V. M. (Nitant) Kenkre

Interplay of Quantum Mechanics with Nonlinearity

Small-Systems Studies of the Discrete Nonlinear Schrödinger Equation

October 5, 2021

Springer Nature

This book is dedicated to a group of wonderful persons I met during the four-year period 1964-68 in Powai, India. It was a little less than sixty years ago then that I joined the Indian Institute of Technology, Bombay, to begin my undergraduate studies. There, I had the good fortune to learn under the guidance of kind and thoughtful teachers who kept my interest in the sciences alive throughout the four years of my instruction. Notable among them were J. S. Murty, R. E. Bedford, M. S. Kamath and C. Balakrishnan. I feel I owe a great debt to them for the personal help and support that they provided me. Even more important in my intellectual formation than their inputs was the exciting atmosphere created by my daily interactions with brilliant colleagues, my classmates. They were an exceptional bunch; I have seldom come across, anywhere in the world, the level of intelligence and overall talent that they were blessed with. I debated, quarreled and discussed, and learned much from them. Some of them are no more. Especially thinking of Rajan M. Ranade and Ashok C. Kulkarni, close friends whose rooms flanked my own, I dedicate this book, with sincere gratitude, to the memories of those of my teachers and colleagues who have departed, and to those who are still around.

Acknowledgements

The work described in this book, specifically on the interaction of quantum mechanics with nonlinearity, was done at various times since the mid 1980s in collaboration with five past Ph. D. students and several other colleagues. It is a pleasure to thank them for joining me in these adventures and helping me understand the nuances of the subject. Considering only the ex-students who chose the topics in this field for their research, in order of our encounters for this particular activity, they were George Tsironis, David Dunlap, John Andersen, Honglu Wu, Ximing Fan, and Srikanth Raghavan. The strongest and the most frequent interactions with other colleagues on this topic were with Marek Kuś whose mathematical wizardry was breathtaking and Alan Bishop whose knowledge of physics was astounding. I learned much from valuable collaborations with David Campbell who was my first coauthor in this field of research, but also Peter Reineker, Markku Salkola, Leonor Cruzeiro-Hansson, Paolo Grigolini, Iris Howard, Augusto Smerzi, Peter Christiansen, M. F. Jorgensen, and Ravindra Amritkar. Associated work done with Vladimir Konotop, Jayanthi Santhanam, and George Kalosakas, while not emphasized in the present book, is also appreciated for aiding my understanding of the subject of nonlinear science. It is a pleasure to recall many illuminating conversations I had with the first Director of the Center for Nonlinear Studies at Los Alamos, the late Alwyn Scott. They were sometimes about matters in this book but more often about life in general and the problem of consciousness in particular.

Various colleagues have helped through comments on preliminary versions of the manuscript: Ravindra Amritkar, Alan Bishop, Leonor Cruzeiro, Robert Knox, ...Two colleagues who were once students of mine gave me a great deal of help in the actual writing of this book: Srikanth Raghavan who educated me about how he applied to Bose-Einstein condensate tunneling what I pretended to have taught him in the polaron field, and most of all John Andersen who came out of his pleasant retirement to kindly render various kinds of invaluable assistance. John's help was especially around his early work on nonlinear trimers and Nmers as well as the recent joint investigation he undertook with me on the nondegenerate nonlinear dimer. It is a special pleasure to acknowledge the help of these two outstanding scientists.

Preface

Procrastination gives you time to consider divergent ideas,
to think in nonlinear ways, to make unexpected leaps.

– Adam Grant

Procrastination, my dear wife has complained for fifty years, is the incessant driving power behind my life. While I do not believe she is right, it is possible, I think, that my fascination with nonlinear science, always from a safe distance so I was not ever compelled to claim any expertise in the field, might have arisen that way, as the modern thinker, Adam Grant, quips in the statement quoted above.

The title of the book you have in your hands, dear reader, is bound to raise your expectations and make you anticipate profound discussions concerning the philosophy of quantum physics and the exquisite nuances of nonlinear science. Walking a fine line between wanting to get your attention by whatever proper means available to me, and my commitment to practice honesty, I must admit, at the outset, that this book is nothing more than a description of a casual but pleasurable adventure I had for about a decade starting in the mid 1980s. That adventure occurred during my efforts to assist a few of my students, who were so inclined, to get their Ph. D.'s doing theoretical research in nonlinear aspects of condensed matter physics. I learned just enough about the subject for that purpose, primarily from my own escapades from what I considered to be my main field of research (statistical mechanics), helped always by books and by colleagues wiser than myself. There are no involved debates, deep ruminations and sudden epiphanies reported here. A single mathematical entity, the "Discrete Nonlinear Schrödinger Equation", is the center of focus in this book, along with simple ideas and calculations based on it. What I can certainly promise the reader, however, is the expression of a tyro's delight at learning about pretty transitions and nifty connections discovered with a beginner's joy in a beautiful field of science.

Similarly to a recent book I have published on the subject of *Memory Functions, Projection Techniques and the Defect Technique* (Kenkre, 2021), the intended reader-

ship here is young starting-out theoretical physicists early in their research career, at their postdoctoral or their advanced graduate stage. I visualize eager fresh researchers searching for weapons of theoretical research, not yet hardened by the requirements and rigors of their profession, inexperienced perhaps, but at their creative peak. I believe that this book will provide them with simple concepts and tools they can use to engage in useful research in theoretical physics even as they acquaint themselves with interesting results in the field of nonlinear physics in condensed matter.

Quantum Mechanics is usually regarded as being linear in its structure. Linear Algebra is, indeed, the underlying mathematical discipline necessary to construct it and linear superposition of its wave functions or state vectors is a frequently occurring phrase in discussions of the subject. Yet, the procedure to extract the expectation value of an observable from the state vector (or wave function) surely involves a nonlinear, to be precise, a *bilinear* operation. It is perhaps partly with an express desire to return to linearity in this operation that von Neumann introduced the density matrix so that observable extraction from the state could be done through the *linear* trace operation. Arguably, the most important and discussed property of quantum mechanical systems is superposition. Linearity is implicit in the statement that, if two independent state vectors, amplitudes, or wave functions are appropriate to describe a process, their superposition, i.e., a sum with constant multiplying coefficients, is also appropriate for such description. Linearity is also inherent in the properties of the operators that represent all quantum mechanical observables. The fact that, typically, the Hamiltonian of the system that operates on the state vector to yield the time derivative of the latter is independent of the state vector, leads to linearity in the time evolution.

However, there is an obvious problem with this way of thinking. While it is true that classical mechanics is often thought of as being generally nonlinear by contrast, it is well known that a reformulation analogous to von Neumann's, that introduces into classical mechanics Liouville densities, at once bestows linearity on classical mechanics as well. The place of the commutation of the Hamiltonian with the system density matrix in quantum mechanics is now taken by Poisson brackets involving the (classical) Hamiltonian and the Liouville density (Balescu, 1975; Reichl, 2009). If one (mistakenly) falls back on the nonlinearity of the classical equations of motion for observables, e.g., the coordinates and momenta of the constituent particles or degrees of freedom, and argues that this is special of *classical* mechanics, one recognizes one's error immediately on noticing that the equations for the corresponding operators for coordinates and momenta are also generally *nonlinear*. Linearity is characteristic of the usual equation of motion for the state vector or wave function, say the Schrödinger equation, or of the Liouville-von Neumann equation for the density or density matrix. This is certainly not true of the Hamiltonian equations for the observables or their corresponding operators.

Surely, we spend much time, as we should, with the process of finding eigenvalues and eigenvectors of the Hamiltonian and other operators and rely, for the purposes of calculation, on the mathematics of linear algebra. However, it is necessary to be precise in one's mind about what one means by the statement that Quantum Mechanics is linear.

We can assert without argument that, by the linearity statement, we at least mean that, in the evolution equation

$$i\hbar \frac{d|\Psi(t)\rangle}{dt} = H|\Psi(t)\rangle,$$

the Hamiltonian operator H is not itself a function of $|\Psi(t)\rangle$. In the title of this book, we consider a violation of this assumption and study the effects of the interplay of familiar quantum features with such nonlinearity. Investigations of a violation of linearity on a *fundamental* level have been carried out by several illustrious scientists (Weinberg, 1989; Leggett, 2002; Jordan, 2009). The last of the authors cited has referred to George Sudarshan's questions and insights into the problem. In the context of the present book, the violation does not arise from any fundamental source, rather from what is an approximate representation of the dynamics supposed to arise from a coarse-grained description through the elimination of some of the variables inherent in the dynamics.[1]

Specifically, our interest is in elucidating the consequences of the *Discrete Nonlinear Schrödinger Equation* (DNLSE). The equation arose originally in polaron physics when phonons interact strongly with moving electrons, or with quasiparticles such as other phonons, from the creative arguments of several investigators (Landau, 1933; Pekar, 1954; Holstein, 1959a,b). Much later it also arose under the guise of the Gross-Pitaevskii equation (Pitaevskii, 1961; Gross, 1961, 1963) in the dynamics of Bose-Einstein condensates, and even formally in optical waveguides and in the dynamics of classical anharmonic oscillators. My interest in this book is primarily in the first area and to some extent in the second. I shall refrain from touching the field of optical waveguides or anharmonic oscillators given that fine expositions (Hennig and Tsironis, 1999; Eilbeck et al., 1985) already contain detailed references to those respective areas.

The subject of nonlinear Schrödinger equations is teeming with activity and encompasses an enormous community of physicists and mathematicians. My purpose will be to focus only on the *discrete* form of the nonlinear Schrödinger equation and that too in spatially *very small* systems. From the multitude of expert treatments in the area of nonlinear Schrödinger equations, even restricting to the discrete variety, I especially mention two, (Ablowitz et al., 2004) and (Kevrikidis, 2009). Both are excellent and can teach the reader valuable techniques and tools in the general field. There are also other, similar, books on the subject with specialized slants, for instance (Christiansen and Scott, 1990). For the general field of soliton physics, an eminently readable presentation is *Physics of Solitons* (Dauxois and Peyrard, 2006). Given all this wealth of material already available in the literature, it is important to understand why I have undertaken to write this one. I believe it has a special pedagogical element. The book is characterized by the fact that it offers a limited treatment of the DNLSE in systems of small spatial extent, always taking advantage of analytical solutions wherever possible. The details of this statement are explained

[1] Thus, in one instance, the nonlinearity arises, or is supposed to arise, from the removal of phonon degrees of freedom from a strongly interacting electron-phonon system.

in Chapter 1. The restriction that we impose on our own sphere of analysis will allow us to focus on simple matters with simple tools.

The work described in the pages of this book stems from about fifty publications primarily within my own research group but also in those of closely connected colleagues, that were produced largely during about a decade starting around 1985. Interest in the so-called Davydov soliton (Scott, 1992) was greatly responsible for the activity in the subject at that time.[2] I believe the lessons learned as well as issues left unresolved during that relatively brief spurt in research on the part of the community focused on that topic are as timely today as they were then. My own activities were not motivated by the Davydov problem except for using it as a backdrop. Despite the elementary nature of the questions raised and treatments offered, I hope that the reader will find something of value in these pages.

Given that I feel that the content of this book might be most useful to starting-out researchers, let me venture to express my opinion to them that research in theoretical physics comes in three flavors. One has to do with the explanation of experiment. The central importance for the advancement of science of this kind of activity is obvious. Einstein unravelling the essence of the temperature dependence of the specific heat of insulators provides a clear example as do Bardeen, Cooper and Schrieffer presenting their explanation for superconductivity. A second flavor is that of seeking relations between formalisms with a view to establishing bridges across theories: an excellent instance is Dyson's building a lexicon that facilitated the understanding of the connections between Feynman's formalism on the one hand and Schwinger's on the other in their investigations of quantum electrodynamics. A third type of activity of the theoretical physicist occurs when, starting with an equation or similar mathematical object, one barges forward and discovers something interesting, unexpected and surprising, and then presents the results to the experimentalist. The discovery of waves of electromagnetic radiation from manipulations of Maxwell's equations happened, as we all know, in this manner. This last of the three flavors is what permeates whatever is described in the present book. Experiments are analyzed seriously but only in the spirit of designing them to see new effects; set puzzles are not solved.[3]

---

[2] Glimpses of the activity around the Davydov soliton proposal can be had in the Dauxois-Peyrard book mentioned above. Much more attention is focused on it in the Christiansen-Scott book on the DNLSE.

[3] Each of these kinds of theoretical research is, no doubt, important to the advancement of our branch of science. Most of us have tried all three, to various extents. The first is perhaps the most difficult. Some among my colleagues consider it the only kind worth pursuing, insisting theorists to be no more than hired hands of experimentalists. At the other extreme lie some theorists who confess that they have the ability only to work in the last of the modes mentioned. That mode is, perhaps, the easiest as there is no goal set by others to meet. Of all three, this 'forward' kind of research activity has less of puzzle-solving and has, I tend to think, more kinship to artistic endeavors. My musician friends have often confided in me that the solving of set problems that they believe to be characteristic of scientific work turns them off. Dancing to one's own tunes is how they describe their own activity. That is why, among the theorist's three avenues, the last one mentioned above is the one I consider most akin to the artist's manner of working.

During the late 1980s in which my private obsession with nonlinear physics proceeded with intensity, David Brown[4] once reminded me that I had expressed to him earlier that nonlinear science was for the birds. I am afraid it is true that I had made that totally irresponsible remark. With hindsight, I conclude it was a consequence of two items. Some contact, when a graduate student myself, with Louis de Broglie's writings on nonlinear quantum mechanics was one of them: I felt convinced, with the irresponsible audacity of youthful ignorance, that they were disjointed. The second reason was my strongly negative reaction later to studies of the subject of chaos that many regarded (and regard) as the essence of nonlinear science. Lack of wisdom, as also perhaps casual shallowness stemming simply from lack of knowledge, had led me to discard the field as not suited to my research aspirations.

What happened in the 1980s then to break my barriers of ignorance? It was simply that, during my study of a simple system, the quantum nonlinear dimer that you will meet in Chapters 1 and 2, I was surprised, in my own analysis, by a bifurcation when I least expected it. Bifurcations and phase transitions are naturally fascinating. From rubber bands that snap, to presidents that get ousted and empires that crumble, instances of "something suddenly happens" always astound and intrigue. It is because a bifurcation or transition sprang in my own simple work that I was turned on to the subject.[5]

I would like to end these thoughts with a few general comments about nonlinearity, particularly in condensed matter physics. The field is of gigantic proportions and I heartily recommend to the reader the book by Alwyn Scott on the Nonlinear Universe (Scott, 2007) in which he tackles a wide spectrum of issues, phenomena, and activities in the subject. I am certain that the reader will be impressed by the breadth of scope, and the intensity of involvement of the writer of the book in a field which he greatly helped expand in his lifetime. Also available and strongly recommended, is Alan Newell's book (Newell, 1985) with focus on solitons. Written by one of the originators of many techniques and insights in the field, it is a delight to read.

At the introductory level, the textbook (Strogatz, 2018) is exceptional in its treatment. Higher level instruction may be found in (Jackson, 1989, 1990) and (Nicolis,

[4] He was an exceptional student who worked for his Ph. D. under my guidance, and was equally comfortable with equations as with nuances of the English language. He went on to make valuable contributions to the debates centering around the Davydov soliton through the publication of a number of widely quoted papers coauthored with Katja Lindenberg and Bruce West.

[5] I must confess I exited the field before I had learned a sufficient amount about the subject. May I amuse the reader by explaining why. The brilliant scientist Elliott Montroll, who was one of my mentors at that time, dispensed to me some advice during a car ride in the late 1970s to Dave Dexter's plantation outside of Rochester. Elliott said he was sharing with me his *modus operandi* in physics research: solve an easy problem and rapidly get out of the field. He claimed that if you did that wisely, others would spend oodles of time and energy on difficult extensions of the problems you had solved and during all that time would keep referring to your work! The strategy did not work for me: Elliott neglected to tell me that the quality of the work also had to be substantial! I happen to know that he himself kept on solving tantalizingly difficult problems and was justifiably credited all his life with outstanding solutions that he produced. I was not helped by attempting to practice what he preached, perhaps jokingly, to his less capable colleagues such as myself.

1995). For a specialized topic such as Synchronization, I suggest Gupta et al. (2018). The numerous contributions of Alan Bishop and David Campbell, working together and separately, are of immense value whether in their own researches (Bishop et al., 1980; Campbell, 1987) or in the exciting conferences they put together and the groups of investigators they helped form in the field of nonlinearity in condensed matter over the years. A nice example is a brief overview (Campbell, 1987) that describes a few selected topics in nonlinearity. For the humorous note in nonlinearity, I cannot resist reminding the reader of the famous statement by Ulam (See for instance its mention in (Campbell, 1987)) that referring to nonlinear science (as normally done) as the study of mathematical systems and natural phenomena that are not linear, is "like defining the bulk of zoology by calling it the study of 'non-elephant animals'." But for more serious musings on the subject I heartily suggest to the reader to peruse the Introductory Section in Landauer's article "Nonlinearity: Historical and Technological View" (Landauer, 1987). I will content myself with the following extract:

> The ambiguity in *nonlinear* is deeper, and reflects the mode of description. We tend to consider classical motion in a constant, linear, or quadratic potential as *linear* and refer to anharmonicity when we go beyond that. But the Hamilton-Jacobi equation, even for a free particle, is already nonlinear. On the other hand the Schrödinger equation is always linear, no matter how complex the potential, and as a limiting case can always describe the classical Hamilton-Jacobi equation. The classical Liouville equation is also linear and represents *the* universal trick for making things look linear, in the case of deterministic problems...The low field Hall current, in crossed electric and magnetic fields, represents a linear conductance, if we consider the magnetic field to be a parameter. If, however, we consider electric and magnetic fields as simultaneous components of a total electromagnetic field, then it is clearly nonlinear...It is possible that there is some kind of rational path through this complexity, and that there is a broadly applicable definition of *nonlinearity*. I do not know about it, and interpret *nonlinear* in a more phenomenological sense. Nonlinearity has to do with thresholds, with multi-stability, with hysteresis, with phenomena which change *qualitatively* as we change excitation.

OUTLINE OF THE BOOK

The mathematical entity around which considerations in this book revolve is, as we have stated above, the Discrete Nonlinear Schrödinger Equation (DNLSE) obeyed by the quantum mechanical amplitude of a particle. An introduction to the equation and to its ability even in the absence of static disorder to localize the particle when the nonlinearity exceeds a critical value is given in Chapter 1. To make exact considerations possible, one introduces the analysis for a dimer, i.e., a system of two sites. Potential considerations and graphical arguments are shown to lead to the possibility of a sharp transition. The analytic tool of elliptic functions, particularly of the Jacobian ilk, is then developed briefly with emphasis on their physical meaning, the goal being to extract with their help explicit solutions of the problem. Such extraction is done in Chapter 2 and the insights applied to two experimental situations, one involving mobility of particles as in electrical conduction and the other having to do with neutron scattering observations. Stationary states of the nonlinear system

and their stability are also investigated here. The effect of the interplay of the initial *quantum phase* of the particle with nonlinearity is studied in Chapter 3. Novel phenomena are found to arise from such interplay and to lead to what appears like another, different, transition. Consequences are analyzed for experiments on fluorescence depolarization of stick dimers under the assumption that the relevant electronic excitation interacts strongly enough with molecular vibrations to justify invoking the nonlinear description.

The quantum mechanical particle obeying the DNLSE studied in most part in the book can be said to be, in the language of the condensed matter physicist, a *polaron*. What the behavior of a polaron owes to its harmonic origins is studied in Chapter 4. The cubic nonlinearity in the quantum amplitude that is characteristic of the DNLSE arises from an interaction of the quantum particle with vibrations which are almost always considered to be harmonic. What happens if the harmonic assumption is relaxed is, thus, the subject of Chapter 4. Rotational polarons as well as those arising from other natural realizations of anharmonicity are investigated. Time evolution is studied as well as stationary states of the system. Appearance of self-trapping on increasing nonlinearity is encountered as in the early chapters of the book but the *disappearance* of self-trapping on further increasing nonlinearity is the primary surprise in these rotational polarons and related systems. Criteria for the continuous versus discontinuous nature of the transitions on varying the parameters are also developed. The study of DNLSE systems with nonlinearities more complex than simple cubic, whatever the mechanism for their turning cubic, can be considered as the primary focus of the analysis in this Chapter.

Dropping back to the standard harmonic situation, equivalently cubic nonlinearities, an attempt is made in Chapters 5 and 6 to understand behavior in systems more complex than the simple site-resonant nonlinear dimer in other ways. A systematic study of the combination of a static energy mismatch and the dynamic energy mismatch produced by the nonlinearity in the DNLSE forms Chapter 5. The first case treated is, thus, the analysis of the *nondegenerate* nonlinear dimer. Weierstrass elliptic functions that have been often used to arrive at final solutions are reviewed and studied. However, a treatment that is based on *Jacobian* elliptic functions that are much more familiar and approachable to the physicist is emphasized. A number of explicit analytic results that will be unfamiliar to most readers are provided concerning quantities such as the period and the average values of site occupation probabilities. Interesting transitions are described. An alternative method for the analysis of the nondegenerate nonlinear dimer resulting in an integrodifferential equation with memory is also provided. In Chapter 6 we study systems of increased size relative to a dimer. To retain the analytic nature of the investigations rather than resort to numerical studies, this enquiry is carried out for systems in which transfer interactions are of long range. Stated precisely, the limit considered is that of *global* interactions, the spirit invoked being, thus, of a mean field theory. Interesting conclusions are drawn and transitions are noticed. The second part of Chapter 6 addresses the study of nonlinear trapping, also limited to global interactions. Bare-bones calculations are presented in the context of the design of what could become artificial photosynthetic machines.

The assumption underlying the analysis reported thus far in the book is that the (vibrational) relaxation that leads to polaronic formation is infinitely fast. This has as its consequence that the energy lowering of the moving particle is instantaneous. The assumption is dropped in Chapter 7. The resulting system, sometimes referred to as the *nonadiabatic* nonlinear dimer, is analyzed in both extremes of damping: high damping so the vibrational relaxation can be considered to be first-order in time, and no damping of the auxiliary subsystem (e.g., the vibrations) so that the full second-order evolution is maintained. The latter analysis tiptoes teasingly around chaotic regions, but can be made to yield precise solutions in terms of elliptic functions for certain values of the system parameters. Thermal effects constitute Chapter 8 and are investigated in two analytic ways: via phase space considerations, and with the help of the standard methodology of Brownian motion. Intriguing phenomena such as Hopf bifurcations arise in the analysis and are shown to be reflected in suggested experiments in fluorescence depolarization.

A brief return to basic questions regarding the emergence of the discrete nonlinear Schrödinger equation from microscopic Hamiltonians involving the interactions of the moving particle and system vibrations is the content of Chapter 9. It includes an explicit comparison between results obtained directly via numerical solutions of the quantum equations of motion and those that arise from two approximation schemes: the memory function formalism on the one hand, and semiclassical equations of motion on the other. This subject of the proper treatment of strong phonon interactions with a quantum particle via semiclassical representations such as the DNLSE is characterized by sharp differences of opinion in the community. One encounters in this connection the extensive publications of Brown et al. (Brown et al., 1986a,c,b) and a transparent analysis by (Lomdahl and Kerr, 1985; Kerr and Lomdahl, 1987). One also finds the strongly critical analysis of Grigolini and his collaborators (Vitali et al., 1992; Bonci et al., 1993; Vitali et al., 1994) who regard the DNLSE as emerging from an erroneous treatment of microscopic interactions between quasiparticles and phonons. No one doubts that the DNLSE, in the systems we discuss, is to be regarded as an approximation to the original linear system but one that describes the essence of the physics when a kind of coarse-graining is performed, eliminating a part of the full system. The differences of opinion refer to whether the approximate description is sensible or whether it throws the baby out with the bath. My development in the book will only scratch the surface in this area and recognize the differences but suggest strongly that they constitute a problem that is still open and deserving of further attention by interested investigators.

Those debates concerning the appropriateness of using nonlinear representations of the quantum evolution equation do not arise in the same manner in the realm of the description of Bose-Einstein condensates via the Gross-Pitaevskii equation although, there too, a semiclassical description is meant in part. In the language used by Scott and his collaborators, Christiansen and Eilbeck, the nonlinearity is essentially intrinsic. Numerous reviews in the Bose-Einstein field, make this clear (Leggett, 2001). My own description in Chapter 10 of this book is spent on treatments of this subject as initiated by Raghavan, Smerzi, Shenoy and their collaborators (Raghavan et al., 1999b,c,d) in close contact with small-system analysis of the DNLSE. They

also include two items to which I might draw the reader's attention. The first is an investigation that Raghavan and Smerzi carried out some time ago (Raghavan et al., 1999d) in collaboration with me on the question of which of the transitions that arise in the DNLSE approach survive when examined for *purely quantum mechanical* systems: a subject that is again coming to the forefront of research in recent years (Pudlik et al., 2014) and derives its importance from the fact that it deals with the important issue of the connection between semiclassical and quantum descriptions. The second consists of very recent proposals for observations that I have constructed in collaboration with Andersen and Raghavan for BEC condensate tunneling and similar systems.[6]

Several miscellaneous issues on the edges of our subject are discussed in Chapter 11. They include an application of projection operators to the derivation of memory functions in a nonlinear system, a brief analysis of external agencies on small nonlinear systems carried out by consideration of time-dependent system parameters, an investigation of the effect of anharmonicities in the vibration on the validity of the semiclassical approximation probed with the help of a Pöschl-Teller potential, a study of soliton propagation in boson-fermion mixtures, treatment of a nonlinear impurity in a linear quantum mechanical chain, and some old but interesting calculations of the formation of excimers and their intermediate so-called Y-states. An overview of the book contents is also presented in this final chapter. Every chapter has, at its end, a brief summary of what has been explained in the chapter. Consonant with the idea that the book targets in part the education of advanced graduate students and young postdoctoral scientists, exercises are sprinkled throughout the book, with hints provided for their solutions in several instances. A bibliography of references is provided at the end.

[6] See John D. Andersen, Srikanth Raghavan, V. M. Kenkre, http://arxiv.org/abs/2108.08711

Contents

Chapter 1
The Discrete Nonlinear Schrödinger Equation and the Two-State System (Dimer)

1.1 Introduction

Consider the motion of a quantum particle moving among the sites of a translationally invariant crystal denoted by $\mathbf{m}$ and $\mathbf{n}$, the latter being vectors in an appropriate number of dimensions, for instance three. The motion is occurring via $V_{\mathbf{mn}}$, which may be taken to be interaction matrix elements between the $\mathbf{m}$th and $\mathbf{n}$th Wannier states of the crystal. The particle might be an electron, an electronic or vibrational excitation, or a heavier object such as a muon or an interstitial atom that is free to move through the crystal. In the theory of electrons in solids (Wannier, 1959; Anderson, 1997) such motion is characterized by Wannier states (or their Fourier transforms, the Bloch states) each associated with a band index and a value of the quasimomentum also known as the crystal momentum. The latter spans the Brillouin zone, its allowed values being equal to the number N of sites in the crystals. The number of bands, on the other hand, is infinite; this corresponds to the intervening space between sites being continuous. Considering only a single band, equivalently under the assumption that we take into account the particle existing only at the sites and not in the space intervening, we might write the equation of motion for the quantum mechanical amplitude $c_{\mathbf{m}}$ for the particle to be at site $\mathbf{m}$ as

$$i\hbar\frac{dc_{\mathbf{m}}}{dt} = \sum_{\mathbf{n}} V_{\mathbf{mn}}c_{\mathbf{n}} - \chi|c_{\mathbf{m}}|^2 c_{\mathbf{m}}. \tag{1.1}$$

The two features of the equation that remind us that the system is quantum mechanical are the presence of $i = \sqrt{-1}$ in the left hand side and the symbol $\hbar$ that represents, of course, the ratio of Planck's constant and 2π. Throughout the book, we will use the notation whereby we put $\hbar = 1$. This means that it has been absorbed into the quantities χ and $V_{\mathbf{mn}}$ by division.[1] Unless mentioned otherwise, we will take the sign of χ to be positive. The motivation arises from its being given in polaronic contexts

[1] This has the obvious consequence that, throughout the book, energies have the same units as frequencies.

by a quantity proportional to $g^2\omega$ (g is a dimensionless coupling constant) and ω is typically a vibrational frequency. Both g^2 and ω have positive sign. It is possible, nevertheless, to have an effective negative sign for χ simply from a negative sign for V. Such can easily arise from the band energy curvature according to whether the moving carrier comes from the bottom or top of the band.

If we restrict our attention to a 1-dimensional chain of sites and consider the particular case of nearest-neighbor interactions, the form of the equation (1.1) we must consider is

$$i\frac{dc_m}{dt} = V(c_{m+1} + c_{m-1}) - \chi|c_m|^2 c_m. \tag{1.2}$$

Because Eq.(1.2) will be the center of our attention throughout the book, it is wise to assign to it a name. The quantity C_m, obtained by multiplying the quantum mechanical amplitude c_m by the phase factor $e^{i\phi(t)}$, obeys

$$i\frac{dC_m}{dt} = V(C_{m+1} + C_{m-1}) - \chi|C_m|^2 C_m + i\left(\frac{d\phi(t)}{dt}\right)C_m. \tag{1.3}$$

The choice $\phi(t) = 2Vt$ yields, therefore, an evolution equation for C_m which, in the continuum limit, leads to

$$i\frac{\partial C(x)}{\partial t} = D\frac{\partial^2 C(x)}{\partial x^2} - B|C(x)|^2 C(x). \tag{1.4}$$

The continuum limit means that the distance a between nearest neighbor sites vanishes, i.e., $a \to 0$ and $V, \chi \to \infty$ such that $Va^2 \to D$ and $\chi a^2 \to B$ and, of course, $C_m/a \to C(x)$.

Equation (1.4) already has a well-established name in the literature: the nonlinear Schrödinger equation. The motivation for the name should be quite clear when one recalls the form that the ordinary (linear) Schrödinger equation takes for a free particle. "The discrete nonlinear Schrödinger equation" thus suggests itself as an appropriate name for Eq. (1.2). This name has been employed in the literature for several decades now.[2] We will use it throughout the book.

There is another equation on the discrete chain, closely allied, that also has Eq. (1.4) as its continuum limit, and is, moreover, exactly soluble. This is the Ablowitz-Ladik equation (Ablowitz and Ladik, 1976) given by

$$i\frac{dc_m}{dt} = V(c_{m+1} + c_{m-1} - 2c_m) - \chi|c_m|^2(c_{m+1} + c_{m-1}). \tag{1.5}$$

It is Eq. (1.2), however, that emerges naturally as a consequence of the physical arguments that we are interested in here. Equation (1.5) represents, instead, a situation in which the cubic nonlinearity modifies the intersite interaction matrix element rather than the site energy. A great deal of work has been done on the Ablowitz-Ladik equation because it constitutes an integrable system. This means that explicit

[2] The phrase the "discrete self-trapping equation" (Eilbeck et al., 1985) has also found use in certain circles.

solutions for the chain with infinite spatial extent can be found and examined with ease, something that is not the case with the DNLSE (1.2).[3]

1.2 A Numerical Study Indicating The Appearance of a Self-trapping Transition

Analytical solutions of the DNLSE, Eq. (1.2), have not been found. One way to understand whether the structure of the equation does result in self-trapping behavior, and how, is to carry out numerical studies. For this, you place the quantum particle at one of the N sites of a periodic ring at the initial time and work out the evolution through numerical algorithms. You change N until it is large enough and further increases do not show much variation in what you observe. Then the finite ring may be taken to emulate the infinite line. Much expert work (Cai et al., 1994) has been done in this manner to investigate various phenomena. Let us implement a simple version of such studies. What is observed as the probability $P_0(t) = |c_0|^2(t)$ of the initially occupied site is plotted in Fig. 1.1 for several values of the nonlinearity χ as shown.

For vanishing nonlinearity, discrete Fourier transforms yield the analytic solution, $P_0(t) = J_0^2(2Vt)$, and the numerical curve computed for this case coincides precisely with that analytic solution. This is clear in the plot. Increase of nonlinearity shows quite transparently that the particle moves with less mobility. Although numerical work of this kind cannot ever show us the consequences with certainty, it does look likely there is a transition which describes self trapping of the particle at a specific value of the nonlinearity parameter. High values of χ appear to result in the particle being essentially stuck around the site at which it is placed initially.

The density matrix evolution equation that is a consequence of the DNLSE, given that $\rho(t) = |\Psi(t)\rangle\langle\Psi(t)|$, is

$$i\frac{d\rho_{m,n}}{dt} = V(\rho_{m+1,n} + \rho_{m-1,n} - \rho_{m,n+1} - \rho_{m,n-1}) - \chi\rho_{m,n}(\rho_{m,m} - \rho_{n,n}). \quad (1.6)$$

Approximate treatments of this equation do also result in indications that a self-trapping transition is in the works. However, given that numerical analysis requires specialized skills to avoid pitfalls that can arise from computing artifacts, in order to be certain of what is going on, let us undertake the analysis of a system of *small size* with the hope that it might be analytically soluble.

[3] Investigators have even analyzed combinations of the two equations in a form that some of us associate with the name of Salerno (Enol'skii et al., 1991, 1992). A cogent explanation of the two extremes is available in (Hennig and Tsironis, 1999).

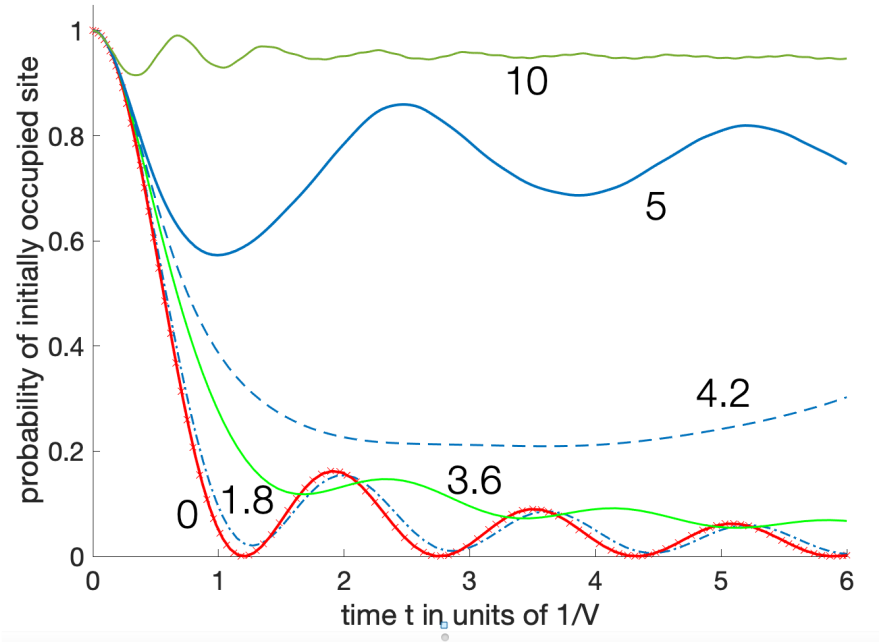

Fig. 1.1 Numerical solution for self-trapping on an infinite chain on which a quantum particle is moving via nearest-neighbor interactions V via Eq. (1.2) which contains a cubic nonlinearity at the occupied site controlled by the parameter χ. A ring of $N = 100$ sites is taken to represent the infinite chain: results do not change visibly on increasing the number of sites beyond that value. The time dependence of the probability of the initially occupied site is plotted as a function of Vt for successively increasing values of χ. Six values of the latter relative to V are considered: 0, 1.8, 3.6, 4.2, 5, and 10. They are indicated next to the respective curves for the time-dependence of the probability of the initially occupied site. The leftmost curve, for $\chi = 0$, is indistinguishable from the analytic solution $J_0^2(2Vt)$ for a linear chain of infinite N, where J_0 is the Bessel function of zero order. The analytic curve is sitting right on top of the numerically computed curve. As χ/V increases, we notice a slowing down of the particle and a transition to what appears to be self-trapping somewhere in the neighborhood of $\chi/V = 4$. For higher nonlinearities, the particle is clearly trapped near where it is placed initially.

1.3 Density Matrix Equations for a System of Very Small Size

If we consider the system to be a dimer, i.e., consist of only two sites 1 and 2, the density matrix equations take the form (Kenkre and Campbell, 1986)

$$\frac{d\rho_{11}}{dt} = -iV(\rho_{21} - \rho_{12}), \tag{1.7a}$$
$$\frac{d\rho_{22}}{dt} = -iV(\rho_{12} - \rho_{21}), \tag{1.7b}$$
$$\frac{d\rho_{12}}{dt} = -iV(\rho_{22} - \rho_{11}) + i\chi(\rho_{22} - \rho_{11})\rho_{12}, \tag{1.7c}$$
$$\frac{d\rho_{21}}{dt} = -iV(\rho_{11} - \rho_{22}) + i\chi(\rho_{11} - \rho_{22})\rho_{21}. \tag{1.7d}$$

and can be written in terms of the probability difference between the two sites, $p = \rho_{11} - \rho_{22}$, and the other two real quantities comprising components of the so-called Bloch vector, $q = i(\rho_{12} - \rho_{21})$ and $r = \rho_{12} + \rho_{21}$.

The time evolution of the Bloch vector follows

$$\frac{dp}{dt} = 2Vq, \tag{1.8a}$$
$$\frac{dq}{dt} = -2Vp - \chi pr, \tag{1.8b}$$
$$\frac{dr}{dt} = \chi pq. \tag{1.8c}$$

Let us focus on the evolution of the probability difference, consider the initial localized condition on one of the sites so that $p(0) = \pm 1$ and $q(0) = 0 = r(0)$, eliminate q and r, and write the closed equation for the probability difference as

$$\frac{d^2p}{dt^2} = Ap - Bp^3, \tag{1.9a}$$
$$A = (\chi^2/2) - 4V^2, \quad B = \chi^2/2. \tag{1.9b}$$

There are two obvious ways to proceed to extract information from this nonlinear equation for p. One is to regard p as representing the displacement of a particle and Eq.(1.9) as describing the acceleration of the particle under a p-dependent force. We can then apply the standard energy method of classical mechanics to proceed further from that equation by multiplying it by dp/dt and integrating once to get a potential $U(p)$:

$$U(p) = (A/2)p^2 - (B/4)p^4. \tag{1.10}$$

The potential can now be plotted and used for graphical studies of the motion.

1.4 Considerations via Potentials

Potentials constructed in this manner are displayed in Fig. 1.2 for various values of the ratio of the nonlinearity χ to V for initial placement of the particle at one of

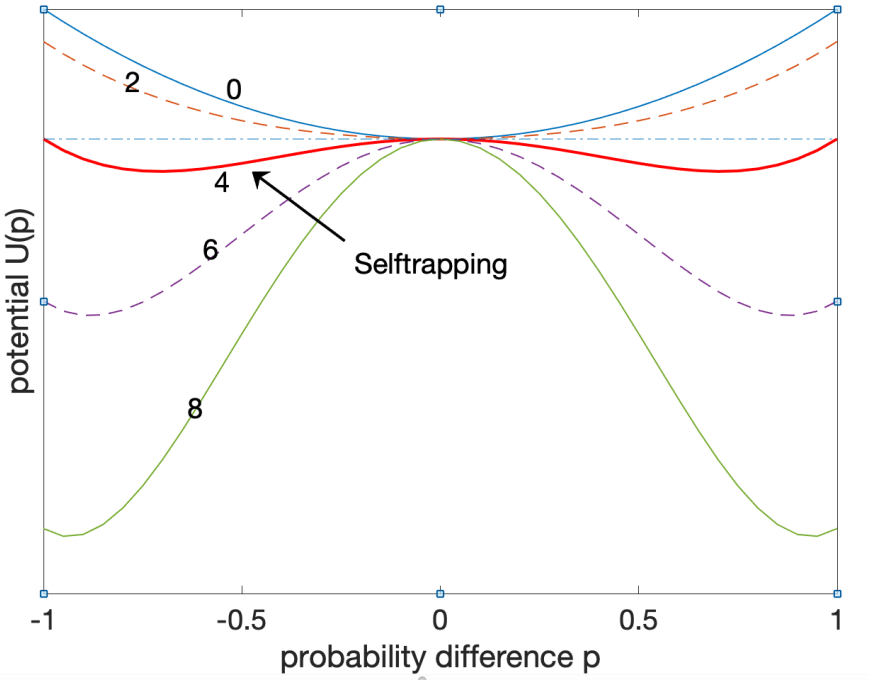

Fig. 1.2 The p-potential $U(p)$ for the dimer given in Eq. (1.10) for various values of the ratio of the nonlinearity parameter to V as marked in the plot: 0, 2, 4, 6, 8. Graphical inspection indicates a transition at the critical value 4 of this parameter as the system would oscillate on both sides of the plot for lower values but only on one side for higher values. Note the importance of the horizontal dash-dot line to the graphical argument behind the transition. It marks the energy of the classical representation of the system with displacement p that remains constant throughout the evolution and thereby shows pictorially that the particle would take infinite time at the transition to go to the other side.

the sites. For vanishing χ, the potential is parabolic (marked 0 in the plot) and the particle rolls back and forth in the potential following a (sinusoidally) oscillating time dependence. As χ/V increases, the potential flattens because of the contribution of its quartic piece with the consequence that the particle clearly takes longer to oscillate within its bounds. See, for instance, the potential marked by the value 2 of χ/V. With further increases in the nonlinearity a double-well nature develops. The value 4 of the ratio is critical and self-trapping sets in (the potential curve is shown thicker for this case). For nonlinearity greater than this value, swishing occurs in only the right well. At the transition, the particle takes infinite time to move to the left well. The horizontal line (dash-dot) drawn leftwards from the point of intersection of the potential with the vertical at value $p = 1$ is *tangential* to the potential curve at its central maximum. It is this graphical feature that shows that we have self-trapping and that the particle takes an infinite amount of time to move from the right of the

plot to the left. Further increase in the nonlinearity makes the (double) wells deeper, signifying less transfer and lower mobility.

More familiarity with what happens in the problem can be gained by obtaining the explicit time dependence of the solutions. For this purpose, let us arm ourselves with some brief essentials of elliptic functions, return to the nonlinear equation (1.9), and obtain the time dependence of p with their help.

1.5 Arming Oneself with Elliptic Functions

Everyone is familiar with the relation that exists between trigonometric and hyperbolic functions as a result of de Moivre's identity

$$e^{i\theta} = \cos\theta + i\sin\theta.$$

The relation is between the trigonometric sine and the hyperbolic sine in that $\sinh i\theta = i\sin\theta$ and $\cosh i\theta = \cos\theta$. However, there also exists a quite different connection between trigonometric and hyperbolic functions, one that teams up the sine with the hyperbolic tangent and the cosine with the hyperbolic secant!

If you can imagine holding two adjacent peaks of a sine function, one positive and the other negative, and pulling them in opposite directions to plus and minus infinity, you will see that the stretch can be said to result in the sine converting itself into a function that rises to the value 1 on one side of the origin and drops to the value -1 on the other side, turning itself into a hyperbolic tangent. In the same way, you can turn a cosine into something that looks like a hyperbolic secant through a stretch by grabbing a cosine at the location of two of its adjacent zeros and stretching it similarly. This is visually apparent in Fig. 1.3 where the stretch of the sine is depicted in the left panel while that of the cosine is in the right panel. In this manner of regarding the functions, the hyperbolic function that the trigonometric sine (cosine) is related to, emerges as the hyperbolic tangent (secant).

1.5.1 Definition of the Elliptic Sine and Related Functions

Let us make this stretching idea more precise by introducing the functions through their integral definition. Let us recall that Newton's equation for the simple pendulum or for the harmonic oscillator of unit frequency,

$$\frac{d^2x}{dt^2} + x = 0$$

has as its solution the trigonometric sine if the initial condition is that $x(0) = 0$ at the initial time. Thus, $x = \sin t$ means that

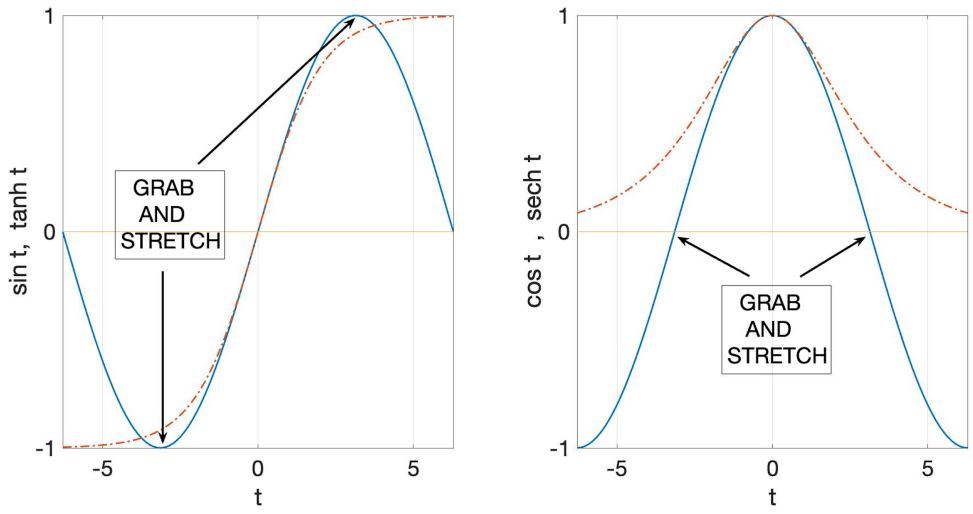

Fig. 1.3 A surprising connection between trigonometric and hyperbolic functions. Holding the peaks of a sine (solid line) and stretching the curve in opposite directions to infinity suggests that one might attain the shape of a hyperbolic tangent (dash-dot line). This is clear in the left panel. Similarly, in the right panel, holding the cosine curve (solid line) at the points where it crosses zero and stretching in a similar manner suggests a transition of a shape to the hyperbolic secant (dash-dot line). Notice that trigonometric functions are profoundly different from their hyperbolic counterparts in that they oscillate and the latter do not. The connection suggests the introduction of elliptic functions as intermediate entities that reduce to trigonometric and hyperbolic limits of a parameter k as it takes on values ranging from 0 to 1. See text.

$$t = \int_0^x \frac{dz}{\sqrt{1-z^2}}. \tag{1.11}$$

We also know that the stretch limit $\tanh t$ suggested by the plots is similarly defined via an integral that has in its denominator the square of the denominator in Eq. (1.11): To say that $x = \tanh t$ means that

$$t = \int_0^x \frac{dz}{1-z^2} = \int_0^x \frac{dz}{\sqrt{1-z^2}\sqrt{1-z^2}}. \tag{1.12}$$

Could we find a way of defining a new intermediate function $\mathrm{fn}(t)$ that might lie between the trigonometric sine and the hyperbolic tangent and tend to each in the appropriate limit? Consider a definition $x = \mathrm{fn}(t)$ such that

$$t = \int_0^x \frac{dz}{\sqrt{1-z^2}\sqrt{1-k^2z^2}}. \tag{1.13}$$

The quantity k should be thought of as continuously changing from 0 to 1 and to yield, at the limits, the sine and the hyperbolic tangent.

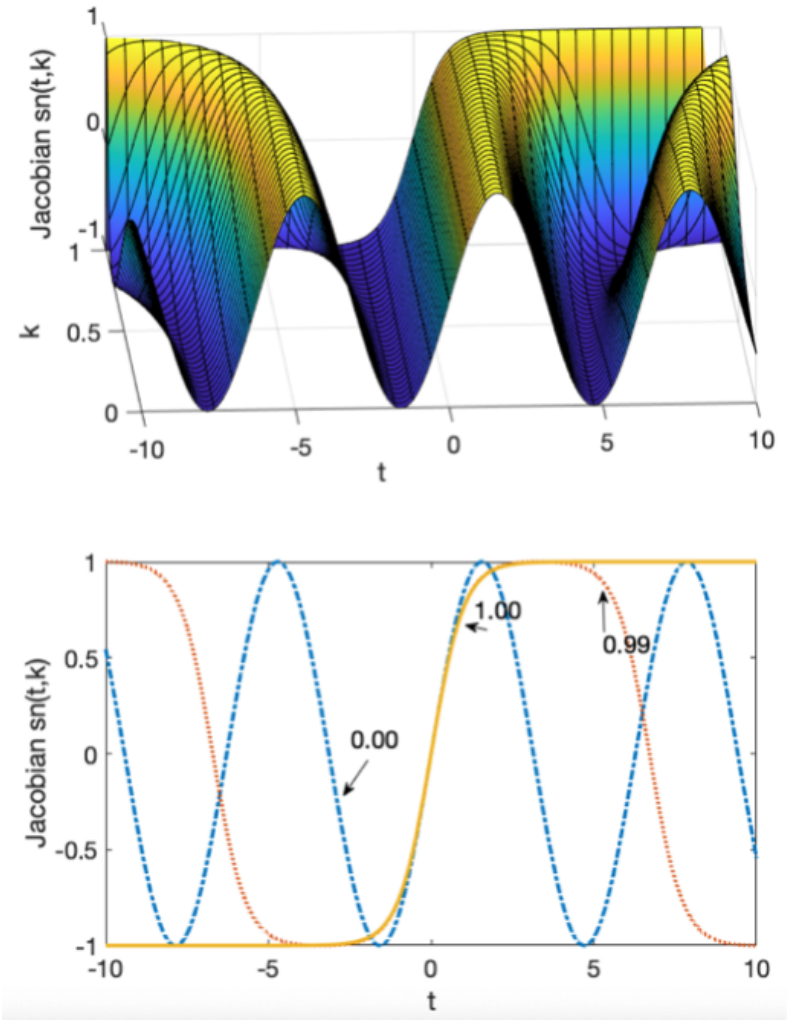

Fig. 1.4 The Jacobian elliptic sine showing its shape variation with the elliptic modulus k. The upper panel is a $3d$ plot showing that for $k = 0$ (front region nearest to the reader) the shape is that of a trigonometric sine but that as k increases the shape varies substantially, taking the form of a hyperbolic tangent as k tends to 1 (back region farthest from the reader). This is made clearer in the $2d$ plots in the lower panel where the k values are indicated as being respectively the extremes 0 and 1 as also an intermediate value 0.99.

The function so defined is called the *elliptic sine*: $x = \mathrm{sn}(t, k)$.[4] We see in Fig. 1.4 a depiction of the elliptic sine showing how it changes its shape as the elliptic

[4] An important point needs to be stressed here about notation that can cause confusion in the literature. Typically, the quantity k defined in Eq. (1.13) is called the 'elliptic modulus' and is written after a comma following the argument of the function. In many places, the notation

modulus (as the parameter k is called, changes from 0 to 1). In the 3-dimensional representation in the top panel, the time evolution of the elliptic sine is seen to change from the circular (trigonometric) sine at the front of the Figure where k is small, to the hyperbolic tangent at the back of the Figure where k is larger, i.e., near 1. How this change in shape happens as k is varied is made clear by the 3-d plot. In the lower panel, the intersection of the surface plotted in the upper panel with three planes produces the time dependence of the elliptic sine not only for the extreme values $k = 0$ (dash-dotted line) and $k = 1$ (solid line) but also for an intermediate value $k = 0.99$ (dotted line). This graphical depiction should make clear to the reader the rich content of the elliptic sine which makes it display such different shapes as k is changed. We will see in the next Chapter that such behavior will be closely related to the sharp behavior of the physics underlying the DNLSE.

Equation (1.13) means that, if you take the derivative of t with respect to x and take the reciprocal of the result, you get

$$\frac{dx}{dt} = \sqrt{1-x^2}\sqrt{1-k^2x^2}.$$

If we define the two factors in the preceding expression as additional functions of t, and call them, respectively, the elliptic cosine $\mathrm{cn}(t,k)$ and the elliptic dn-function $\mathrm{dn}(t,k)$, we add several new tools to our repertoire of elliptic functions:

$$\mathrm{sn}^2(t,k) + \mathrm{cn}^2(t,k) = 1, \tag{1.14a}$$

$$k^2\mathrm{sn}^2(t,k) + \mathrm{dn}^2(t,k) = 1, \tag{1.14b}$$

$$\frac{d}{dt}\mathrm{sn}(t,k) = \mathrm{cn}(t,k)\mathrm{dn}(t,k), \tag{1.14c}$$

$$\frac{d}{dt}\mathrm{cn}(t,k) = -\mathrm{sn}(t,k)\mathrm{dn}(t,k), \tag{1.14d}$$

$$\frac{d}{dt}\mathrm{dn}(t,k) = -k^2\mathrm{sn}(t,k)\mathrm{cn}(t,k). \tag{1.14e}$$

Equations (1.14d) and (1.14e) come from differentiating (1.14a) and (1.14b). An application of the last three entries of Eq. (1.14) carried out twice in succession results in closed second-order equations obeyed by each of the elliptic functions involving their first and third powers. For the cn function the result is, as the reader should explicitly demonstrate,

$$\frac{d^2y}{dt^2} = (2k^2-1)y - 2k^2y^3, \tag{1.15}$$

$x = \mathrm{sn}(t\,|m)$ is used the quantity $m = k^2$ being called the 'elliptic parameter'. The separator used is the vertical bar rather than a comma. The specific terminology has been sometimes mixed up or misrepresented in the literature. This can be particularly dangerous in calculations. For instance, in software implementations, m is often used with a comma separator. It is safe to define the elliptic function through an explicit statement such as (1.13). Throughout this book we will use k as the quantity, comma as a separator, and 'elliptic modulus' as the term.

where $y = \mathrm{cn}(t, k)$.

An equivalent manner of introducing sn, cn, and dn is from the integral representation

$$t = \int_0^{\varphi} \frac{d\theta}{\sqrt{1 - k^2 \sin^2 \theta}}, \tag{1.16}$$

the three Jacobian elliptic functions being simultaneously defined as

$$\mathrm{sn}(t, k) = \sin \varphi, \qquad \mathrm{cn}(t, k) = \cos \varphi, \qquad \mathrm{dn}(t, k) = \sqrt{1 - k^2 \sin^2 \varphi}. \tag{1.17}$$

It is straightforward to see that the elliptic sine becomes identical to the hyperbolic tangent at $k = 1$ and to the trigonometric sine at $k = 0$, that the elliptic cosine becomes the hyperbolic secant and the trigonometric cosine at these respective limits, and that the dn-function equals the hyperbolic secant just as the cn-function does at $k = 1$, but is the constant 1 at $k = 0$. If you have not encountered elliptic functions earlier, their visual shapeshifting illustrated in the example of the elliptic sine displayed in Fig. 1.4 should instruct and impress you at the same time.

Of direct use in the description of the DNLSE is the time dependence of the elliptic cosine. We show it in Fig. 1.5 for four values of $k : 0, 0.99, 0.999, 1$. The first case is the trigonometric cosine. As k increases, the period of the function increases until at $k = 1$ it becomes infinite and the function becomes identical to the hyperbolic secant. We will find below that the variation of k corresponds directly to the variation of physical observables of interest and that when k increases beyond the value 1, the elliptic cosine becomes the dn function (not shown in Fig. 1.5) and oscillates only above the value 0.5.

1.5.2 Some Useful Properties of the Jacobian Elliptic Functions

My intent in providing some of the results and rules of Jacobian elliptic functions here is by no means to serve as a substitute for standard instruction in a book on the subject such as (Abramowitz and Stegun, 1965; Bowman, 1953; Byrd and Friedman, 1971). Rather, the purpose here is to make the reader familiar with the functions so that it will become easier to think in terms of them. With that in mind, allow me to display a small sampling of their properties selected from what we will use in our book.

The period $T$of the elliptic sine and cosine is $4K$ while the period of the elliptic dn function is $2K$ where K is the so-called complete elliptic integral of the first kind defined by putting $x = 1$ in the upper limit of integration in Eq. (1.13):

$$K(k) = \int_0^1 \frac{dz}{\sqrt{1 - z^2}\sqrt{1 - k^2 z^2}}. \tag{1.18}$$

This quantity equals $\pi/2$ for $k = 0$ and increases as k increases, becoming infinite at $k = 1$. The period of the dn-function is half of the period of the other two functions:

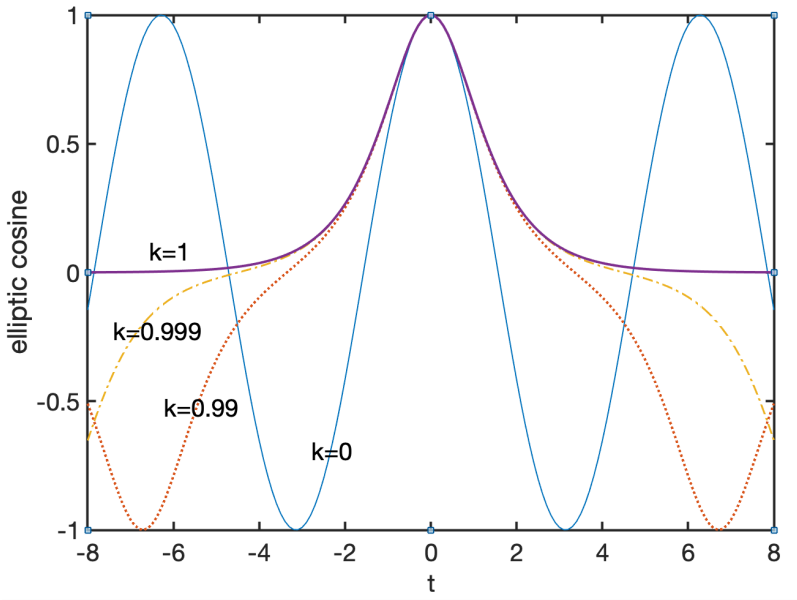

Fig. 1.5 The variation of the shape of the Jacobian elliptic cosine as the elliptic modulus k is varied with the respective (indicated) values 0, 0.99, 0.999 and 1. In the first and the last cases the function is identical to the trigonometric cosine and the hyperbolic secant respectively. When k exceeds 1, the elliptic cosine turns into a dn function (not shown) that oscillates only in the upper half of the plot and this marks a physical transition as will be shown in Chapter 3.

it is $2K(k)$. The dn-function oscillates twice as fast as its two companions. An associated period, useful in the complex plane, is K' defined as (we give here the alternate angle form of the integral),

$$K' = \int_0^{\pi/2} \frac{d\theta}{\sqrt{1-(1-k^2)\sin^2\theta}}. \tag{1.19}$$

We will use K' only to define the 'nome' $q = e^{-\pi K'/K}$ that will appear in an expansion of the functions.

1.5.3 Trigonometric and Hyperbolic Approximations

For small values of k, the following trigonometric approximations apply,

$$\mathrm{sn}(t,k) \approx \sin t - (k^2/4)(t - \sin t \cos t)\cos t, \tag{1.20a}$$

$$\mathrm{cn}(t,k) \approx \cos t + (k^2/4)(t - \sin t \cos t)\sin t, \tag{1.20b}$$

$$\mathrm{dn}(t,k) \approx 1 - (k^2/2)\sin^2 t, \tag{1.20c}$$

while for k nearing 1, the following approximations in terms of hyperbolic functions exist:

$$\mathrm{sn}(t,k) \approx \tanh t + (1/4)(1-k^2)(\sinh t \cosh t - t)\mathrm{sech}^2 t, \tag{1.21a}$$

$$\mathrm{cn}(t,k) \approx \mathrm{sech} t - (1/4)(1-k^2)(\sinh t \cosh t - t)\tanh t\,\mathrm{sech}\, t, \tag{1.21b}$$

$$\mathrm{dn}(t,k) \approx \mathrm{sech} t + (1/4)(1-k^2)(\sinh t \cosh t + t)\tanh t\,\mathrm{sech}\, t. \tag{1.21c}$$

1.5.4 Shifting the Elliptic Modulus

What happens when k exceeds 1? This will turn out to be a particularly relevant question for our investigations. The simplest manner of establishing a result is to flip k to $1/k$ in Eq. (1.16) and work out the consequences. Another way is to define kz in a defining integral of the form (1.13) as a new variable z'. The answer to the question posed in terms of the so-called reciprocal parameter or Jacobi's transformation is that, when the modulus of the elliptic cn function exceeds 1, the function can be written as a dn function with a modulus which is the reciprocal of the original modulus, with a constant multiplying the argument of the function. The constant is the original modulus (of the cn function). Precisely the same happens when the modulus of a dn function exceeds 1. In the case of the sn, the function remains an sn while the modulus undergoes a change to its reciprocal, but not only does the argument change in the same way as for the other two functions but a scaling to reduce the amplitude also occurs. Thus, if $k > 1$,

$$\mathrm{cn}(t,k) = \mathrm{dn}(kt, 1/k), \tag{1.22a}$$

$$\mathrm{dn}(t,k) = \mathrm{cn}(kt, 1/k), \tag{1.22b}$$

$$\mathrm{sn}(t,k) = (1/k)\mathrm{sn}(kt, 1/k), \tag{1.22c}$$

provide explicit expressions while returning k to the standard range.

The above is often referred to as Jacobi's reciprocal parameter transformation: it brings back into the 0, 1 range any k that strays beyond 1. We will also have occasion to use a transformation that allows a shift from one k-value to a specific different (either larger or smaller) value accompanied by a more complicated combination of elliptic functions (Abramowitz and Stegun, 1965). One of them changes k to a higher value (within the 0, 1 range) and the other to a lower value and they are called, respectively, ascending and descending Landen transformations. An example is

$$\mathrm{dn}(t,k) = \frac{\mathrm{dn}^2\left(\frac{t}{(1+\kappa)},\kappa\right) - (1-\kappa)}{(1+\kappa) - \mathrm{dn}^2\left(\frac{t}{(1+\kappa)},\kappa\right)}, \tag{1.23}$$

where $\kappa = \frac{1-\sqrt{1-k^2}}{1+\sqrt{1-k^2}}$. More details will be found in the literature.

1.5.5 Jacobi's Imaginary Transformation

By using the definitions of the elliptic functions, it is similarly straightforward to transform the functions when the argument becomes imaginary (Byrd and Friedman, 1971):

$$\mathrm{cn}(it,k) = \frac{1}{\mathrm{cn}\left(t,\sqrt{1-k^2}\right)} = \mathrm{nc}\left(t,\sqrt{1-k^2}\right), \tag{1.24a}$$

$$\mathrm{dn}(it,k) = \frac{\mathrm{dn}\left(t,\sqrt{1-k^2}\right)}{\mathrm{cn}\left(t,\sqrt{1-k^2}\right)} = \frac{\mathrm{nc}\left(t,\sqrt{1-k^2}\right)}{\mathrm{nd}\left(t,\sqrt{1-k^2}\right)}, \tag{1.24b}$$

$$\mathrm{sn}(it,k) = i\frac{\mathrm{sn}\left(t,\sqrt{1-k^2}\right)}{\mathrm{cn}\left(t,\sqrt{1-k^2}\right)} = i\frac{\mathrm{nc}\left(t,\sqrt{1-k^2}\right)}{\mathrm{ns}\left(t,\sqrt{1-k^2}\right)}. \tag{1.24c}$$

where the functions nc, nd and ns are respectively defined as the reciprocals of cn, dn and sn, respectively. We will have occasion to use these during our study of the effect of initial phase on the evolution of the particle.

1.5.6 Weierestrass and Other Elliptic Functions

Useful generally in physics applications are also theta and zeta elliptic functions that we will not discuss because we do not apply them in this book. We will find much use for the Weierstrass function $\wp$ in Chapter 4 where we employ it to study the nonlinear nondegenerate dimer, and systems more complex than a dimer. There are several connections between the two kinds of elliptic functions (see, e.g., Abramowitz and Stegun (1965)) but we will have the occasion, in Chapter 4, to use one that connects $\wp$ to the reciprocal of the square of the sn-function. Details are explained in Eq. (5.12) and the ensuing discussion.

1.6 Application of Elliptic Functions to a Familiar System

Examples of elliptic functions put to use in physics are in rigid body motion such as spinning tops, the physical pendulum subject to gravity, the theory of relativity, and even population dynamics of bacteria in a Petri dish. In order to gain familiarity with elliptic functions, let us briefly examine them in a simple physical system, a standard textbook case of a planar pendulum that is not restricted to *small* oscillations, and let us solve it in two different ways to gain expertise in elliptic connections. We will also make passing allusion to the analysis of bacteria in a Petri dish.

A physical pendulum of mass m inclined at an angle θ to the vertical at time t obviously obeys Newton's equation of motion

$$m\ell \frac{d^2\theta(t)}{dt^2} = -mg \sin\theta(t). \tag{1.25}$$

Here g is the acceleration due to gravity and ℓ is the length of the pendulum. By defining

$$\Omega = \sqrt{g/\ell}$$

we can rescale time to the dimensionless form $\tau = \Omega t$, and simplify Eq. (1.25) to

$$\frac{d^2\theta}{d\tau^2} + \sin\theta = 0. \tag{1.26}$$

Let us now solve Eq. (1.26) in two different ways to familiarize ourselves with the use as well as behavior of elliptic functions.

1.6.1 The Displacement of the Physical Pendulum

First, let us simply use the standard 'energy method' familiar to us from elementary classical mechanics (that was mentioned in Eq. (1.10) to derive a potential) whereby we multiply the equation by $d\theta/d\tau$ to get a first-order derivative equation,

$$\frac{d}{d\tau}\left[\frac{1}{2}\left(\frac{d\theta}{d\tau}\right)^2 - \cos\theta\right] = 0, \tag{1.27}$$

and, consequently,

$$\frac{1}{2}\left(\frac{d\theta}{d\tau}\right)^2 - \cos\theta = \frac{1}{2}\left(\frac{d\theta}{d\tau}\right)_0^2 - \cos\theta_0. \tag{1.28}$$

Here the angular displacement θ_0 and the angular velocity $(d\theta/d\tau)_0$ correspond to any point 0 on the trajectory. Taking that point as the one at which the displacement is maximum, θ_m, and the velocity is zero, i.e., the point at which the pendulum

reverses the direction of its oscillation, we find

$$\frac{d\theta}{d\tau} = \sqrt{2\,(\cos\theta - \cos\theta_m)}. \tag{1.29}$$

This can be rewritten as

$$\frac{\tau}{k_1} = \int_0^{\theta/2} \frac{d\theta'}{\sqrt{1 - k_1^2 \sin^2\theta'}}, \tag{1.30}$$

under the convention that $\theta = 0$ at $\tau = 0$, and k_1 is the cosecant of half the maximum angle. Identification with the definition (1.16) then gives us the solution

$$\sin\left(\frac{\theta}{2}\right) = \mathrm{sn}\left(\frac{t}{k_1}\sqrt{\frac{g}{\ell}}, k_1\right), \quad k_1 = 1/\sin(\theta_m/2). \tag{1.31}$$

Because k_1 that we have chosen as the elliptic modulus can exceed 1 (being the reciprocal of a sine), we might use the reciprocal transformation, choose $k = 1/k_1$ as the new modulus and write, using (1.22c),

$$\sin\left(\frac{\theta}{2}\right) = k\,\mathrm{sn}\left(t\sqrt{\frac{g}{\ell}}, k\right), \quad k = \sin(\theta_m/2). \tag{1.32}$$

For small angles (short times or small amplitude of oscillations), $\sin(\theta/2) \approx \theta/2$ as well as $\mathrm{sn}(t\sqrt{g/\ell}, k_1) \approx \sin(t\sqrt{g/\ell})$, not to mention that $k \approx \theta_m/2$, which gives us back the simple harmonic approximation as a small-oscillation limit

$$\theta \approx \theta_m \sin(t\sqrt{g/\ell}),$$

appropriate to the stated initial condition. The solution retains, nevertheless, the complexities of the large-oscillation features in the opposite limit.

Although all this development is straightforward, we must remain alert to subtleties. We know that Eq. (1.31) expresses a trigonometric sine as equal to an elliptic sine; both are known to be limited to ±1 and so there is no problem. But Eq. (1.32) equates a trigonometric sine as the product of k and an elliptic sine. Could this create a problem if the k and consequently its product with the elliptic sine were to exceed 1? You might argue that k itself is restricted to being not greater than 1 because it equals a sine ($k = sin(\theta_m/2)$). However, this presupposes the existence of a maximum angular displacement θ_m from which the mass retraces its motion. What if there is no such maximum and the motion of the pendulum is such that θ always increases as would happen for sufficient energy when the pendulum never reverses direction and the motion consists of rotations rather than librations?

The alert reader will realize that Eq. (1.31) is built for this eventuality, the elliptic modulus k_1 being generally larger than 1 in its context. Indeed, although Eqs. (1.31) and (1.32) are formally equivalent to each other through the prescription $k = 1/k_1$,

they are respectively appropriate to the description of rotatory and librational motion of the pendulum, the demarcation situation being $k = 1$ or $\theta_m = \pi$.

Perhaps these matters become clearer if we regard Eq. (1.26) to describe, rather than a pendulum under the action of gravity, an atom moving in a 1-dimensional sinusoidal potential as it might in a material. The variable θ is then a true distance rather than an angle. Depending on its initial energy, the atom might either remain oscillating in its starting well (elliptic modulus confined to the 0 to 1 range) remaining thereby restricted to vibrations around the starting position, or escape that starting well (elliptic modulus with magnitude larger than 1) and keep moving away from the starting position, never reversing its direction.

1.6.2 The Angular Velocity of the Pendulum

It is instructive to inspect the velocity $\omega(\tau) = d\theta(\tau)/d\tau$ (angular if it is a pendulum we study but standard linear if it is the atom in the sinusoidal well we investigate) by differentiating Eqs. (1.31) and (1.32). Such an operation results in both cases in the velocity emerging as a dn function,

$$\omega(\tau) = \frac{d\theta}{d\tau} = \frac{2}{k_1}\mathrm{dn}\left(\frac{\tau}{k_1}, k_1\right) = 2k\,\mathrm{dn}(\tau, k), \tag{1.33}$$

which, as we know, can be expressed equivalently as a cn function with inverted modulus. It should be clear to the reader that, although these expressions are equivalent, the dn (cn) functions with modulus restricted to the 0 to 1 range are more appropriate to rotational (librational) motion of the pendulum or the translational, well-to-well (oscillatory, intra-well) motion of the atom.

Let us attempt something unusual at this point: return to Eq. (1.26) and rather than attempt to integrate it, *differentiate* it one more time with respect to τ:

$$\frac{d^3\theta}{d\tau^3} + \cos\theta\frac{d\theta}{d\tau} = 0. \tag{1.34}$$

The reason to step further into differentiation of Eq. (1.26) is not to make life more difficult by increasing the order of the equation to solve but to notice that it is identical to a *second order* differential equation for the angular velocity $\omega(\tau) = d\theta/d\tau$. For $\cos\theta$ appearing in Eq. (1.34), we substitute the expression obtained from Eq. (1.28). The result is an evolution with a cubic nonlinearity in ω:

$$\frac{d^2\omega}{d\tau^2} = E\omega - \frac{\omega^3}{2}, \tag{1.35}$$

The constant E is equal to the right hand side of Eq. (1.28) and can be evaluated from the initial conditions. Comparison of Eq. (1.35) with a result we have already seen, that the cn function obeys Eq. (1.15b), allows us, after a straightforward scaling, to express the angular velocity of the pendulum as being proportional to the cn:

$$\omega(t) = \omega(0)\mathrm{cn}(\tau, k). \tag{1.36}$$

The reader is strongly encouraged to undertake the exercise of completing the process of filling in the intermediate steps in going from Eq. (1.35) to Eq. (1.36).

What we have achieved through this unusual procedure of differentiating the second order equation for θ is to convert its trigonometric nonlinearity to a cubic one in an equivalent equation for $\omega(\tau)$ so that we could find the solution directly in terms of the elliptic functions. The solution, thus obtained, describes the velocity rather than the displacement of the pendulum. Furthermore, the reader is invited to notice the isomorphism of the ω-equation in the pendulum case to the p-equation for the quantum nonlinear dimer.[5]

1.7 Application to Bacterial Populations in a Petri dish

Finally, let us examine a relatively rare application of elliptic functions, this time to an ecological problem concerning the evolution of a bacterial population.

The population of bacteria in a Petri dish increases in the well-known Malthusian manner but is limited by competition for nutrition. Denoting the bacterial density at a location x in a 1-dimensional representation at time t by $u(x,t)$, the evolution is often modeled (Lin et al., 2004; Kenkre and Kuperman, 2003) as obeying (see also the recent review in Kenkre and Giuggioli (2020)),

$$\frac{\partial u(x,t)}{\partial t} = Au(x,t) - Bu^2(x,t) + D\frac{\partial^2 u(x,t)}{\partial x^2}, \tag{1.37}$$

where A and B are constants and D is the diffusion constant that controls the random walk that the bacteria perform. The three terms on the right hand side of Eq. (1.37) respectively describe increase in the population controlled by nutrition, depletion from competition and random walk motion. A simple experiment designed to test the equation or to measure its parameters consists of placing a mask in the Petri dish while simultaneously shining lethal radiation that destroys the bacteria outside the mask. Such an experimental setup was analyzed (Kenkre and Kuperman, 2003) and the theoretical predictions verified (Perry, 2005). Extensions relevant to the use of multiple masks may be found in (Kenkre and Kumar, 2008; Kumar and Kenkre, 2011). What is involved is the solution of the steady state version of the Fisher equation which is the ordinary differential equation

$$\frac{d^2u(\xi)}{d\xi^2} + Au(\xi) - Bu^2(\xi) = 0 \tag{1.38}$$

in the scaled variable $\xi = x/\sqrt{D}$.

[5] With the restriction that p has to lie in the interval ± 1.

The setup is that the mask proceeds from $\xi = -w$ to $\xi = +w$ and thus has width $2w$. The parameters are constant except that A outside the mask is supposed to be negative and infinite in magnitude with the result that at the mask edges and outside, the density vanishes. One way to solve (1.38) is to notice that it is very similar, but not identical, to the equation obeyed by $y = \mathrm{sn}^2(\xi, k)$:

$$\frac{d^2y}{d\xi^2} + 4(1 + k^2)y - 6k^2y^2 = 2 \tag{1.39}$$

the difference being, for instance, an extra constant in the evolution. To bring the two equations into alignment with each other, one considers a phase and amplitude change and consider as a solution,

$$u(\xi) = \alpha \mathrm{sn}^2(\beta\xi + \delta, k) + \gamma. \tag{1.40}$$

A bit of somewhat tedious algebra leads to explicit expressions relating α, β and γ to the elliptic modulus k and to the constants A and B then produces a convenient solution in terms of $\mathrm{cd}^2(\xi, k)$ where $\mathrm{cd}(\xi, k)$ is the ratio of the cn function to the dn function,

$$\mathrm{cd}^2\left(\frac{w}{2}\sqrt{\frac{A}{D}}\left(1 - k^2 + k^4\right)^{-1/4}, k\right) = \frac{1}{1 + k^2 + \left(1 - k^2 + k^4\right)^{-1/2}}. \tag{1.41}$$

This solution[6] is then used to deduce a fitting function that is compared to the spatial dependence of the observed density of the bacteria. The elliptic modulus k, the diffusion constant D, and the growth rate A (B drops out of the evaluation under the conditions of experiment) are obtained from fitting the expression to the observed spatial variation of the population. The mask width is found then to be related to the system parameters through

$$w = 2\sqrt{\frac{D}{A}}\left(1 - k^2 + k^4\right)^{1/4} \mathrm{cd}^{-1}\left(\sqrt{\frac{1}{1 + k^2 + \left(1 - k^2 + k^4\right)^{-1/2}}}\right). \tag{1.42}$$

A confirmation of the theory is recovered by observing that an abrupt transition occurs as one lowers the width of the mask and reaches, when $k = 0$, at a critical value w_c of the width satisfying the simple relation

$$2w_c = \pi\sqrt{D/A}.$$

---

[6] Some typographical errors were left inadvertently in earlier publications, specifically in Kenkre and Kuperman (2003) and Kenkre and Giuggioli (2020). It is always difficult to provide errata to already published material. I take this opportunity to correct the typos here. It could help the rare reader who might have come across those typos and, maintaining some sort of reading continuity, might have arrived at this book. Equations (1.41) and (1.42) given above should respectively replace Eqs. (5.33) and (5.35) in Kenkre and Giuggioli (2020) and Eqs. (10) and (12) in Kenkre and Kuperman (2003). I am indebted to Marcelo Kuperman for assistance in setting this right.

Based on their calculations from bacterial data on E. coli, Kenkre and Kuperman (2003) calculated the crucial mask width to be of the order of $0.5\,cm$, a prediction that was verified satisfactorily a few years later (Perry, 2005) as stated above.

Our purpose in this description has been to show the reader another example of an application of elliptic functions particularly when the equations obeyed are not precisely the same as the ones that we need to analyze.

1.8 Chapter 1 in Summary

The discrete nonlinear Schrödinger equation appears naturally in the polaron problem where strong interaction of a quantum particle such as an electron moving among the sites of a crystal with phonons could lead to a suppression of the site energy of the particle. Self-trapping is expected but difficult or impossible to study analytically from the equation on an extended system. A simple numerical investigation was shown to lead to what looks like such self-trapping. In order to have a precise analysis, attention was then restricted to a system of small spatial extent, a dimer. Density matrix equations were derived and a closed nonlinear equation for the probability difference in the dimer obtained. Arguments based on a study of the potential associated with the equation, in the manner of a well-known procedure in classical mechanics, were shown to lead to a transition. In order to prepare for an explicit solution of the probability difference in terms of analytical functions, background was provided on Jacobian elliptic functions and it was shown how they may be applied to two physical problems, a pendulum not restricted to small amplitudes of oscillation, and bacterial populations in a Petri dish. These considerations were presented as a prelude to the solution to be presented in the succeeding Chapter.

Chapter 2
Dimer Solutions, Mobility Reduction, and Neutron Scattering

The simple numerical study of the discrete nonlinear Schrödinger equation (DNLSE) for a particle moving on the sites of a linear chain suggests as we saw in Chapter 1 (see Fig. 1.1) that a self-trapping transition is probably in the air and that it occurs at a finite value of the ratio χ/V of the nonlinearity parameter to the nearest-neighbor intersite transfer matrix element. On restricting the study to a small system of two sites 1 and 2, the transition seems graphically to occur (see Fig. 1.2) when the above mentioned ratio takes the value 4 if the particle is initially completely localized on one of the two sites. The last sections of Chapter 1 armed us with elliptic functions, thereby providing us with a tool to obtain an analytic solution for the probability difference $p(t)$. We will now see how the solution arises in the dimer and exhibits curious behavior with physical significance and describes the self-trapping transition in the DNLSE in a very natural manner (Kenkre and Campbell, 1986).

Throughout this present Chapter we will assume that the quantum particle is initially localized on one of the two sites, leaving partially distributed initial conditions for the next Chapter. Here we will address interesting consequences of the solution in reduction of mobility and effects on neutron scattering.

2.1 Self-trapping as the cn-dn Transition

Standard recasting of the integral representation of the solution of Eq. (1.9) that describes the time evolution of the probability difference for initial localization is quite straightforward. It is, however, even quicker to identify Eq. (1.9) with the second-order equation obeyed by the elliptic function cn, Eq. (1.15). This is done as follows.

Divide (1.9) by $4V^2$, define $\tau = 2Vt$ and rewrite the derivatives with respect to this dimensionless time. The identification of the two quantities relevant to Eq. (1.9),

$$\frac{A}{4V^2} = \frac{\chi^2}{8V^2} - 1, \quad \frac{B}{4V^2} = \frac{\chi^2}{8V^2},$$

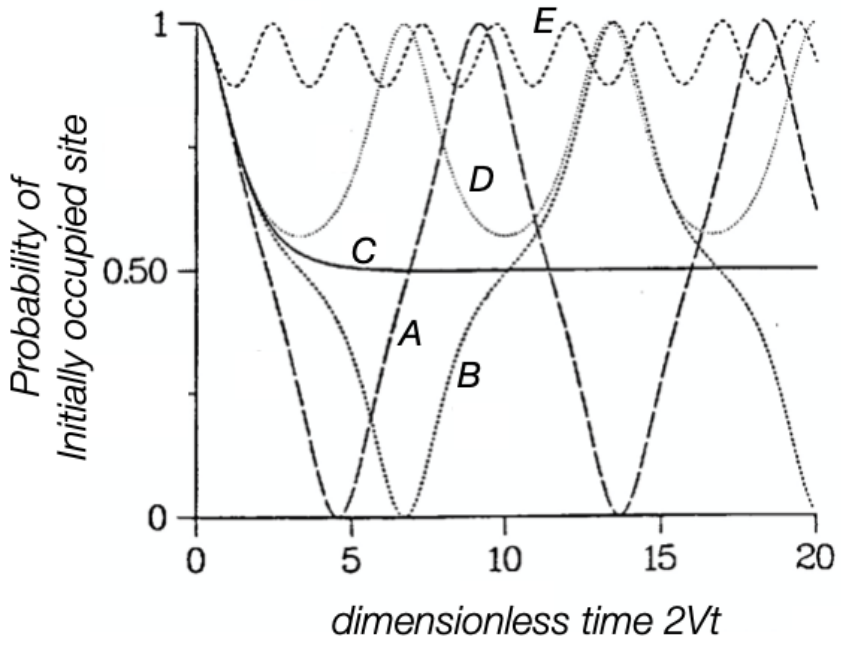

Fig. 2.1 The time evolution of the probability of the initially occupied site in the degenerate nonlinear dimer showing the self-trapping transition. The different curves correspond to different values of the nonlinearity ratio $\chi/4V$. For values near 0, the probability is sinusoidal (not shown in the Figure) but changes shape as the ratio increases from (A) 0.95 to (B) 0.9995, with a clear increase in the period of the oscillation. Curve (C) has the nonlinearity ratio equal 1 and marks the self-trapping transition: the probability is proportional to the hyperbolic secant and the period of oscillation is infinite. As $\chi/4V$ increases further, with values (D) 1.0001 and (E) 1.75 as shown, the probability oscillates only in the upper half, its average value increasing further from 0.5 and towards 1, signifying less and less mobility of the quasiparticle.

with $2k^2 - 1$ and $2k^2$ of Eq. (1.15) respectively, leads directly to the conclusion that, for initial placement ($t = 0$) on site 1, the probability difference $p(t) = P_1(t) - P_2(t)$ of the site occupation probabilities is given by the elliptic cosine with argument $2Vt$ and elliptic modulus $\chi/4V$,

$$p(t) = \mathrm{cn}\left(2Vt, \frac{\chi}{4V}\right) \text{ for } \chi \leq 4V. \tag{2.1}$$

Equation (2.1) predicts (Kenkre and Campbell, 1986) that in the absence of the nonlinearity, the particle oscillates back and forth between the sites sinusoidally, $p(t)$ being simply a cosine of the argument $2Vt$ in this case of vanishing nonlinearity. However, the shape of the time evolution changes as the nonlinearity increases and the oscillation period increases. The change of shape is pronounced as the elliptic

modulus $\chi/4V$ nears 1, following the sequence of cases shown in Fig. 1.5. At the point that χ equals $4V$, the critical value, $p(t)$ assumes the shape of the hyperbolic secant, the period becoming infinite.

What happens as the nonlinearity exceeds $4V$? For this, we appeal to the transformation (1.22b) which tells us that the cn function becomes a dn function, i.e.,

$$p(t) = \mathrm{dn}\left(\frac{\chi t}{2}, \frac{4V}{\chi}\right) \text{ for } \chi \geq 4V. \tag{2.2}$$

Notice that the transformation has brought the elliptic modulus back into the 0 to 1 range as the nonlinearity parameter χ has stepped beyond $4V$. Equation (2.2) predicts that, if the nonlinearity is larger than its critical value, $p(t)$ oscillates, taking only positive values. This signifies that the particle tends to stay near the initial site of occupation: we are now in a situation of hampered mobility. Within the limitations of a representation of a real extended system by a system (dimer) of such limited size, we can say that, for the initial condition considered, the particle motion is free if $4V$ exceeds χ (given that it attains equally large values on both sites) whereas it is self-trapped if χ exceeds $4V$ (given that it clearly occupies the initial site for longer intervals). As a function of the nonlinearity, the detailed behavior is as follows.

For vanishing nonlinearity, the particle oscillates between the two sites with period π/V. As χ increases, the oscillations depart from trigonometric behavior. The period of oscillations T is always given by the complete elliptic integral of the first kind $K(k)$ with elliptic modulus $k = \chi/4V$,

$$T = \frac{2K(k)}{V} = \frac{2}{V}\int_0^1 \frac{dz}{\sqrt{1-z^2}\sqrt{1-k^2z^2}}. \tag{2.3}$$

As χ approaches very close to $4V$, the oscillations show a marked departure from those of a trigonometric nature. The period becomes huge as the particle oscillates sluggishly between the sites. The logarithmic approximation is appropriate and we can express the period as

$$T \approx \frac{1}{V}\ln\left(\frac{16}{1-(\chi/4V)^2}\right). \tag{2.4}$$

At the transition, $p(t) = \mathrm{sech}(2Vt) = \mathrm{sech}(\chi t/2)$ showing an infinite period and this clearly refers to moving in the right well in Fig. 1.2 constrained by the dashed-dotted line and taking an infinite time to cross to the left well, unable to perform a proper oscillation. Far away from the transition, on the self-trapped side, as $\chi/4V$ approaches infinity, the oscillations are well approximated by the trigonometric expression for the dn-function

$$p(t) \approx 1 - (8V^2/\chi^2)\sin^2(\chi t/2). \tag{2.5}$$

This is precisely the evolution of the probability of a *linear* dimer with a true energy mismatch $\Delta = \chi$ if it is much larger than $2V$ (see Eq. (2.9) below). This similarity prompts the discussion in the next Section.

2.1.1 Kinship to Two Linear Systems

The nonlinear degenerate dimer, i.e., one with equal site energies, that we are treating in this chapter bears kinship to two different *linear* counterparts, the linear nondegenerate dimer and the linear damped dimer. For the former, the site energies differ by $\Delta = E_1 - E_2$. For the latter, interactions with the environment tend to equalize the occupation of the site probabilities by damping p at rate α. For instance, note that the latter system obeys

$$\frac{d^2p(t)}{dt^2} + \alpha\frac{dp(t)}{dt} + 4V^2p(t) = 0, \tag{2.6}$$

and has the solution

$$p(t) = e^{-\alpha t/2}\cos\left(2Vt\sqrt{1-(\alpha/2V)^2}\right), \tag{2.7}$$

if we use the condition that $p(0) = 1$ and $dp(t)/dt$ vanishes initially. We have seen that, in the nonlinear dimer, there is a critical value of the nonlinearity χ, viz. $4V$, at which the behavior changes abruptly. In the linear damped dimer, there is also a critical value of its parameter, the damping rate α, (viz. $2V$), at which the behavior of the evolution changes abruptly from being underdamped to turning overdamped. The demarcation is known widely in elementary contexts as 'critical damping'. Oscillations of $p(t)$ disappear at this point and, for higher values of the damping rate, the time evolution changes from sinusoidal variation to exponential decay.

Particularly important is that the period of oscillation increases from the value π/V it had for zero damping and becomes infinite at the transition. Beyond the transition, the behavior of the time evolution is different in the case of the linear damped dimer as compared to the case of the nonlinear dimer in that the former shows a decay while the latter does not. Nevertheless, as we will see below in our examination of neutron scattering, the phenomenon of motional narrowing that is typical of the linear damped dimer also occurs for the nonlinear (undamped) dimer.

Let us now compare the nonlinear dimer evolution to the other simple system, the linear *nondegenerate* dimer. The time evolution equation it obeys is

$$\frac{d^2p(t)}{dt^2} + (4V^2 + \Delta^2)p(t) = \Delta^2, \tag{2.8}$$

and has the solution

$$p(t) = 1 - \left[\frac{2}{1+(\Delta/2V)^2}\right]\sin^2\left[Vt\sqrt{1+(\Delta/2V)^2}\right], \tag{2.9}$$

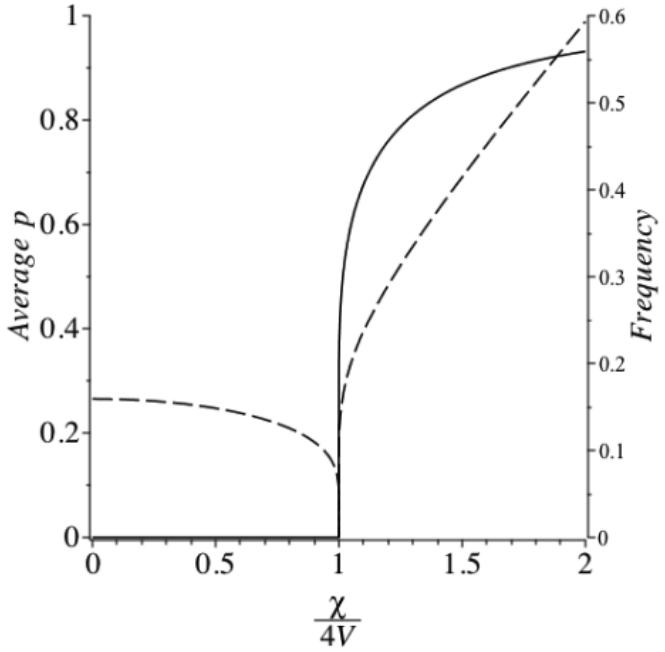

Fig. 2.2 The self-trapping transition illustrated by plots against the nonlinearity ratio $\chi/4V$ of two properties of the probability difference: its average over a cycle of its time dependence (solid line, left axis) and of its frequency of oscillation (dashed line, right axis). The average p remains zero for all values of the nonlinearity less than the critical value 1 as the quantum particle oscillates equally on both sites. It then undergoes the self-trapping transition as the nonlinearity increases further. With further increase in χ, the average p (solid line) tends to 1, indicating total self trapping. The oscillation frequency (dashed line) starts at a value proportional to the bandwidth, drops logarithmically at the transition and, for nonlinearities beyond the critical value, increases without bound. See Eq. (2.3).

for the same initial condition considered above. See, e.g., (Tiwari and Kenkre, 2014). While this solution exhibits no transition at a specific value of Δ relative to V, it does display the property of non-resonance: the average value around which $p(t)$ oscillates increases with an increase in Δ similarly to the way it does in the nonlinear dimer with an increase in χ *beyond* the transition. If $\Delta >> 2V$, it agrees with Eq. (2.5) as commented, with the correspondence $\Delta \rightarrow \chi$.

Qualitatively speaking, for nonlinearities less than the critical value $4V$, the nonlinear degenerate dimer is similar to the damped linear dimer in that the period increases and becomes infinitely long at the critical point, and as we shall see in the

sequel, exhibits motional narrowing.[1] Beyond the transition, the similarity is to the nondegenerate (undamped) dimer in the behavior of the average value of p.

The takeaway from these brief comments is that, for the analysis of the nonlinear dimer, it is instructive to focus on two quantities having to do with the probability difference: $\langle p \rangle$, its average over a cycle, and its period of oscillation, equivalently its reciprocal, the frequency. A plot of these two quantities is provided in Fig. 2.2. The nonlinearity ratio $\chi/4V$ is plotted on the x-axis. On the y-axis, $\langle p \rangle$ is shown on the left and the frequency, equivalently the reciprocal of the period, is plotted on the right. The first quantity remains zero for all points on the left of the transition and then rises on its right whereas the second decreases to zero precipitously at the transition and then rises beyond the transition.

We will have occasion to use these two quantities, $\langle p \rangle$ and the frequency of oscillations, for a detailed analysis of the nonlinear nonresonant dimer in Chapters 4 and 5.

2.1.2 Reduction of Mobility from the DNLSE

How would the transition behavior we have discovered in the simple system of the degenerate nonlinear dimer reflect itself in an observed experiment? The simplest consequence to imagine would be in the sudden reduction of the mobility of a quantum particle moving in a system as the nonlinearity parameter is increased from below the transition value to one higher than the critical amount. As the theory of linear response (Kubo, 1957) explains, the mobility of a particle moving on the sites of a crystal can be looked upon as an infinite time integral of the velocity autocorrelation function which involves in it the square of the matrix element for intersite transfer. An examination of the detail of various formalisms constructed for the calculation of transport coefficients (Chester and Thellung, 1959; Kenkre and Dresden, 1971) should not be necessary here. We need focus only on the square of the matrix element of the velocity (or the site-to-site transfer interaction) that is proportional to the mobility in any such way of calculating the mobility or conductivity. We see by equating the frequency of oscillation of the probability difference in the presence of the nonlinearity to a quantity proportional to the effective matrix element (bandwidth) V_{eff}, that the latter can be regarded as V divided by a complete elliptic integral of the first kind that blows up at the transition, causing V_{eff} to vanish. Thus, Fig. 2.3 shows the bandwidth, consequently the mobility, undergoing a sharp logarithmic reduction at the transition. It should be noted that the effective transfer matrix element is also the first part of the dashed curve in Fig. 2.2.

A similar simple way of understanding the mobility reduction is to calculate directly the transfer rate of the quantum particle to move from site to site. In a linear chain of sites separated by the distance (lattice constant) a, the evolution being

[1] The dimer subjected simultaneously to damping and nonlinearity has been analyzed in (Tsironis et al., 1988) but has less relevance to the present discussion.

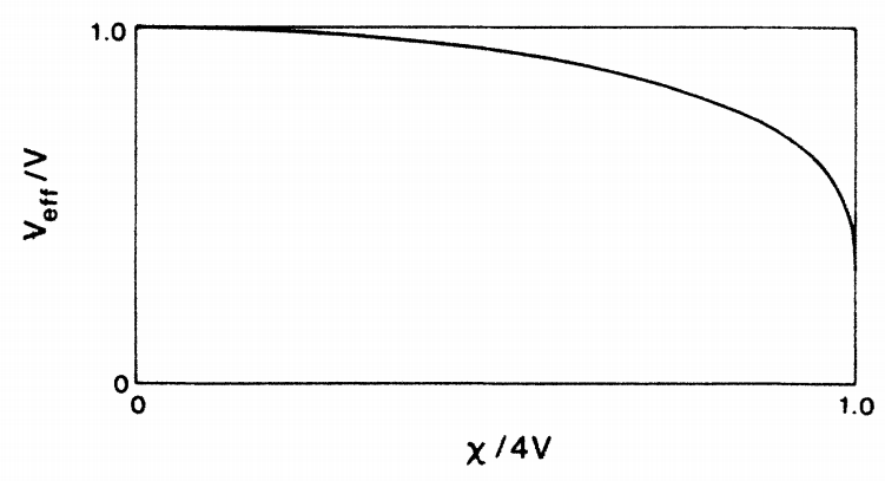

Fig. 2.3 Mobility Reduction as a result of self-trapping from the DNLSE. Being proportional to the time integral of a velocity autocorrelation function, the mobility is proportional to the square of the effective intersite matrix element V_{eff}. The ratio of the latter to V is plotted here as being proportional to $[(2/\pi)K(\chi/4V)]^{-1} \approx \left[\pi/\ln\left(16/1-(\chi/4V)^2\right)\right]$, the logarithmic approximation being pretty accurate near the transition. The abscissa is the nonlinearity ratio $\chi/4V$. Reprinted with permission from fig. 2 of Ref. (Kenkre and Campbell, 1986); copyright (1986) by American Physical Society.

governed by the DNLSE (1.2), it is possible to derive a generalized master equation of the form

$$\frac{dP_m(t)}{dt} = \int_0^t ds \sum_n \left[\mathcal{W}_{mn}(t,s)P_n(s) - \mathcal{W}_{nm}(t,s)P_m(s)\right], \tag{2.10}$$

via a weak-coupling approximation (Wu and Kenkre, 1989). Here the $P_m(t)$ are the probabilities of occupation of sites m and the memories $\mathcal{W}_{mn}(t,s)$ are found to be approximately given by nonlinear expressions

$$\mathcal{W}_{mn}(t,s) = 2V^2(\delta_{m,n+1} + \delta_{m,n-1}) \cos\left(\chi \int_s^t dz\ [P_m(z) - P_n(z)]\right). \tag{2.11}$$

Some of the details of the procedure will be indicated in Chapter 11. The definition of the intersite transfer rate as the reciprocal of the time taken for the mean square displacement to rise from the value 0 to a^2 as the particle moves from a site to its nearest-neighbor may then be used with the approximate equation (2.11) in the generalized master equation as well as with the exact DNLSE (1.2). One is then led to Fig. 2.4 in which one sees in (A) that the exact and the approximate equation of evolution both predict, very similarly, the abrupt decrease in the rate (therefore the

mobility) in the region of self-trapping as the nonlinearity ratio $\chi/4V$ crosses the neighborhood of the critical value (Wu and Kenkre, 1989).

Manifestations of nonlinearity effects on mobility reduction as predicted by the DNLSE can be seen in a variety of other contexts including in the application carried out by Wu and Kenkre to muon spin relaxation as shown in (B) of Fig. 2.4. They followed ideas developed by Kehr and Kitahara (1987, 1988) who studied spin depolarization of quantum particles moving in lattices using the stochastic Liouville equation which combines quantum features with random scattering, and focusing attention on two-state features of the system. In a system such as a ferromagnetic crystal with magnetically inequivalent sites, e.g. BCC iron, a spin-polarized muon undergoes spin relaxation as a combined result of its motion and of the different Larmor frequencies at the different sites. An idealization of this system is a linear chain with alternating Larmor frequencies ω and $-\omega$. In such a simplified system, the muon may be looked upon as a quantum particle whose state evolves under the combined action of transport via nearest-neighbor matrix elements V from site to site, spin rotation with the Larmor frequencies, and strong interactions with the vibrations of the lattice. Wu and Kenkre calculated the oscillations and decay of the x-component of the muon spin, specifically of $S_x(t) = \sum_m (1/2)[\rho^{+-}_{mm}(t) + \rho^{-+}_{mm}(t)$. Behavior such as emerges from the analysis of Kehr and collaborators was seen. However, because we employed the DNLSE, we could also predict an abrupt

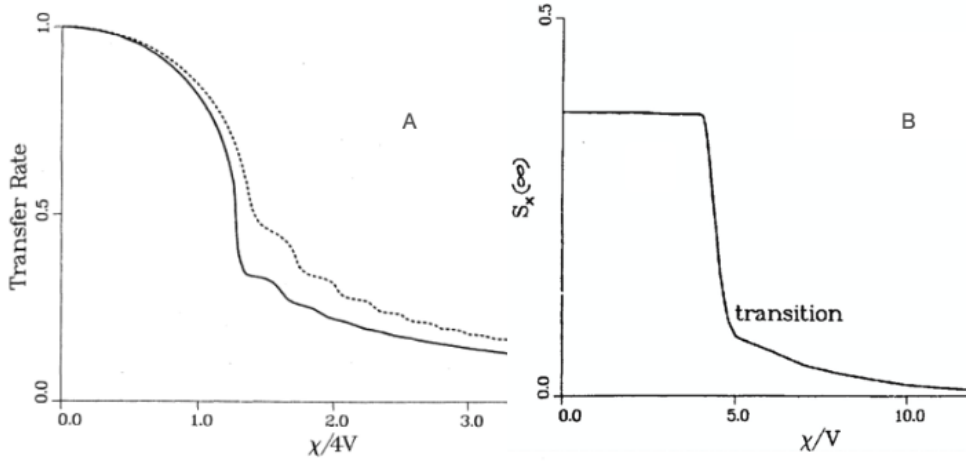

Fig. 2.4 The self-trapping transition reflected in consequences of the DNLSE for muon spin relaxation. The transfer rate defined as the reciprocal of the time taken for the particle to move the distance of a lattice site is displayed in (A) as calculated from Eq. (2.11), exactly as well as via a weak-coupling transition, and the steady state (infinite-time) $x-$ component of the muon spin is displayed in (B). Both are plotted against the nonlinearity and both show an abrupt decrease arising from mobility reduction at the transition.

transition. It is graphically depicted in (B) in fig. 2.4 and the reader is referred to a complete description in (Kenkre, 1989, 1994a).

2.2 Neutron Scattering Lineshapes

The clearest and perhaps the most interesting consequences of self-trapping are, however, seen in the traditionally used probe of neutron scattering. Let us investigate it extensively in the following.

2.2.1 Introduction to the Experiment and Basic Formalism

The motion of a particle in a lattice, such as a hydrogen atom or a muon in a metal, is often studied experimentally by scattering a beam of probe particles that interact weakly with the particle, a neutron being an excellent candidate for the probe particle. See, e.g., Sköld (1978). The general theory is due to Van Hove (1954). The key quantity that needs to be calculated to address experiment is the so-called scattering function which is the Fourier transform $S(k,\omega) = (1/2\pi)\int_{-\infty}^{\infty} dt\, e^{-i\omega t} I(k,t)$ of the correlation function

$$I(k,t) = Tr\, \rho e^{-ikx} e^{-ikx(t)}. \tag{2.12}$$

Here, ρ is the equilibrium density matrix of the moving particles taken to be noninteracting, k is the momentum transfer, and x is the position operator.

If the target system is initially in thermal equilibrium, as we will assume to be the case, the appropriate form of ρ is canonical. In narrow-band materials, wherein k_B times the temperature is large enough (with respect to the particle bandwidth) that the infinite temperature approximation is applicable to a reasonable extent, the correlation function $I(k,t)$ becomes simply the spatial Fourier transform of a conditional probability, i.e., $\sum_m e^{ikam} P(m,t)$, where a is the lattice constant in a 1-dimensional representation. Details of how to calculate the neutron line shape from various equations of motion underlying the particle motion have been given by (Brown and Kenkre, 1983, 1987; Kenkre and Brown, 1985) and reviewed in Chapter 4 of Kenkre (2021).

2.2.2 Calculation of the Lineshape

The application of the formalism to the calculation of the neutron scattering function for a particle moving between the two sites of a nonlinear dimer becomes simplified because of the assumption of the temperature being high enough as explained above and by the fact that the only two values of ka need be considered, 0 and π. This at once makes the correlation function $I(k,t)$ equal to the probability difference $p(t)$,

and we call the relevant line shape simply $S(\omega)$. Fourier transforms of the elliptic function cn are not difficult to calculate (Abramowitz and Stegun, 1965) and lead to

$$S(\omega) = [\pi/2kK(k)] \sum_{n=0}^{\infty} \text{sech}(\omega R_<)[\delta(\omega - \omega_n) + \delta(\omega + \omega_n)], \tag{2.13a}$$

$$S(\omega) = (1/4V)\text{sech}(\omega\pi/4V) = (1/\chi)\text{sech}(\omega\pi/\chi), \tag{2.13b}$$

$$S(\omega) = [\pi/2kK(1/k)] \left(\delta(\omega) + \sum_{n=1}^{\infty} \text{sech}(\omega R_>[\delta(\omega - \tilde{\omega}_n) + \delta(\omega + \tilde{\omega}_n)] \right). \tag{2.13c}$$

The three cases (a) $\chi < 4V$, (b) $\chi = 4V$ and (c) $\chi > 4V$ are indicated individually here for obvious reasons of clarity. The handling is best done in terms of the nome $q = \exp[-\pi K(k')/K(k)]$ where K is the complete elliptic integral of the first kind and $k' = \sqrt{1-k^2}$. Here, $R_<(k) = K(\sqrt{1-k^2})/2V$ and $R_>(k) = (1/k)R_<(1/k)$. The peak locations are at $\omega_n = 2(2n+1)V_{eff} = 2V(2n+1)\left[(2/\pi)K(\chi/4V)\right]^{-1}$ and $\tilde{\omega}_n = (n\pi\chi)/2K(4V/\chi)$. These explicit expressions were provided along with a graphical display by Kenkre and Tsironis (1987) . Let us reproduce them here and examine what they convey about the nonlinear dimer.

2.2.3 Transition Behavior and Motional Narrowing

The nuances of the behavior of $p(t)$ are naturally reflected in the scattering function. In the free region ($\chi < 4V$), symmetrically placed lines appear on the ω-axis but there is no peak at $\omega = 0$. In the self-trapped region ($\chi > 4V$), an additional peak emerges at $\omega = 0$, to signify the fact that the average of $p(t)$ does not vanish for this case, in keeping with the energy mismatch that is a consequence in this region of the nonlinearity in the evolution.

In the absence of the nonlinearity, the elliptic modulus k starts out at zero in Eqs. (2.13). In this limit, $K(k)$ tends to $\pi/2$ while $K(k')$ tends to infinity. The identity

$$\lim_{k\to 0} \frac{e^{-\pi K(k')}}{2kK(k)} = \frac{1}{4}$$

results in the spectrum of $S(\omega)$ consisting of the two δ-function lines at $\pm 2V$ appropriate to a dimer with no nonlinearity. See (a) of Fig. 2.5.

As the nonlinearity χ becomes nonzero, an infinite number of δ-lines spring up throughout the frequency region, specifically at $\omega_n = \pm(n + \frac{1}{2})(\Delta\omega)$. For this below-threshold case ($\chi < 4V$), the frequency interval is given by

$$\Delta\omega = 4V_{eff} = 4V\left[(2/\pi)K(\chi/4V)\right]^{-1}. \tag{2.14}$$

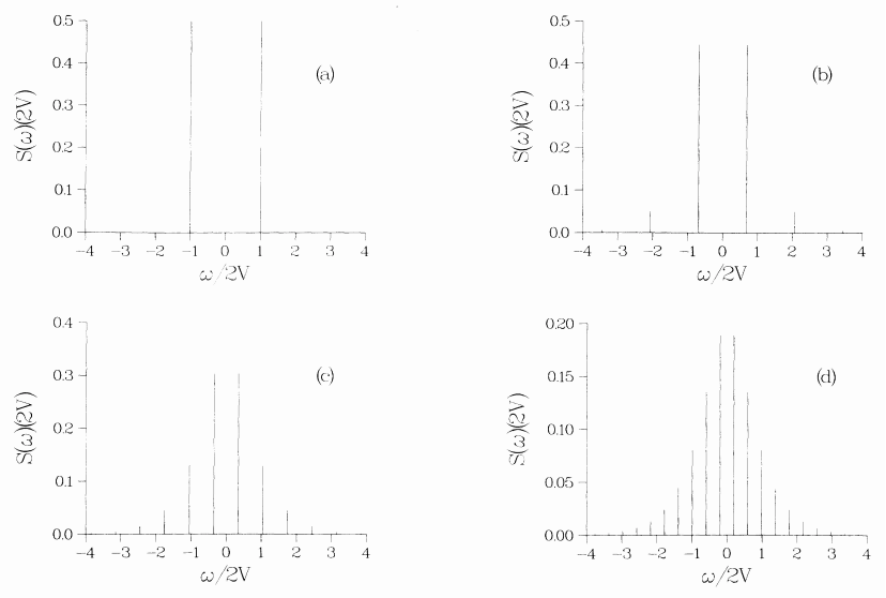

Fig. 2.5 Neutron scattering lineshape $S(\omega)$ for values of the nonlinearity χ below the critical value $4V$. To be appreciated is the march of the lines as one progresses from (a), the case of the linear dimer with $\chi = 0$ through (d), and the narrowing of the interval between them as nonlinearity is increased until the critical value is reached. The product of $S(\omega)$ and $2V$ is plotted along the y-axis, and the frequency ω in units of $2V$ along the x-axis. See text for details. Reprinted with permission from fig. 1 of Ref. (Kenkre and Tsironis, 1987); copyright (1987) by American Physical Society.

Increasing nonlinearity causes the intensity of the two original lines to decrease whereas that of the new lines increases. All lines march towards the origin. The frequency interval between neighboring lines decreases. All this is clear in (b), (c) and (d) of Fig. 2.5.

At the transition, i.e., for $\chi = 4V$, shown in Fig. 2.6(a), the frequency interval $\Delta\omega$ vanishes and the δ-functions collapse into a continuous nonsingular curve. The $p(t)$ at the transition being a hyperbolic secant, the $S(\omega)$ is its Fourier transform which is also[2] the hyperbolic secant (in frequency space), see Eq. (2.13b). As the nonlinearity increases beyond its critical value, the continuous scattering line shapes breaks up into an infinite number of δ-functions again. A line appears at $\omega = 0$ which was not there for the case of χ lower than its critical value and it increases in intensity as the nonlinearity increases further. Clearly, it represents the effective energy mismatch arising from the nonlinearity corresponding to the fact that $p(t)$ oscillates with a nonzero average. The other lines march outwards away from the origin and *decrease*

[2] It has always been amusing to me that just like the Gaussian, the hyperbolic secant is its own Fourier transform! I am not sure I would quite agree, but I have heard it said by reluctant companions in theoretical physics that such punctuations of the rigors of a physicist's life make it bearable.

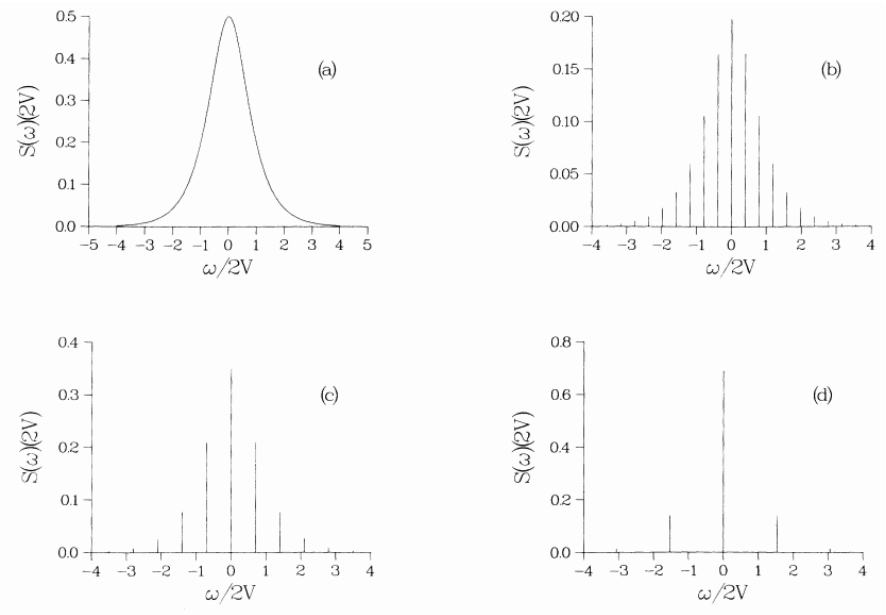

Fig. 2.6 The second half of the graphical depiction of the neutron scattering lineshape $S(\omega)$ as the nonlinearity χ is, respectively at, and above, the critical value $4V$. The critical case $\chi = 4V$ corresponds to (a), where the δ-functions collapse into a *nonsingular* hyperbolic secant curve. Above the critical value, the phenomenon of motional narrowing is observed. The interval between successive lines now *increases* as $\chi/4V$ increases and the central line becomes more and more intense. See text. Reprinted with permission from fig. 2 of Ref. (Kenkre and Tsironis, 1987); copyright (1987) by American Physical Society.

in intensity as the nonlinearity increases. This behavior, evident in (b), (c) and (d) of Fig. 2.6 is surely fascinating. It is nothing that other than *motional narrowing* well known for a linear damped system!

While Eq. (2.14) describes the pre-transition frequency interval, the expression for nonlinearities greater than the critical value ($\chi > 4V$) is

$$\Delta\omega = \chi \left[(2/\pi)K(4V/\chi)\right]^{-1} . \tag{2.15}$$

To a good approximation, the behavior of the frequency interval is logarithmic near the transition on both sides of it:

$$\Delta\omega \approx 4V\pi/\ln\left(\frac{16}{1-(\chi/4V)^2}\right) \quad \text{for}\, \chi \leq 4V, \tag{2.16a}$$

$$\Delta\omega \approx \chi\pi/\ln\left(\frac{16}{1-(4V/\chi)^2}\right) \quad \text{for}\, \chi \geq 4V. \tag{2.16b}$$

2.3 Comparison of the Motional Narrowing to the Linear Damped Result

The behavior of the neutron scattering lineshape for the nonlinear dimer is remarkably similar to that of a *linear* dimer with damping present. The evolution of $p(t)$ in the latter case is governed by Eq. (2.6), with the solutions in the three regimes, underdamped, critically damped, and over damped, given, respectively by

$$p(t) = e^{-t\alpha/2}\left[\cos(\Omega_< t) + (\alpha/2\Omega_<)\sin(\Omega_< t)\right] \quad \text{for } \alpha \le 4V, \tag{2.17a}$$

$$p(t) = e^{-t\alpha/2}\left[1 + (t\alpha/2)\right] = e^{-2Vt}\left[1 + 2Vt\right] \quad \text{for } \alpha = 4V, \tag{2.17b}$$

$$p(t) = e^{-t\alpha/2}\left[\cosh(\Omega_> t) + (\alpha/2\Omega_>)\sinh(\Omega_> t)\right] \quad \text{for } \alpha \ge 4V. \tag{2.17c}$$

The frequency $\Omega_<$ here is $\sqrt{4V^2 - (\alpha/2)^2}$ and the symbol $\Omega_>$ stands for $\sqrt{(\alpha/2)^2 - 4V^2}$.

What scattering lineshapes would result from neutron scattering off a linear damped dimer? Fourier-transforming Eqs. (2.17), and employing the notation that $\mathcal{L}_\alpha(\omega)$ is $1/2\pi$ times the Lorentzian $(\alpha/2)[(\alpha/2)^2 + \omega^2]^{-1}$, and that $\mathcal{H}_\pm(\omega)$ denote the combinations $\mathcal{L}_{\alpha-2\Omega}(\omega) \pm \mathcal{L}_{\alpha+2\Omega}(\omega)$, we get the result

$$S(\omega) = \left(2 + \frac{\omega}{\Omega_<}\right)\mathcal{L}_\alpha(\omega + \Omega_<) + \left(2 - \frac{\omega}{\Omega_<}\right)\mathcal{L}_\alpha(\omega - \Omega_<) \quad \text{for } \alpha < 4V, \tag{2.18a}$$

$$S(\omega) = 2\left[1 + \cos\left(2\tan^{-1}\frac{2\omega}{\alpha}\right)\right]\mathcal{L}_\alpha(\omega) \quad \text{for } \alpha = 4V, \tag{2.18b}$$

$$S(\omega) = \left[\mathcal{H}_+(\omega) + \frac{\alpha}{2\Omega_>}\mathcal{H}_-(\omega)\right] \quad \text{for } \alpha > 4V. \tag{2.18c}$$

The astute reader will have correctly concluded that the reason to display the scattering lineshape for the linear damped dimer in the more complicated form of Eq. (2.18) rather than simply as

$$S(\omega) = \frac{1}{\pi}\frac{4V^2\alpha}{(4V^2 - \omega^2)^2 + (\alpha\omega)^2} \tag{2.19}$$

is merely to facilitate comparison with Eqs. (2.13). The linear damped dimer lineshape is displayed in Fig. 2.7. For no damping, the lineshape consists of two δ-function lines (not shown) that undergo true broadening on introducing and increasing the damping rate α, with their peaks moving towards the origin. It is clear that true broadening, i.e., the appearance of a continuous curve that is not singular, does not happen in the nonlinear dimer lineshape but the overall effect appears the same particularly if instrumental broadening agents are present as they would be in any realistic experimental situation. At critical damping marked by $\alpha = 4V$, we see only a single central peak in the linear damped dimer lineshape. This is identical to the nonlinear dimer system. The peak is then seen to narrow and rise in its value at the origin here as the damping rate α is increased beyond $4V$. The qualitative behavior

is thus the same in the nonlinear dimer with no damping and the linear dimer with damping. The ratio $\alpha/4V$ in the latter case plays the role of the ratio $\chi/4V$ in the former.[3]

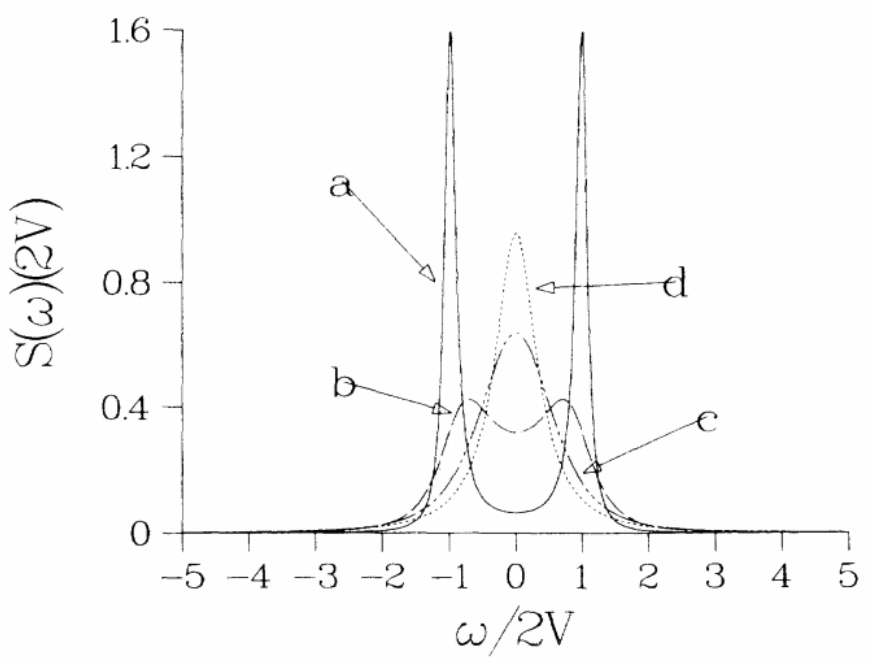

Fig. 2.7 Neutron scattering lineshape $S(\omega)$ for the linear damped dimer from Eqs. (2.18) for various values of $\alpha/4V$: (a) 0.1, (b) 0.5 for underdamped motion, (c) 1 for critical damping, and (d) 1.5 showing standard motional narrowing. The similarity to Figs. 2.5 and 2.6 is noteworthy. Modified with permission from fig. 4 of Ref. (Kenkre and Tsironis, 1987); copyright (1987) by American Physical Society.

Where does the similarity come from? It is clear that the transition situation $\chi = 4V$ in the nonlinear and $\alpha = 4V$ in the linear damped dimer both correspond to infinitely sluggish equalization of site probabilities. Fig. 2.8 might help in the understanding. In the left panel, the position on the ω-axis of the main (largest) peak in the "free/underdamped" region is plotted as a function of a, the nonlinearity parameter $\chi/4V$ for the nonlinear dimer, and of b, the damping parameter $\alpha/4V$ for the linear dimer. In the right panel, the relative intensity of the central peak is plotted as a function of the two ratios respectively in a and b. This intensity is clear in the case of the nonlinear dimer. Although it is more difficult an appropriate quantity

[3] As is well known, expected behavior of a lineshape on superficial examination is broadening which clearly happens on the underdamped region. The phenomenon of motional narrowing is somewhat of a surprise to the casual investigator.

to represent it in the case of the damped linear dimer because of the absence of δ-functions, let us take it to be $2\Omega_>/\alpha$ which is the ratio of the value of $\mathcal{H}_-(\omega)|_{\omega=0}$ to that of $\mathcal{H}_+(\omega)|_{\omega=0}$. Fig. 2.8 shows that, in this manner, the position of the main peak as well as the intensity of the central peak in the region where it exists, exhibit essentially identical behavior for the two systems.

The source of this impressive similarity can be traced to the fact that, if the nonlinearity parameter χ is taken to be the imaginary quantity $i\alpha$ in the original DNLSE (1.2) for the amplitudes, α being taken real, the off-diagonal part of the density matrix equation becomes identical to the equation representing the linear damped dimer, equivalently to replacing the DNLSE by the standard stochastic Liouville equation.

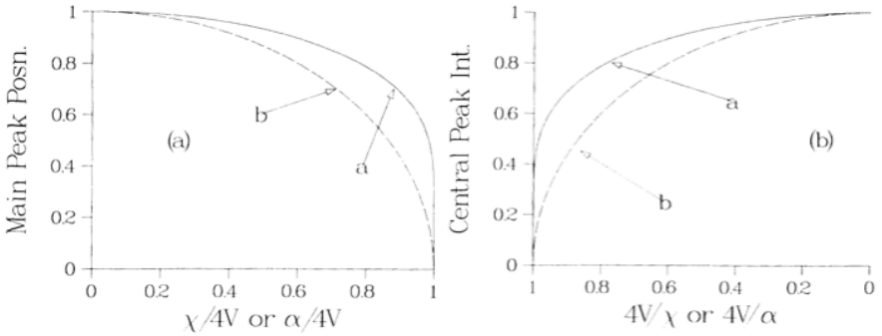

Fig. 2.8 Comparison of the position of the main peak and the intensity of the central peak in the spectrum for the nonlinear and the linear damped dimers. See text. Modified with permission from fig. 5 of Ref. (Kenkre and Tsironis, 1987); copyright (1987) by American Physical Society.

Thus, although the nonlinear and linear damped cases correspond to quite different equations and solutions in appearance, they both arise from essentially the same source. If χ is pure real, what we have seen as the nonlinear dimer evolution results. If it is taken pure imaginary the linear damped evolution ensues. If it is taken to be generally complex, an integro-differential equation can be derived, the real (imaginary) part of the complex χ being the nonlinear (linear damped) parameter. The consequent scattering spectrum can be shown to interpolate between that shown in Figs. 2.7 on the one hand and, on the other, 2.5 and 2.6, respectively.[4]

It is worthwhile asking whether it is possible to differentiate between linear damped and undamped nonlinear behaviors in the lineshape, particularly given that there are no real δ-functions in the spectrum as a result of instrumental broadening. Such differentiation would be possible, at least in principle, if the following require-

[4] Needless to emphasize, whenever one uses a χ that is not pure real, the diagonal part of the ρ equation must be left untouched in the same spirit as in the construction of the standard stochastic Liouville equation to ensure that the total particle probability does not decay and the particle does not disappear.

ments are met: (i) The instrument broadening width should be small enough, (ii) the frequency interval $\Delta\omega$ should be large enough, and (iii) the neighboring peaks should not be disparate in intensity. The spectrum for the nonlinear dimer would then consist of a *multitude* of peaks, visually differentiable, whereas that for the linear damped dimer would have at most two peaks. The first requirement refers to the quality of instrumentation and the extent to which the lines are free of extraneous interference. Given a specific instrumental broadening width, the third requirement places a window on the value of $\chi/4V$ (or of $\alpha/4V$) for which the difference in the two spectra is easily discernible. Much more detailed considerations into this realistic (nonlinearity) interpretation problem have been given in Kenkre and Tsironis (1987). Their analysis also shows how to apply methods derived by Kenkre and Brown (1985) can be applied to the nonlinear dimer to obtain, to a good approximation, the effect of temperature variation on the scattering lineshapes. The reader is referred to the original paper for details.

2.4 Solution for Arbitrary Initial Conditions

The solutions in Eq. (2.1) or (2.2) on which the development in this Chapter has been based, take the initial condition to be localized on one of the two sites of a dimer and thus with q_0 and r_0 vanishing while $p_0 = \pm 1$. In order to study the effect of initial quantum *phases* on the dynamics, a matter we will take up in Chapter 3, it is necessary to have the full solution unencumbered by the localization restriction. Let us obtain the general solution here (Kenkre et al., 1987; Kenkre and Tsironis, 1987) and employ it in the next Chapter.

Returning to the original Eq. (1.8), one finds that relaxing the restrictions on the initial condition does not change the form of the solutions but only results in the replacement of the simpler expression for the coefficient A (leaving even B unchanged) by one containing full information about q_0 and r_0 as well as about p_0:

$$\frac{d^2p}{dt^2} = Ap - Bp^3, \tag{2.20a}$$

$$A = (\chi^2/2)p_0^2 - 4V^2 - 2V\chi r_0, \quad B = \chi^2/2. \tag{2.20b}$$

Because the three components of the Bloch vector must obey the condition $p_0^2 + q_0^2 + r_0^2 = 1$ for a pure state (which is the only kind we are analyzing here), it is necessary to specify only two of the three components.

Let us present the fully general solution of Eq. (2.20) through two stages of generalization. First, let us consider situations in which the initial time derivative of p vanishes, in other words, $q_0 = q(0) = 0$. The solution then continues to be a cn that transitions into a dn when the elliptic modulus crosses 1 but k now depends on the initial phases as well as the probability difference. The general solution is then

$$p(t) = p_0 \mathrm{cn}[(p_0\chi/2k)t, k] = p_0 \mathrm{dn}[(p_0\chi/2)t, 1/k], \tag{2.21}$$

the elliptic modulus being given by

$$1/k^2 = 2 + (1/p_0^2)[(4V/\chi)^2 + (8V/\chi)r_0 - 2p_0^2], \tag{2.22}$$

which, with the definition that $k_0 = \chi/4V$, can be written in the simple form

$$k^2 = \frac{k_0^2 p_0^2}{1 + 2k_0 r_0}. \tag{2.23}$$

What happens in the completely general case when the initial time derivative of p is arbitrary? If it does not vanish, we must write

$$p(t) = C\mathrm{cn}[(C\chi/2k)(t - t_0), k] = C\mathrm{dn}[(C\chi/2)(t - t_0), 1/k], \tag{2.24}$$

and evaluate C and/or t_0 in terms of p_0, r_0, and $q_0 = (dp/dt)_0$. The result, as given explicitly in Kenkre and Tsironis (1987) is

$$t_0 = (2k/C\chi)F\left(\cos^{-1}(p_0/C), k\right), \tag{2.25}$$

where $F(\varphi, k)$ is the *incomplete* elliptic integral of the first kind given by[5]

$$F(\varphi, k) = \int_0^{\varphi} \frac{d\varphi'}{\sqrt{1 - k^2 \sin^2 \varphi'}}.$$

The elliptic modulus k which is obviously a very important quantity governing the evolution is given by

$$k^2 = \frac{1}{2}\left[1 + \frac{p_0^2 - \zeta^2}{\sqrt{\zeta^4 + (q_0/k_0)^2}}\right], \tag{2.26}$$

with

$$\frac{1}{2\zeta^2} = \frac{k_0^2}{1 + 2k_0 r_0}. \tag{2.27}$$

Clearly, the fully general expression (2.26) reduces to (2.23) whenever $q_0 = 0$. We will have occasion to put both these expressions to use in the next Chapter.

2.5 Stationary States and Stability Analysis

As the final subject of this Chapter we investigate stationary states and their stability, a topic first analyzed for the DNLSE for large as well as small systems by Eilbeck et al. (1985) in a thorough, impressively detailed, and clear manner. While those

[5] You have encountered this quantity already in Eq. (1.16) for an alternate definition of the sn function whose inverse it is.

authors started directly from the equations obeyed by the amplitudes in the DNLSE, we will give here an equivalent study useful for small systems such as the dimer that was derived by requiring that time derivatives of the probability difference for arbitrary initial conditions (see Eq. (2.24) vanish for all times (Kenkre and Tsironis, 1987; Kenkre et al., 1987). To be able to make appropriate linkages to more general systems treated in the book further on, let us study the stationary states by demanding that all three components p, q and r of the Bloch vector in Eqs. (1.8) be independent of time for all time. This is obviously what we mean by stationary states. We will call the resultant stationary values, respectively p_{ss}, q_{ss} and r_{ss}.

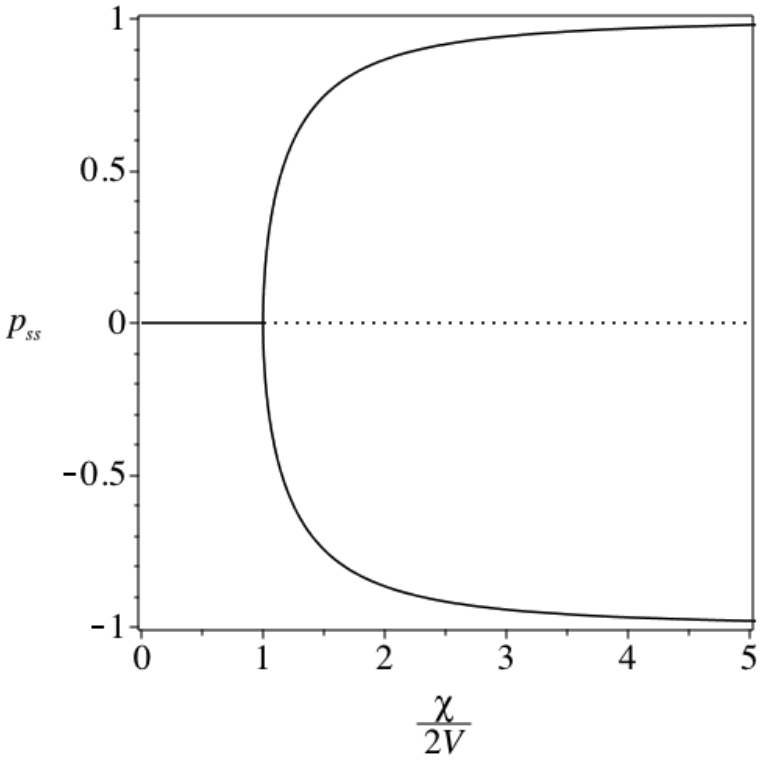

Fig. 2.9 Stationary state probability differences p_{ss} plotted versus the nonlinearity ration $\chi/2V$ showing bifurcation behavior when the latter reaches the value 1. For nonlinearities smaller than this critical value, the probability difference vanishes. For $\chi/2V > 1$, on the other hand, that symmetrical solution becomes unstable (as shown by the dotted line). The stable solution then has two branches corresponding to the two signs in Eq. (2.28). The upper branch has state $|1\rangle$ occupied more, while the lower branch has it occupied less, than the state $|2\rangle$ as quantitatively given in Eq. (2.29).

The first and the third equations in (1.8) merely confirm that $q_{ss} = 0$. The second equation supplies important independent information that stationarity requires that either p_{ss} vanish or that $r_{ss} = -2V/\chi$. Given the interrelation among the three Bloch components from probability conservation, and additionally that $q_{ss} = 0$, stationarity means that p_{ss} must either vanish or be given by

$$p_{ss} = \pm\sqrt{1 - \frac{4V^2}{\chi^2}}. \tag{2.28}$$

In terms of the stationary values of the quantum mechanical amplitudes c_1 and c_2, the result is

$$|c_1| = \frac{1}{\sqrt{2}}\sqrt{1 + \sqrt{1 - \left(\frac{2V}{\chi}\right)^2}}, \tag{2.29a}$$

$$|c_2| = \frac{1}{\sqrt{2}}\sqrt{1 - \sqrt{1 - \left(\frac{2V}{\chi}\right)^2}}. \tag{2.29b}$$

These are the self-trapped values, applicable only for $\chi \geq 2V$. For $\chi \leq 2V$, the symmetrical solution of vanishing p_{ss} takes over.

In order to determine the stability of the stationary states, let us follow the standard procedure of expanding the three Bloch vector components around the stationary values, linearizing the evolution, and requiring that in the linear approximation the values tend to return to the stationary ones. The consequence is that for nonlinearities less than the critical value $\chi = 2V$, the $p_{ss} = 0$ solution is stable but for nonlinearities larger than the critical value that solution becomes unstable.[6] The stable solutions are then the self-trapped values given in Eq. (2.28). Fig. 2.9 displays this graphically, with solid (dotted) lines representing the stable (metastable) solutions. Stationary states are of physical importance for at least two reasons. They are often directly accessible in experiments involving spectra. And in the presence of a damping agent, the system evolves to them with the passage of time as will be seen in Chapter 7.

2.6 Chapter 2 in Summary

The solution of the discrete nonlinear Schrödinger equation for a quantum mechanical particle shuttling between the two sites of a degenerate (resonant in energy) dimer was given in terms of Jacobian elliptic functions explained in Chapter 1. The inherent nature of the relationship of the cn and dn functions as their elliptic modulus crosses the critical value 1 was shown to be naturally connected to the physical connection

[6] Putting time derivatives to zero in the equations for the Bloch vector components finds *all* the possible stationary states. Which are stable among them and which not is decided by the stability analysis which, thus, results in the $p_{ss} = 0$ line becoming dotted in the plot beyond $\chi = 2V$.

between the particle being free or self-trapped. Connections to the simpler systems of a linear damped dimer and a nonresonant linear dimer to the given system were examined and explored and suggested the use of two quantities for investigation in the latter: the average of the probability difference over a cycle and the period of oscillation. Their characteristic behavior as the nonlinearity parameter is varied was indicated. Applications of the self-trapping were described to several experimental investigations including mobility or conductivity of particles such as electrons, the spin relaxation of muons and hydrogen atoms in solids, and neutron scattering. The latter experiment was explored in considerable detail. The van Hove theory of lineshapes simplified for the spatially limited system was used for calculations of the neutron scattering lineshape. The self-trapping transition was investigated in detail through Fourier transforms of the Jacobian elliptic function solutions we obtained. Comparison of the spectrum to that of a linear damped dimer was studied and the reasons for the phenomenon of motional narrowing observed in the nonlinear dimer as well were investigated. The generalized solution for the probability difference was shown to have the same elliptic function form as for the localized initial condition (although shifted in time to account for initial time derivatives) and explicit expressions were provided in readiness for application in subsequent Chapters. Finally, stationary states were analyzed along with a brief indication of stability analysis.

Chapter 3
Initial Delocalization, Phase-Nonlinearity Interplay, and Fluorescence Depolarization

In Chapter 2, we analyzed the condition of extreme initial localization. This meant that the particle is initially entirely on one of the two sites of the dimer. Let us devote this Chapter to the investigation of the effects of initial *delocalization* as also the consequences initial *quantum phases* have on the evolution of the dimer. We will use for the purpose the solution for $p(t)$ for arbitrary initial conditions obtained at the end of Chapter 2. In a certain sense, the present Chapter justifies the title of the entire book because of its immediate engagement with the interplay of quantum phases and nonlinearity.

We will carry out the study only for *pure* initial states, which demand, as a result of the conservation of probability, that the components of the Bloch vector satisfy

$$p^2(t) + q^2(t) + r^2(t) = p_0^2 + q_0^2 + r_0^2 = 1. \tag{3.1}$$

This represents the fact that the tip of the Bloch vector must lie on the surface of a sphere of radius 1. The phases of the system are determined by the inclination of the Bloch vector.

We do not consider mixed states (i.e., those involving an ensemble) because we consider the DNLSE as an approximation to whatever original evolution equation governs the system under study. It is quite possible that forming a proper mixed state might conflict with the range of validity of the approximation that leads to the DNLSE. An ensemble average of a property is computed by calculating the property for each member of the ensemble and then summing the results with weights appropriate to the ensemble. This is a linear operation. If the actual system we start our investigations on is, as we have assumed, linear in the full expanded space required for its description, the standard expectations of linearity will apply during our construction of mixed states. However, it should be obvious that a subtle question arises: whether the operation of the approximation that replaces the actual linear evolution by the contracted nonlinear counterpart (as provided, for instance, by the DNLSE) is equally valid if performed before or after the ensemble averaging approximation is carried out. In general, the two will not *commute*. To be assured of the correctness of the analysis, let us restrict it, therefore, to pure states.

Of our two questions, how is self-trapping affected by a delocalized initial condition, and what does phase-nonlinearity interplay introduce into the evolution, the first is easier to reason about on physical grounds. We have seen that the lowering of the site energy through occupation of the site by the quantum particle leads to resonance being lost between the sites of a system that certainly started out being resonant as given. The greater this effective difference at the sites, the greater the contribution to the self-trapping transition. One might expect, therefore, that larger initial delocalization will cause *lesser* loss of effective resonance for a given amount of nonlinearity. The amount of nonlinearity required to cause self-trapping might then be larger than for a totally localized initial condition case. Let us see if this really comes about.

Rather than taking a truly arbitrary initial state at once, let us do so in two stages. Let us take p_0 to be less than 1 in magnitude but begin with the assumption

$$q_0 = \rho_{12}(0) - \rho_{21}(0) = 0. \tag{3.2}$$

Observe, for instance, that this condition holds for the stationary state (because q is proportional to the time derivative of p; all time derivatives must vanish in the stationary state) and notice that this means that knowing p_0, the *magnitude* of r_0 is specified immediately. Let us investigate the two cases for the two signs of $r_0 = \pm\sqrt{1 - p_0^2}$, and only then proceed to the study of the effects of non-zero q_0. We thus study the simpler case of real initial conditions first and only later add complex ones. We will find that expected behavior is seen for the positive sign (in-phase case) but striking new behavior for the negative sign (out-of-phase case), and that complex initial conditions add a bit, but not much that is dramatic, to our understanding of the interplay of initial phases with nonlinearity.

3.1 Real Initial Conditions

The substitution of the assumed values of the initial components of the Bloch vector in the expression (2.23) for the elliptic modulus of the cn or dn solution (2.21) of the dimer probability difference gives us, for real initial conditions,

$$k^2 = \frac{k_0^2 p_0^2}{1 \pm k_0\sqrt{1 - p_0^2}}. \tag{3.3}$$

A cursory glance at Eq. (3.3) confirms, particularly from the numerator, that a delocalized initial placement should require a larger amount of nonlinearity χ to cause a transition. To keep in mind is that self-trapping occurs at $k = 1$ when the elliptic functions involved change character. The cursory glance also shows that something dramatic may occur when the nonlinearity reaches a value that makes k_0 equal the reciprocal of $\sqrt{1 - p_0^2}$ in the case when the minus sign is operative. The

expectation is thus that the out-of-phase initial condition may be more interesting. We will examine all this below.

3.1.1 In-phase Case: $r_0 = +\sqrt{1 - p_0^2}$, Expected Behavior

For the in-phase case, let us take as an illustrative real initial condition, $P_1(0) = 0.8$ which, from conservation of probability means $P_2(0) = 0.2$ and $p_0 = 0.6$. We

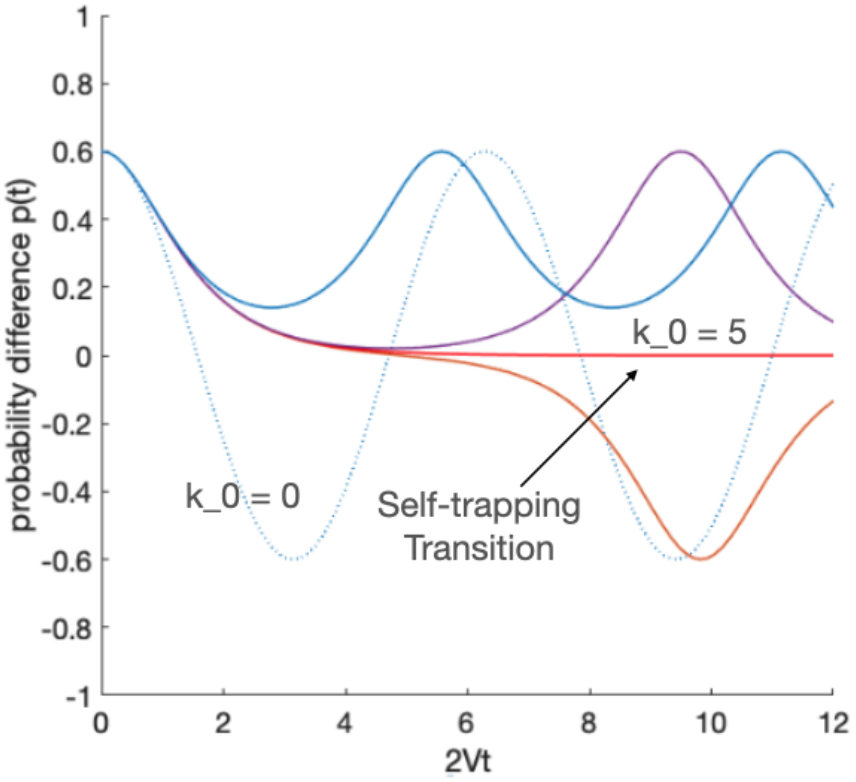

Fig. 3.1 Time evolution of the probability difference $p(t)$ between the two sites of the nonlinear dimer for a real initial condition that is in-phase. The system begins to oscillate sinusoidally in the linear extreme limit ($k_0 = \chi/4V = 0$). The oscillations become more strenuous, i. e., with with larger period, as k_0 reaches the critical value 5. For still larger nonlinearity, the probability difference oscillates only on one side of zero. The evolution for this delocalized initial condition is thus identical to that for the localized one except for the critical value of k_0 which is a factor of 5 larger here and for the fact that oscillations occur between ±0.6 rather than between ±1.

additionally assume $q_0 = 0$, $r_0 = +\sqrt{1 - p_0^2} = 0.8$.

As Fig. 3.1 shows, the time evolution of the probability difference simply emulates the situation in the case treated in Chapter 2 where the initial condition was completely localized, with only the maximum of $p(t)$ changed from 1 in that case to $p_0 = 0.6$ here. The expectation that a higher degree of nonlinearity is required to cause the self-trapping transition is borne out: The value of $k_0 = \chi/4V$ required, as shown in the plot, happens to be 5, certainly larger than the value 1 for the localized case. We have indicated only that critical value and the value 0 (linear dimer) in the plot. The marching of the evolution towards the transition from the linear situation and then, beyond the self-trapping transition, the oscillations becoming with greater frequency with increase of nonlinearity are clear from the graph. In contrast to what we will see in the out-of-phase case to be treated next, the value of nonlinearity χ required for the $p(t)$ evolution to reach the constant at the top limit 0.6 is *infinite*.

For $\chi/4V < 5$, the probability difference shows symmetrical oscillations about zero and is given by

$$p(t) = 0.6\,\mathrm{cn}[(1.2)Vt, \chi/4V].$$

At the transition, this turns into the familiar hyperbolic secant curve that does not oscillate. And for $\chi/4V > 5$, it follows

$$p(t) = 0.6\,\mathrm{dn}[(0.3)\chi t, 4V/\chi],$$

oscillating only on one side of zero, signifying self-trapping.

3.1.2 Out-of-phase Case: $r_0 = -\sqrt{1 - p_0^2}$, a New Transition

Similarly to the in-phase case, let us take, for this out-of-phase example, the real initial condition $P_1(0) = 0.8$ and therefore $P_2(0) = 0.2$ and $p_0 = 0.6$ with the additional assumption that $q_0 = 0$. However, now we choose the minus sign, in other words assume the initial quantum phases to be such that $r_0 = -\sqrt{1 - p_0^2} = -0.8$. We find in the consequent evolution three consequences that are worthy of note. The first is expected but the other two are surprising. Fig. 3.2 displays two of them, the expected and and one of the surprising ones.

We see that $p(t)$ starts out by oscillating sinusoidally between the limits of ± 0.6 for zero nonlinearity. The period of the oscillation becomes longer as the nonlinearity increases, the evolution being described by the cn function, until the self-trapping transition is reached. This behavior is the same as in the in-phase case but for this out-of-phase case the self-trapping occurs for a much lower value of the nonlinearity ratio, 5/9, rather than at 5 as in the in-phase case. The cn turns into the hyperbolic secant at this point. For higher nonlinearities, the evolution follows the oscillations of a dn function on only one side of zero. This is the expected feature, being similar to the localized and the in-phase delocalized counterparts.

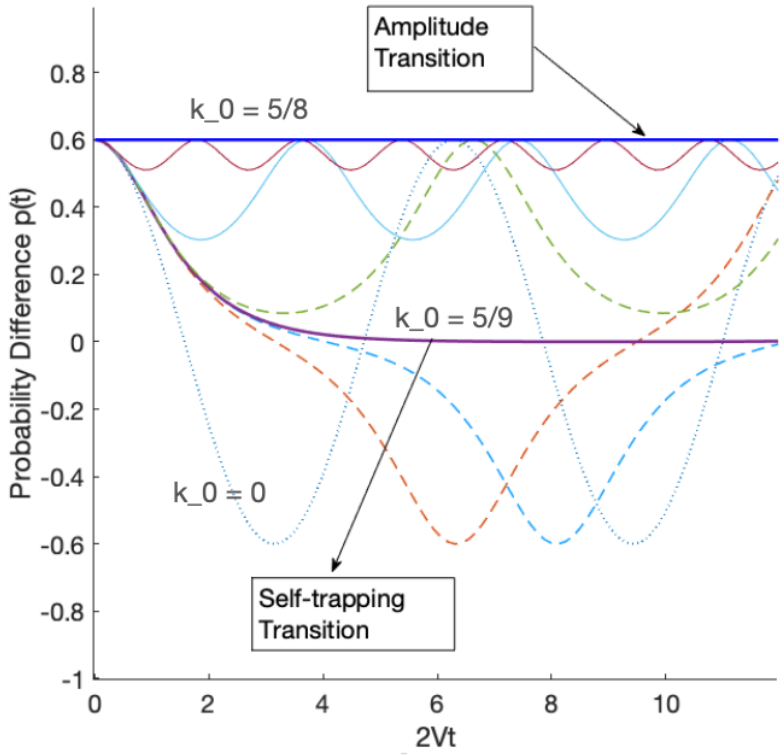

Fig. 3.2 Striking behavior of the probability difference $p(t)$ for the out-of-phase initial condition. The sinusoidal oscillations for the linear limit ($k_0 = 0$) turn into the hyperbolic secant saturation at $k_0 = 5/9$ signifying the self-trapping transition but on further increase of the nonlinearity display unexpected behavior: a new (amplitude) transition occurs at $k_0 = 5/8$ which, as the text will explain, signifies the initial state of the dimer being one of its stationary states thus having no time dependence whatsoever. What is remarkable is that this happens at a finite value of the nonlinearity.

The surprise occurs as the nonlinearity increases beyond the critical value for the self-trapping transition. The dn oscillations decrease in amplitude and increase in frequency as in the localized or the in-phase delocalized cases. However, when $\chi/4V = k_0$ hits the value 5/8, the probability difference $p(t)$ becomes completely independent of time.

Losing all time dependence in this fashion occurs for the other two cases studied, the fully localized and the in-phase delocalized, only at an infinite value of the nonlinearity. For the out-of-phase case it happens, by contrast, at the finite value of 5/8. This is a new kind of transition. When we discovered it (Tsironis and Kenkre, 1988), I decided to name it the *amplitude* transition to distinguish it from self-trapping which we thought of as a frequency transition.

It turns out that increasing the nonlinearity beyond the characteristic value 5/8 for the amplitude transition uncovers another unexpected behavior. It is displayed in Fig. 3.3. The oscillations of the probability difference now lie entirely on the *other side* of 0.6. What this means is that, on the average, the initially more populated state tends to get *more* populated than the initially less populated one! In the other two cases (localized and in-phase delocalized, respectively) the evolution tended to equalize the site occupations. Here the opposite is true.[1]

For the purposes of reference, Fig. 3.3 shows the self-trapping transition curve (dashed line), i.e., the secant hyperbolic that results for $k_0 = 5/9$, an intermediate curve (dotted line) for $k_0 = 7/12$, and the amplitude transition curve (solid blue), the constant that occurs for $k_0 = 5/8$. This links to what we have seen in Fig. 3.2. The focus of the display in Fig. 3.3 is, however, on the solid curves marked (a) $k_0 = 6/9$, (b) $k_0 = 7/9$, (c) $k_0 = 1$, and (d) $k_0 = 5$.

First, we see that, on exceeding the k_0 characteristic of the amplitude transition, the oscillations of $p(t)$ occur with steadily increasing frequency. Further investigations uncover even more interesting behavior. The amplitude of the oscillations of $p(t)$ first increases on increasing the nonlinearity, $p(t)$ always oscillating only on the other side of the stationary state constant value 0.6 as we have seen. But subsequently, the amplitude begins to decrease slowly, on a logarithmic scale: for large increases in k_0, $p(t)$ *returns* to the constant value 0.6. This is made more clear by Fig. 3.4 in which the average $< p >$ of the probability difference as well as the amplitude of its oscillations are plotted on the same graph.

There is little question that exciting new features emerge in the out-of-phase case. In order to understand their origin, it is natural to examine the variation of the elliptic modulus k as the nonlinearity χ, consequently $k_0 = \chi/4V$, is varied. This we do next.

3.1.3 Meaning of the Amplitude Transition

Let us examine how the square of the elliptic modulus k behaves as the nonlinearity ratio $k_0 = \chi/4V$ is varied. Fig. 3.5 shows the variation. The main figure addresses the out-of-phase case and the corresponding variation is shown in the inset for the in-phase initial condition. Both the inset and the main figure show k^2 increasing as the nonlinearity is increased, the intersection with the horizontal at $k = 1$ marking the self-trapping transition (at $k_0 = 5/9$ for the out-of-phase case in the main figure but at the much larger value $k_0 = 5$ for the in-phase case in the inset). The out-of-phase case shows an additional feature: k^2 blows up to infinity at $k_0 = 5/8$. This is the amplitude transition. As shown by Tsironis and Kenkre (1988), it is indicative of the initial state being coincident with a stationary state of the nonlinear dimer.

Further increase of the nonlinearity brings k up from negative infinity to a maximum value. It then undergoes a slow decrease, eventually to negative infinity. While

[1] What is happening here is confirmation of a principle that in real life is known as the 'rich get richer' phenomenon.

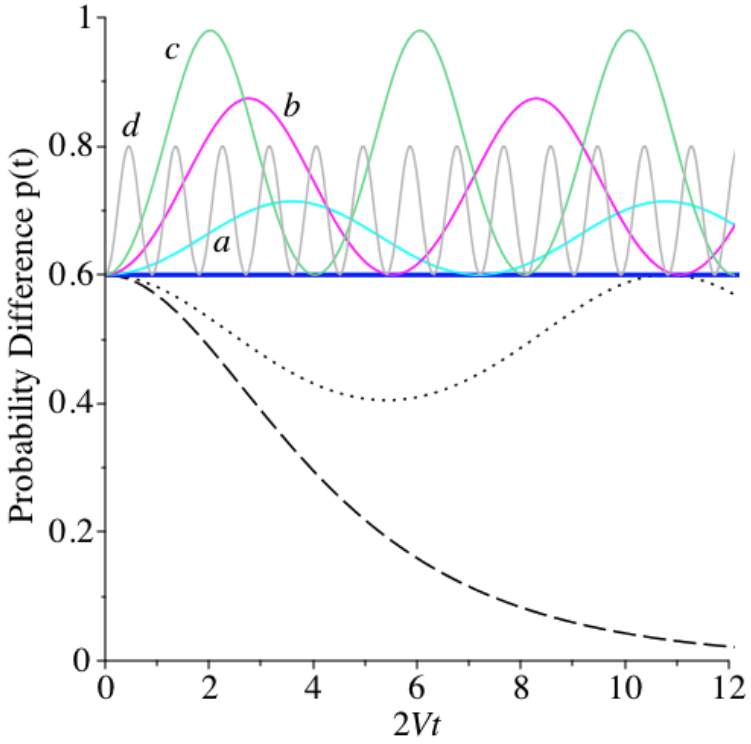

Fig. 3.3 What happens for values of the nonlinearity parameter k_0 beyond that characteristic of the amplitude transition. As in Fig. 3.2, the time evolution of the probability difference $p(t)$ is plotted but the range of p values is restricted from 0 to 1 to make new features clearer. Two of the curves shown are repeated for reference from Fig. 3.2: the (dashed) self-trapping transition for $k_0 = \chi/4V = 5/9$ and the solid blue amplitude transition curve for $k_0 = 5/8$ that marks the stationary state as explained earlier. An intermediate (dotted) curve is also shown for $k_0 = 7/12$. New curves for $k_0 > 5/8$ show oscillations occurring on the other side, i.e., maintaining $p(t)$ always *larger* than the initial value 0.6. The first three, for values of k_0 equaling (a) 6/9, (b) 7/9 and (c) 2, show the oscillation amplitude increasing but the fourth, (d) for $k_0 = 5$, shows a decrease in the amplitude. See Fig. 3.4 for more on this last observation.

this may not necessarily be appreciated from the plot, it is quite clear form the expression. The behavior of k^2 explains all the behavior observed visually in the evolution of $p(t)$ and also suggests transformations of k, one to bring it within the 0 to 1 range and the other associated with the imaginary Jacobi transformation of the argument.[2] The essence of this combination of transformations is that, as k changes by variation of k_0 via the negative-sign expression in Eq. (3.3), we start with $p = p_0 \mathrm{cn}(p_0 k_0 k^{-1}\tau, k)$, go through $p = p_0 \mathrm{dn}(p_0 k_0 \tau, k^{-1})$, and end up with

[2] These transformations have been introduced in Chapter 1.

$$p = p_0 \,\mathrm{nd}\left(p_0 k_0 |k|^{-1} \tau \sqrt{1+|k|^2}, \frac{1}{\sqrt{1+|k|^2}}\right). \tag{3.4}$$

This expression, given by Eq. (3.4), is the appropriate one to use, and has been so used, to plot the probability difference curves for k values greater than that characteristic of the amplitude transition. The reader is reminded that the Jacobian elliptic function nd is nothing other than the reciprocal of the dn function.

In order to support their assertion that the meaning of the amplitude transition was the initial state coming into coincidence with a stationary state of the nonlinear dimer, Tsironis and Kenkre (1988) showed that precisely the same happens to the *linear* nonresonant dimer. For that simple system, the solution for $p(t)$ has been provided for a localized initial condition as Eq. (2.9). It is straightforward to write the full equation of motion for abitrary initial conditions as

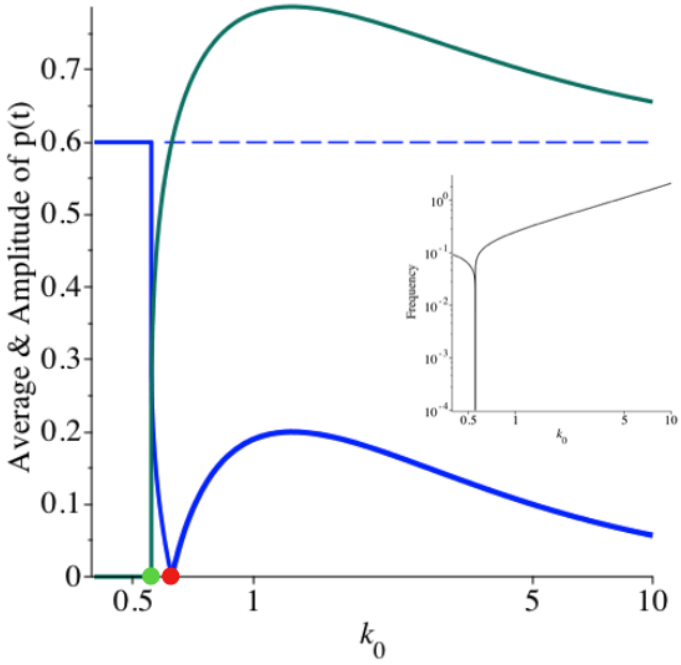

Fig. 3.4 Further display of the behavior of the probability difference $p(t)$ for the out-of-phase real initial condition case. The average of $p(t)$ over a cycle (green line) and its amplitude of oscillations (blue line) are both plotted as a function of k_0 in the main Figure, with their transition points (self-trapping and amplitude transitions, respectively, at $k_0 = 5/9, 5/8$) marked with little circles on the x-axis. Both display an increase for increasing k_0 beyond the transitions but then a decrease, the average $< p >$ to the initial value 0.6 and the amplitude to the value 0. The inset shows the corresponding variation of the frequency of $p(t)$ behaving similarly to the initially localized case in Fig. 2.2.

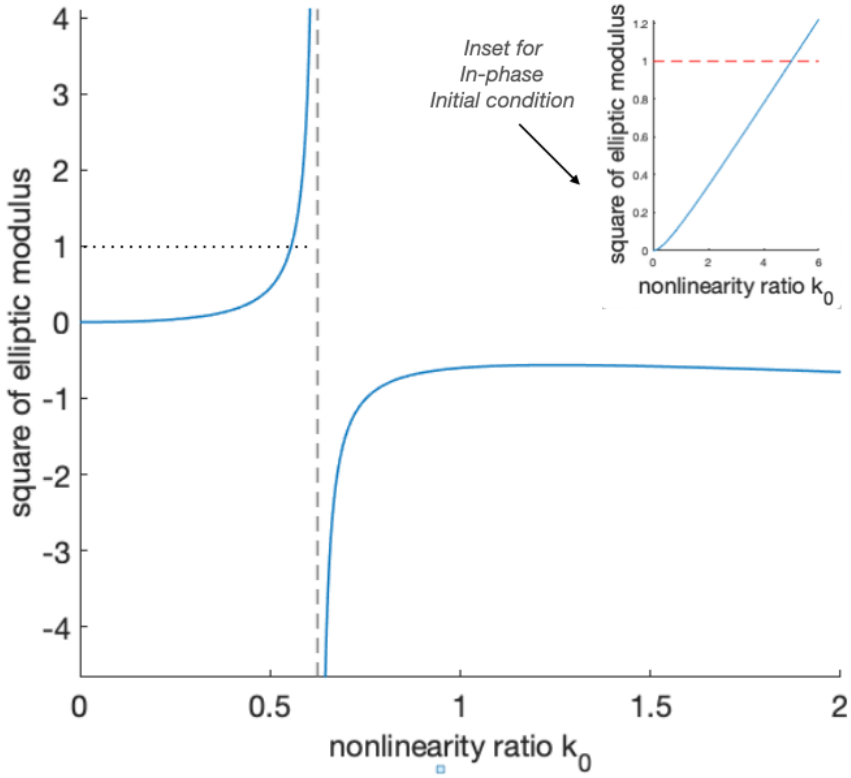

Fig. 3.5 The elliptic parameter, i.e., the square of the elliptic modulus, plotted as a function of the nonlinearity ratio $k_0 = \chi/4V$ for the out-of-phase real initial condition in the main figure and for the in-phase real initial condition in the inset. The latter has only one interesting transition (self-trapping) where the modulus attains the value 1, which for the case treated in this section occurs at $k_0 = 5$. In the main figure, i.e., for the out-of-phase case, two transitions occur: self-trapping where the modulus equals 1 ($k_0 = 5/9$) but, on further increase of k_0, the amplitude transition where the modulus becomes infinite ($k_0 = 5/9$) as the initial state comes in coincidence with a stationary state of the system. These values correspond to $p_0 = 0.6$ as in Figs. 3.1 and 3.2. See text.

$$\frac{d^2p}{d\tau^2} + (1+\delta^2)p = \delta r_0 + \delta^2 p_0 \tag{3.5}$$

with $\delta = \Delta/2V$, the energy of site 1 being Δ larger than that of site 2. Stationary states are obtained by putting time derivatives to zero. It is now entirely straightforward to prove that, starting from $\delta = 0$, it is possible to make an initial out-of-phase real state ($q_0 = 0$) coincide precisely with the stationary state by simply varying the magnitude of Δ, maintaining its sign. It also follows that it impossible to do the same for an

initial in-phase real state.[3] The reader is strongly encouraged to go through this easy exercise.

The natural question asked by Tsironis and Kenkre (1988) when they discovered the unexpected amplitude transition was whether it was a consequence simply of the nondegeneracy created by the nonlinearity through the self-trapping phenomenon or an individual independent consequence of the interplay of quantum dynamics and the nonlinearity. It was particularly relevant to ask this question because the transition occurred only in the region of nonlinearity values already larger than that required for the onset of effective loss of resonance induced by the nonlinearity. The answer is clearly that it is not an additional consequence of nonlinearity-quantum interplay: it occurs even without nonlinearity for a nonresonant situation. The demonstration in (Tsironis and Kenkre, 1988) makes this quite clear.

3.2 Complex Initial Conditions

Let us now relax the constraint of real initial conditions, introduce a non-vanishing q_0, and accordingly replace the earlier relation $r_0 = \pm\sqrt{1 - p_0^2}$ by

$$r_0 = \pm\sqrt{1 - p_0^2 - q_0^2}. \tag{3.6}$$

We know that the condition for self-trapping is that the modulus reach and exceed 1. The critical value of the nonlinearity, χ_c is now still given by a simple expression:

$$\frac{\chi_c}{4V} = \frac{1 + r_0}{p_0^2} = \left(\frac{1}{p_0^2}\right)\left(1 \pm \sqrt{1 - p_0^2 - q_0^2}\right). \tag{3.7}$$

If $\chi < \chi_c$, the particle executes periodic motion, and $p(t)$ follows cn function behavior. When χ exceeds the critical value, the particle is trapped. As in the q_0 case, the negative sign option in Eq. (3.7) corresponds to particularly interesting behavior and will be the only one treated here. It is clear at the outset that there is no way that an initial state with $q_0 \neq 0$ could be made to coincide with a stationary state of the dimer. This is so because stationarity implies $q_0 = 0$, the quantity q being the time derivative of p for all time obviously including the initial time.

Raghavan et al. (1997) addressed the variation of the square of the elliptic modulus as in Fig. 3.5 and showed that, in the presence of a non-vanishing q_0, no blow-up of k^2 occurs. Around where the nonlinearity ratio attains values characteristic of the blow-up in the $q_0 = 0$ case, now for nonvanishing q_0, all one sees is a characteristic modification looking like a discontinuity. There is little other change. They also gave a detailed comparison between the nonlinear and the linear *nondegenerate* dimers in the context of the dependence of the amplitude of oscillations past the amplitude

[3] The reader who consults the original reference cited is gently warned that the symbols used in the original references do not necessarily represent the same quantities as here in the book.

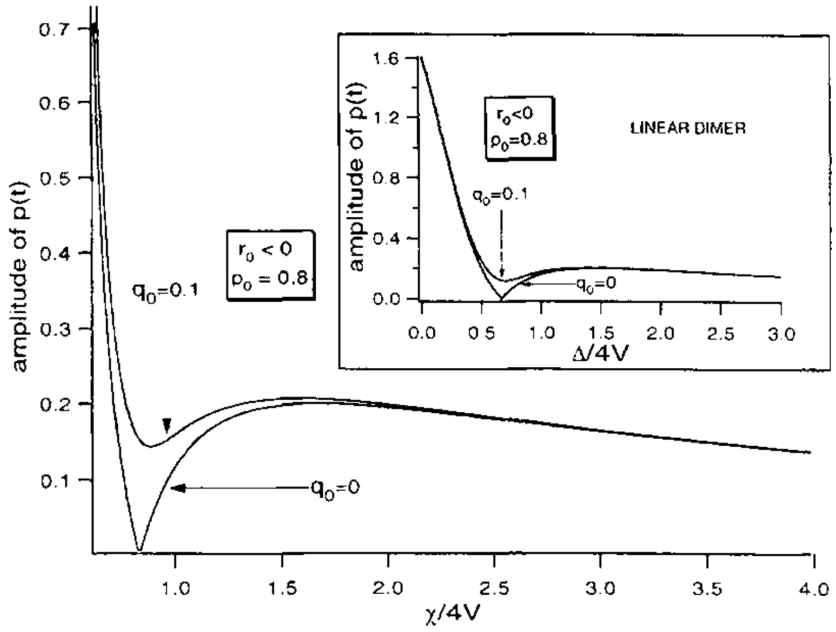

Fig. 3.6 Comparison of the variation of the amplitude of oscillations in the nonlinear dimer (main plot) and in a linear nondegenerate dimer (inset) with changes in the nonlinearity ratio $\chi/4V$ for $r_0 < 0$ and $p_0 = 0.8$ for two values of q_0: 0 and 0.1, respectively. Plotted in the inset along the x-axis is the nondegeneracy $\Delta/4V$ rather than the nonlinearity given that the dimer considered in there is linear. The display shows both the effect of $q_0 \neq 0$ and the fact that nondegeneracy in a *linear* system has the same consequences for the phenomenon studied as nonlinearity in a degenerate system provided the nonlinearity is beyond the value required for the self-trapping transition to set in.

transition and showed visually as well as analytically that the argument we have presented above is borne out in detail. We reproduce their graphical display in Fig. 3.6 and refer the reader to the original paper for details.[4]

Of the two questions we posed at the beginning of this Chapter, how is self-trapping affected by a delocalized initial condition, and what does phase-nonlinearity interplay introduce into the evolution, we have seen that the second has complex answers. Interesting discussions and insights have emerged throughout the foregoing analysis.

In order to readdress the first, easier, question succinctly, let us inspect Fig. 3.7 in which, for the restricted case of real initial conditions, we display, following Raghavan et al. (1997), the critical value $\chi_c/4V$ of the nonlinearity ratio. That is

[4] Although the plot displayed here from the publication of Raghavan et al. (1997) refers to $p_0 = 0.8$ while we have considered $p_0 = 0.6$ throughout this Chapter, all considerations and conclusions remain the same.

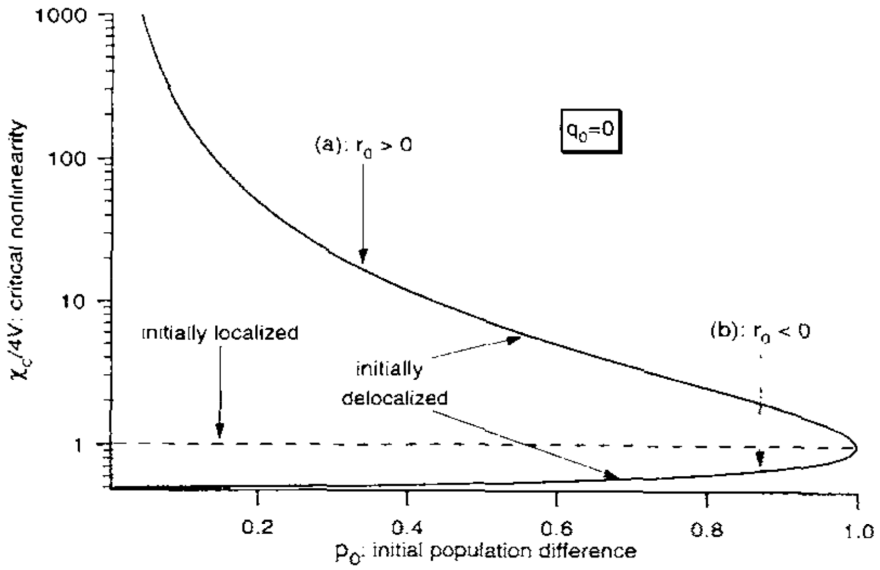

Fig. 3.7 The critical value χ_c required for the self-trapping transition in units of $4V$ plotted logarithmically as a function of the initial population difference p_0 to show the effect of initial differentiation of site occupation on the self-trapping. Eq.(3.7) is used by putting $q_0 = 0$ (real initial conditions) for simplicity. The dashed line represents the localized initial condition ($r_0 = 0 = q_0$ and $p_0 = \pm 1$ as a result) and r_0 is positive in (a) but negative in (b).

the value required to cause the self-trapping transition. In Fig. 3.7 we see it plotted against the initial probability difference p_0 for real initial conditions, for the in-phase as well as the out-of-phase cases. The dashed line at $\chi_c/4V = 1$ represents the case of the initially localized condition. As indicated in the plot, the curve above (below) that dashed line corresponds to the in-phase (out-of-phase) initial condition. Graphically, we see that initial delocalization has opposite effects in this regard: the critical nonlinearity decreases as the magnitude of the initial probability difference decreases in the in-phase case but increases in the out-of-phase case.

3.3 Fluorescence Depolarization in Stick Dimers

Thinking hard about a system in the laboratory that could display some of these effects in principle, I thought of fluorescence depolarization in stick dimers that I had worked on with my colleague Bob Knox and his then-student Talat Rahman several years prior to these nonlinear investigations (Rahman et al., 1979).[5] Sophisticated

[5] In that work, what I had been called upon to do was to act as the local EEE (evolution equation expert) and fix the equation of motion that would properly describe the motion of electronic

instrumentation, clever ideas, and intriguing systems of study such as optical lattices and Bose-Einstein condensates have sprung to the fore in recent times. It is my hope that the concepts of phase-nonlinearity interplay that I have described here will attract the attention of experimentalists to such systems. It is possible that the relatively simple proposals for observations that I made during the work on the nonlinear dimer with Tsironis, and later, will communicate the essence of what is expected to be observed.

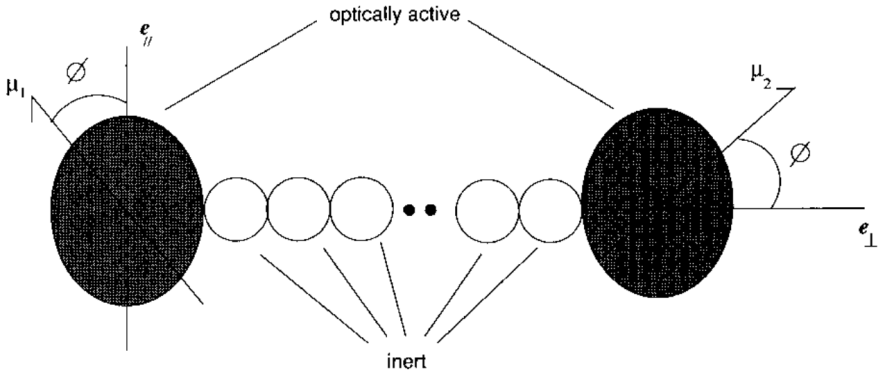

Fig. 3.8 Schematic of the fluorescence depolarization setup. Circles at the end of the molecular dimer shown indicate optically active molecules that give rise to electronic excitation upon the incidence of light. Unshaded circles indicate optically inert molecules so controlling their number (the two dots in the center of the figure represent that the number is controllable) allows one to control quantitatively the transfer interaction between end molecules. Angled arrows note the two induced dipole moments on each optically active molecule, the μ's being dipole moments. The polarization vector $e_{//}$ is at an angle ϕ with dipole moment μ_1. Reprinted with permission from fig. 1 of (Raghavan et al., 1996). Copyright 1996 by American Physical Society.

The system I proposed for experimental investigations of what Tsironis and I discovered in our theoretical studies of the nonlinear dimer, led by what I learnt from my participation in (Rahman et al., 1979), is a variable-distance noninteracting donor-acceptor pair of molecules (Stryer and Haugland, 1967). A fine example is that of the so-called "stick-dimer" in which poly-L-proline oligomers of controllable length are used to separate an α-naphthyl group at the carboxyl end - the donor - from the dansyl group at the imino end - the acceptor -, and the efficiency of energy transfer is studied through measurements of fluorescence excitation, emission and polarization spectra. Here let us take the donor and acceptor to be identical molecules. On illumination, either of the molecules in the pair may undergo electronic excitation.

---

excitation across the two sites of a stick dimer. What I had succeeded in doing for the Knox-Rahman research was to modify a stochastic Liouville equation so it gave the correct thermal equilibrium and moreover allow the investigator to move from representation to representation while using it.

The direction of the transition dipole moment produced on the molecule through the process of excitation depends on geometrical factors and is generally different for the two molecules in the pair. Not to complicate the example too much, let us take the two dipole moments to be coplanar and mutually perpendicular. Shining (broad-band) polarized light in such a way that the excitation beam is incident perpendicular to the plane in which the transition dipoles lie, and varying the angle of polarization of the incident light beam results, in principle, in varying the relative amplitude of probability of excitation of either molecule.

3.3.1 The Observable and Relation to the Dimer Density Matrix

If $I_{//}$ and $I_{\perp}$ are the intensities of fluorescence polarized respectively parallel and perpendicular to the direction of polarization of the incident light, the observable we will focus on is the "degree of fluorescence polarization" f defined as[6]

$$f = \frac{I_{//} - I_{\perp}}{I_{//} + I_{\perp}}. \tag{3.8}$$

For details of the formalism I refer the reader to the work of Rahman et al. (1979). Generally, the intensity of fluorescence in the direction of the unit vector e_λ is given by

$$I_\lambda = \sum_{m,n} \rho_{mn} (\mu_m \bullet e_\lambda)(\mu_n \bullet e_\lambda)$$

In terms of the product of density matrix elements and dot products (represented by bullets here) of the (induced) dipole moments μ in each state in a complete representation, e.g., at each site. The assumption of mutually perpendicular dipole moments allows us to focus on the essentials of our problem and write

$$\mu_1 \bullet e_{//} = \mu_2 \bullet e_{\perp} = \cos\phi; \quad -\mu_1 \bullet e_{\perp} = \mu_2 \bullet e_{//} = \sin\phi. \tag{3.9}$$

Here ϕ is the angle made by the polarization of the incident light with the induced dipole moment on molecule 1. Equation (3.8) then allows us to calculate the central observable f in terms of the Bloch vector components p and r whose evolution here in this section of the book is given by the DNLSE:

$$f(t) = p(t)\cos 2\phi + r(t)\sin 2\phi. \tag{3.10}$$

Here and elsewhere in the book, I will display this observable either as the time-dependent $f(t)$ directly from Eq. (3.10) or, in its steady-state version, with τ_0 as the radiative lifetime of the excitation[7] as

[6] I have departed from the common usage in the fluorescence depolarization community which uses p for this quantity. That symbol already stands for the probability difference in our discussions here.

[7] Not to confuse it with the dimensionless time $\tau = 2Vt$.

$$f_s = \frac{1}{\tau_0}\int_0^\infty dt'\, f(t')e^{-t'/\tau_0}. \tag{3.11}$$

3.3.2 Observable in the Absence of the DNSLE

In order to appreciate how motion characteristics of the excitation are reflected in the fluorescence observable, let us first examine what f would be if the DNSLE and possibilities of self-trapping were *not operative*. Only after we have internalized the connection between motion and the observable, we will inspect the consequences of the DNLSE.[8]

In the absence of nonlinearity, i.e., in a linear undamped dimer, $\chi = 0$ and one obtains, from Eq.(3.10),

$$f(t) = \sin^2 2\phi + (\cos^2 2\phi)\cos 2Vt, \tag{3.12}$$

with the consequence from Eq. (3.11) that the steady-state result is

$$f_s = \frac{\cos^2 2\phi}{1 + 4(V\tau_0)^2} + \sin^2 2\phi. \tag{3.13}$$

What happens to the observable if we include scattering of the excitation (stochastic interaction with a reservoir) represented in the standard simple manner of the stochastic Liouville equation where α is the scattering or rephrasing rate, the equation of evolution being (2.6) for $p(t)$ with an associated equation for $r(t)$? The result is (Kenkre, 1994c)

$$f(t) = (\cos^2 2\phi)e^{-\alpha t/2}\left[\cos\Omega t + (\alpha/2\Omega)\sin\Omega t\right] + (\sin 2\phi)\left(r_{eq} + [\sin 2\phi - r_{eq}]e^{-\alpha t}\right). \tag{3.14}$$

Here the value of r_{eq} is $\tanh(V/k_BT)$ at temperature T, with k_B as the Boltzmann constant, and the quantity $\Omega = \sqrt{4V^2 - (\alpha/2)^2}$ arises from a combination of the transfer interaction and the damping interaction.[9]

The degree of fluorescence polarization evolves from an initial value of 1 to $(\sin 2\phi)\tanh(V/k_BT)$. We see that this value is dependent on the polarization angle ϕ. Thus, if the incident light has its plane of polarization parallel to the induced dipole moment on one of the molecules (and perpendicular to that on the other molecule), the degree of fluorescence polarization f vanishes at large times. For other inclinations of the incident polarization plane, $f(t)$ does not vanish at long times.

The steady-state f_s from Eq. (3.11) then emerges, in agreement with the results of (Rahman et al., 1979), to be:

---

[8] Although these expressions were not made available in the original publication (Kenkre and Tsironis, 1988), I have published the results elsewhere later (Kenkre, 1994c) in the context of application of thermal effects.

[9] Needless to say, if Ω is real (imaginary), the evolution of f is underdamped (overdamped).

$$f_s = \frac{(4\cos^2 2\phi)(1+\alpha\tau_0)}{(2+\alpha\tau_0)^2 + (16V^2 - \alpha^2)\tau_0^2} + \frac{\sin 2\phi}{1+\alpha\tau_0}\left[\sin 2\phi + \alpha\tau_0 \tanh\left(\frac{V}{k_B T}\right)\right]. \quad (3.15)$$

3.3.3 Self-trapping Effects on Fluorescence Depolarization

Now that we have seen what the fluorescence polarization observable does with linear (including stochastic linear) equations of motion, let us calculate what our elliptic function results are from the DNLSE. As given explicitly elsewhere (Kenkre, 1994c), the time-dependent expression is

$$f(t) = (\cos^2 2\phi)\mathrm{cn}(ut,\sigma) + (\sin 2\phi)[\sin 2\phi - \sigma(\cos^2 2\phi)\mathrm{sn}^2(ut,\sigma)], \quad (3.16)$$

with

$$u = 2V\xi\cos 2\phi, \quad (3.17a)$$

$$\sigma = \frac{\xi\chi}{4V}, \quad (3.17b)$$

$$\xi = \frac{\cos 2\phi}{\sqrt{1 + (\chi/2V)\sin 2\phi}}. \quad (3.17c)$$

A graphical display by Kenkre and Tsironis (1988) reveals the effects of self trapping clearly as shown in Fig. 3.9. It is interesting that the noteworthy features appear for polarization angles larger than than 90 deg and for nonlinearities larger than 2V; it is in the latter region that self-trapped states appear in the energy spectrum of the dimer.

It is clear from a perusal of Figs. 3.10 (and 3.9) that the consequences of nonlinearity that our analysis predicts are the mild variation of $f_s(\phi)$ with the nonlinearity χ in the region $\chi < 2V$, the transition at $\chi = 2V$, the minima that develop in the dependence near $\phi = 135$ deg and the unmistakable cusp at 135 deg.[10] The fact that the variation of the angle of polarization ϕ spans the two transitions that we have discussed as consequences of the phase-nonlinearity interplay, the self-trapping and the amplitude transition, is what is behind the peculiar behavior. The stationary states of the linear resonant dimer are characterized by the site-state amplitudes $c_{1,2} = 1/\sqrt{2}$ for the symmetric case and $c_{1,2} = \pm 1/\sqrt{2}$ for the antisymmetric case, respectively. The two states thus possess resultant dipole moments that make respectively the angles 45 deg and 135 deg with the dipole moment of molecule 1. At these values of the polarization angle, the excitation would find itself initially (and consequently forever) in a stationary state. Curve (a) of Fig. 3.10 which is for $\chi = 0$, indeed shows that f_s equals 1 at these stationary state angles 45 deg and 135 deg.

[10] The inset in Fig. 3.10 visually clarifies the meaning of the angle ϕ. Transition dipole moment pairs $\mu_{1,2}$ are in the site-representation directions and $\mu_{+,-}$ in what would have been eigenstates in the absence of the nonlinearity. The vector e_λ lies along the polarization vector of exciting or emitted light and ϕ is measured from the direction of μ_1.

As χ increases in value but is still lower than $2V$, the stationary state angles remain identical to those of the linear dimer. Effects of nonlinearity are there but not significant. When χ hits the value $2V$, however, the characteristic effects of the nonlinearity set in. The trivial stationary states with equal occupation of both sites is reflected in the plots in the fact that the peak at 45 deg is maintained for all values of the nonlinearity. As χ exceeds $2V$, a second stationary state appears in the nonlinear dimer. It is this state that is responsible for the novel features of the figures. The site amplitudes in this state are quite different and represent self-trapping,

$$c_{1,2} = \frac{\sqrt{1 \pm (2V/\chi)^2}}{\sqrt{2}}.$$

For values of χ in excess of $2V$, the nonlinear dimer acts like a *non-resonant* dimer although it is inherently resonant. The site amplitudes in the stationary state are clearly unequal and the resultant dipole moment of the stationary state, which was at 135 deg to that of molecule 1, now slips away from that orientation. The value of χ determines the amount of this slipping. Curves (d) and (e) in Fig 3.10 show this slipping or shift of the maximum of f_s. with 1 and 2 corresponding to the plus and the minus signs respectively.

The source of the visually dramatic 'pinning' effect at 135 deg visible in the plots is merely conflicting symmetries in the nonlinear dimer. When the self-trapping

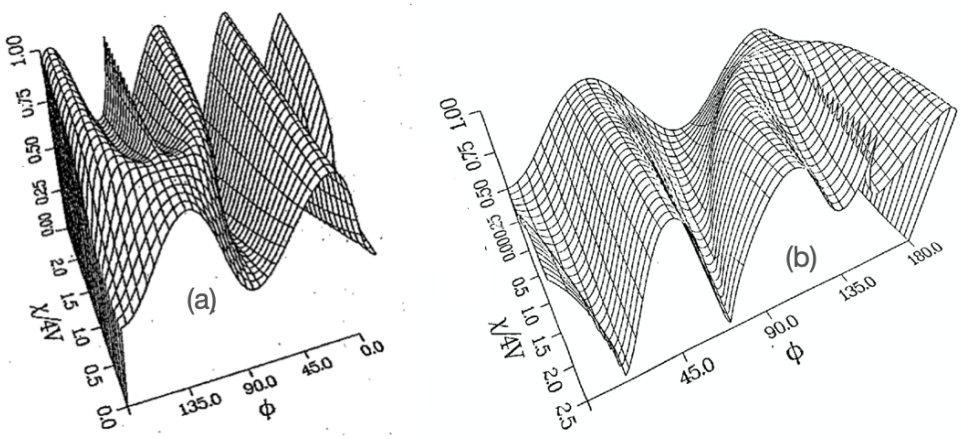

Fig. 3.9 The steady-state fluorescence polarization degree f_s, i.e., integrated over time, plotted as a function of the angle of polarization ϕ (in deg) and of the nonlinearity ratio $\chi/4V$. The linear limit is clear in the foreground in (a) and the result of large nonlinearity is clear in the foreground in (b). The displacement of the $f_s - \phi$ maximum as one moves along t he the nonlinearity axis and an apparent "pinning" of the $f_s - \phi$ curve at $\phi = 135$ deg as well as the value $\chi/4V = 1/2$ at which one sees a transition in the ϕ-dependence are noteworthy features. The value of $2V\tau$ has been assumed to be 1 for simplicity. Reprinted with permission from fig. 1 of Ref. (Kenkre and Tsironis, 1988); copyright (1988) by Elsevier Publishing.

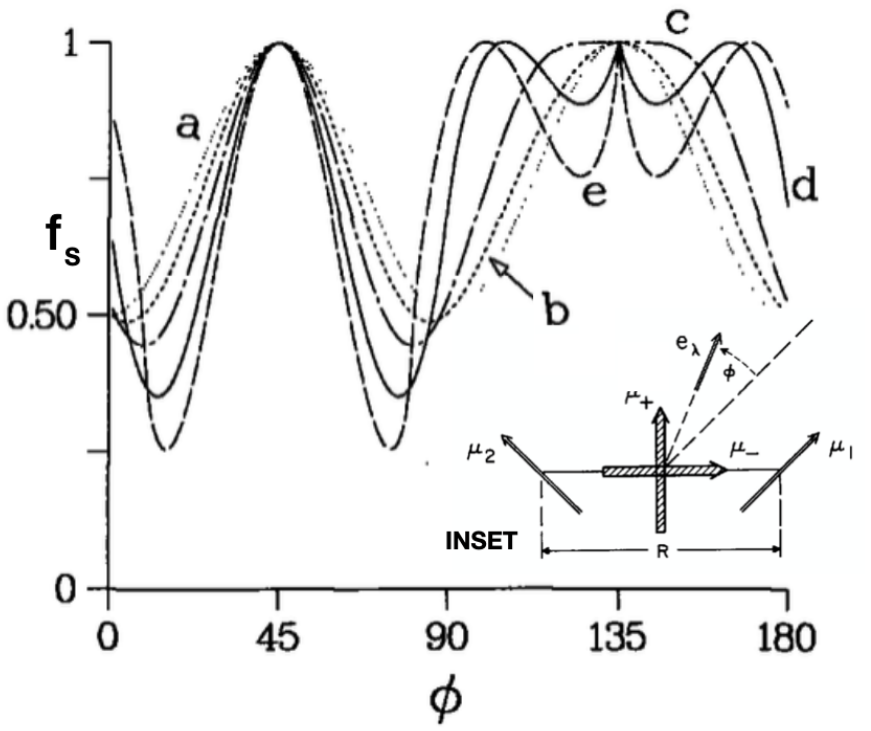

Fig. 3.10 Nonlinearity effects on the steady-state degree of fluorescence polarization f_s in Eq. (3.11). This is a projection of the f_s-ϕ-χ surface shown in Fig. 3.9 on the f_s-ϕ plane. The nonlinearity ratio $\chi/4V$ has the respective values (a) 0, (b) 0.2, (c) 0.5, (d) 1, and (e) 1.5. The variation of f_s is sinusoidal for the linear case (a) and shows only a small change brought about by the nonlinearity. The stationary state is self-trapped for curve (c) as $\chi = 2V$ and the shape of the curve makes clear the occurrence of the transition. Unmistakable effects of self trapping are clear for higher nonlinearities in curves (d) and (e): the formation of a cusp at $\phi = 135$ deg and the minima that appear nearby as a result. The inset explains the geometrical set-up. See text. Reprinted with permission from fig. 2 of Ref. (Kenkre and Tsironis, 1988); copyright (1988) by Elsevier Publishing.

transition sets in, the nonlinear dimer takes on the behavior of a nonresonant (linear) dimer. A true linear nonresonant dimer does not have its stationary state dipole moment at 135 deg and possesses no symmetry around that particular angle. Yet the equations underlying the nonlinear dimer, which is really a resonant entity, favor no site or angle: there is complete symmetry around 135 deg. The emergence of the peculiar cusp in the plots is thus the consequence of the combination of this

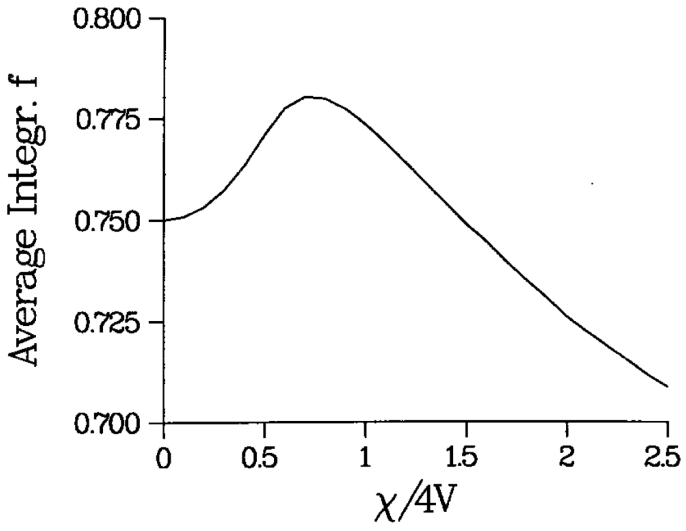

Fig. 3.11 Steady-state (integrated) degree of fluorescence polarization f_s averaged over orientations plotted as a function of the nonlinearity ratio showing a hump around the critical value of the nonlinearity signifying the occurrence of the self trapping transition. The system studied is a solution in which the stick-dimers are oriented at random and values along the abscissa correspond to variation of the intermolecular distance, i.e., the length of the dimer as this can be used observationally to control the V. Reprinted with permission from fig. 4 of Ref. (Kenkre and Tsironis, 1988); copyright (1988) by Elsevier Publishing.

symmetry requirement around 135 deg and the shift of the f_s peak stemming from the shift of the stationary state.[11]

The experimental observation of the effects predicted in Kenkre and Tsironis (1988) requires the construction of appropriate dimers and investigations which involve orientations that are not random. The difficulty in the construction of such systems could be one of the reasons that this experiment that we proposed more than 30 years ago was never performed. Anticipating this possibility, we calculated nonlinearity effects of the same kind in solution systems by performing an average over orientations. Surely, most of the clear effects are lost through the averaging procedure but a discernible hump appears around the critical nonlinearity value as shown in Fig. 3.11.

[11] For the sake of clarity, the effect has been displayed graphically under the assumption that the self-trapped state that contributes has a lower energy at 135 deg. Symmetry of both the dimer and the excitation process requires, however, precisely the same to occur at 45 deg. What is expected to be observed is an equal superposition of the variation shown in Fig. 3.10 with one mirror-imaged around 90 deg.

3.4 Chapter 3 in Summary

A number of expected as well as surprising effects of the interplay of initial quantum phases with nonlinearity were studied in this Chapter, justifying thereby the title of the entire book. The analysis went beyond localized initial conditions, asked a simple question as to what consequences differential occupation of the two sites has on the evolution and the richer question as well as how how phase-nonlinearity interplay modifies the dynamics. The answer we found to the first question was that it depends on whether the particle starts out in phase or out of phase at the two sites. A visual summing of what happens was given towards the end of the Chapter in Fig. 3.7. The behavior for the localized initial placement was found to be followed in essence for the delocalized in-phase real condition scenario, and self-trapping occurred at a higher value of the nonlinearity. For the out-of-phase placement there were several surprises. Self-trapping was found to occur at smaller values of the nonlinearity relative to the localized case. As the nonlinearity increased beyond that for self-trapping another transition was observed at which the initial placement was completely undisturbed with the passage of time. This happened because of the coincidence of the initial state with a stationary self-trapped state of the dimer. For increases of nonlinearity beyond this 'amplitude transition', the frequency of oscillations of the probability difference increased. The amplitude of oscillations first increased and then decreased with yet larger nonlinearity, the limit of extremely large nonlinearity resulting in the amplitude of oscillations vanishing and the probability difference becoming time-independent. An explanation of all the occurrences was given in several different ways and an application to fluorescence depolarization of stick dimers was worked out.

Chapter 4
What Polarons Owe to their Harmonic Origins

Where does the nonlinearity in the DNLSE that gives rise to all the interesting phenomena we saw in Chapters 2 and 3 come from? We have touched upon this question in the Preface[1] where we have warned the reader that in certain situations intense debates have raged over the question particularly in the context of polaronic physics. Chapter 9 has been designated for a description of those discussions in the polaronic area, and Chapter 10 to an analysis of Bose-Einstein condensates, sidestepping that issue. Although we will certainly wait for those Chapters to undertake the matter in detail, it is helpful to understand right away that a traditional way of arriving at the DNLSE has been to consider a simple physical representation of a standard polaronic situation wherein a relatively slower moving particle is envisaged as slaving faster excitations that interact strongly with it.

A polaron is, by definition, a quasiparticle such as an electron, an exciton, a vibrational excitation, or a light interstitial particle, e.g., a muon or a hydrogen atom, in *such strong interaction* with oscillations, such as lattice vibrations or intramolecular motions, that it displays unusual properties in its transport and other characteristics. Unusual properties of this kind include dramatic features such as self-trapping and counterintuitive behavior such as an increase in the mobility with increasing temperature. Such behavior is typically considered contrary to the intuition that temperature increase should lower the mobility because a hotter environment presents the moving particle with larger-amplitude irregular motions that break the translational invariance of a crystal. The underlying physical picture that has been developed to explain such (polaronic) phenomena is that the quasiparticle 'digs its own well' as a result of its interactions with the oscillations and thereby gets self-trapped. Increasing the temperature helps the quasiparticle to climb out of its well and move *more* efficiently than at lower temperatures. This is in contrast to nonpolaronic motion wherein an

[1] As the wise say, there are two types of people in this world: those who read a book's preface and those who don't. If you belong to the former class, you know what is meant by the previous statement. If you are more relaxed about inspecting books in that you normally skip prefaces considering them filler material, you might want to hurry back and read what you have missed; the present author considers his preface an integral part of the book that is best read before starting on the individual chapters.

increase in temperature results, as mentioned, merely in greater scattering through an increase in the oscillation amplitudes. In that non-polaronic case, the quasiparticle moves *less* efficiently than at lower temperatures. The well-digging process in this picture corresponds to the lowering of the site energy that we have encountered in, and is the central process leading to, the DNLSE.[2]

It will help the reader to inspect the basic Hamiltonian H with which most polaronic studies begin:

$$H = \sum_m \varepsilon_m a_m^\dagger a_m + \sum_{m,n} V_{mn} a_m^\dagger a_n + \sum_q \hbar\omega_q \left(b_q^\dagger b_q + \frac{1}{2} \right) + \frac{1}{\sqrt{N}} \sum_{m,q} \hbar\omega_q g_q e^{iq\cdot R_m} \left(b_q + b_{-q}^\dagger \right) a_m^\dagger a_m. \tag{4.1}$$

Here, $a_m^\dagger$ creates the traveling quasiparticle at site m, ε_m is its site energy, V_{mn} is its matrix element for moving from site n to site m, R_m is the position of site m, $b_q^\dagger$ creates boson excitations of an oscillator of mode q with frequency ω_q, and $\hbar$ has been explicitly included in the Hamiltonian to avoid possible confusion. The most important quantity is the coupling constant g_q of the quasiparticle-oscillator interaction. If it is small enough to treat via a perturbation treatment, standard transport theory is used as in descriptions of electron dynamics in metals. If it is large, various methods have been invented including dressing transformations of various kinds and also the DNLSE. Unfortunately, little interconnection is to be found in the literature between the methods.

4.1 A Graphical Understanding of How the DNLSE Could Arise

In order to understand how it is thought that the DNLSE arises here, it is important to inspect the third and fourth terms in the right-hand-side of Eq. (4.1). If of two mutually interacting agents, one is much is faster than the other in its dynamics, it often finds itself *slaved* by the slower variable and it moves quickly to adjust to the latter. This ubiquitous situation has been argued often to occur in strongly interacting systems with fast vibrations (created by the $b_q^\dagger$'s in Eq. (4.1)). The resulting effective Hamiltonian involving only those moving particles (created by the $a_m^\dagger$'s in Eq. (4.1) may then be viewed as depending simply on themselves with energies lowered from their bare values ε_m. The lowering is by an amount that is given essentially by $\sum_q g_q^2 \omega_q$ and happens only at the sites that are occupied. The proportionality constant involved contains the probability that the given site is occupied by the moving particle. Whereas many have assumed this argument as providing the source of the nonlinearity as well as of a dynamical breaking of translational invariance

[2] If you find this picture of the feedback process of the particle digging the well and then moving in the consequent symmetrical structure physically appealing, you might claim membership in a group of followers of the physical ideas set in motion by Landau, Pekar and Holstein.

in the system, you will meet in Chapter 9 objections to this line of reasoning.[3] The oscillators of a given mode have a fixed frequency in the third term and are, thus, *harmonic*. Typically, it is also assumed that the restoring force that brings the oscillators to their equilibrium follows the (linear) Hooke's law. The quasiparticle-oscillator interaction in the fourth term describes the site energy of the quasiparticle as being modulated by an amount linear in the oscillation amplitude.

For the purposes of the present Chapter, let us ask the following question: what are the consequences of taking the oscillators to be *not Hookian* and/or of the quasiparticle-oscillation interaction to be *not linear* in the oscillation amplitude?

Our interest here in raising this question will be not in slight excursions from harmonicity or linearity, which can be easily addressed through perturbation methods. Rather it will be in seeking qualitatively significant departures from traditional analysis of the polaron. Unexpected answers such as the disappearance of self-trapping on increasing the nonlinearity beyond a threshold will emerge below (Kenkre, 1989; Kenkre et al., 1995; Wu and Kenkre, 1995; Kenkre, 1994a; Kenkre et al., 1996b; Kenkre, 1998b; Amritkar and Kenkre, 1999). These results were the consequences of the study I carried out in collaboration initially with my student Honglu Wu[4] and also with my colleague Iris Howard. Later joint work with Christiansen and Jorgensen from Lyngby, and most notably with Ravindra Amritkar from Pune who added important corrections to our insights, will also be described below.

Fig. 4.1 shows the harmonic nature of the oscillators as given by the third term in Eq. (4.1), symbolically, via a sketch of the parabolic potential (dotted line) that governs the oscillators. It also represents the linear nature of the interaction between the quasiparticle and the oscillators by the linear potential (dash-dotted line). Both these are simplifications, of course, both motivated by a Taylor's series representation of the force in each case.

What is important to observe is that the graphical addition of a parabola and a straight line results in just a parabola; indeed, one that is lowered and shifted as seen in Fig. 4.1. Irrespective of the sign of the interaction, the equilibrium position of the resultant parabola is lowered, although the sign does control the lateral direction of the shift. The amount of lowering is proportional to the slope of the straight line representing the interaction and this corresponds to the energy lowering varying as the square of the coupling constant g_q. These are all well-known facts that underlie elementary understanding of the Stokes shift phenomenon in the chemical physicists' community or in polaron matters in the solid state physics context. Having understood in graphical terms how the DNLSE might be arising, let us now ask how it would be modified if the coordinate dependence of the potential and the restoring force are *qualitatively* different from being linear. Such a situation could be imagined to occur in liquid crystals (Chandrasekhar, 1992). These materials consist of partially ordered aggregates of molecules possessing directed shapes such as rods or discs, the coordinate of interest being *rotational*. Rotational polarons discussed below

[3] You will also meet with an alternative argument that is free from those objections. Originated in (Kenkre, 1989; Kenkre and Wu, 1989a,b), it is based on damping produced by the bath rather than on the standard arguments relying on time scale disparity of two parts of the system itself.

[4] He was one of the most efficient of my students in calculations.

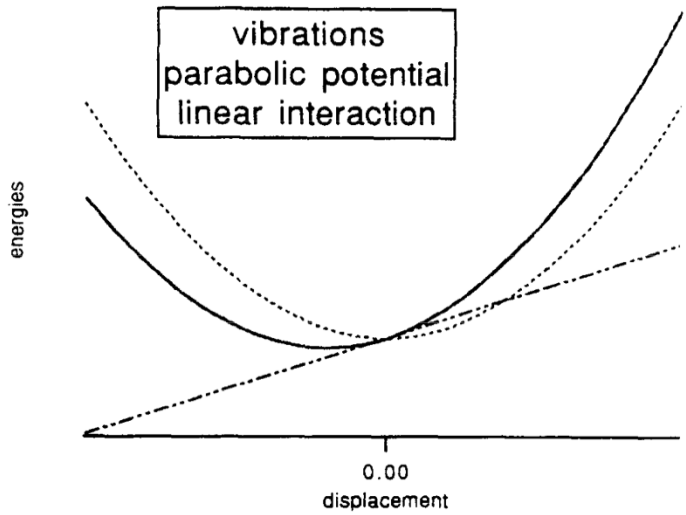

Fig. 4.1 A qualitative sketch of the standard polaronic situation wherein the basic potential is harmonic (the dotted parabola). The interaction potential is linear (shown in dash-doubledotted line). The two when added to each other produce a shifted parabola whose curvature is retained but whose equilibrium position is shifted laterally and the equilibrium energy is lowered. This is the standard situation used for explaining Stokes shifts and polaron systems. Reprinted with permission from fig. 2 of Ref. (Kenkre, 1998b); copyright (1998) by Elsevier Publishing.

could arise generally in any system in which a quasiparticle such as an electron or electronic or vibrational excitation interacts with angular oscillations so strongly that the presence of the quasiparticle has an appreciable effect on the equilibrium direction of the molecule.

4.2 Rotational Coordinates and Nonlinear Dependence

While the left panel of Fig. 4.2 shows an alternate possibility for the restoring potential and the interaction that is based on hyperbolic functions, let us focus on the right panel where the potential and the interaction both have sinusoidal dependence on the displacement.

It is easy to understand graphically what adding a sinusoid to a sinusoid does. Let us nevertheless demonstrate it explicitly. The simple semiclassical argument of how the DNLSE could come about[5] can be envisaged as stemming from an interaction term in the Hamiltonian of the coupled particle-oscillation system,

[5] Let us here assume the reasoning on physical grounds and postpone a rigorous examination of the validity of the semiclassical argument to Chapter 9.

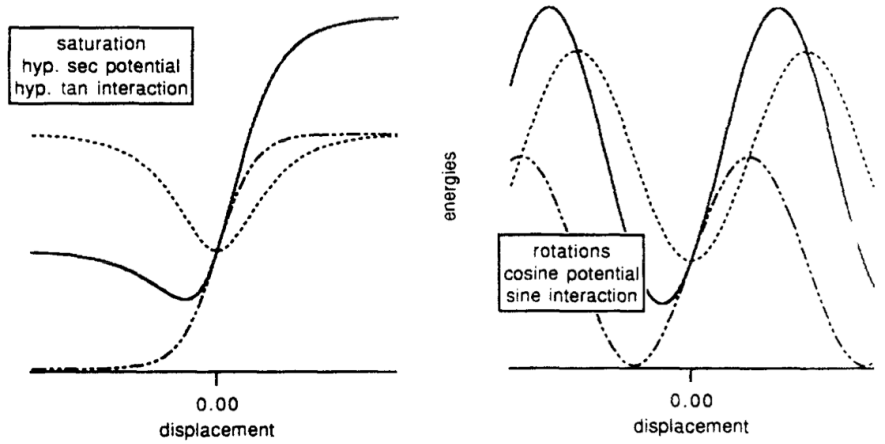

Fig. 4.2 A qualitative sketch of the suggested generalization that leads to the novel features analyzed in this Chapter. The right panel depicts a system in which rotational motions might be represented by a sinusoidal potential rather than parabolic. The interaction potential is also sinusoidal rather than linear. When added to each other they produce a shifted sinusoid rather than a shifted parabola. It should be clear that whereas in the case of Fig. 4.1 larger slopes of the interaction potential always increase the shift effects, this is not true of the present case which can lead to disappearance of polaron effects. See text. Modified with permission from fig. 1 of Ref. (Kenkre, 1998b); copyright (1998) by Elsevier Publishing.

$$\mathcal{E}(x_m, c_m) = E_0 x_m |c_m|^2, \tag{4.2}$$

c_m being the quantum particle amplitude to be at site m and x_m the oscillation coordinate of an Einstein oscillator situated at that site, and considered classical. The usual DNLSE can then be said to arise from a time scale disparity argument applied to the coupled equations of motion

$$i\frac{dc_m}{dt} = \sum_n V_{mn} c_n + E_0 x_m c_m, \tag{4.3a}$$

$$\frac{d^2 x_m}{dt^2} + \omega^2 x_m + S|c_m|^2 = 0. \tag{4.3b}$$

The coupling terms in this equation are taken to arise from differentiation of the interaction term $\mathcal{E}(x_m, c_m)$ in Eq. (4.2) with respect to c_m^* and x_m respectively. And the time scale disparity is argued to slave the oscillation coordinate to the expression obtained by dropping the time derivatives. The constant S then is nothing other than E_0/M where M is the mass of the Einstein oscillator at the mth site.

The two assumptions of linearity in the above standard procedure, both arise from a Taylor series argument. The interaction term $\mathcal{E}(x_m, c_m)$ is linear in x_m and so is the restoring force which is the product of the oscillator mass M and the term $\omega^2 x_m$ in Eq. (4.5b). Our interest here lies in relaxing these two linearity assumptions and

considering nonlinear restoring forces $Mf(x_m)$. We will not be interested in further complexities that can be introduced by nonlinearities of $\mathcal{E}(x_m, c_m)$ in $|c_m|^2$.

Systems in which nonlinearities might be particularly relevant are ones in which x_m is a rotation rather than a vibration. (Hence the title of this chapter.) To emphasize this, we will describe x_m here as an angle variable θ_m. The system could thus be an electron/exciton moving among the sites m of a chain, there being a rotator (for instance a dipole) at each site m whose angle from a fixed direction is θ_m. Periodicity in θ_m is obviously essential at least at every interval of 2π: this means that nonlinear effects of the kind we seek could be quite important for rotations that are not too small compared to 2π. Thus, we replace Eq. (4.2) by

$$\mathcal{E}(x_m, c_m) = E(\theta_m)|c_m|^2, \tag{4.4}$$

and obtain thereby, in place of Eqs. (4.5),

$$i\frac{dc_m}{dt} = \sum_n V_{mn}c_n + E(\theta_m)c_m, \tag{4.5a}$$

$$\frac{d^2x_m}{dt^2} + \omega^2 f(\theta_m) + RE'(\theta_m)|c_m|^2 = 0. \tag{4.5b}$$

The constant R is essentially the moment of inertia of the rotator. The prime denotes differentiation with respect to the argument.

The time scale disparity argument mentioned earlier, used to eliminate the angle variable θ_m, then produces the new DNLSE

$$i\frac{dc_m}{dt} = \sum_n V_{mn}c_n - h(|c_m|^2)c_m, \tag{4.6}$$

where $h(|c_m|^2)$ is simply $-E(\theta_m)$, the quantity θ_m being expressed as a function of $|c_m|^2$ obtained as the solution of

$$f(\theta_m) = -(R/\omega^2)E'(\theta_m)(|c_m|^2). \tag{4.7}$$

What Eq. (4.6) tells us in a physical sense is that, for this rotational system, the energy of an occupied site is lowered by the nonlinearity effect just as in the simple DNLSE but not merely by an amount proportional to the probability of occupation. Instead, the lowering happens by an amount which is a *function h* of that probability. The function is determined in turn by the dependence of the restoring agent f and of the particle-displacement interaction E on the (angular) displacement θ_m. The specific manner in which h depends on the probability of occupation of the mth site is given by Eq. (4.7). We will see that exciting novel effects await us as a result.

We now have, generally as a consequence of Eq. (4.7), the density matrix equation

$$i\frac{d\rho_{mn}}{dt} = \sum_s (V_{ms}\rho_{sn} - V_{sn}\rho_{ms}) - \rho_{mn}\left[h(\rho_{mm}) - h(\rho_{nn})\right]. \tag{4.8}$$

For nearest neighbor interactions $V_{mn} = V(\delta_{m,n+1} + \delta_{m,n-1})$, it takes, as expected, a form similar to Eq. (1.6). The striking difference is, however in the content of the factor in the last term of Eq. (4.8) in that what multiplies ρ_{mn} is not merely proportional to the difference of the probabilities of occupation at sites m and n. Instead, it is the difference of the h-functions evaluated at those probabilities. For the dimer ($m = 1, 2$), reduces to the generalized Bloch vector equations[6]

$$\frac{dp}{dt} = 2Vq, \tag{4.9a}$$

$$\frac{dq}{dt} = -2Vp - rj(p), \tag{4.9b}$$

$$\frac{dr}{dt} = qj(p). \tag{4.9c}$$

where $j(p)$ is given by

$$j(p) = h\left(\frac{1+p}{2}\right) - h\left(\frac{1-p}{2}\right). \tag{4.10}$$

To maintain our own orientation in these systems wherein the rotating molecules may change theirs, let us point out to ourselves that, for the simple DNLSE that we have studied so far in the book, h is linear in the probability, the proportional constant being what we have termed throughout as the nonlinearity χ. Thus,

$$h(y) = \chi y; \qquad j(p) = \chi p.$$

For the rotational polaron, however, both h and j are strongly nonlinear in their argument.[7] The dynamical equations (4.9) are thus a simple generalization of Eqs. (1.8) and might be approached in essentially the same manner.

In order to solve for the dynamics of the system we use the methods we learned for the simple DNLSE dimer. We obtain a closed second order equation for the probability difference $p(t)$ from Eqs. (4.9), use the potential method to solve for the classical mechanical motion of the representative particle whose displacement is $p(t)$, and inspect the solutions obtained to quadratures. However, the procedure must be preceded by an precise identification of the nonlinearity function h and consequently j. For the sake of simplicity, let us examine what we get for the simplest assumption that both the restoring force $f(\theta_m)$ and the interaction energy $E(\theta_m)$ are proportional to the sine of a multiple of the angular displacement $\theta = \theta_1 - \theta_2$,

---

[6] For the sake of the reader who might consult the original publications on this material, I point out that the function $j(p)$ introduced here in the book is related to the $g(p)$ in the original publications by the simple relation $j(p) = dg(p)/dp$. The reader will meet the $g(p)$ explicitly in Eq. (4.17).

[7] I am enormously tempted to state here that the ordinary DNLSE (1.2) is, thus, characterized by a linear nonlinearity. And that the present Chapter is the exploration of the departure from linearity of the nonlinearity functions h or j. However, I control myself. Let me desist from making such an assertion because I am afraid that what might win out in the mind of the reader is a demand for clarity rather than entertainment via confusion over a sense of (peculiar) word-play humor.

$$f(\theta) = \frac{\sin(\Lambda\theta)}{\Lambda}, \tag{4.11a}$$

$$E(\theta) = \frac{E_0}{\Lambda}\sin(\Lambda\theta)\,. \tag{4.11b}$$

I have selected the expressions so that under the single limit $\Lambda \to 0$, we recover the linear case and, through it, the standard DNLSE situation. With the definitions of a new 'saturation parameter' Δ_s and the old nonlinearity parameter χ, we write

$$\Delta_s = \frac{E_0}{\Lambda}, \tag{4.12a}$$

$$\chi = \frac{E_0^2 R}{\omega^2}. \tag{4.12b}$$

In subsequent discussions, the dimensionless ratio $\chi/2\Delta_s$ that measures the nonlinearity relative to the saturation energy will acquire significance. We note in passing that, in terms of the internal parameters specified here, it is given by

$$\frac{\chi}{2\Delta_s} = \frac{E_0 R\Lambda}{2\omega^2}. \tag{4.13}$$

Straightforward calculations lead to an h-function that involves not only the probability of occupation but its square as well. For low values of the nonlinearity parameter, the h-function behaves linearly as in the standard case but it has the remarkable feature that it saturates[8] to a constant independent of the probability for high values of the nonlinearity:

$$h(|c_m|^2) = \frac{\chi|c_m|^2}{\sqrt{1+(\chi/\Delta_s)^2|c_m|^4}}. \tag{4.14}$$

The all-important $j(p)$ appearing in the generalized Bloch vector equations (4.9) then has the form

$$j(p) = \frac{\chi}{2}\left[\frac{1+p}{\sqrt{1+(\chi/2\Delta_s)^2(1+p)^2}} - \frac{1-p}{\sqrt{1+(\chi/2\Delta_s)^2(1-p)^2}}\right], \tag{4.15}$$

which can also be rewritten as

$$j(p) = \Delta_s\left[\frac{1+p}{\sqrt{(1+p)^2+(2\Delta_s/\chi)^2}} - \frac{1-p}{\sqrt{(1-p)^2+(2\Delta_s/\chi)^2}}\right]. \tag{4.16}$$

Equation (4.15) shows that if the saturation energy Δ_s is large with respect to the nonlinearity χ so that $\chi/2\Delta_s$ may be neglected, the function $j(p)$ is linear in the probability difference and the standard DNLSE is recovered. On the other hand, Eq.

[8] Here we have arrived at one of the striking consequences of the rotational idea. Inspection of the sinusoids in Fig 4.2 has already prepared the astute reader, I am certain, to this occurrence. There is more to come.

(4.16) shows that in the opposite limit, when the saturation energy is vanishing, more interesting and varied behavior emerges. It will be the focus of our discussions in further sections.

4.3 Surprises in the Dynamics of the Rotational Polaron

What do we obtain when we follow the standard program of converting the Bloch equations (4.9) into a second order equation for the probability difference p and solving it to quadratures? Let us examine the time dependence of the probability difference in this manner for the simplest localized case, i.e., when one of the two sites is fully occupied? I urge the reader strongly to verbalize the expectation before calculating or reading on. What do you expect to happen to the time dependence given that we have sighted the possibility of a saturation with increasing nonlinearity?

Figure 4.3 shows the result graphically. The probability difference p is plotted as a function of the dimensionless time $2Vt$ for 3 values of the nonlinearity ratio $\chi/2V$ in three panels (upper, central and lower) each characterized by one value of the saturation energy Δ_s relative to $2V$. Respectively, the value $\Delta_s/2V$ is large, i.e., 100 (upper panel (a)), relatively small, 2.5 (central panel (b)), and subcritical, 2 (lower panel (c)). In each panel, the solid lines denote small nonlinearity ($\chi/2V = 0.5$) relative to the bandwidth, the dotted lines describe intermediate nonlinearity ($\chi/2V = 5$), and the dashed (faintest) lines represent the highest nonlinearity ($\chi/2V = 9$). The uppermost panel shows behavior similar to that predicted by the standard DNLSE. It is what we have come to look upon as natural (see, e.g., Fig. 2.1) in that free motion for small nonlinearity is replaced by slower motion showing strong nonlinearity effects of slowing down as the period of the oscillation becomes large and then, finally for the largest nonlinearity, self-trapping occurs.

Two surprises emerge, however, in panels (b) and (c).

In the central panel (b), nonlinearity displays a non-monotonic effect. The free motion depicted by the solid line gives way to self-trapping shown by the dotted line as p oscillates only on one side of the dimer but further increase in χ brings the oscillation to acquire again its free character as p oscillates on both sides.

In the lower panel (c), self-trapping is completely destroyed. The saturation parameter Δ_s is low enough to make it impossible for the particle to be self trapped no matter what the value of the nonlinearity $\chi/2V$. The oscillation for all values of the nonlinearity is on both sides and the motion is fundamentally different from the situation in the standard DNLSE represented in the upper panel (a).

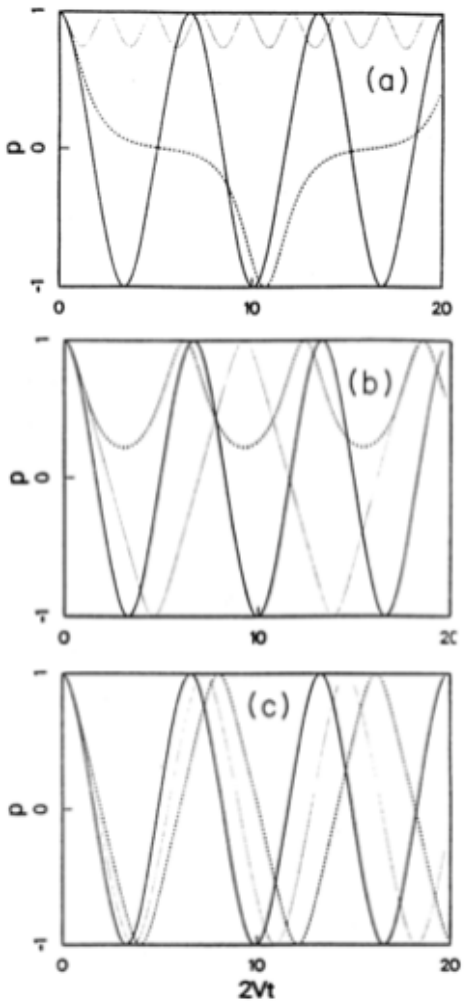

Fig. 4.3 Noteworthy effects in the Rotational Polaron: The time evolution of the probability difference $p(t)$ is plotted for initial localization on one site for various parameter combinations. Behavior akin to the standard DNLSE is observed in the top panel: free motion changes into self-trapped motion as nonlinearity is increased. A new feature is observed in the middle panel: further increase of nonlinearity destroys the self-trapping and the motion becomes free again. Another new feature appears in the bottom panel for another parameter combination: no self-trapping ever occurs no matter what the value of nonlinearity. Adapted with permission from fig. 3 of Ref. (Kenkre et al., 1995); copyright (1995) by American Physical Society.

4.4 Non-monotonicity and Stationary States

In order to gain a better understanding of the origin of the novel results, let us inspect how the potential $U(p)$ constructed to obtain the time-dependent solution to quadratures changes its shape as the nonlinearity is changed.

4.4.1 Potential Considerations

The form of (4.16) facilitates the integration of $j(p)$ into a function $g(p)$ such that its p-derivative equals $j(p)$ and $g(0) = 0$. It is obviously given by

$$g(p) = \Delta_s \left[\sqrt{(p+1)^2 + (2\Delta_s/\chi)^2} + \sqrt{p-1)^2 + (2\Delta_s/\chi)^2} - 2\sqrt{1 + (2\Delta_s/\chi)^2} \right]. \tag{4.17}$$

The potential expression which, for the simple case of the infinite Δ_s limit (equivalently, the standard DNLSE case) is given by

$$U(p) = (\chi^2/8)\left(p^2 - p_0^2\right)^2 + V(2V - r_0\chi)\left(p^2 - p_0^2\right), \tag{4.18}$$

for arbitrary initial conditions, involves Δ_s and gains interesting new properties. The general expression for arbitrary Δ_s, being tedious, is not shown here but, for the localized case specifically, its peculiar properties are displayed in Fig. 4.4.

The case considered in the plot addresses initial localization on one site ($p(0) = p_0 = 1$) and a saturation parameter Δ_s having the value 6 in units of $2V$. Three values of nonlinearity are considered, characterized by $\chi/2V = 2, 8, 12$. Initial localization with $p(0) = 1$ means that the system starts on the extreme right where the horizontal line intersects the vertical line at $p = 1$. In the lowermost curve (solid), the motion is free as the particle oscillates on both sides of the dimer. The thick blue arrow pointing upwards shows the next higher nonlinearity curve (dotted) for which the nonlinearity is 3 times larger than in the first case. The intersection of the horizontal line with the potential curve clearly shows that self-trapping has occurred as the particle oscillates only between the values 1 and a little over 0.6 only on the right side. The thick blue arrow pointing downward shows the next higher nonlinearity curve (dash-dotted) which is the central curve. We see that the particle motion has *become free again* with oscillations of p between 1 and -1. The potential $U(p)$ thus explains in total clarity the first of the two effects shown in the time-dependent plots of Fig. 4.3. The second effect, *no self-trapping for any nonlinearity*, arises from the Δ_s being so small that self-trapping does not have a chance to occur in the first place. In order to gain a full understanding of it, let us now study the stationary states of the rotational polaron (Wu and Kenkre, 1995).

4.4.2 Stationary States of the Rotational Polaron

Essential insights into the nature of a nonlinear system can be gained by studying its stationary states. To obtain the states, one puts all time derivatives in the dynamical equations such as (4.9) to zero. Let us denote all stationary state values by the suffix ss. From the first and the third of (4.9) we deduce that $q_{ss} = 0$. Because the condition $p^2 + q^2 + r^2 = 1$ must be satisfied at all times and consequently also in the stationary states, we can be certain of

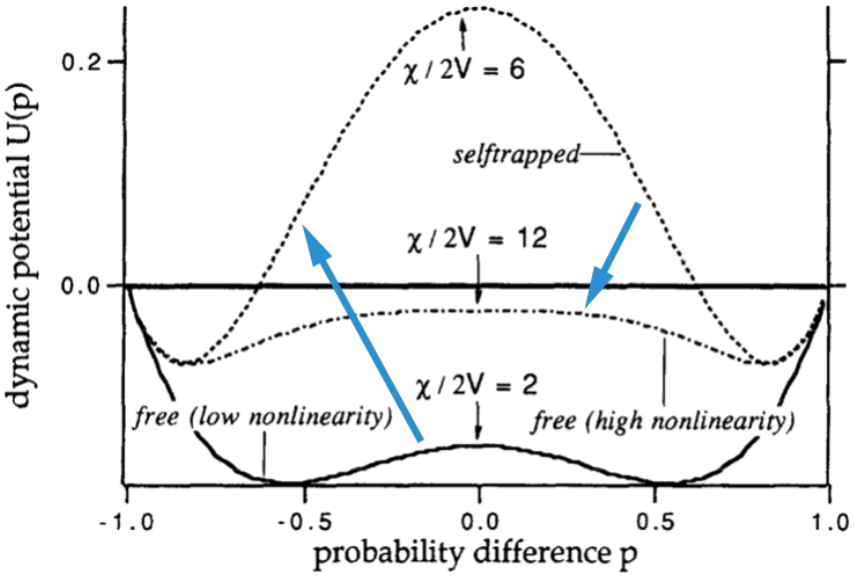

Fig. 4.4 Onset of self-trapping and its eventual disappearance with increase of nonlinearity χ shown through the dependence of the dynamic potential $U(p)$ plotted as a function of the probability difference p in the rotational polaron dimer. The saturation parameter $\Delta_s = 6$ for all three curves shown for respective values 2, 6, and 12 of the nonlinearity ratio $\chi/2V$ as indicated on the plot. Thick arrows show that the increase in nonlinearity takes the system from the lowermost curve (low nonlinearity) that represents free motion to the uppermost curve (intermediate nonlinearity) that signifies self-trapped motion. However, further increase in the nonlinearity frees the quasiparticle. Whether the motion is free or self-trapped is visible from where the horizontal line at the zero of $U(p)$ cuts the potential curve. See text. Modified with permission from fig. 2 of Ref. (Kenkre et al., 1995); copyright (1995) by American Physical Society.

$$r_{ss} = \pm\sqrt{1 - p_{ss}^2},$$

whose substitution in the information obtained from Eq. (4.9b) yields the relation satisfied by p_{ss}:

$$2Vp_{ss} \pm j(p_{ss})\sqrt{1 - p_{ss}^2} = 0, \tag{4.19}$$

where $j(p)$ is available from Eq. (4.15) or (4.16) and directly involves the saturation parameter Δ_s. From the explicit form of $j(p_{ss})$ that we know, for instance from Eq. (4.15), it is clear that $p_{ss} = 0$, the free state, is always a stationary state. It refers to the plus sign in Eq. (4.19). The minus sign case leads to self-trapping.

Not all the stationary states identified via (4.19) are stable. In order to determine their stability, we analyze whether small departures in the Bloch vector components from their stationary states have a tendency to grow as time evolves, thus leading to the destruction of the states, or decay to zero, thereby causing the system to return to them. This standard procedure (see, e.g., (Nicolis, 1995; Strogatz, 2018)), consists

of writing $u = u_{ss} + \epsilon_u$ for $u = p, q, r$ in turn, substituting in the dynamical equations (4.9) and determining whether the departures tend to become larger or to disappear. In the former (latter) case the stationary states are unstable (stable). Examination of the eigenvalues of the dynamical matrix completes the analysis for this purpose in the standard manner.

Wu and Kenkre (1995) showed that the second of the Eqs. (4.9) conveys the most useful part of the required information. As a result of their argument it is found that the departure from the stationary value q_{ss} obeys

$$\frac{d\epsilon_q}{dt} = -2V\epsilon_p \left(1 + r_{ss}(\chi/2V)\left[1 + (\chi/2V)^2\right]^{-3/2}\right),$$

and leads to the stability condition

$$1 + r_{ss}(\chi/2V)\left[1 + (\chi/2\Delta_s)^2\right]^{-3/2} > 0. \tag{4.20}$$

The stationary state with $r_{ss} = 1$ always satisfies[9] this condition. For $r_{ss} = -1$, we have the transition condition

$$(\chi/2V)^2 = \left[1 + (\chi/2\Delta_s)^2\right]^3. \tag{4.21}$$

In the limit that the saturation energy Δ_s is infinitely large, this result reduces to the known simple DNLSE consequence we have explored in the previous Chapters: an increase in the nonlinearity continues to strengthen the self-trapping that occurs at $\chi = 2V$. Generally, we find that the nonlinearity value at the transition is given by the solution of the cubic equation in the parameter $z = (\chi/2V)^2$:

$$z^3 + 3z^2 + \left[3 - (\Delta_s/V)^2\right] z + 1 = 0. \tag{4.22}$$

Equation (4.22) has two real roots, one corresponding to the appearance and the other to the disappearance of the self-trapping stationary states. Start with an infinite saturation energy Δ_s and reduce its value to so that the interesting new features begin to emerge. As Δ_s decreases, the two roots of Eq. (4.22) merge into one another and become imaginary. Once that happens, self-trapping stationary states cannot occur no matter what the value of the nonlinearity χ. From the standard lore of cubic equations (see, e.g., (Abramowitz and Stegun, 1965)), the condition for the disappearance of the stationary states, *whatever* the value of χ relative to $2V$, is

$$\frac{\Delta_s}{V} < \sqrt{\frac{27}{4}}. \tag{4.23}$$

We will encounter an almost identical condition in the next Chapter.

The foregoing analysis has explained satisfactorily both surprises we were hit with in the quadrature solutions of the time dependence in Fig. 4.3: the appearance followed by the disappearance of self-trapping as nonlinearity is increased, and

[9] As can be expected, this is the relatively uninspiring state that is symmetric in the probabilities.

the complete absence of self-trapping for *any* value of the nonlinearity for certain parameter combinations.

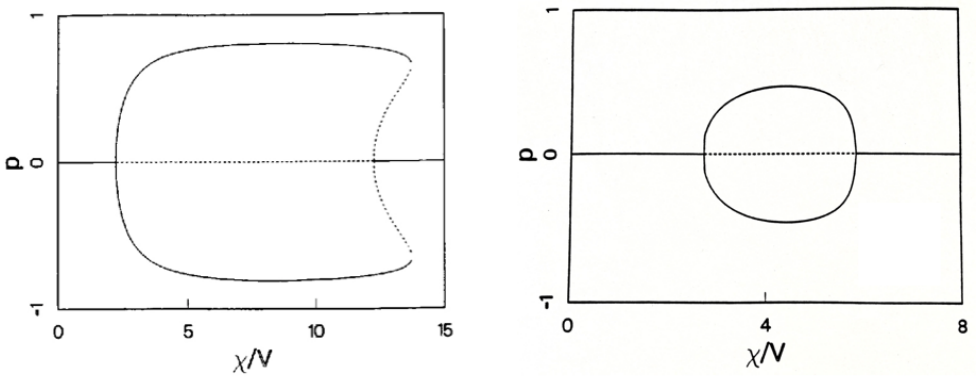

Fig. 4.5 Discontinuous (left panel) as well as continuous (right panel) transitions of the stationary state probability difference in the rotational dimer as a function of the nonlinearity. Solid (dotted) lines represent stable (unstable) states. The free state is the only stationary state for low values of the nonlinearity in both panels. A continuous transition (sometimes referred to as 'second order') is seen in the left panel at a value of χ/V close to 2.5 in the left panel and close to 3 in the right panel. Further intermediate values of the nonlinearity ratio produce self-trapping which means that $p \neq 0$. The two possible values, equal in magnitude but opposite in sign arise from the symmetry of the dimer. In the intermediate region, the free state is stationary but not stable. The remarkable destruction of self-trapping for large nonlinearity in both panels occurs in a discontinuous manner in the left panel with resultant multiple stationary stable states at a given value the nonlinearity but continuously in the right panel. The former means that hysteresis would occur: a different stationary state would be selected by the system according to the direction of the change of nonlinearity. Adapted with permission from fig. 1 of Ref. (Wu and Kenkre, 1995); copyright (1995) by Elsevier Publishing.

Observe that the conjunction of Eqs. (4.15) and (4.19) yields

$$\frac{4V}{\chi}\frac{p}{\sqrt{1-p^2}} = \frac{1+p}{\sqrt{1+(\chi/2\Delta_s)^2(1+p)^2}} - \frac{1-p}{\sqrt{1+(\chi/2\Delta_s)^2(1-p)^2}}. \tag{4.24}$$

Let us now follow Wu and Kenkre (1995) in their demonstration that the self-trapping occurrence and disappearance on increasing nonlinearity can be understood by plotting the functional dependence of the stationary state values of p relative the nonlinearity ratio χ/V for different combinations of the parameters χ and Δ_s relative to $2V$.

Two possible consequences of choosing parameter values are displayed in Fig. 4.5. In both panels, self-trapping occurs as the nonlinearity exceeds a critical value and the onset of the appearance of self-trapping is continuous. Further increases of the nonlinearity merely increase the probability difference at first which means an intensifying of the self-trapping effect. However, beyond another critical value

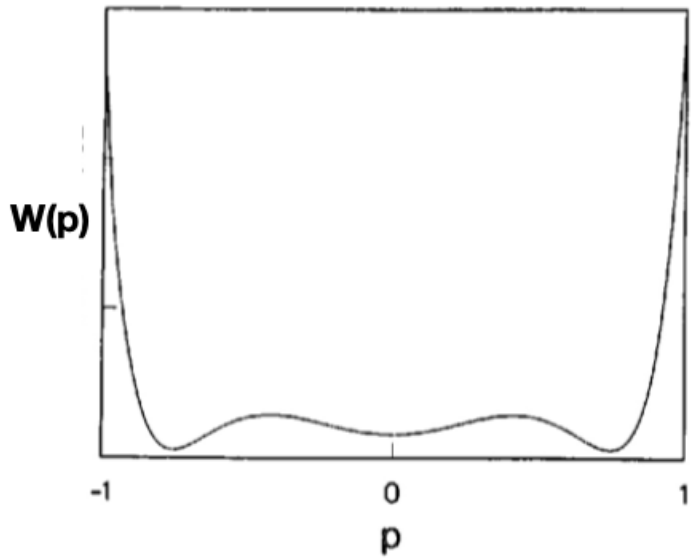

Fig. 4.6 Stationary state potential $W(p)$ as a function of the probability difference p for $\chi/2V$=13 and $\Delta/2V$=4. Multiple stationary states exist, each corresponding to a potential minimum. In the plot as shown, the central stationary state at zero p is metastable as indicated by the central minimum being higher than the side minima. Self-trapping, which is indicated in the plot, is destroyed when the central minimum dips below the other two. Adapted with permission from fig. 2 of Ref. (Wu and Kenkre, 1995); copyright (1995) by Elsevier Publishing.

of χ/V, self-trapping disappears in both panels. This disappearance transition is continuous (second order as it is often called in phase transitions terminology) in the right panel but discontinuous (first order) in the left panel. In the left panel one clearly sees the possibility of hysteresis as in magnetic systems. Multiple possible values of the probability difference occur in this latter case.

It is also straightforward to understand (Wu and Kenkre, 1995) that, as an alternative to the above explanation, one may construct a potential $W(p)$ whose derivative is given by the difference of the left hand and right hand sides of Eq. (4.24) and plotted in Fig. 4.6. Multiple stationary states are seen as minima of $W(p)$ in the plot, free at $p = 0$ and self-trapped at nonzero values of p. Whether the transition is discontinuous or not is decided by whether the central minimum dips below the side minima abruptly resulting in a jump in p_{ss} or not as the nonlinearity ratio is varied. This is determined by the value of Δ_s relative to the other system energies. The precise numerical values used have not been specified in Fig. 4.5 to emphasize the qualitative aspect. The quantitative values are indicated in detail below in the general considerations.

4.4.3 Some General Comments

The nature of the underlying oscillation (rotational rather than translational) and specific forms of interaction (anharmonic and nonlinear rather than harmonic and linear) are the ingredients that led us to the analysis described initially in this Chapter. However, it is important to keep in mind that their role was only to provide a *segway* into the physics that I have wanted to emphasize in this Chapter. The primary motivation here is to investigate the effects of nonlinearity terms in the DNLSE that can have *more complexity than being merely cubic* in the quantum mechanical amplitude.

Two comments, one minor and the other major, need to be made here. The first is that the effects we have seen, saturation energies leading to the destruction of self-trapping for *large* nonlinearity (indeed, to the impossibility of a self-trapping transition away from free motion for *any* nonlinearity for sufficiently small saturation-nonlinearity ratio) can arise for systems vastly different from what we have called the rotational polaron. Consider the case wherein the oscillator potential is proportional to $[1 - \mathrm{sech}(\Lambda x)]/\Lambda^2$ and $f(x), E(x)$ are given by

$$f(x) = \frac{1}{\Lambda}\mathrm{sech}(\Lambda x)\tanh(\Lambda x), \qquad E(x) = \frac{E_0}{\Lambda}\tanh(\Lambda x).$$

It is easy to show that the form of the resulting $h(|c|^2)$ is *precisely* the same as in Eq. (4.14). This is true in spite of the fact that one can hardly imagine rotations among this multitude of hyperbolic functions. The left panel of Fig. 4.2, which was introduced in one of the original publications that explained these matters (Kenkre, 1998b), has as its role, the conveying of the message that, although rotational polarons have helped us understand the physics or mathematics of the material in this Chapter, they are not essential for providing the underlying mechanism. Angular dynamics are dispensable. All that is important is that the dependence of the h-function be nonlinear on the probability in the manner shown. The stark differences in this regard in the shapes seen in the two panels of Fig. 4.2 should make this amply clear.

Indeed, neither sinusoids as in the right panel nor exponentials as in the left (of Fig. 4.2) are essential. The same h-function and identical physical consequences also emerge from Jacobian elliptic functions making up the $f(x), E(x)$! [10] It can be shown that

$$f(x) = \frac{1}{\Lambda}\mathrm{sn}(\Lambda x, k)\mathrm{dn}(\Lambda x, k), \qquad E(x) = \frac{E_0}{\Lambda}\mathrm{sn}(\Lambda x, k),$$

also end up producing the exact same h-function as in Eq. (4.14). The k appearing here is the elliptic modulus. When it equals 0, the elliptic functions become the trigonometric functions whereas when it equals 1, they turn into the corresponding hyperbolic functions. At any k they produce the same h-function.

[10] I realized this early on when I introduced the rotational polaron idea and conveyed it through oral presentations in the ensuing years but put in print the relevant comment only years later in the publication (Amritkar and Kenkre, 1999).

The second comment that is relevant here is, perhaps, even more important. At the beginning of the Chapter, I emphasized that this manner of introducing nonlinear equations of the Schrödinger kind by eliminating an underlying motion has a few objectors (see Chapter 9). I have also pointed out that those objections disappear (as shown in Chapter 9) when time scale disparity arguments are based on considerations of the bath rather than of parts of the system itself. It might detract from the arguments presented here, however, if the (unconvinced) reader were to incorrectly conclude that eliminating the underlying motion, rotational or otherwise, is an essential prerequisite to what we have learned. These novel effects we have discussed are to be expected whenever the nonlinearity in the DNLSE has complexity beyond the mere cubic which is characteristic of Eq. (1.2). Whatever the manner it arises, it is the peculiarities of the h-function in Eq. (4.8), its dependence on the probabilities, that is responsible for the matters discussed. We have seen how the probability dependence of the h-function controls the nature of $j(p)$ and how that controls saturation, destruction of self-trapping, and related effects. I want to invite the reader, therefore, to look upon the contents of this Chapter independently of the precise manner we have so far arrived at the h-function.[11]

4.5 Further Work on the Nature of the Transitions and Additional Examples

Let us now look into further interesting insights that it is possible to gain into our subject of generalized nonlinearities in the DNLSE.[12]

4.5.1 General Considerations

The equivalence of the standard analysis of the dynamical matrix in the linear approximation of the departures from the stationary states (Nicolis, 1995), and of considerations of the potential shown in Fig. 4.6 had already been shown in Wu and Kenkre (1995). If we define a function $G(p)$ to represent the second term of Eq. (4.19),

---

[11] It is to be kept in mind that cubic nonlinearity is known to arise in the Gross-Pitaevski equation for the wave function of Bose-Einstein condensates (see Chapter 10) in a manner that appears immune to the objections that some have raised to the polaron manner of introducing it.

[12] In a highly fruitful collaboration, Ravindra Amritkar, then of the University of Pune and later of the Physical Research Laboratory in Ahmedabad, gained these insights and extended the ideas explained so far in the Chapter in novel directions as in studies of the nature of the transitions, continuous or discontinuous, alternative manners of arriving at the criteria we have studied for the transitions to occur, and phase diagrams for various situations. The collaboration started with his correcting a slightly embarrassing sign error my later coauthors and I had made in one of our examples. It ended up with his masterful analyses into our subject. The details he carried out may be read in Amritkar and Kenkre (1999). Only a brief description is provided here.

$$G(p) = \sqrt{1-p^2}\, j(p), \tag{4.25}$$

we find that obtaining the transition is the same as looking for the intersection of a plot of this $G(p)$ with a straight line of slope $2V$ passing through the origin. This is a standard procedure we all learned in elementary treatments of mean field theories and is illustrated in Fig. 4.7.

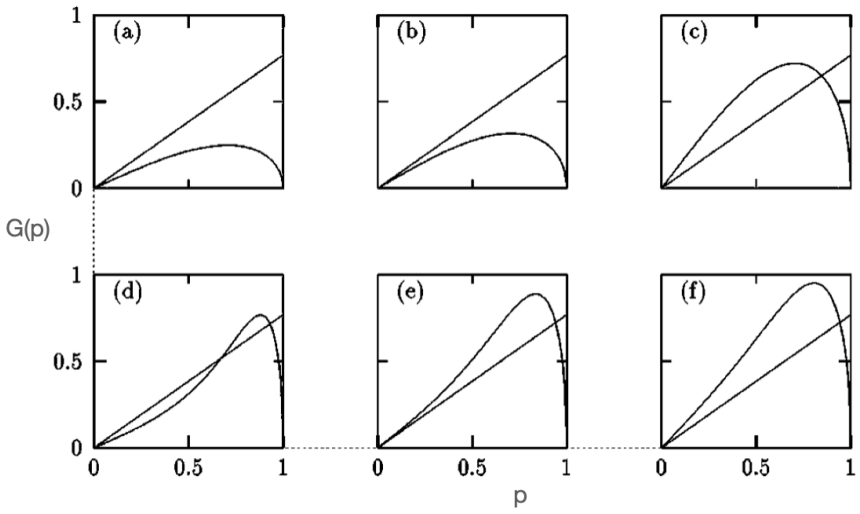

Fig. 4.7 Schematic representation of the graphical procedure to find the self-trapping states. The function $G(p)$ that represents the second term of Eq. (4.19) is plotted along with a straight line of slope $2V$ against the probability difference p. An intersection at a nonzero p shows the stationary state. If the straight line is tangential to the $G(p)$ curve we are on the threshold of the transtion. Both continuous (upper three panels) and discontinuous (lower three panels) are shown. See text. Reprinted with permission from fig. 1 of Ref. (Amritkar and Kenkre, 1999); copyright (1999) by American Physical Society.

Given the relation (4.10) between the h-function and the $j(p)$, we can rewrite the condition for the transition between the stable and unstable free polaron state as given by Amritkar and Kenkre (1999)

$$\left[\frac{dj(p)}{dp}\right]_{p=0} = \left[\frac{dh(y)}{dy}\right]_{y=1/2} = 2V. \tag{4.26}$$

As $[dh(y)/dy]_{y=1/2}$, which we will call from now as $h'(1/2)$ for brevity, increases with the nonlinearity parameter and crosses the value $2V$, we obtain a transition from the free to the self-trapping state. As the nonlinearity increases even further, it is possible for the self-trapping state to be destroyed if $h'(1/2)$ decreases again and falls below the value $2V$. An interesting situation arises if $h'(1/2) < 2V$ for *all*

values of the system parameters. Then the free state always retains its stability and self-trapping tends not to occur at all.

If Fig. 4.7, the plots (a), (b) and (c) refer to what is often called a second-order transition[13] from a free to a self-trapping state. Panel (a) shows the situation in which the free state is stable whereas panel (b) shows the self-trapping transition. Panel (c) where the straight line just touches the $G(p)$-function tangentially, describes the transition.

The point of inflection present in the march of $G(p)$ in the lower three panels of Fig. 4.7 gives rise to *discontinuous* transitions typically called first-order. Panel (d) shows that the free state is stable while panel (f) indicates the self-trapping state being stable. Panel (e) is the transition. By expanding $G(p)$ in a Taylor series for small p to include cubic terms, one obtains the condition for crossover from continuous transition to the discontinuous counterpart (see panels (b) and (e)) as (Amritkar and Kenkre, 1999)

$$\left[\frac{d^3 j(p)}{dp}\right]_{p=0} = \left[\frac{d^3 h(y)}{dy}\right]_{y=1/2} = 24V. \tag{4.27}$$

What this means is, for instance, that continuous transitions occur when both $h'''(1/2) < 24V$ and $h'(1/2) = 2V$. This also means that hysteresis effects may be observed and manipulated if the nonlinearity χ is experimentally controllable. One end of the hysteresis loop would be given by $h'(1/2) = 2V$; the other by the simultaneous solution of $G(p) = 2Vp$ and a new condition (Amritkar and Kenkre, 1999)

$$4V = \left[h'\left(\frac{1+p}{2}\right) + h'\left(\frac{1-p}{2}\right)\right](1-p)^{3/2} \tag{4.28}$$

evaluated at $p = p_{ss}$.[14]

4.5.2 Illustrative Applications for and beyond Rotational Polarons

Let us study the conditions derived above and explore phase diagrams with their help first for the rotational polaron case and then for a few other examples of non-cubic nonlinearities.

For the standard cubic nonlinearity, $h(y) = \chi y$, and Eq. (4.26) gives $\chi = 2V$. The free state becomes and remains unstable as χ is increased beyond $2V$. Condition (4.27) is never satisfied (except for $V = 0$). Consequently, the transition from free to self-trapping state is always continuous.

---

[13] I personally prefer to distinguish the transitions by the usage 'continuous' versus 'discontinuous' to avoid the confusion that might arise from the acceptance by some of the Ehrenfest classification and the appearance of the enthalpy function in that classification.

[14] Needless to say the p's in these stationary state conditions refer to their values p_{ss} in the stationary states as they do in Fig. 4.7 as well.

4.5.2.1 Rotational Polarons

For this system, $h(y)$ is given by Eq. (4.14) and is thus seen to have saturation character. The condition in Eq. (4.26) now gives

$$h'(1/2) = \frac{\chi}{\left[1 + (\chi/2\Delta_s)^2\right]^{3/2}} = 2V, \tag{4.29}$$

which shows that the maximum of $h'(1/2)$ occurs when $\chi/2\Delta_s)^2$ attains the value 2. A significant outcome is that, if the maximum value of $h'(1/2)$ is less than 'particle bandwidth' $2V$, the occurrence of self-trapping is *impossible*. This recovers the remarkable condition (4.23) obtained in Wu and Kenkre (1995) for the impossibility of self-trapping as the ratio of the saturation energy Δ_s to the transfer interaction V becoming less than the square root of 27/4.

Now that we have the general conditions that characterize the crossover from continuous to discontinuous transitions in our tool-bag, we can go beyond the old results of Wu and Kenkre (1995), note that, for $(\Delta_s/V)^2 > 27/4$, Eq. (4.29) has two solutions as χ is varied, and use our criterion in Eq. (4.27).

For this specific rotational polaron case, we obtain

$$h'''(1/2) = 3\chi(\chi/\Delta_s)^2 \left[\frac{\chi(\chi/\Delta_s)^2 - 1}{\left[1 + (\chi/\Delta_s)^2\right]^{7/2}}\right] = 24V. \tag{4.30}$$

With the help of Eqs. (4.29) and (4.30) the crossover from continuous to discontinuous transitions is found for the rotational polaron to occur at, with the notation that $b = \frac{3+\sqrt{21}}{6}$,

$$(\chi/2V)^2 = (1+b)^2, \qquad (\Delta_s/V)^2 = (1+b)^3/b. \tag{4.31}$$

The reader should be now in a position to appreciate the quantitative version of Fig. 4.5 and also a phase diagram on the basis of the analysis presented. These are presented as left and right panels of Fig. 4.8, respectively. The left panel shows a continuous appearance as well as continuous disappearance of self-trapping in curve (a) for $\Delta_s/V = 2.8$ and continuous appearance but disappearance of self-trapping in curve (b) for $\Delta_s/V = 6$. Stable states are shown by solid lines and unstable ones by dashed lines. Hysteresis manipulations are clearly possible for curve (b) as one either increases or decreases the nonlinearity at the higher end. In the right panel, which is a phase diagram in the space of Δ_s and χ plotted relative to V, I and II denote regions of free and self-trapping states, respectively. Solid line in this right panel corresponds to continuous transitions, dashed line to discontinuous transitions and the dash-dot lines on the two sides of the discontinuous (dashed) line mark the limits of hysteresis effects denoted by III.

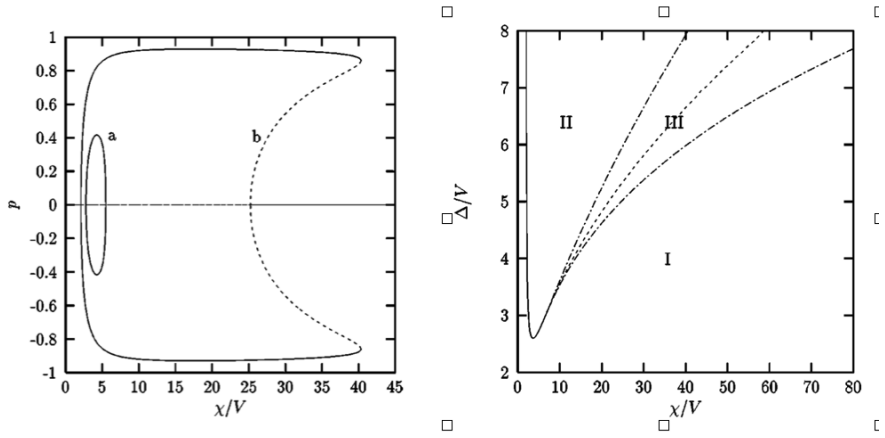

Fig. 4.8 Studies for the rotational polaron. The stationary state values of the probability difference are shown plotted as a function of the nonlinearity ratio χ/V in the left panel and a phase diagram with χ/V as the abscissa and Δ_s/V as the ordinate are shown in the right panel. Adapted with permission from figs. 2 and 3 of Ref. (Amritkar and Kenkre, 1999); copyright (1999) by American Physical Society.

4.5.2.2 Logarithmically Hard and Soft Oscillators

As examples of nonlinear systems which have features similar to the rotational polarons in spite of the fact that they arise from quite different internal mechanisms, let us consider the logarithmic oscillators.[15] If the harmonic oscillations that interact strongly with the moving quantum particle in the context of the standard DNLSE are replaced by oscillations arising from not the quadratic potential but from

$$\mathcal{U}(x) = ka(a - |x|)\left[\ln\left(1 - \frac{|x|}{a}\right) + |x|\right], \tag{4.32}$$

and the particle-oscillation interaction is kept simple in the form $E(x) = E_0 x$, our aim is achieved. Note that $\mathcal{U}(x)$ is defined only for $|x| < a$, it reduces to the harmonic potential $kx^2/2$ for small x/a, and diverges as $|x| \to a$. In the terminology we have used in this chapter,

[15] In collaboration with Christiansen and Jørgensen of Lyngby, I analyzed one such system (Kenkre et al., 1996b) during a sabbatical in Denmark. The reader should find that original publication interesting to examine. An unfortunate sign error that crept into that analysis and affected its terminology was spotted a couple of years later by Amritkar and corrected satisfactorily in (Amritkar and Kenkre, 1999). We use the corrected terminology and expressions in this book.

$$f(x) = -\,ka \ln\left(1 - \frac{|x|}{a}\right) \text{ for } x > 0, \tag{4.33a}$$

$$f(x) = +\,ka \ln\left(1 + \frac{|x|}{a}\right) \text{ for } x < 0. \tag{4.33b}$$

What h-function does this system result in? If we define

$$\chi = G_0 E_0 / k, \quad \chi_0 = E_0 a, \tag{4.34}$$

where G_0 is an appropriate constant, we find

$$h(|c_m|^2) = \chi_0 \left(1 - e^{-\frac{\chi}{\chi_0}|c_m|^2}\right). \tag{4.35}$$

Comparison with Eq. (4.14) reveals that the similarities with the rotational polaron are considerable in spite of the basic potentials being quite different. For nonlinearity small with respect to the saturation energy χ_0, the h-function starts out proportional to the probability $|c_m|^2$ but as the nonlinearity becomes much larger than the saturation energy, h saturates. The parameter χ_0 plays the role of Δ_s.

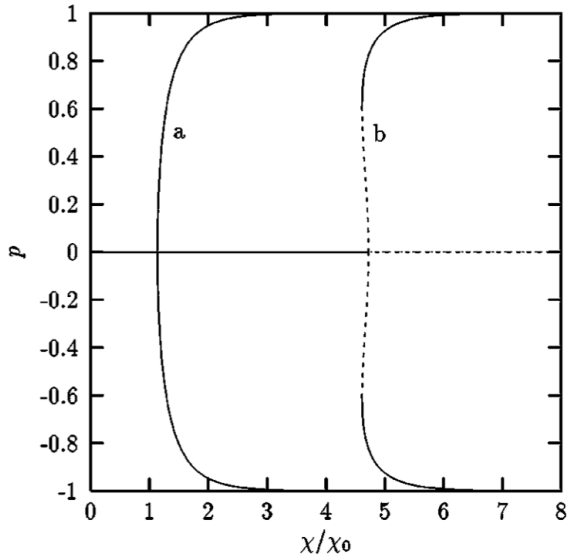

Fig. 4.9 Onset of transitions for the logarithmically hard oscillator. The probability difference in the stationary states p (meaning p_{ss}) is plotted as a function of the nonlinearity ratio that is appropriate to be taken as χ/χ_0. Curves (a) and (b) correspond to $V/\chi_0 = 1$ and 25, respectively, and denote, in turn, a continuous and a discontinuous transition. Stable (unstable) states are shown by solid (dashed) lines. The region of stability of the free state ($p_{ss} = 0$ is shown only for curve (b). Adapted with permission from fig.6 of Ref. (Amritkar and Kenkre, 1999); copyright (1999) by American Physical Society.

The transition to self-trapping happens at

$$h'(1/2) = \chi e^{-\chi/2\chi_0} = 2V. \tag{4.36}$$

By considering the maxima of $h'(1/2)$, one finds that self-trapping does not occur at all if $(\chi_0/V) < e$. For $(\chi_0/V) > e$, two solutions appear as χ is varied. The condition for the passage from continuous to discontinuous nature of transitions is now

$$h'''(1/2) = \frac{\chi^3}{\chi_0^2} e^{-\chi/2\chi_0} = 24V. \tag{4.37}$$

The crossover from continuous to discontinuous transition therefore happens at

$$V/\chi_0 = \sqrt{3}e^{-\sqrt{3}}, \quad \chi/\chi_0 = 2\sqrt{3}.$$

The onset of transitions is shown n Fig. 4.9 where the probability difference in the stationary states p (meaning p_{ss} is plotted as a function of the nonlinearity ratio that is appropriate to be taken as χ/χ_0 for the present system.

Let us now consider, briefly, the logarithmically soft oscillator which has a sign change at some of the places in the appropriate expressions relative to the logarithmically hard counterpart. The oscillations take place in the potential

$$\mathcal{U}(x) = ka(a + |x|)\left[\ln\left(1 + \frac{|x|}{a}\right) - |x|\right], \tag{4.38}$$

with the consequence that we now have

$$f(x) = +\, ka \ln\left(1 + \frac{|x|}{a}\right) \text{ for } x > 0, \tag{4.39a}$$

$$f(x) = -\, ka \ln\left(1 - \frac{|x|}{a}\right) \text{ for } x < 0. \tag{4.39b}$$

We have once again $E(x) = E_0 x$ which results in an h-function given by

$$h(|c_m|^2 = \chi_0 \left(e^{\frac{\chi}{\chi_0}|c_m|^2} - 1\right). \tag{4.40}$$

The condition for the transition to self-trapping is now

$$h'(1/2) = \chi e^{+\chi/2\chi_0} = 2V. \tag{4.41}$$

The great similarity to the corresponding expressions for the logarithmically hard oscillator but with change of sign should be noticed. Observe therefore that now $h'(1/2)$ is a monotonically increasing function of χ and there is consequently a solution for all values of V. This is similar to the case of a harmonic oscillator rather than of the rotational polaron. However, there is a sharp difference. Unlike in the case of a harmonic oscillator, the transition for the logarithmically soft oscillator can be both continuous and discontinuous. The condition that determines this nature of

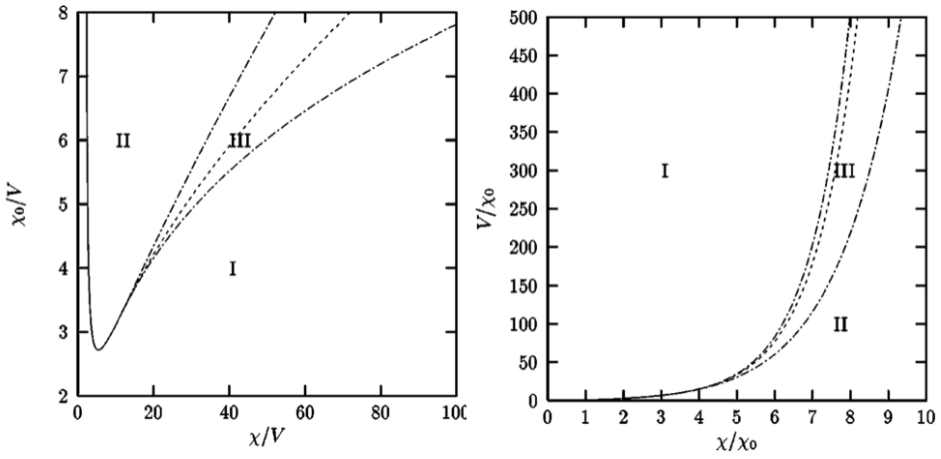

Fig. 4.10 Phase diagram for the logarithmically hard (left panel) and logarithmically soft potentials (right panel) similar to the right panel of Fig. 4.8. Adapted with permission from fig. 4 of Ref. (Amritkar and Kenkre, 1999); copyright (1999) by American Physical Society.

the transition is now

$$h'''(1/2) = \frac{\chi^3}{\chi_0^2} e^{+\chi/2\chi_0} = 24V. \tag{4.42}$$

The result is that the crossover from discontinuous to continuous transitions happens now when

$$V/\chi_0 = \sqrt{3}e^{\sqrt{3}}, \quad \chi/\chi_0 = 2\sqrt{3}.$$

The phase diagrams for both logarithmical oscillators are displayed in Fig. 4.10 side by side on the basis of these considerations. Once again, as in the right panel of Fig. 4.8 which is a phase diagram for the rotational polaron, solid lines denote continuous transitions, a dashed line a discontinuous transition, and the dash-dot lines limit the region of hysteresis effects marked by III. Free states are in the region marked I and self-trapped states in that marked II.

Although the expressions for all conditions are nearly identical for the two systems, the change of sign makes all the difference.

4.6 Chapter 4 in Summary

Novel effects that arise for nonlinearities that interact with the quantum mechanical shuttling of excitations with greater complexity than a simple cubic expression might have were the subject of this Chapter. It was shown that such complex nonlinearities

appear naturally through the feedback effect when one eliminates oscillations in the standard manner for *rotational* polarons when the oscillation involved is in an angular coordinate. The richer forms of the DNLSE that arose displayed saturation effects. One such effect was that increase of nonlinearity caused self-trapping to occur for intermediate values of nonlinearity but that further increases destroyed the self-trapping. Another was that for certain values of the ratio of the saturation energy to the transfer interaction, self-trapping *never* occurred, free states being always stable. Yet another effect was the existence of both discontinuous and continuous transitions. A detailed study of conditions for these effects to be manifested in terms of relative values of the system parameters was presented and applied to several systems including logarithmic oscillators.

Chapter 5
Static Energy Mismatch in the Nonlinear Dimer: Nondegeneracy

Let us return in this Chapter to a DNLSE dimer with cubic nonlinearity, thus no longer addressing the harmonic origin (or not) of an underlying motion but complicate the system by considering *nondegeneracy*, i.e., a lack of energetic resonance between the two sites. In other words, we ask here what happens if there is a static energy mismatch in addition to the dynamic mismatch provided by the nonlinearity.

5.1 Evolution of the Nondegenerate Nonlinear Dimer

Given that we have understood, in Chapters 2 and 3, the primary behavior of the degenerate nonlinear dimer stemming from the *dynamic* mismatch in energy, let us compare how the time evolution of its nondegenerate counterpart is different, and richer, as a result of the static energy mismatch present in addition to the dynamic mismatch.

The amplitude equations of motion, if site energies at the two dimer sites 1 and 2 are not equal to each other but E_1 and E_2, respectively, are

$$\frac{dc_1}{dt} = -iVc_2 - i\left(E_1 - \chi|c_1|^2\right)c_1,$$
$$\frac{dc_2}{dt} = -iVc_1 - i\left(E_2 - \chi|c_2|^2\right)c_2,$$

and lead, with the definition $\Delta = E_1 - E_2$, to the nonlinear Bloch vector equations

$$\frac{dp}{dt} = 2Vq, \tag{5.1a}$$
$$\frac{dq}{dt} = -2Vp - (\chi p - \Delta)r, \tag{5.1b}$$
$$\frac{dr}{dt} = (\chi p - \Delta)q. \tag{5.1c}$$

These are identical to the degenerate (nonlinear) counterparts except for the replacement of χp in them by $\chi p - \Delta$, signifying that the site energy difference is, in general, simply the sum of the dynamic and static contributions. Notice that the evolution equations for the linear dimer with a static energy mismatch Δ are obtained from Eqs. (5.1) by putting $\chi = 0$. Let us initially restrict the analysis to the localized initial condition $p_0 = 1$.

The obvious questions to ask are how the self-trapping transition that we saw in the degenerate nonlinear dimer is modified by the presence of the *static energy mismatch* Δ in the nondegenerate dimer, and how the time dependence changes from the simple cn-dn evolution we have examined in Chapter 2 for $\Delta = 0$.

Before we explain the analytic procedures to arrive at the solutions, we display graphically the answer to these two questions by making use of those solutions. To answer the second question, how does the time dependence of the probability difference in the nondegenerate dimer at and near the self-trapping transition compare to that in the degenerate counterpart, we show Fig. 5.1. The left panel shows time

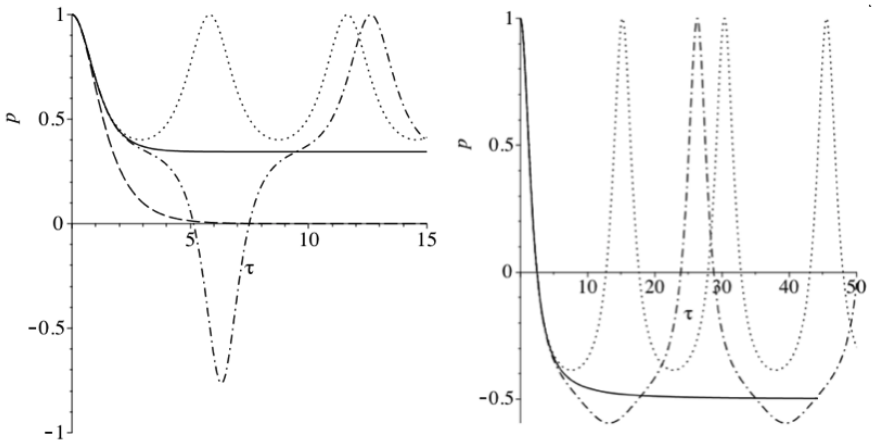

Fig. 5.1 Time dependence of the probability difference p in the nondegenerate nonlinear dimer at and near the self-trapping transition that appears similar (left panel) and quite dissimilar (right panel) relative to the degenerate case. Displayed is the plot of p versus τ which is the time t in units of $1/2V$. See text.

evolution that is largely similar to what is seen in a *degenerate* nonlinear dimer (see, e.g., Fig. 2.1), whereas the right panel depicts evolution that shows substantial differences relative to the degenerate case. The static energy mismatch $\delta = \Delta/2V$ equals 3/4 in the left panel. The solid line depicts the self-trapping transition in the nondegenerate case. It corresponds to the nonlinearity ratio $\chi/4V = 1.623$ while the curves of $p(t)$ *near, but not at,* the transition are for $\chi/4V = 1.621$ (dash-dotted)

on the free side of the transition and $\chi/4V = 1.627$ (dotted) on the trapped side, respectively. To emphasize the qualitative similarity to the degenerate case ($\delta = 0$) that we know from Chapter 2, we have included its evolution at the self-trapping transition (dashed line). We see that $p(t)$ vanishes at long times. The saturation value at the transition (solid line) of the nondegenerate dimer on the other hand, is not zero but is appropriate to the specific value of the static energy mismatch. The qualitative evolution (shape of the curve) is, however, the same. The time dependence on the two sides of the transition looks a bit different, i.e., p is not symmetrical above and below the transition line. Despite these slight effects of the static energy mismatch, it is visually clear that the evolution is quite similar to that in the degenerate case.

By contrast, the right panel of Fig. 5.1 illustrates considerable dissimilarity of the nondegenerate situation relative to the degenerate counterpart. The value of $\delta = \Delta/2V$ here happens to be $-1/\sqrt{27}$ and the nonlinearity $\chi/4V$ at the transition is $4/\sqrt{27}$. The range of p just above the transition and just below it are not very different from each other unlike in the case of the left panel where they are substantially different. What this means is that, in contrast to the case treated in the left panel, the values the probability difference roams over do not change much from one side of the transition to the other. The shapes of the curves seem markedly different in the free versus trapped regions in the right panel. The conclusion to be drawn is that the variation of shape at the transition can be profoundly different as a result of the static energy mismatch.

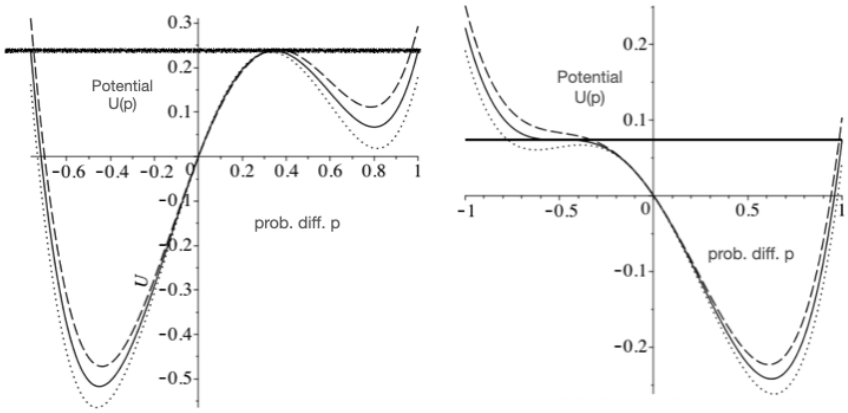

Fig. 5.2 The dependence on the probability difference p of the potentials $U(p)$ corresponding, respectively, to the left and right panels of Fig. 5.1. The solid line in either case depicts the transition case.

5.1.1 Potential Shapes and Physical Arguments to Gain Insight into the Time Dependence

The reader will not be surprised that the procedure used to find analytic solutions for the evolution in the nondegenerate dimer involves a p-potential in a way similar to Eq. (1.10) relevant to the degenerate case except that here the expression is more complicated. In order to gain some insight into the reasons for the changes shown in the left versus the right panels of Fig. 5.1, let us plot that potential $U(p)$ as done for the degenerate case of Fig. 1.2. The precise expression for $U(p)$ may be found in Eq. (5.4).

We depict the transition situation by a solid line and represent values of the nonlinearity slightly different from its critical (transition) value by the dashed and dotted lines in each case. The initial value of the probability difference is $p_0 = 1$. We start therefore at $p = 1$ at the right end of each of the two panels in Fig. 1.2 and draw a vertical line upwards to see where on the potential curve the system lies initially. From the intersection with the transition curve in both panels we draw a horizontal line (thick trace). It is tangential to the potential curve at the transition representing the fact that it takes infinite time for the system to cross over the maximum of the potential in the left panel and over its inflection region in the right panel. The fact that the potential curve in Fig. 1.2 exhibits an extremum in the left panel but does not in the right panel is responsible for the difference in the observed time dependence shapes.

In a degenerate nonlinear dimer, the site energies are equal but as soon as one of the two sites is occupied by the quantum particle, the nonlinearity causes the energy at that site to be *effectively* lowered by the amount χ (For simplicity we take χ to be positive throughout our analysis.) As intersite transfer begins, the decrease in the probability of occupation that the transfer causes results in an increase in the effective site energy at the initial site. The transfer also causes a decrease in the effective energy of the other site as the probability of that site increases. The transfer process decreases in this manner the effective difference in the site energies. If this results in bringing the sites in resonance, the process can happen in reverse in that the energy of the initially unoccupied site can become less than that of the other site. Transfer that is overall resonant can then occur. This happens for sufficiently small (but non-zero) values of χ. If χ assumes its critical value ($4V$), the process described fails to bring the two sites in effective resonance, the energy of the initially occupied site always remaining less than (or equal to) that of the initially unoccupied site. This leads to the dynamic energy mismatch playing the same role as would a static energy mismatch. That is how self-trapping occurs.

What is different in a *non*degenerate dimer? If $\Delta = E_1 - E_2 > 0$, the energy of the initially occupied site (always labeled as 1) starts out being larger than that of the other site before occupation. The dynamic effect of the nonlinearity can bring the two sites energetically closer. If the reverse is true, i.e., if the energy of the initially occupied site starts out less, i.e., if $\Delta < 0$, would the effect of the nonlinearity be to pull the two sites energetically further apart and thus to make it impossible to have a transition as one increases the nonlinearity? Superficial considerations might tend to

make one think so but it is not to be forgotten that the complexities of the dynamics as transfer occurs may invalidate this process. Fortunately, we have exact analytic solutions with the help of which we can know for certain. We now develop them and apply them to study systematically the effects of lack of resonance.

5.2 Specifics of the Weierstrass Calculation

The standard Weierstrass method of analysis starts with the solution of r in terms of p in the Bloch vector Equation (5.1c) and substitution in (5.1b). This allows one to derive a closed second order equation in p as in the case of the degenerate dimer. Its right hand side is a fourth-order polynomial in p as in the degenerate case but with non-vanishing terms for the zeroth and second power of p:

$$\frac{d^2p}{d\tau^2} = -2\gamma_0 - 6\gamma_1 p - 6\gamma_2 p^2 - 2\gamma_3 p^3. \tag{5.2}$$

The coefficients are given by, with $k_0 = \chi/4V$ for brevity,

$$\gamma_0 = \delta\left(p_0^2 k_0 - p_0\delta - r_0\right)/2, \tag{5.3a}$$

$$\gamma_1 = \left(-2p_0^2k_0^2 + 2k_0r_0 + 1 + 2p_0\delta k_0 + \delta^2\right)/6, \tag{5.3b}$$

$$\gamma_2 = -\delta k_0/2, \tag{5.3c}$$

$$\gamma_3 = k_0^2. \tag{5.3d}$$

They are dependent, as they should be, on both the system parameters δ and k_0 and the initial conditions p_0 and r_0.[1] The standard 'energy method' well-known in classical mechanics, involving a multiplication by $dp/d\tau$, leads to the p-potential $U(p)$ as in the case of the degenerate nonlinear dimer, Eq. (1.2):

$$U(p) = 4\gamma_0 p + 6\gamma_1 p^2 + 4\gamma_2 p^3 + \gamma_3 p^4. \tag{5.4}$$

In the use of the 'energy method' for the solution of differential equations, the result

$$\left(\frac{dp}{d\tau}\right)^2 = \left(\frac{dp}{d\tau}\right)^2_{\tau=0} + U(p_0) - U(p) = f(p) \tag{5.5}$$

appears naturally. The second equality defines $f(p)$ as the right side of the equation. Observe that $dp/d\tau$ is nothing but q, the second component of the Bloch vector. Equation (5.5) is integrated from the initial value p_0 to the 'current' value p in two segments,

[1] They are determined by q_0 as well, of course. But we know that only two of the components of the Bloch vector can be independent quantities since the squares of all three must add up to 1.

$$\tau = \int_{p_0}^{p} \frac{dp'}{\sqrt{f(p')}} = \int_{p_0}^{p_1} \frac{dp'}{\sqrt{f(p')}} + \int_{p_1}^{p} \frac{dp'}{\sqrt{f(p')}} \tag{5.6}$$

where p_1 satisfies $f(p_1) = 0$. The "representative particle" that moves in the potential U with $p(t)$ as its time-dependent "displacement", reverses its direction at $p = p_1$. If we call the first term on the extreme right hand side τ_1, our problem is solved to quadratures as

$$\tau - \tau_1 = \int_{p_1}^{p} \frac{dp'}{\sqrt{f(p')}}. \tag{5.7}$$

What one is really looking for, however, is some known special function that can be identified in some form in the integral of the right hand side. This was easy for the simple pendulum discussed in Chapter 1 where we recognized an integral that had a similar form related to the expression for the inverse sinusoid. For the physical pendulum, equivalently the degenerate nonlinear dimer, we did not look at the quadrature form; instead the differential equation obeyed by the Jacobian elliptic functions had the same aspect as that obeyed by the pendulum velocity or by the probability difference, In the bacterial problem analyzed in Chapter 1, we got a taste of the difficult manipulations that are necessary to make in order to force known differential equations into the form we encounter in the problem we solve.

The present problem straddles us with a still higher level of difficulty. Inspection of Eq. (5.7) with (5.5) suggests the use of the Weierstrass function but not directly. It is the reciprocal of a shifted form of it that does the trick.

If we define the quantities g_2 and g_3 in terms of the systems parameters and initial conditions through

$$g_2 = 3\gamma_1^2 - 4\gamma_0\gamma_2 - \gamma_3 U(p_1), \tag{5.8a}$$

$$g_3 = \gamma_1^3 + \gamma_0^2\gamma_3 - 2\gamma_0\gamma_1\gamma_2 + (\gamma_1\gamma_3 - \gamma_2^2)U(p_1), \tag{5.8b}$$

and introduce the symbols $U_1' = dU/dp|_{p=p_1}$ and $U_1'' = d^2U/dp^2|_{p=p_1}$ to denote the potential derivatives, the theory of Weierstrass functions allows us to write the solution of Eq. (5.5) explicitly and analytically as[2]

$$p(\tau) = p_1 - \frac{6U_1'}{24\wp(\tau - \tau_1; g_2, g_3) + U_1''}. \tag{5.9}$$

If you, the reader, are already well initiated in the properties of Weierstrass elliptic functions, you will notice that the explicit result (5.9) connecting the time evolution of the probability difference to the Weierstrass function may be equivalently said to come from defining from $p(\tau)$ the quantity

$$\sigma(p) = -\frac{1}{4}\left(\frac{1}{p - p_1}\left.\frac{dU}{dp}\right|_{p=p_1} + \frac{1}{6}\left.\frac{d^2U}{\mathrm{d}p^2}\right|_{p=p_1}\right).$$

[2] You may or may not find it significant that, although we have expressed the probability difference in terms of the Weierstrass function $\wp$, the latter has had to be shifted by a constant and put in the denominator before one can identify it as being closely related to $p(\tau)$!

This is so because this transformation leads on the one hand to Eq. (5.7) taking the form

$$\tau - \tau_1 = \int_{\sigma}^{\infty} \frac{d\sigma'}{\sqrt{4\sigma'^3 - g_2\sigma' - g3}}, \tag{5.10}$$

and on the other to our being able to identify $\sigma(\tau)$ as the Weierstrass function,

$$\sigma(\tau) = \wp(\tau - \tau_1; g_2, g_3).$$

It is also known that σ obeys the cubic equation

$$\sigma^3 - g_2\sigma - g_3 = (\sigma - e_1)(\sigma - e_2)(\sigma - e_3) = 0. \tag{5.11}$$

The roots e_i of the equation ($i = 1, 2, 3$) will be of particular calculational convenience for us further into our analysis.

Thus, in summary, we see that the system parameters $\delta = \Delta/2V$ and $k_0 = \chi/4V$ of the nonlinear nondegenerate dimer, along with the initial conditions p_0 and r_0, determine[3] the γ's in Eq. (5.3). The g's are known from Eq. (5.8). Substitution into Eq. (5.9) gives us then the complete evolution of nondegenerate dimer. Notice that the solution provided is now for *arbitrary* initial conditions involving any extent of delocalization and phases.

The first instance of an analytic study of the nonlinear nondegenerate dimer that I am aware of is by George Tsironis.[4] Similar, but not identical, calculations emerged independently, first in Andersen's work that he reported in Bull. Am. Phys. Soc. 34, 967 (1989), see also (Andersen and Kenkre, 1993a,b) on spatially extended nonlinear systems such as the trimer and the globally connected N-mer, as well as in nonlinear trapping work performed by Kuś (Kenkre and Kuś , 1992). I recommend to the reader two fine articles by Tsironis on this subject (Tsironis, 1993; Molina and Tsironis, 1995). While they pursue the same system, the nondegenerate nonlinear dimer, as the topic of the present Chapter, they emphasize different matters relative to what is described here and, in several cases, predate the matters touched upon here. For general background on Weierstrass matters, I suggest to the reader a lucid exposition by Brizard (2009) as well as the standard treatments by Abramowitz and Stegun (1965) and Byrd and Friedman (1971).

---

[3] As has been mentioned several times, the condition $p_0^2 + q_0^2 + r_0^2 = 1$ determines the third of the Bloch vector values once the other two are specified and that we are considering only pure states that allow us to use this identity.

[4] He was the first of the Ph. D. students of mine to join me on the adventures whose retelling constitutes this book. He undertook the study of the nondegenerate dimer at my suggestion to extend the degenerate version that had been investigated in (Kenkre and Campbell, 1986; Kenkre et al., 1987; Kenkre and Tsironis, 1987). George showed that the investigation called for the introduction of Weierstrass elliptic functions into the analysis. We included his work in his dissertation but George and I did not publish or exploit the analysis further at that time. He went on to make many outstanding contributions to the study of nonlinear systems, and in 1996 was the recipient of the Stephanos Pnevmatikos award.

5.3 Analytic Results in terms of Jacobian Functions

The study of the nonlinear nondegenerate dimer presented in the foregoing sections of this chapter has been based on exact expressions obtained for the time evolution of the probability difference $p(t) = P_1(t) - P_2(t)$ for initial occupation of site 1 expressed as a function of the dimensionless time, $\tau = 2Vt$. Treatment in terms of Weierstrass functions has been available since Tsironis' study in his dissertation (Tsironis, 1993; Andersen and Kenkre, 1993b,a; Kenkre and Kuś, 1992; Molina and Tsironis, 1995). However, Jacobian functions are more familiar than the former (and with more intimate significance) to the physicist. It has been recognized (Scott, 1990; Scott and Christiansen, 1990; Tsironis, 1993) and often stated, that an equivalent Jacobian function analysis is possible but no expressions and derivations using them have been offered, to the best of my knowledge. A special feature of the presentation I provide in this Chapter is such an explicit analysis.[5]

5.3.1 Jacobian Results

Equation (5.9) can be used directly for displaying the probability difference and studying its consequences analytically. However, Weierstrass functions happen to be less familiar to the physicist than Jacobian elliptic functions which, as we have seen in Chapter 1, can be looked upon as natural intermediates between oscillating trigonometric functions and non-oscillating hyperbolic counterparts. Furthermore, fewer software programs make the Weierstrass functions easily available to the user.[6] For this reason, I have been wishing for a long time to have available the analytics of this nonlinear system in terms of Jacobian functions. This we do here with the help of one of several known results (Abramowitz and Stegun, 1965; Byrd and Friedman, 1971) that connect the two kinds of elliptic functions:

$$\wp(u; g_2, g_3) = e_3 + \frac{e_1 - e_3}{\mathrm{sn}^2\left(u\sqrt{e_1 - e_3}, k_1\right)}, \tag{5.12}$$

The e's in Eq. (5.12) are the roots of the cubic equation (5.11) that we have referred to in the earlier section.

Let us focus on the specific quantities $p(t)$, its period of oscillation, and its average over a cycle. Direct substitution of the correspondence relation, Eq. (5.12), in Eq.

---

[5] I am indebted to John Andersen for the close collaboration that has led to that analysis. His work with me has included an investigation to stationary states using methods developed by Honglu Wu in his Ph.D. dissertation (1990), a generalization of Eq. (5.2) to deal with arbitrary quantum phases in the initial state, and the application of both these to the dynamics of Bose-Einstein condensates (Andersen, Raghavan and Kenkre, *Quantum Oscillations between weakly coupled Bose-Einstein Condensates: Evolution in a Non-degenerate Double Well*, 2021, preprint.)

[6] For instance, at the time of this writing, the Weierstrass function can be called simply via a command in Mathematica and Maple but not in Matlab, except, I am told, through the acquisition of an add-on package.

(5.9) yields the solution in terms of Jacobian functions. Explicitly,

$$\frac{p(\tau)}{p_1} = \frac{1 + (a-b)\,\mathrm{sn}^2\left[\sqrt{e_1 - e_3}\,(\tau - \tau_1)\,, k_1\right]}{1 + a\,\mathrm{sn}^2\left[\sqrt{e_1 - e_3}\,(\tau - \tau_1)\,, k_1\right]}, \tag{5.13}$$

with the understanding that the elliptic modulus is given by

$$k_1^2 = \frac{e_2 - e_3}{e_1 - e_3}, \tag{5.14}$$

and the coefficients a and b are to be obtained through

$$a = \frac{e_3 + (U_1''/24)}{e_1 - e_3}, \tag{5.15a}$$

$$b = \frac{(U_1'/4)}{p_1(e_1 - e_3)}, \tag{5.15b}$$

by calculating potential derivatives from Eq. (5.4).

The period T of the solution is given by the simple expression

$$T = \frac{2K(k_1)}{\sqrt{e_1 - e_3}} \tag{5.16}$$

if g_3 in Eq. (5.8) is positive and leads to corresponding simplifications. However, in general, it is necessary to use a more involved procedure[7] with the help of which we arrive at the general expression for the period:

$$T = \frac{2K(k_2)}{(48e_1^2 - 4g_2)^{1/4}}. \tag{5.17}$$

Here,

$$k_2^2 = \frac{1}{2}\left[1 - \frac{3e_1}{(12e_1^2 - g_2)^{1/2}}\right], \tag{5.18}$$

and it should be noticed that the full g_2 has to be used, rather than simply the root e_3 for the evaluation of the elliptic modulus. The quantity e_1 in Eqs. (5.17) and (5.18) is the largest real root of the three e_i.

In order to calculate $\langle p \rangle$, the average of the probability difference over a cycle, let us introduce the incomplete elliptic integral of the third kind[8] via its definition

---

[7] Relation (18.9.8,) column $\Delta < 0$, in the notation of Abramowitz and Stegun (1965) corresponds to this situation.

[8] It is amusing that in a book I published as recently as a few months back (Kenkre, 2021), I wrote that a (complete) elliptic integral of the third kind had appeared in my own research only once, courtesy of Yiu-man Wong, one of the earliest of my Ph. D. students. I must now confess lightening has struck again, this time while I worked with John Andersen. Beware of the rare beast! It can chase you in your old age and appear unannounced, bounding after you even in its *incomplete* garb.

$$\Pi(n;u,k) = \int_0^u dw\, \frac{1}{1 - n\,\mathrm{sn}^2(w,k)}.$$

Manipulation of Eq. (5.13) before the evaluation of the average of a cycle, assisted by the use of an identity such as (17.2.16) in Abramowitz and Stegun (1965)), then yields directly a highly useful analytic expression of the average,

$$\frac{\langle p\rangle}{p_1} = \frac{\langle p(\tau)\rangle}{p_1} = 1 - \frac{b}{a}\left(1 - \frac{\Pi(-a;\beta,k_1)}{\beta}\right). \tag{5.19}$$

The quantity β introduced here is not to be confused with any inverse temperature-like entity you might encounter in your analysis but is simply proportional to the period T given by Eq, (5.17):

$$\beta = T\frac{\sqrt{e_1 - e_3}}{2} = \sqrt{2}(12e_1^2 - g_2)^{-1/4}\mathrm{K}(k_2)\frac{\sqrt{e_1 - e_3}}{2}.$$

When the simpler expression for the period, Eq. (5.16), holds, i.e., for $g_3 > 0$, the quantity β is given by $K(k_1)$. In that simpler case, the average of the probability difference can be expressed in terms of the more straightforward *complete* elliptic integral of the third kind:

$$\frac{\langle p\rangle}{p_1} = 1 - \frac{b}{a}\left(1 - \frac{\Pi(-a,k_1)}{\mathrm{K}(k_1)}\right), \tag{5.20}$$

the definition of the complete integral being

$$\Pi(n,k) = \int_0^1 \frac{dt}{\left(1 - nt^2\right)\sqrt{(1-t^2)(1-k^2t^2)}} = \int_0^{K(k)} \frac{dw}{1 - n\,\mathrm{sn}^2(w,k)}.$$

The general *Jacobian* form expression and the consequent results (5.13)-(5.20) that we have obtained, including the relations via (incomplete and complete) elliptic integrals of the third kind, are especially useful. Displayed probably for the first time in this book, they allow one to perform systematic studies of the nondegenerate dimer as will be discussed in the following sections.

5.3.2 Reduction to the Case of the Degenerate Dimer

Expressions for the probability difference in the case of the nonlinear nondegenerate dimer, even when expressed in terms of Jacobian elliptic functions in the form of (5.13), have an aspect that appears quite different from the degenerate case. Equation (5.13) involves the ratio of two expressions each containing as a term the square of an sn function, whereas the degenerate case is simply a single cn (equivalently a dn) function. It is instructive to understand how the simplification occurs when the static energy mismatch is put equal to zero in the non degenerate dimer expressions. For

the sake of simplicity, let us restrict the calculation to the localized initial condition. Taking thus $\delta = 0$, $p_1 = p_0 = 1$, the potential $U(p)$ is simplified to

$$U(p) = -(2k_0^2 - 1)p^2 + k_0^2 p^4. \tag{5.21}$$

The initial values of the potential and the first two derivatives are, respectively, $1-k_0^2$, 2, and $8k_0^2 + 2$. The roots e_i are calculated to be

$$e_1 = \frac{k_0^2}{6} - \frac{1}{12} + \frac{\sqrt{k_0^4 - k_0^2}}{2}, \tag{5.22a}$$

$$e_2 = \frac{k_0^2}{6} - \frac{1}{12} - \frac{\sqrt{k_0^4 - k_0^2}}{2}, \tag{5.22b}$$

$$e_3 = \frac{1}{6} - \frac{k_0^2}{3}. \tag{5.22c}$$

Their substitution into Eq. (5.14) leads to an expression for k_1 that is not equal to $k_0 = \chi/4V$, the expected result for the degenerate nonlinear dimer. This is so because k_1 is relevant to the sn function in Eq. (5.13) rather than to the cn or dn function that describes the probability difference in the degenerate case. Note also that the coefficients a, b, given by Eq. (5.15) that determine the expression for $p(\tau)$ that is provided in Eq. (5.13) simplifies in the degenerate case to

$$a = b/2 = k_1,$$

yielding

$$p(\tau) = \frac{1 - k_1 \mathrm{sn}^2\,(u, k_1)}{1 + k_1 \mathrm{sn}^2\,(u, k_1)}. \tag{5.23}$$

The Landen transformation detailed in Chapter 1 allows the reexpression of a Jacobian elliptic function in terms of another with a different elliptic modulus. In particular,

$$\mathrm{dn}(t, \kappa) = \frac{\mathrm{dn}^2(u, k) + k - 1}{1 + k + \mathrm{dn}^2(u, k)} = \frac{1 - k\mathrm{sn}^2(u, k)}{1 + k\mathrm{sn}^2(u, k)}$$

with $t = u(1 + k)$ and $\kappa = 2\sqrt{k}/(1 + k)$. Substitution turns the somewhat unfamiliar form for $p(\tau)$ obtained in Eq. (5.23) into the familiar form

$$p(t) = \mathrm{dn}\left(\frac{\chi t}{2}, \frac{4V}{\chi}\right)$$

that we know well for the degenerate nonlinear dimer treated in Chapters 2 and 3. This analysis in the limit $\delta = 0$ should reinforce confidence in the Jacobian elliptic expressions that we have derived.

Before undertaking a study of the time evolution of the nondegenerate dimer with the help of the expressions shown, it might be useful to detail the steps involved. The

program thus follows these steps in succession:

1. From the system parameters $\Delta = E_1 - E_2$, V and χ, respectively the static energy mismatch, the intersite transfer interaction and the nonlinearity, as well as the initial conditions, for instance p_0 and r_0, the two independent components of the Bloch vector, obtain the coefficients γ through Eqs. (5.3).

2. Construct the p-potential through Eq. (5.4) and obtain its value at $p(0)$ and, with its help, calculate p_1 at which there is direction reversal in the motion of the representative point by putting the right hand side of Eq. (5.5) equal to zero. Obtain the time shift τ_1 as the definite integral that constitutes the first term on the extreme right side of Eq. (5.6).

3. Calculate from Eq. (5.8) g_2 and g_3 from the γ coefficients evaluated in step 1 and the potential value at $p = p_1$ evaluated in step 2.

The solution for the probability difference $p(\tau)$ is then given in Eq. (5.9) in terms of the calculated quantities in steps 2 and 3 and from the values of the first two p-derivatives of the potential $U(p)$ at $p = p_1$. This is the Weierstrass solution used in the literature earlier. A fourth step that we provide in this book gives greater analytical convenience than has been available in the literature. It may be had from the Jacobian elliptic sn-function solution given here. For that additional step that bypasses the Weierstrass function,

4. Find the roots e_1 , e_2 and e_3 of Eq. (5.11) and obtain the probability difference $p(\tau)$ from Eq. (5.13), the elliptic modulus k_1 being given by Eq. (5.14). Particularly useful results on which we have based our analysis in the Chapter are then available as Eqs. (5.19).

5.4 Systematic Study of the Effect of Nondegeneracy

Let us use the analytic solutions we have obtained to focus on the observable $\langle p \rangle$, i.e., the average of the probability difference over a cycle to produce a plot against the nonlinearity ratio $\chi/4V$ for different values of the static energy mismatch. I have come across a remark in the literature where analysis with the help of this average observable has been implied to be in some sense inferior to the full time dependence of $p(t)$. This misses the power of integrated observables that assist in our understanding of the physics by probing the *overall effect* of the entire time dependence rather than the separate value at each instant of time.[9] The quantum yield in exciton capture investigations in the field of sensitized luminescence is a well-known example of such an integrated observable. See, e.g., (Kenkre, 2021) for a discussion.

[9] Our analysis also provides, easily, the computation of the instantaneous time evolution of any quantity in the system, if desired. This should be clear from Fig. 5.1.

In other words, what we are doing here is extending systematically the left plot of Fig. 2.2 that was made for the degenerate nonlinear dimer to various cases of static mismatch for the nondegenerate system, learning about features of the transition for each case. We will also inspect the extension of the right side of the plot of Fig. 2.2 in one instance. Denoting the static mismatch by the ratio $\delta = \Delta/2V$, and taking three values $\delta = -3/4, 0, and + 3/4$, we present Fig. 5.3.

In the first of these cases, $\delta = -3/4$, (dotted line), the effect of the static energy mismatch adds directly to the effect of the nonlinearity. The nonlinear suppression of the initially occupied site makes the energy mismatch always larger as the nonlinearity increases. We therefore encounter no transition: the average of the probability difference always increases as the nonlinearity increases. The second case with $\delta = 0$, (solid line) represents the degenerate dimer with no static mismatch. As we know, the average p is zero until χ hits the critical value at which point the transition occurs. In the third case, $\delta = 3/4$, (dashed line), the average value of p is the same as

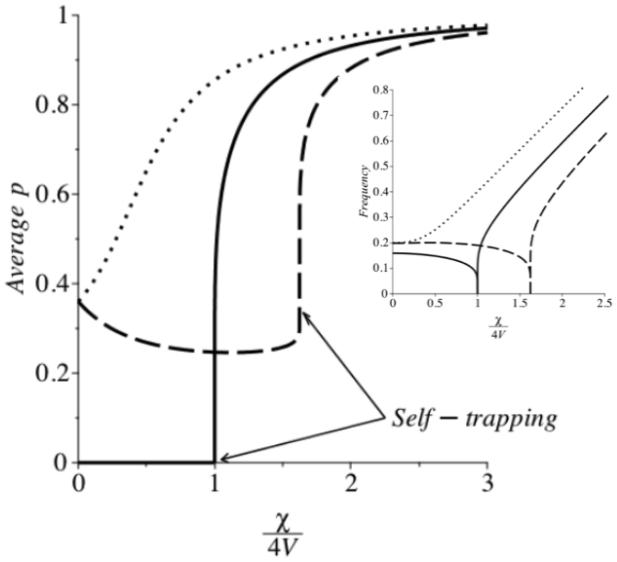

Fig. 5.3 Probability difference p averaged over a cycle plotted in the main figure as a function of the nonlinearity ratio $\chi/4V$ for three different values of the static energy mismatch $\Delta = E_1 - E_2$ expressed as a dimensionless ratio $\delta = \Delta/2V$: $-3/4$ (dotted), 0 (solid), and $+3/4$ (dashed). The initial placement of the particle is always on site 1. This is the energetically lower site in the first case (dotted line) and so the nonlinearity effectively increases the energy mismatch. No transition occurs. In the opposite case when the initially occupied site is energetically higher (dashed line), increase in nonlinearity tends to bring the sites to a resonance situation when the self-trapping transition occurs as displayed. In the degenerate dimer case (solid line), the average value of p is zero for all nonlinearity values lower than the critical one, at which the self-trapping occurs. The inset shows the frequency (reciprocal of period) of the probability difference time evolution as a function of the nonlinearity for the corresponding cases. See text.

for $\delta = -3/4$ for vanishing nonlinearity: we know, for instance from Eq. (2.9), that $\langle p \rangle$ for the linear dimer is insensitive to the sign of the site energy difference whose square determines that average. Indeed, the value is $\delta^2/(1+\delta^2)$ which, for $\delta = \pm 3/4$ equals 0.36 where both the dotted and the dashed lines start at $\chi = 0$. While the former rises always, encountering no transition in its journey to the value 1, the latter has an interesting trek: it comes down with an increase in the nonlinearity, undergoes the trapping transition, jumping thereby abruptly to a higher value and then continues to the value 1 as a result of further increase in nonlinearity. The inset shows the corresponding variation of the frequency of the probability difference (reciprocal of the period of oscillation) for the corresponding three cases in the main plot with the same line styles as in the main plot. In the two cases (dashed and solid lines) in which there is a transition, the frequency drops (logarithmically) to zero at the transition and increases without limit beyond the transition. In the case of no transition (dotted line), the frequency increases for all nonlinearities, as expected.

The reader is reminded that the time dependence of the probability difference $p(t)$ at the transition, as well as for slightly lower and larger values of nonlinearity relative to the critical value, corresponding to the dashed line in Fig. 5.3, is shown explicitly in the respective three curves of the left panel of Fig. 5.1.

Having seen that the sign of the static energy mismatch has a clear influence on the existence of the transition, we are ready to explore the effect of the static mismatch more systematically.

5.4.1 Difference in Positive and Negative Static Mismatch in Site Energy

The effect of positive energy mismatch $E_1 > E_2$ is examined by taking several specific instances as shown in Fig. 5.4. All cases shown display change of average p as the nonlinearity is varied, a transition at the corresponding critical values represented by a jump upwards, and an eventual saturation to the value 1 for large values of the nonlinearity signifying total self trapping. Curves (a), (b) and (c), for which $\delta = \Delta/2V$ takes the respective values 0.1 (solid), 0.25 (dotted) and 0.4 (space-dashed), show an increase for all increases in χ whereas curves (d), (e), and (f), for which δ takes the respective values 0.6 (dotted-dashed), 0.8 (dashed), and 1.0 (space-dotted), display a decrease before the transition but an increase beyond it. The complexity of the interaction between static and dynamic mismatch should be clear from this lack of uniformity.

In order to inspect how the sign of the energy mismatch affects the transition, we show Fig. 5.5 similarly to what we see in Fig. 5.3. The two solid lines represent the variation of the average value of p with changes in nonlinearity expressed as $\chi/4V$ with values $\delta = -0.1, -0.19245$ of the same magnitude but opposite sign as the two dotted lines. The second value is actually precisely $-1/\sqrt{27}$ and emerges from the

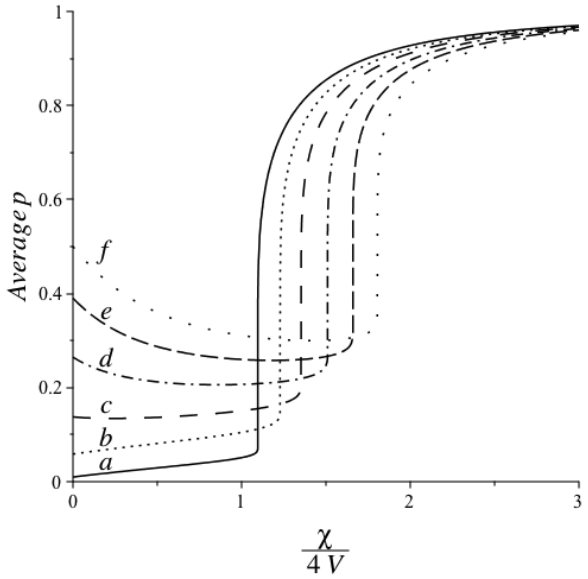

Fig. 5.4 Average of the probability difference p plotted as a function of the nonlinearity ratio $\chi/4V$ for six different cases of static energy mismatch $\delta/2V$ as detailed in the text, all displaying a self-trapping transition marked by abrupt upwards jumps. Three of the cases, (a), (b), and (c), show an increase throughout while the other three decrease first and then increase as the nonlinearity is increase. This stems from the complexity of the interaction of the static and dynamic mismatch. See text.

Weierstrass analysis as a significant number for this system. For any δ values more negative than that value, there are no transitions as we will see below.[10]

As explained earlier, the sign of the static mismatch is irrelevant to the value of $\langle p \rangle$ at zero nonlinearity. This has the consequence that each solid-dotted pair starts at the same place on the y-axis. As χ increases, the negative δ curves bend down but the positive δ counterparts go up. All four cases shown involve the self-trapping transition but the negative mismatch cases have a much sharper appearance. We also show the $\delta = 0$ case (thick solid line) that describes the nonlinear degenerate dimer, for comparison. The negative static mismatch situations require a lower nonlinearity value to cause the self-trapping transition.

This result is worth noting as it corrects a superficial expectation. We might mistakenly assume that a negative mismatch, which means populating initially the site which as a consequence of its static mismatch is lower in energy than the

[10] The curious appearance of the numbers 4 and $\sqrt{27}$ in these systems should not be surprising once one notices their connection to the square of 2 and the cube of 3. They appear in (Kenkre, 1989) in the context of the rotational polarons study of (Kenkre et al., 1995; Wu and Kenkre, 1995), they have appeared much earlier in Kenkre, Wu and Howard, Bull. Am. Phys. Soc. 33, K22-6 (1988), additionally in Tsironis (1993), and can be found even in the 1986 dissertation of Tsironis.

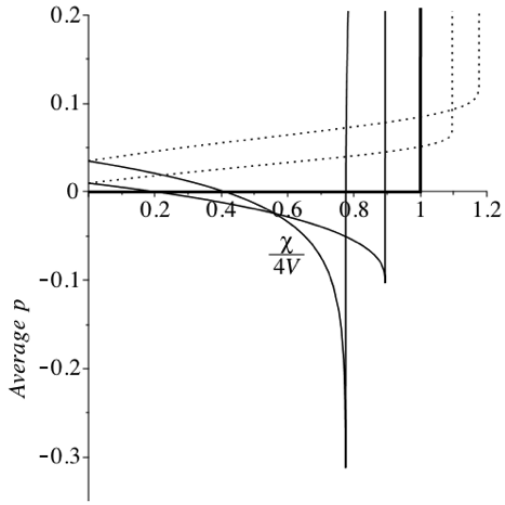

Fig. 5.5 Comparison of cases of static mismatch of positive and negative sign. Plotted is the variation of the probability difference average $\langle p \rangle$ as a function of the nonlinearity for five values of the static energy mismatch δ: positive values $+1/\sqrt{27}$ and $+0.1$ shown by dotted lines, the value 0 representative of the degenerate dimer depicted by a thick solid line, and negative values -0.1 and $-1/\sqrt{27}$ shown by solid lines. The order mentioned is as we go from right to left or top to bottom in the Figure. Negative energy mismatch shows sharper transitions. Note by the way that the imperfection of numerical procedures makes the sharp peak appear to be at -0.3 (similarly in Fig. 4.6 below) but in actuality it extends to -0.5 as analytic results further into this explanation show. See text.

unoccupied one, would necessarily increase the overall mismatch in the subsequent evolution and therefore disallow a transition. The complex process of interaction of the static and dynamic mismatches has the consequence that a small negative δ helps the nonlinearity (i.e., requires a lower value of χ) in causing self-trapping to occur. And yet, the leftmost solid curve in Fig. 5.5 is a demarcation curve. Notice the supersharp nature of its transition. For more negative static energy mismatch, there is no transition!

This disappearance of the transition is seen unequivocally in Fig. 5.6 where, in addition to repeating the two negative δ curves that are part of Fig. 5.5, we display two more results for more negative δ values. Both (dotted) variations of the average of the probability difference show smooth variation, in other words, no transition. Of those two, the one on the right ($\delta = -0.25$) displays a decrease followed by an increase as the nonlinearity increases, whereas the one on the (extreme) left ($\delta = -0.40$) increases always with χ. Both curves manifest inflection in their shapes which is an indicator of transition-like behavior. It is clear nevertheless that there is no self-trapping.

As we increase the magnitude of the negative static energy mismatch further, it is clear that we return to the case we started with the beginning of the study in Fig. 5.3

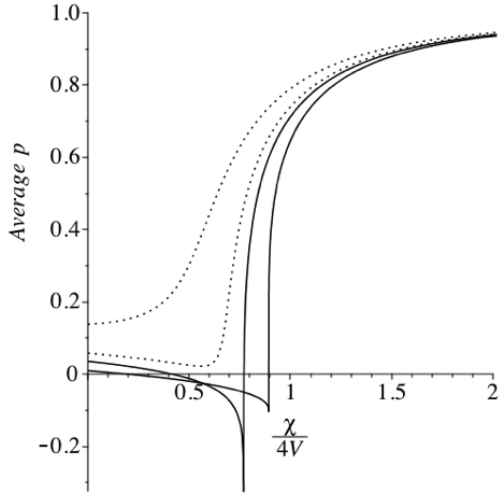

Fig. 5.6 Disappearance of the self-trapping transition as the static energy mismatch is made more negative. Plotted are four cases of variation of the average of the probability difference over a cycle as a function of the nonlinearity ratio $\chi/4V$. The rightmost curve ($\delta = -0.1$ and the curve to its left ($\delta = -1/\sqrt{27}$), both solid lines, exhibit the self-trapping transition, the latter being a demarcation case. For negative δ's of larger magnitude the transition disappears as shown by the two dotted curves on the left. They are for $\delta = -0.25$ and $\delta = -0.40$ as one moves to the left. See text.

where we considered the static energy mismatch $\delta = -3/4$ and saw that there was no transition.

In order to emphasize the disappearance of the self-trapping transition at the value $-1/\sqrt{27} \approx 0.192$ of the static energy mismatch δ, we also show the variation of the *frequency* of oscillations of the probability difference p as a function of the nonlinearity ratio $\chi/4V$ in Fig. 5.7. We display that variation along with two companion cases on either side of the critical value. The solid line represents the demarcation value $-1/\sqrt{27}$ while to its right we have the space-dotted line for $\delta = -0.18$ that does have a transition (at a value of the nonlinearity ratio slightly over 0.79) and to its left the dotted line for $\delta = -0.20$ that has no transition but only a vestige of the transition shown by the frequency turning around from descent to ascent at a value of the nonlinearity ratio a little over 0.75.

5.4.2 Graphical Perspective of Potential Plots

In order to understand some of these cases we have studied from the perspective of potential plots, we provide Fig. 5.8 for four cases selected from the nine analyzed

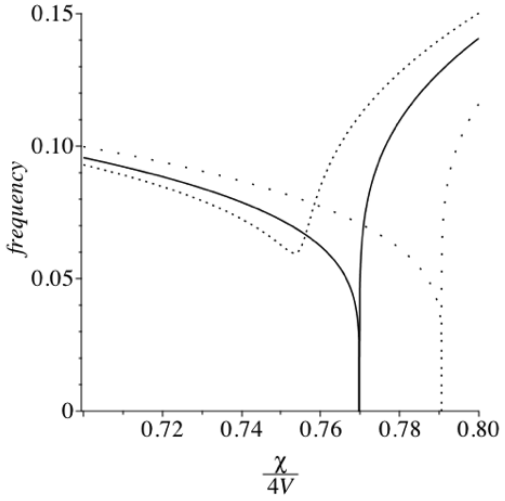

Fig. 5.7 Frequency of oscillations of the probability difference p plotted as a function of the nonlinearity ratio $\chi/4V$ to show the disappearance of the self-trapping transition as the static energy mismatch is made more negative. Shown is the demarcation case (solid line) $\delta = -1/\sqrt{27} \approx 0.192$ along with a negative static mismatch $\delta = -0.18$ of smaller magnitude for which there is a transition on its right and a negative mismatch case of $\delta = -0.20$ of larger magnitude for which there is no transition. See text.

above. Each of the four panels corresponds to a value of the static energy mismatch $\Delta/2V$ as shown.

The transition curve in each panel is a solid line and the dashed and dotted lines represent the same value of δ as the solid line does but nonlinearities respectively 1.01 and 0.99 times the transition value. How free and self-trapped behavior follows from the potential curves is clear from the plots.

All nine cases analyzed in this Chapter so far, inclusive therefore of the four cases represented in Fig. 5.8, have the quantum particle starting on site 1 and thus on the right-most point in each panel. The nature of the critical point example, the lower-right panel, is different from all others in that the horizontal line drawn from the initial point is tangential to the potential curve at a point of *inflection*. It is tangential to maxima portions in all the other panels. The lower minima are on the right for the lower panels but on the left for the upper panels.

5.5 The Blend of Static and Dynamic Mismatch

To summarize how the interplay of static and dynamic mismatch occurs in the nonlinear nondegenerate dimer and produces, or fails to produce, the self-trapping

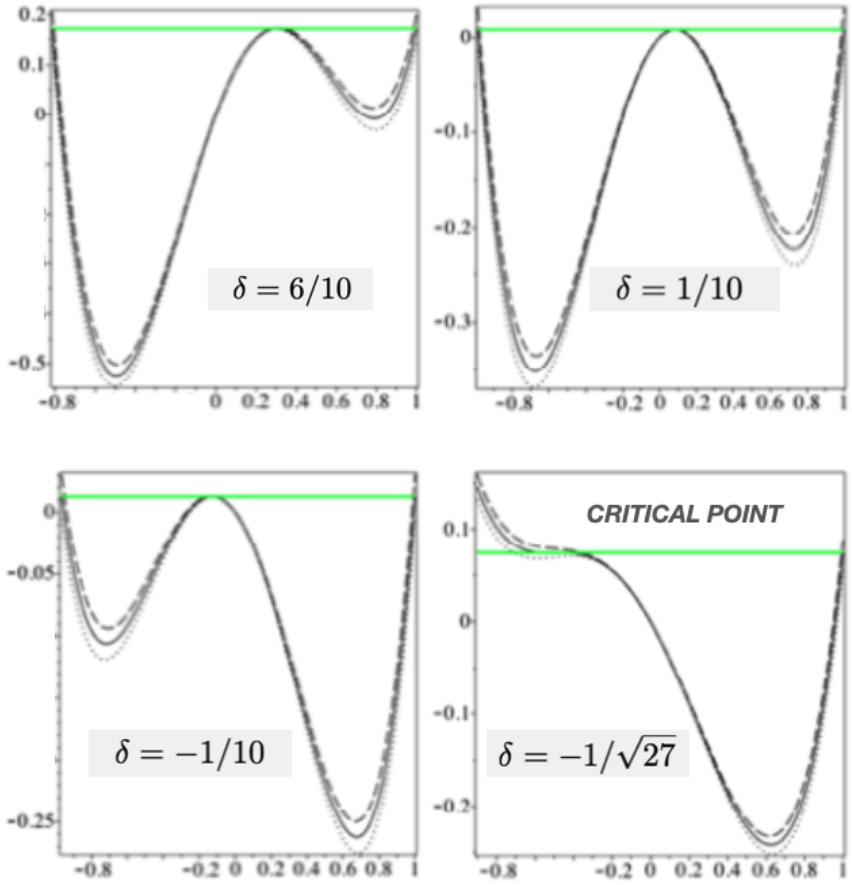

Fig. 5.8 Transition behavior studied with the help of potential curves, $U(p)$. Of the nine cases denoted by filled circles in Fig. 5.10, four have been selected here to show the p-dependence of the plot of $U(p)$ calculated from Eq. (5.4). In each, the self-trapping transition is shown as a solid line and a dashed curve and a dotted curve represent, respectively, cases near but not at the transition. The static energy mismatch $\delta = (E_1 - E_2)/2V$ is positive in the upper panels and negative in the lower panels, the respective values being displayed in the Figure. The abscissa in each plot is the probability difference extending from -1 to +1. The lower right panel depicts the critical point.

transition, we collect the various cases studied and present in the form of a single 3-dimensional plot. It depicts the frequency of oscillation $1/T$ calculated as the reciprocal of the period of oscillation of $p(t)$ in Fig. 5.9. The construction of this plot is made possible by Eq. (5.17) which is itself obtained from the analytical expressions we have obtained in terms of Jacobian elliptic functions. The static

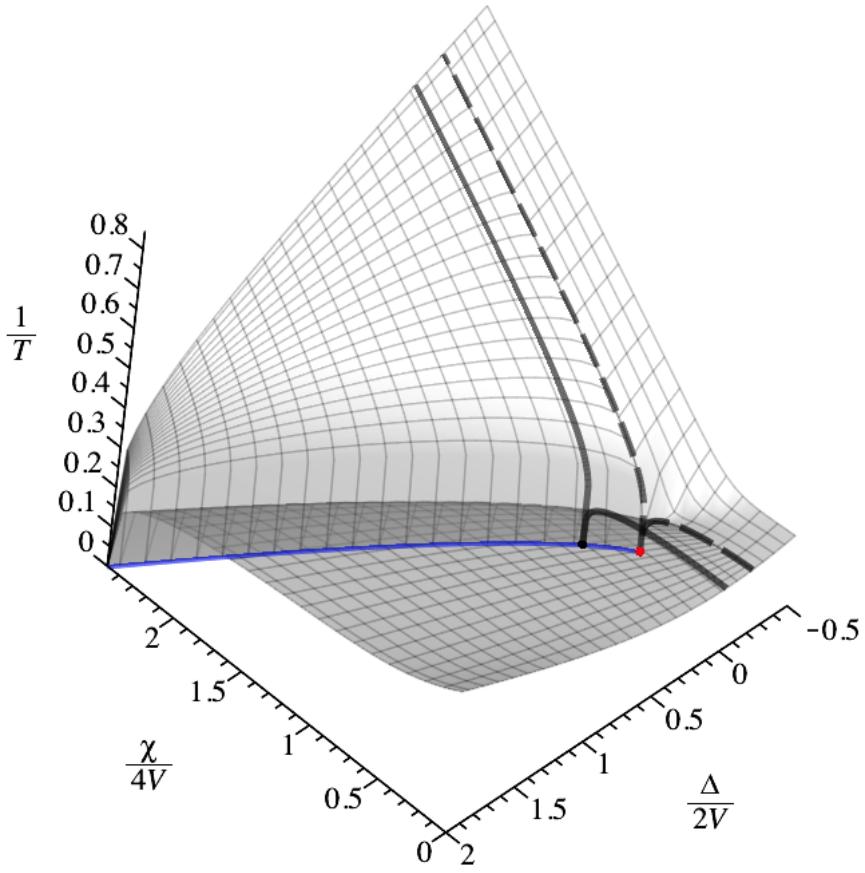

Fig. 5.9 3-dimensional representation of the variation of $1/T$, the reciprocal of the period of oscillation of the probability difference $p(t)$, in the nonlinear nondegenerate dimer for localized initial placement on one of its two sites. The nonlinearity ratio $\chi/4V$, and the non-degeneracy ratio $\delta = (E_1 - E_2)/2V$, are respectively plotted on the x-axis and y-axis as shown. The sudden logarithmic reduction in the oscillation frequency as one nears the self-trapping transition is clear from the solid and dashed lines as is its unrestrained increase beyond the transition. The intersection of the plot with the 'floor', marked by the blue line, locates the line of the self-trapping transitions: the period T is infinite along the curve. This line ends in the critical point marked in red, beyond which there is no self-trapping. The plot is obtained from our analytic expression for the period, Eq. (5.17). See text.

energy mismatch $\delta = \Delta/2V$ is plotted on the y-axis, the dynamic mismatch $\chi/4V$ on the x-axis, and the frequency of oscillation on the z-axis as shown.

Four important messages can be gathered from the plot. The first is shown by the solid and dashed lines in the back towards the right of the figure where we notice the sudden decrease of the frequency on approach to the self-trapping transition. The solid line is for the degenerate dimer ($\delta = 0$) while the dashed line is the limit beyond

which there is no self-trapping ($\delta = -1/\sqrt{27}$). This frequency variation connects with that in the 2d plots of Fig. 5.7 and is the extension to the nondegenerate situation of the mobility reduction plot given in (Kenkre and Campbell, 1986), shown in this book as Fig. 2.3.

The second point of note is the unrestricted rise of the frequency beyond the transition as the nonlinearity χ increases beyond the critical value. It is indicative of the phenomenon of motional narrowing in the line shape that would be seen in an experiment such as neutron scattering. This is the nonresonant extension of Fig. 2.2 in this book, its essence being clear in Kenkre and Tsironis (1987). The third interesting display is the blue line that marks the intersection of the plot with 'the floor', i.e., marks an infinite period T. This is the transition curve and indicates the value of nonlinearity required for the self-trapping transition to occur for any given static energy mismatch Δ. The curve ends in the red dot (the fourth point of note) which is the critical point[11] with coordinates $\delta = -1/\sqrt{27}$ and $\chi/4V = 4/\sqrt{27}$.

It is straightforward to derive the equation of the blue line and the coordinates of the red dot from our theoretical development. The equation is

$$8\delta k_{cr}^3 - (12\delta^2 - 1)k_{cr}^2 + 2\delta(3\delta^2 - 5)k_{cr} - (\delta^2 + 1)^2 = 0, \qquad (5.24)$$

and is graphically displayed by itself in Fig. 5.10. Reorientation in the χ-δ space with attention to the senses in which the variables increase along the respective axes will help understand the connection between the blue line on the floor of Fig. 5.9 and the (black) line of Fig. 5.10.

It is appropriate at this point to show how Eq. (5.24) emerges as a relationship between the nonlinearity and the nondegeneracy at the self-trapping transition. At the occurrence of the transition, the period of oscillations becomes infinite which means from the expression for the period presented in Eq. (5.19b) that either the elliptic modulus becomes 1 or the denominator vanishes. While the second of these alternatives means that $e_1 = e_3$, in the light of Eq. (5.14), the first of these alternatives requires $e_1 = e_2$. These equality conditions on the roots of the cubic equation (5.11) place restrictions on g_2 and g_3 appearing in (5.11). Imposing them in Eqs. (5.8) and using the relations (5.3) between the γ's and the system parameters δ and χ leads, finally, to (5.24) that predicts the critical point.

5.6 Behavior at the Critical Point

There are three interesting features of the behavior of the system at the critical point marked by $\delta = -1/\sqrt{27}$, $\chi_{cr}/4V = 4/\sqrt{27}$. Two of them are striking. They are all

[11] The equation for our blue line and the coordinates of the red dot have appeared first in (Tsironis, 1993); note that δ is reversed in sign there with respect of our usage here, that ζ there represents our k_0 here, and that the derivation is restricted as is our Eq. (5.24), to a localized initial condition. Our analysis permits us to generalize Eq. (5.24) to *arbitrary* initial conditions. The striking dependence of the critical line on initial conditions has been obtained in the present book and discussed in Chapter 10 in the context of Bose-Einstein condensate tunneling.

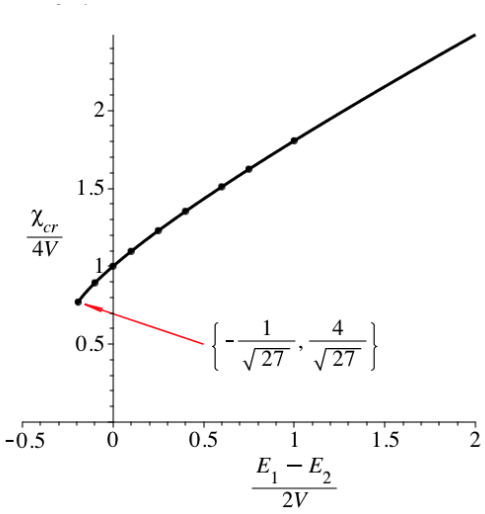

Fig. 5.10 Self-trapping properties of the nonlinear nondegenerate dimer for localized initial placement on one of its two sites. Plotted is the relationship between the critical value of the nonlinearity ratio, $\chi_{cr}/4V$ to the nondegeneracy ratio $\delta = (E_1 - E_2)/2V$. The little filled circles represent the nine situations studied in the previous plots in this Chapter, 4.1 through 4.7. As discovered by Tsironis (1993), the point at the very left end of the curve, marked by an arrow, is special in that no self-trapping transition is possible beyond it. The values of δ and of the critical nonlinearity ratio $\chi_{cr}/4V$ that mark that special point are as shown in the curly brackets in the plot. See text.

illustrated in Fig. 5.11 where the saturation value of the probability difference at the self-trapping transition is plotted as a function of the static energy mismatch.

Initial occupation is of site 1, i.e., $P_1(0) = 1$, $P_2 = 0$, and p_s is the value the probability difference attains its saturation value at infinite time *at the transition*. The energy of the initially occupied site is lower (by an amount $2V/\sqrt{27}$); the eventual occupation is more at the initially unoccupied site, the difference of $P_2(t) - P_1(t)$ as $t \to \infty$ being 0.5. The two noteworthy features are that there is no transition beyond the critical point as we have remarked in connection with Fig. 5.10, and that the slope of p_s with respect to variations of the static energy mismatch δ is *infinite* as shown by the dashed line in Fig. 5.11. Analytic proofs can be given as follows.

The signature of the self-trapping transition at which p becomes p_s, is that k_1 in Eq. (5.13) should tend to 1. The complete elliptic integral of the first kind then becomes infinite and so does the period T which is proportional to it as Eq. (5.19b) shows. The *average* value of p, given by substituting $k_1 \to 1$ in Eq. (5.19a), with a and b from Eqs. (5.15), is

$$p_s = 1 - \frac{6U_0'}{24e_1 + U_0''}. \tag{5.25}$$

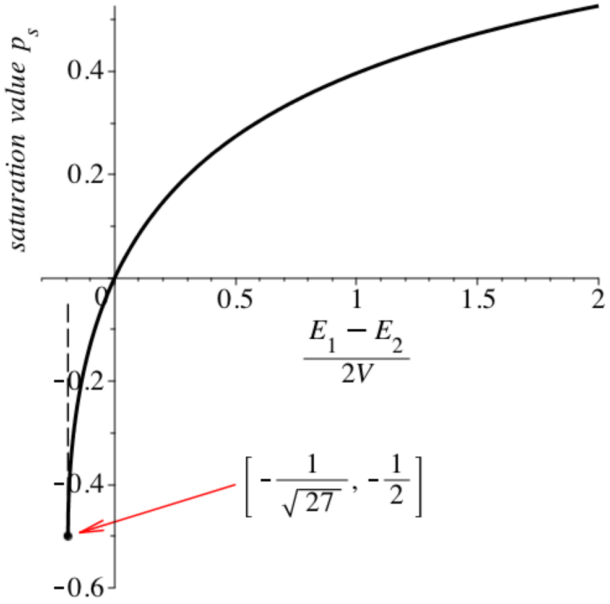

Fig. 5.11 Plot of p_s, the saturation value of the probability difference $P_1(t) - P_2(t)$, i.e., its limit as $t \to \infty$ as a function of the static energy mismatch $\delta = (E_1 - E_2)/2V$. Initially, $P_1(0) = 1$ and $P_2(0) = 0$. The two striking features here are that the p_s curve *stops* at the value -0.5 where $\delta = -1/\sqrt{27}$, there being no transition beyond that point ; and that the slope of p_s at that point is infinite. See text for the analytic proof of both these conclusions.

where U_0' and U_0'' denote, respectively, the first and second p-derivatives of the potential $U(p)$ evaluated at $p = p(0)$. Expanding relevant expressions in powers of a small departure ϵ around the critical point $\delta = -1/\sqrt{27}$, $k_0 = 4/\sqrt{27}$, Eq. (5.24) and other equations such as (5.8) and (5.4) yield, on the neglect of higher powers of ε, the root e_1 to be

$$e_1 \approx \frac{3^{3/4}\sqrt{2}}{6}\sqrt{\varepsilon} + \mathrm{O}(\varepsilon^1). \tag{5.26}$$

On combining this result with Eq. (5.25) we find

$$p_s \approx -\frac{1}{2} + \frac{3^{7/4}}{2^{3/2}}\sqrt{\varepsilon} + \mathrm{O}(\varepsilon^1), \tag{5.27a}$$

$$\frac{dp_s}{d\varepsilon} \approx \frac{3^{7/4}}{2^{5/2}}\frac{1}{\sqrt{\varepsilon}} + \mathrm{O}(\varepsilon^0). \tag{5.27b}$$

The passage $\varepsilon \to 0$ then allows us to recover the results, clear from Fig. 5.11, that the limiting values of $dp_s/d\delta$ and p_s at the critical point are infinity and -1/2, respectively.

Although most of the focus in the present Chapter so far has been to initial conditions that are localized on one site, our develop can easily cover more general initial conditions. We have performed such general studies that show how the critical point (as well as the entire transition line given by Tsironis for localized initial conditions) moves as the degree of localization is changed. Some of that will appear in Chapter 10 in the context of the dynamics of Bose-Einstein condensates.

5.7 Stationary States

The analysis of stationary states of the nonlinear nondegenerate dimer is easy to perform. Putting the time derivatives to zero in Eq. (4.6) and noticing that given that q equals $dp/d\tau$, it must also vanish in the stationary state, we get the condition that for a stationary state,

$$\frac{\chi}{2V} = \frac{\delta}{p_{ss}} - \frac{1}{r_{ss}} = \frac{\delta}{p_{ss}} \mp \frac{1}{\sqrt{1-p_{ss}^2}} \tag{5.28}$$

where ss denotes stationary states and r_{ss} equals $\sqrt{1-p_{ss}^2}$ given that $q_{ss} = 0$ as explained above. This links to Eq. (2.28) provided in Chapter 2 which treats the degenerate case $\delta = 0$. It is easy to show that if nonlinearity vanishes, the stationary state probability difference satisfies

$$\frac{\Delta}{2V} = \delta = \pm \frac{p_{ss}}{\sqrt{1-p_{ss}^2}}. \tag{5.29}$$

It is thus noteworthy that Eq. (5.28) describing stationary states in the nonresonant nonlinear dimer is made up from additive contributions from the nonlinearity and the nondegeneracy which each can be separately simply be put equal to zero to get the respective result.

In order to determine which of these stationary states are stable and which not, we follow the method used by Honglu Wu in an Appendix to his 1990 dissertation for this system. Similarly to his analysis of the stability of stationary states of the rotational polaronic dimer that we detailed in Chapter 4, he expanded the three Bloch vector components around the stationary values as

$$p = p_{ss} + \epsilon_p, \qquad q = q_{ss} + \epsilon_q = 0 + \epsilon_q, \qquad r = r_{ss} + \epsilon_r,$$

and, linearizing the equations of motion in the variations $\epsilon_{p,q,r}$, arrived at[12]

[12] While not all steps of the calculation are visible in the dissertation, the prominent results have been worked out and shown here in the book for completeness. My thanks to John Andersen for help in the detailed verification of these results during the writing of the book.

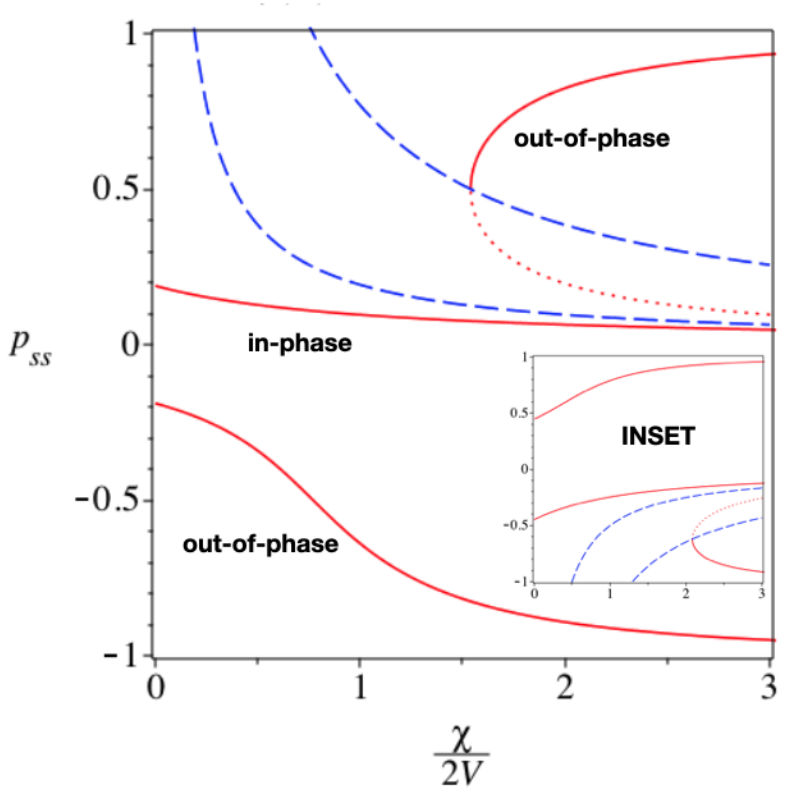

Fig. 5.12 Stationary states of the nonlinear nondegenerate dimer. Plots are of the probability difference p_{ss} in the stationary states as the nonlinearity ratio $\chi/2V$ is varied. Comparison of the solid (red) lines here to the pitchfork bifurcation of the *resonant* nonlinear dimer ($\delta = 0$) shown in Fig. 2.9 makes clear the effects of non-resonance. The in-phase (near-horizontal) branch is stable. Of the two out-of-phase branches, the lower is stable but only part of the upper branch is stable (dotted line represents lack of stability). The two dashed lines in the upper half of the figure depict the limits of the inequality that mark the stability criterion given in Eq. (5.33), see text. The static energy mismatch $\delta = \Delta/2V$ is $1/\sqrt{27}$ in the main figure. The inset shows the same plot as in the main figure for the static mismatch δ having a *negative* value $-1/2$. The axes in the inset are the same as in the main figure and we see all features qualitatively reproduced but upside down.

$$\frac{d}{d\tau}\begin{pmatrix}\epsilon_p\\ \epsilon_q\\ \epsilon_r\end{pmatrix} = \begin{pmatrix}0 & 1 & 0\\ -(1+2k_0r_{ss}) & 0 & +\frac{p_{ss}}{r_{ss}}\\ 0 & -\frac{p_{ss}}{r_{ss}} & 0.\end{pmatrix}\begin{pmatrix}\epsilon_p\\ \epsilon_q\\ \epsilon_r\end{pmatrix} \tag{5.30}$$

If any of the three eigenvalues of the matrix has a positive real part, the stationary state is unstable. The eigenvalues λ are, explicitly,

$$-\lambda[\lambda^2 + (p_{ss}/r_{ss})^2] - (1)[(1+2k_0r_{ss})\lambda - 0] = 0. \tag{5.31}$$

One of the eigenvalues is zero. The other two are

$$\lambda^2 = -(2k_0 p_{ss} - \delta)^2 + \frac{\delta}{2k_0 p_{ss} - \delta}. \tag{5.32}$$

This then allows us to conclude that the stationary state is unstable if

$$\delta/2k_0 < p_{ss} < (\delta^{1/3} + \delta)/2k_0, \quad \text{for } \delta > 0, \tag{5.33a}$$

$$\delta/2k_0 > p_{ss} > (\delta^{1/3} + \delta)/2k_0, \quad \text{for } \delta < 0 \tag{5.33b}$$

The final results that Wu arrived at, which apparently have not been published in the open literature, are displayed in Fig. 5.12 where the probability difference in the stationary states is plotted as a function of $\chi/2V$ for two values of the static energy mismatch. The main plot is for a positive value $\delta = \Delta/2V = 1/\sqrt{27}$ and the inset (for the same axes and scales as in the main plot) for the negative value $\delta = -1/2$. As the inset shows slight changes of values and an up-down inversion because of change of sign, let us focus only on the main plot. The solid (red) lines represent the stable stationary states while the dotted line represents the unstable situation. The two lines marked 'out-of-phase' have $r_{ss} = -\sqrt{1 - p_{ss}^2}$ while for those marked 'in-phase', $r_{ss} = +\sqrt{1 - p_{ss}^2}$. The dashed (blue) lines are the limits that mark the region in which the stationary states are unstable as shown by Wu's analysis.

5.8 Alternative Method for the Analysis of the Nonlinear Dimer

In ending this Chapter, let us examine an alternative method for the analysis of the nondegenerate nonlinear dimer and some interesting generalizations thereof on the basis of expressions that are non-local in time.

Equation (5.1) describes the nonlinear time evolution of the Bloch vector whose components are p, q and r. Begin by recasting the evolution in matrix form as

$$\frac{d}{dt}\begin{pmatrix} p \\ q \\ r \end{pmatrix} + \begin{pmatrix} 0 & -2V & 0 \\ 2V & 0 & -\mathcal{E}(t) \\ 0 & \mathcal{E}(t) & 0 \end{pmatrix}\begin{pmatrix} p \\ q \\ r \end{pmatrix} = 0. \tag{5.34}$$

where the quantity $\mathcal{E}(t)$ that we have introduced equals the total energy mismatch between the two sites of the nondegenerate nonlinear dimer as the difference

$$\mathcal{E}(t) = \chi p(t) - \Delta. \tag{5.35}$$

Because our focus is on the probability difference p, the first element of the Bloch vector, let us derive a closed equation for it by first separating from the 3×3 evolution in Eq. (5.34) the problem of the evolution of the 2×2 matrix that is the rest of the Bloch problem. Solving that problem formally, and substituting the solution in the evolution of p alone will fulfill our task. Although problems of this ilk are often

approached via Zwanzig projection operators (Zwanzig, 1961, 1964; Kenkre, 2021) let us not use those operators here and extract from (5.34),

$$\frac{d}{dt}\begin{pmatrix} q(t) \\ r(t) \end{pmatrix} + \mathcal{E}(t)\begin{pmatrix} 0 & -1 \\ 1 & 0 \end{pmatrix}\begin{pmatrix} q(t) \\ r(t) \end{pmatrix} = 2V\begin{pmatrix} p(t) \\ 0 \end{pmatrix}. \tag{5.36}$$

Let us regard Eq. (5.36 as an inhomogeneous linear differential equation in which the driving term is $2V$ times the vector with the elements $p(t)$ and 0 as displayed, and the homogeneous part is controlled by the matrix

$$\zeta(t) = \mathcal{E}(t)\begin{pmatrix} 0 & -1 \\ 1 & 0 \end{pmatrix}.$$

Because it is a traceless 2×2 matrix, its exponentiation is easily performed by using the result that, for such a matrix,

$$e^{\zeta} = \left(\cos\sqrt{D}\right) I + \left(\frac{\sin\sqrt{D}}{\sqrt{D}}\right)\zeta$$

where I is the identity and D is the determinant of ζ. The homogeneous part of the problem is solved by

$$\begin{pmatrix} q(t) \\ r(t) \end{pmatrix} = e^{-\int_0^t ds\, \zeta(s)}\begin{pmatrix} q(0) \\ r(0) \end{pmatrix}, \tag{5.37}$$

time ordering being assumed, as customary, in the exponentiation of the time-dependent matrix. The Green function apparent in Eq. (5.37), the exponential of the (time-ordered) integral of the ζ matrix, is then applied to the driving term involving $p(t)$ and the result used in Eq. (5.36) to obtain a closed equation for $p(t)$ which is, however, non-local in time. The case when $q(0)$ and $r(0)$ are non-vanishing is left as an exercise for the reader. For the localized initial placement $p(0) = 1$ and $q(0) = 0 = r(0)$, one arrives at the integrodifferential equation

$$\frac{dp(t)}{dt} + 2\int_0^t ds\, \mathcal{W}(t,s)p(s) = 0. \tag{5.38}$$

The memory $\mathcal{W}(t,s)$ is not a function of the difference $t - s$: a consequence of the time dependence of $\mathcal{E}(t)$ in the Hamiltonian. It is given explicitly by

$$\mathcal{W}(t,s) = 2V^2 \cos\left[\int_s^t dz\, \mathcal{E}(z)\right]. \tag{5.39}$$

Although this method does not appear to have been presented earlier, the final result, Eq. (5.38) with (5.39), has been (Kenkre, 2000), the derivation route having been through the application of Wu's generalization (Wu and Kenkre, 1989) of Zwanzig's projection techniques (Zwanzig, 1961, 1964) to nonlinear situations. That application of the diagonalizing projection operators will be one of the stand-alone topics discussed in the Miscellaneous Chapter 11.

There are five physically interesting cases of the integrodifferential Eq. (5.38) which might be worth mentioning passingly. Explicit solutions are easily derived for three of them. The first of these is when $\chi = 0$ so this is not a nonlinear situation at all and Δ is a constant so we are here analyzing a linear dimer with static energy mismatch. The second is when Δ is time-dependent (with $\chi = 0$). This situation is connected to the bursts in transfer (Agarwal and Harshawardhan, 1994) that had been predicted in two-level atomic systems but mistaken in the literature for the phenomenon of dynamic localization (Dunlap and Kenkre, 1986b), and treated with the help of projection techniques in (Kenkre, 2000). The third is for a nonlinear dimer (χ non-vanishing) that is degenerate ($\Delta = 0$) and this leads to the equations of motion that are like those for a physical pendulum and to explicit solutions in terms of Jacobian elliptic functions. It is thus possible in all these cases to provide explicit solutions in terms of analytic functions. For the last two cases in which χ and Δ are both nonvanishing (Δ being time-dependent in the last of the examples) represent the nonlinear nondegenerate dimer, the last of the examples being descriptive of an external time-dependent field applied to it. Equations can be set up but solutions are not straightforward to obtain. These matters will be taken up along with other miscellaneous issues in Chapter 11.

5.9 Chapter 5 in Summary

The simultaneous effects of a static and a dynamic energy mismatch in the dimer were studied in this Chapter, the former arising from nondegeneracy, i.e., from the inequivalence of the site energies and the latter from nonlinearity. A systematic study of the dynamics was carried out as well as of the stationary states of the system. The quantities investigated for various amounts of the blend of static and dynamic disorder were the average of the probability difference over a cycle and the period of oscillation. The study was facilitated by new expressions presented for the probability difference in terms of Jacobian rather than Weierstrass elliptic functions. These expressions not only showed simply the passage to the dynamics of the nonlinear degenerate dimer analytically but also made it possible to calculate the saturation value of the probability difference and of the singular manner in which its derivative blows up. Visual displays of the period confirmed critical behavior and clarified how the self-trapping transition ceases to be for negative mismatch beyond a certain point. Stationary state considerations were presented along the lines of the development in Chapter 2 but enriched appropriately for the nondegenerate dimer. At the end of the Chapter an alternative way of analyzing the time evolution of the nondegenearate nonlinear dimer was also presented.

Chapter 6
Extended Systems with Global Interactions, and Nonlinear Trapping

Consider a benzene molecule. It is often looked upon as having a planar ring structure. An excitation, electronic or vibrational for instance, may be imagined as moving among the atoms of the molecule. Analysis appropriate to motion of a quasiparticle via nearest-neighbor interactions may be one way of studying such as a system. It would be particularly appropriate if the transfer interactions are of short range so that an atom may be considered to be in communication primarily with adjacent atoms. However, if the transfer interactions are of long range, the situation would be more complicated. Yet in the other extreme limit, the interactions may be considered to be equal between any two of the atoms constituting the system so that we have what is called an N-mer rather than a ring. Analysis may then be simplified because of the global nature of the interactions.

A different physical example of such a situation is provided by hydrogen in metals, a subject of great technological importance (Sköld, 1978; Brown and Kenkre, 1987). The moving particles are now the hydrogen ions that get trapped at the interstices near impurities such as oxygen. They are light enough that quantum effects may be discernible. In both the cases mentioned, benzene-like systems and hydrogen in metals, if the moving particle interacts strongly with vibrations of the environment it may be describable by the DNLSE. Let us therefore investigate in the following, quasiparticle motion and self-trapping via a discrete nonlinear Schrödinger equation by considering the limit of equal transfer interaction between *any pair* in a group of N sites.

Returning to Eq. (1.1), we will take its form which, rather than Eq. (1.2), is one obtained for $V_{mn} = V$ for all m and n in the system, thus starting with

$$i\frac{dc_m}{dt} = V\left(\sum_{m'} c_{m'} - c_m\right) - \chi|c_m|^2 c_m, \tag{6.1}$$

where the sum over m' has been kept unrestricted over all sites in the system. Such systems have been occasionally referred to as (globally interacting) N-mers. In keeping with the underlying theme of the book (and of the spirit of our researches into this otherwise difficult and extensive field), the idea here is to seek, whenever possible,

systems which can be approachable analytically, taking the help of numerical or approximate studies only when essential to do so.[1]

6.1 Trimers and N-mers with any Pair of Sites in Equal Communication

Let us begin by converting Eq. (6.1) for our n-site system into the corresponding equation for the elements of the density matrix ρ_{mn}:

$$\frac{d\rho_{mn}}{dt} = -iV \sum_s (\rho_{sn} - \rho_{ms}) + i\chi (\rho_{mm} - \rho_{nn}) \rho_{mn}, \tag{6.2}$$

and make the decision, in the spirit of our intention to study only analytically reachable conclusions here, to restrict our study to initial conditions for which the particle is either localized on a single site, partially localized over a group of identical sites ($m_A < N$ in number), or partially localized over these sites and over a different group of identical sites ($m_B = N - m_A$ in number). The idea here is to achieve high symmetry in the evolution by high symmetry in the initial conditions. Thus, the initial conditions on the amplitudes c_m are taken to be exactly the same within each of two groups A and B, and thus to be given by $c_m(0) = |c_{A0}|$ and $c_m(0) = |c_{B0}|$, respectively, with two possibilities on their interrelation: $|c_{A0}| = \pm|c_{B0}|$. We are *initially in our analysis* considering, thus, only "real conditions" in the language of Chapter 3. The probability of occupation within the A group is ρ_{AA} and that within the B group is $\rho_{BB} = 1 - \rho_{AA}$.

Following Andersen and Kenkre (1993b,a), let us define p, q and r via

$$p = m_A\rho_{AA} - m_B\rho_{BB}, \tag{6.3a}$$

$$q = i\sqrt{m_A m_B}\,(\rho_{AB} - \rho_{BA})\,, \tag{6.3b}$$

$$r = \sqrt{m_A m_B}\,(\rho_{AB} + \rho_{BA})\,, \tag{6.3c}$$

and notice that they satisfy $p^2 + q^2 + r^2 = 1$ just as do the components of the Bloch vector in a dimer. The time evolution of these three Bloch components obeys

[1] In the late 1980's I suggested these investigations to John Andersen who undertook them with me with immediate success as will be described in the first part of this Chapter. John had been a Ph. D. student of mine who had acquired expertise in standard polaron theory for his dissertation, working on the resolution of the long-standing naphthalene puzzle (Pope and Swenberg, 1982, 1999; Andersen et al., 1983; Kenkre et al., 1989) and discovered many noteworthy results in this N-mer scenario. While my interest in the N-mer behavior was stimulated by the motion of trapped hydrogen ions in metal hydrides, this subject had been started already earlier by Eilbeck et al. (1985) motivated by excitation motion in a molecule like methane (or benzene) as mentioned at the beginning of this Chapter. Our studies proceeded, independently, with different focus as will be seen below.

$$\frac{dp}{dt} = 2V\sqrt{m_A m_B}\, q, \tag{6.4a}$$

$$\frac{dq}{dt} = -2V\sqrt{m_A m_B}\, p + \left[\frac{(m_A - m_B)(\chi + 2m_A m_B V) - N\chi p}{2m_A m_B}\right] r, \tag{6.4b}$$

$$\frac{dr}{dt} = -\left[\frac{(m_A - m_B)(\chi + 2m_A m_B V) - N\chi p}{2m_A m_B}\right] q. \tag{6.4c}$$

The initial conditions we are studying may be expressed in terms of the initial values p_0, q_0 and r_0 of these Bloch-like components through the relations

$$\rho_{AA}(0) = |c_{A0}|^2 = c_{A0}^2 = \frac{1 + p_0}{2m_A}, \tag{6.5a}$$

$$\rho_{BB}(0) = |c_{B0}|^2 = c_{B0}^2 = \frac{1 - p_0}{2m_B}, \tag{6.5b}$$

$$\rho_{AB}(0) = \rho_{BA}(0) = c_{A0}c_{B0} = s\sqrt{\frac{(1 - p_0)^2}{4m_A m_B}}, \tag{6.5c}$$

with the restriction that $s = 0$ (localized), $s = 1$ (delocalized in-phase) or $s = -1$ (delocalized out-of-phase), or more simply as

$$p_0 = 2m_A c_{A0}^2 - 1, \tag{6.6a}$$

$$q_0 = 0, \tag{6.6b}$$

$$r_0 = s\sqrt{1 - p_0^2}. \tag{6.6c}$$

By introducing the dimensionless quantities $u = NVt$, $\eta = (m_A - m_B)/N = -1 + 2m_A/N$ and $k_0' = \chi/\left[N^2V(1 - \eta^2)\right]$, Andersen and Kenkre (1993b,a) were able to obtain the closed second-order equation for $p(u)$,

$$\frac{d^2p}{du^2} = -2\gamma_0' - 6\gamma_1' p - 6\gamma_2' p^2 - 2\gamma_3' p^3, \tag{6.7}$$

the coefficients γ' being given by

$$\gamma_0' = (\eta/2)(2k_0' + 1)\left(p_0\left[k_0' p_0 - \eta(2k_0 + 1)\right] - r_0\sqrt{1 - \eta^2}\right), \tag{6.8a}$$

$$6\gamma_1' = (1 - \eta^2) - 2k_0'\left(k_0' p_0^2 - r_0\right)\sqrt{1 - \eta^2} + \eta(2k_0' + 1)\left[2k_0' p_0 + \eta(2k_0' + 1)\right], \tag{6.8b}$$

$$2\gamma_2' = -\eta k_0'(2k_0' + 1), \tag{6.8c}$$

$$\gamma_3' = k_0'^2. \tag{6.8d}$$

The reason primes have been placed on k_0 and for that reason on the γ's is that we will be rescaling them in the next section to establish a useful link with the

nonlinear nondegenerate dimer. They appear in Andersen and Kenkre (1993b,a) without primes and precisely as defined here.

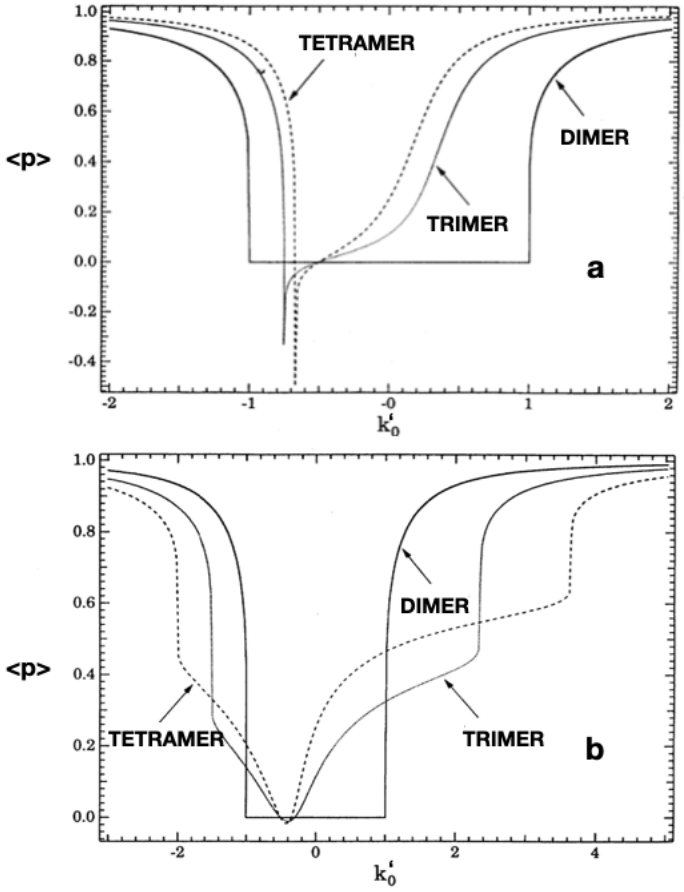

Fig. 6.1 Comparison of the self-trapping transitions exhibited by globally interacting N-mers (particularly dimers, trimers and tetramers) obeying the DNLSE for an initially localized condition ($p_0 = 1$ and $q_0 = 0 = r_0$). The plots are taken directly from (Andersen and Kenkre, 1993b) but a prime has been placed on k_0 appropriate to the scaling discussed in the text. The average of $p(t)$ over a cycle is plotted as a function of k_0', a quantity which, except for proportionality constants, measures the nonlinearity. Systems treated are the two simplest N-mers, the trimer and the tetramer, along with the resonant dimer for comparison. Both negative and positive values of k_0' are included. See text for discussion. Modified with permission from figs. 3 and 4 of Ref. (Andersen and Kenkre, 1993b); copyright (1993) by American Physical Society.

Andersen and Kenkre (1993b,a) employed Weierstrass functions to find solutions to Eq. (6.7). From the detailed analysis of the behavior of trimer, tetramer and

generally N-mer systems that they published in those papers, let us display Figs. 3 and 4 of (Andersen and Kenkre, 1993b) as our combined Fig. 6.1 here.

Perhaps the most striking of the results in Fig. 6.1 is that the dimer possesses an extended k_0' region over which the average over a cycle of the probability difference is constant at 0 whereas that is not true for the trimer and the tetramer.[2]

Although this N-mer analysis leading to Fig. 6.1 as well as numerous other results discussed in the original publications in the 1990's was carried out independently of any connection to the nonlinear nondegenerate dimer described in Chapter 4, I have always felt that there must be a close connection, at least conceptual, between the two. Part of the reason for this belief is that the symmetry that we imposed on the initial conditions separated the site-space into two groups which are dissimilar but in all other respects quite like the sites of a nonlinear nondegenerate dimer. Furthermore, inspection of Fig. 6.1a relative to Fig. 5.5 of Chapter 5 reveals an impressive kinship of the flat versus spiked transition behavior as does the inspection of Fig. 6.1b relative to Fig. 5.4 of Chapter 5 which brings out the difference in the behavior of the curves before and after the self-trapping transition. This led John Andersen and me in the very recent investigation we undertook for the purposes of this book to seek out an explicit transformation that might connect our N-mer analysis of the 1990's to the nonlinear nondegenerate study we reported in Chapter 5. We succeeded in the study, linking thereby our investigations with the Weierstrass investigations initiated in the Tsironis 1988 dissertation. We present the explicit transformation in the next Section and work out on its basis a few noteworthy results.

6.2 Rescaling to Connect the N-mer to the Nonlinear Nondegenerate Dimer

The equations of motion for the N-mer developed in Andersen and Kenkre (1993b) chose the natural dimensionless time $u = NVt$ and used the symbol k_0, which we have rewritten here with a prime, i.e., as k_0', to denote the nonlinearity in the combination

$$k_0' = \frac{\chi}{N^2 V(1-\eta^2)}. \tag{6.9}$$

In order to establish a relation that will allow us to use it as a conduit to travel between the N-mer and the nonlinear nondegenerate dimer, let us now return to Eqs. (6.4) and rewrite them in terms of new parameters V', χ' and Δ' that explicitly depend on the condition we imposed via the choice of dissimilar groups of sites numbering m_A and m_B respectively, with identical evolution at each site within the

[2] Graphical displays similar to those in Fig. 6.1 have appeared several times in the literature, some with citation to (Andersen and Kenkre, 1993b) as in the BEC tunneling analysis of Raghavan et al. (1999c) and and some without citation as in the paper by Molina (1999). To whichever class they belong, they all support our earlier findings and strengthen our faith in their correctness and relevance. I have recently come across some well thought-out analysis on this subject presented by Tsironis (2011). I particularly encourage the reader to consult it as it emphasizes additional features.

group.

$$V' = V\sqrt{m_A m_B}, \tag{6.10a}$$

$$\chi' = \frac{N\chi}{2m_A m_B}, \tag{6.10b}$$

$$\Delta' = (m_A - m_B)\left(V + \frac{\chi}{2m_A m_B}\right) = (m_A - m_B)\left(V + \frac{\chi'}{N}\right). \tag{6.10c}$$

We find that the resulting evolution equations governing the N-mer,

$$\frac{dp}{dt} = 2V'q, \tag{6.11a}$$

$$\frac{dq}{dt} = -2V'p - (\chi' p - \Delta')r, \tag{6.11b}$$

$$\frac{dr}{dt} = (\chi' p - \Delta')q, \tag{6.11c}$$

are completely identical to Eqs. (5.1) that govern the nonlinear nondegenerate dimer, except for the primes in (6.11)!

This isomorphism allows one to deduce, in a nontrivial way as we shall show below, the N-mer dynamics from the known dynamics of the nonlinear nondegenerate dimer examined in Chapter 5.

Inspection of Eq. (6.10) shows transparently that the nondegeneracy Δ' arises directly from the difference $m_A - m_B$ and would vanish if there were no assumed separation into unequal A and B groups of sites. It also shows, the (perhaps unexpected) contribution to the nondegeneracy that comes from the nonlinearity χ in the system.

Dividing by $2V'$ all the entries in Eqs. (6.11), defining $\tau = 2V't$, $k_0 = \chi'/4V'$ and particularly $\delta = \Delta'/2V$ which is to be identified as the dimensionless nondegeneracy in the effective dimer, we can rewrite the evolution as proceeding from

$$\frac{dp}{d\tau} = q, \tag{6.12a}$$

$$\frac{dq}{d\tau} = -p - (2k_0 p - \delta)r, \tag{6.12b}$$

$$\frac{dr}{d\tau} = (2k_0 p - \delta)q. \tag{6.12c}$$

The k_0 that appears (without a prime) in Eq. (6.12) is now found to be

$$k_0 = \frac{\chi}{N^2 V(1-\eta^2)^{3/2}}. \tag{6.13}$$

with a change in the exponent of $(1 - \eta^2)$ from 1 to 3/2, relative to Eq. (6.9). Particularly important to note is that the key quantity in the effective nondegenerate nonlinear dimer is δ and is given by

$$\delta = \beta + 2k_0 \left(\frac{\beta}{\sqrt{1+\beta^2}} \right) = \eta \left(2k_0 + \frac{1}{\sqrt{1-\eta^2}} \right). \tag{6.14}$$

The first of these expressions involves $\beta = \eta/\sqrt{1-\eta^2}$, a quantity that is purely determined by the difference of m_A and m_B. Its appearance makes clear how the effective nondegeneracy arises from the separation of sites we have imposed through the inequality of m_A and m_B. The second expresses the effective nondegeneracy in terms of the quantity η introduced by Andersen and Kenkre (1993b),

$$\eta = \frac{m_A - m_B}{N} = \frac{2m_A}{N} - 1. \tag{6.15}$$

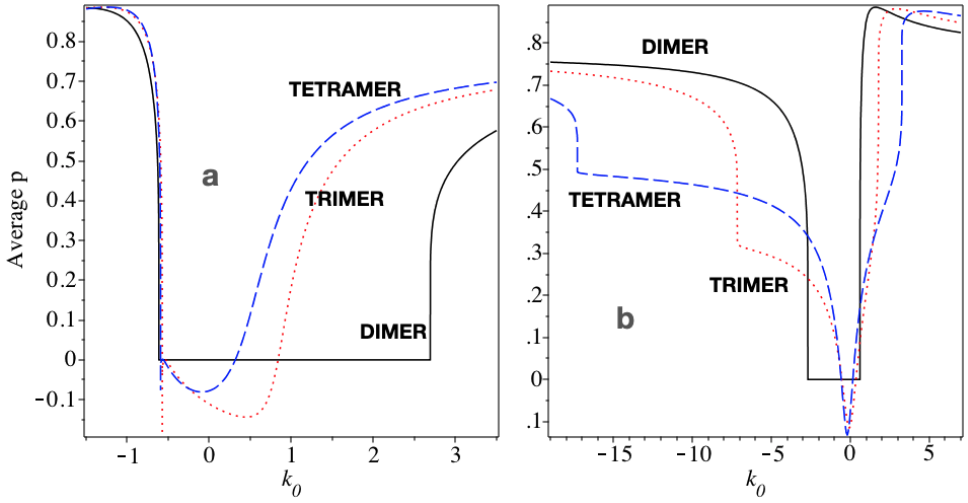

Fig. 6.2 Comparison similar to that shown in Fig. 6.1 but for partially delocalized initial conditions with $p_0 = 7/9$ and $q_0 = 0$. The left panel (a) is for in-phase conditions $r_0 = \sqrt{1-p_0^2}$ while the right panel (b) is for out-of-phase conditions $r_0 = -\sqrt{1-p_0^2}$. Modified with permission from figs. 5 and 8 of Ref. (Andersen and Kenkre, 1993b); copyright (1993) by American Physical Society.

We have thus constructed a bridge to port over results collected over the years for the nondegenerate dimer and the N-mer from one side to the other.

As the first example of the new rescaled equations of motion we reconstruct with their help two transition plots of the dependence of the average probability difference in the N-mers for *delocalized* (real) initial conditions that had been presented in Andersen and Kenkre (1993b) as Figs. 5 and 8, here blended as (a) and (b) in Fig. 6.2 for in-phase ($s = 1$) and out-of-phase ($s = -1$) cases respectively. The similarity between the plot produced here in this book from the nonlinear nondegenerate dimer

expressions and the one given in the publication almost three decades ago (without using the connection) is noteworthy. The only slight difference is a relative shift in the locations of the sharp dips in the left panel of Fig. 6.4. The source of this shift is the difference in the exponents in the k_0 expressions (6.9) and (6.13).

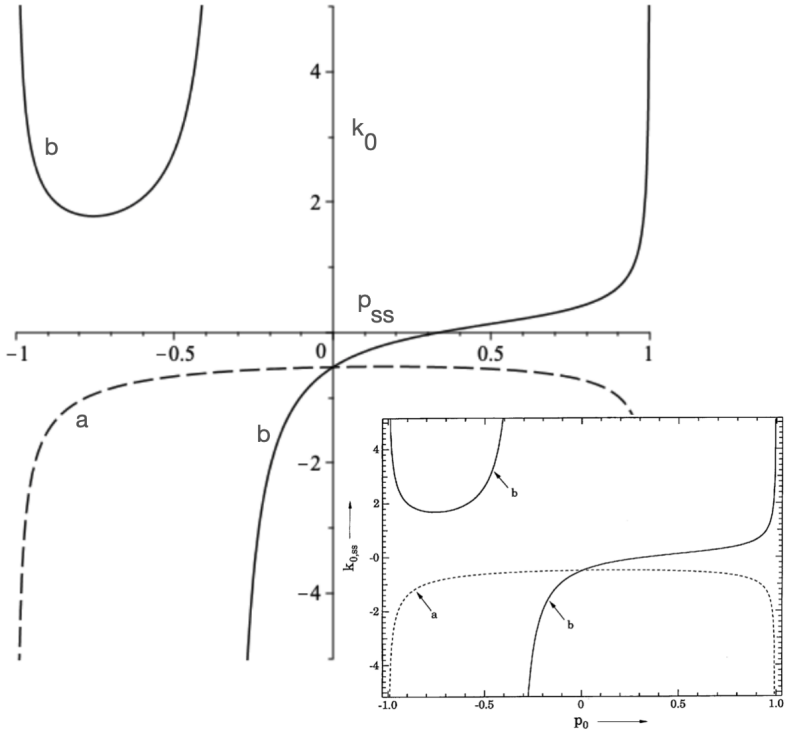

Fig. 6.3 A consequence of the bridge we have established to port over results from the nonlinear nondegenerate dimer to N-mers and vice-versa. The main plot has the stationary state probability difference p_{ss} plotted on the x-axis and the nonlinearity parameter $k_0 = \chi'/4V'$ plotted on the y-axis as calculated by putting the time derivatives to zero in Eq. (6.12). It can also be considered to be obtained by a rotation of the nonlinear nondegenerate plot of Fig. 5.12 concomitant with Eq. (6.14). The inset is a miniature representation of the precise corresponding plot from fig. 1 of Ref. (Andersen and Kenkre, 1993a). Solid (dotted or dashed) lines represent out-of-phase (in-phase) cases. The identity of the main plot and the inset proves beyond doubt, graphically, the validity of our prescription (6.14) that connects the two systems, the nonresonant dimer and the N-mer. Inset modified with permission from fig. 1 of Ref. (Andersen and Kenkre, 1993a); copyright (1993) by American Physical Society. Main figure, copyright Vasudev M Kenkre, 2021. All rights reserved.

As additional examples of the use of the bridge that Eq. (6.14) represents across the N-mers and the nonlinear nondegenerate dimer, we show Figs. 6.3 and 6.4. In the first of these, the stationary state probability plot shown in Chapter 5 for the nonlinear nondegenerate dimer yields the stationary state plot for the N-mers through a simple

rotation. The caption explains further detail. Trimers and tetramers are both shown in the plots.

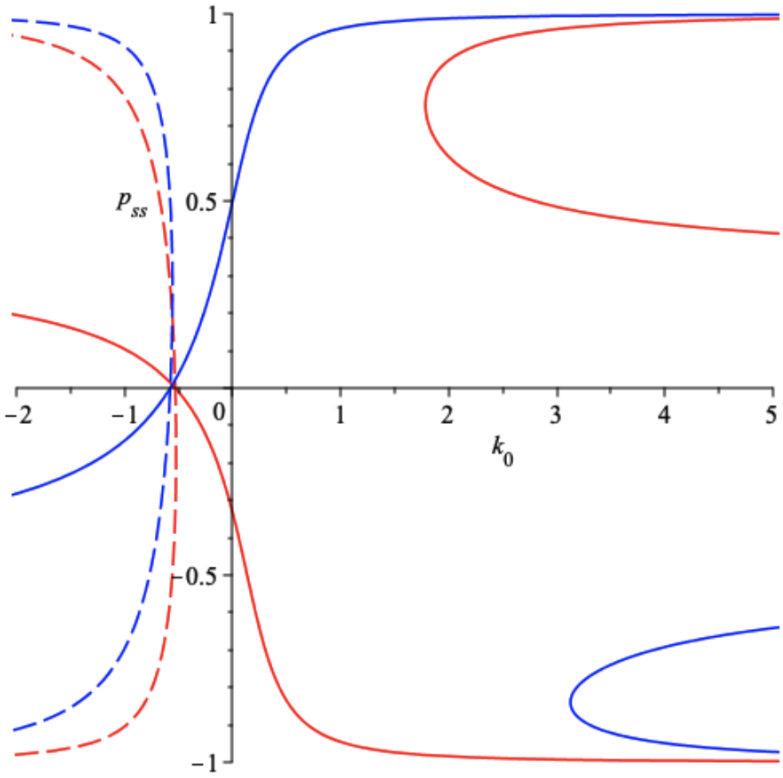

Fig. 6.4 Stationary states of N-mers shown to emphasize another example of the bridge we have established to port over results from the nonlinear nondegenerate dimer to N-mers and vice-versa. Solid (dashed) lines represent out-of-phase (in-phase) cases and red (blue) lines correspond to the trimer (tetramer). A comparison of the plot to Fig. 5.12 makes amply clear the validity of the prescription we have provided in Eq. (6.14) to establish the connection between the two systems.

As our final application of our bridge relation between N-mers and the nonlinear nondegenerate dimer we provide Fig. 6.5. It results from using the relation in conjunction with the fascinating finding by Tsironis (1993) that no self-trapping transitions occur in the nonlinear nondegenerate dimer beyond a critical point in the δ-k_0 plane[3]. The relevant question to ask is what may be expected for the N-mers as

[3] The plane is displayed clearly in Fig. 5.10. It can be regarded also as the floor of the Fig. 5.9 we have constructed from our theoretical analysis.

a corresponding result. The focus here is on the feature of Eq. (6.14) that it offers the effective nondegeneracy δ as arising from a superposition of the contribution of the nonlinearity with that of β or η which stems merely from the division of the N-mer into site groups for symmetry.

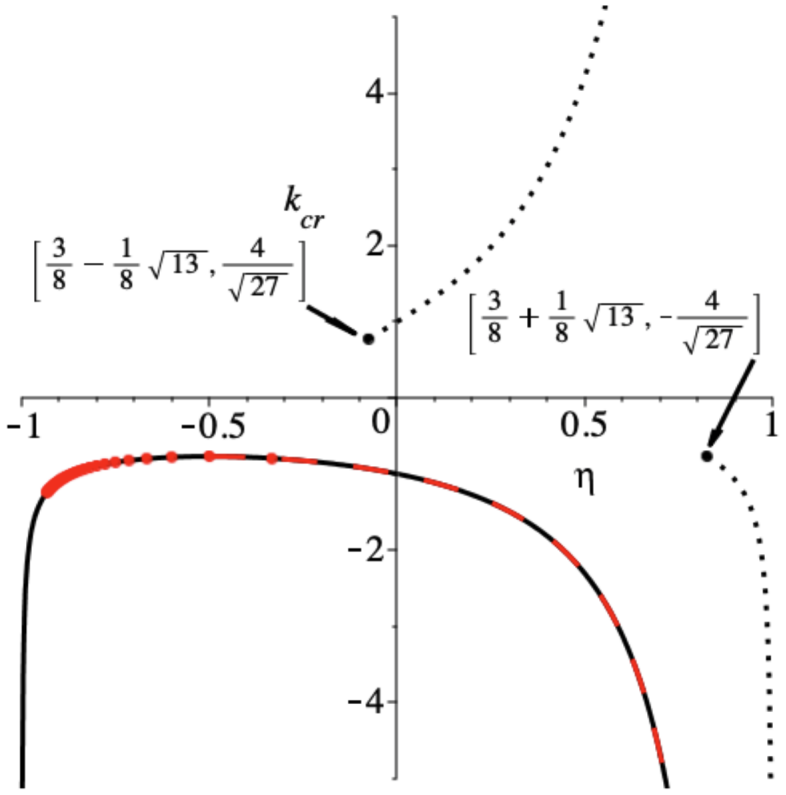

Fig. 6.5 Graphical depiction of the critical point and critical line situation in N-mers calculated via the the application of the bridge relation, Eq. (6.14), to the corresponding situation in the nonlinear nondegenerate dimer. The critical nonlinearity for self-trapping in the N-mer is shown as a function of the lattice asymmetry as solid and dotted black lines. Self-trapping stops along the dotted curves at their respective critical points, as it does in the nonlinear nondegenerate dimer (see Tsironis (1993)). The dashed red curve for $-1/2 \leq \eta < 1$ from (Andersen and Kenkre, 1993a) and the red circles from Molina (1999) follow the solid black curve. These earlier results provide clear additional validation of the bridge that we have presented. Although not apparent for all curves, the vertical asymptotes are at $\eta = \pm 1$. See text.

The answer is that the rotation implied by the mixing of the two contributions produces Fig. 6.5 for the N-mers with its multiple branches denoted by dotted lines in addition to the solid line (see plot). The dotted lines start at critical points

marked by arrows pointing to filled black circles whose coordinates are also shown in the Figure. Of particular interest are the previously reported results we show in red on the black solid trace in Fig. 6.5. Note in the plot the following. When the two symmetrically equivalent nondegenerate nonlinear dimer critical points lying at $(\delta, k_{cr}) = \left(\frac{\mp 1}{\sqrt{27}}, \frac{\pm 4}{\sqrt{27}}\right)$ are used in the relation (6.14), the resultant locations of the N-mer critical points are found to be at symmetrically inequivalent positions $(\eta, k_{cr}) = \left(\frac{3\mp\sqrt{13}}{8}, \frac{\pm 4}{\sqrt{27}}\right)$ and the maximum value $(\eta, k_{cr}) = \left(\frac{-1}{2}, \frac{-4}{\sqrt{27}}\right)$ of the solid curve.

The critical nonlinearity for localized initial conditions ($p(0) = 1$) has been found for N-mers for specific cases of η. The results of Andersen and Kenkre (1993b) were for the continuous range $-1/2 \leq \eta < 1$, while those given by Molina (1999) were for $m_A = 1$ (equivalently, $\eta = (2/\eta) - 1$) with $N \geq 3$. These two sets of results overlap only at $\eta = -1/3$ and $\eta = -1/2$. Modifying these earlier results so that they have the same scaling as the present k_0, displayed in the plot as k_{cr}, those from Andersen and Kenkre (1993b) are plotted in as a dashed red line, while those from Molina (1999) are shown as filled red circles. What is important to realize is that the bridge condition we have provided here has allowed us to arrive, with hardly any effort, at the *entire self-trapping phase space* for all N-mers.[4] It has also allowed us to unify the results of earlier investigations, obtained by different authors and over a span of half a dozen years, into a single context.

6.3 Additional Results from Considerations of *N*-mers

There is an interesting extension of the usefulness of the results obtained from the globally interacting N-mers with symmetric conditions that Andersen and Kenkre (1993b) argued in their analysis. Given that we are assured that the occupation of any of the A (or B) sites is as that of another of the group for all time, the intersite matrix element connecting any of these sites to each other is of no importance and can be set equal to zero. It follows then that the solution obtained for a trimer ring is also the solution for a trimer chain by which we mean a 3-site system without periodic boundary conditions, subject to initial conditions in which the two end sites have equal amplitudes. In exactly the same way, a tetramer reduces to a 2-dimensional star shape or to a 4-site ring with alternating A and B sites. This extension of the results to systems with lower symmetry but for initial conditions that are symmetric can be understood from Fig. 6.6.

[4] We have shown the analysis here only for localized initial conditions.

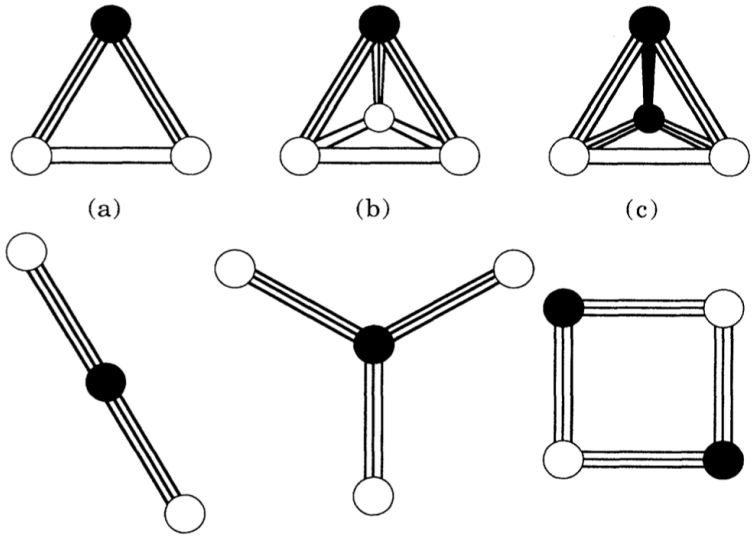

Fig. 6.6 Extension of the applicability of results obtained for N-mers by breaking bonds connecting equivalent sites. The upper three systems in the Figure are as analyzed in the text and the corresponding lower three are extended versions. In the upper row, white space represents bonds through which excitation flow is vanishing as a result of symmetry, and the corresponding bonds are simply disconnected (broken) in the lower row. We thus get an open trimer chain in (a), an open star in (b) and an alternating site type tetramer in (c). Modified with permission from fig. 2 of Ref. (Andersen and Kenkre, 1993b); copyright (1993) by American Physical Society.

6.4 Nonlinear Trapping from a Linear Lattice Antenna

In this and subsequent sections of this Chapter, we now turn to a different example of complex but analytically soluble systems approachable via the DNLSE and characterized by global interactions. They deal with the excitation capture problem in such globally interacting systems, analyzed by Kenkre and Kuś (1992).

The reaction diffusion problem of the motion (diffusion) of a quasiparticle in some environment followed by its arrival at a special location where it undergoes some characteristic process (reaction) is ubiquitous in physics. Sensitized luminescence, mutual anhhilation, chemical reactions are among phenomena whose study is linked to such reaction diffusion scenarios. An enormous literature exists on the subject and the interested reader might wish to learn about techniques, problems and subtleties from recent discussions in chapters 11 and 12 of a book I have recently published (Kenkre, 2021). Here let us focus on the analysis carried out by Kenkre and Kuś (1992) with a photosynthetic antenna and capturing center in mind.

Let us assume that the excitation whose trapping we study, moves quantum mechanically on a ring (chain with periodic boundary conditions) of sites m, n, etc.,

via nearest neighbor interactions V and is captured at a site that has the nonlinear behavior characteristic of the DNLSE arising, for example, from strong interactions with vibrations. It is then natural to think of three separate models. In the first, one of the sites in the chain is itself the capturing site and is inherently nonlinear in its behavior. This could arise from the energy of the excitation being lowered by an amount proportional to the probability of occupation of that site (indexed below by the label 0) by the excitation, leading to the evolution of the amplitude c_m at the mth site as

$$i\frac{dc_m}{dt} = V(c_{m+1} + c_{m-1}) - \delta_{m,0}\chi|c_0|^2 c_0. \tag{6.16}$$

A different model would correspond to the situation in which the capturing site is indexed by θ and a particular chain site, for instance the one at $m = 0$, communicates with that capturing site via a matrix element W. The capturing site is here considered external to the chain. The evolution would then obey

$$i\frac{dc_m}{dt} = V(c_{m+1} + c_{m-1}) + \delta_{m,0}Wc_\theta \tag{6.17}$$

in what may be called the *antenna* part of the system, with

$$i\frac{dc_\theta}{dt} = Wc_0 - \chi|c_\theta|^2 c_\theta \tag{6.18}$$

describing the evolution of the amplitude of the capturing center. It is explicit here that the capturing site is outside the antenna.

A third model could involve global capture from all antenna sites. It is characterized by

$$i\frac{dc_m}{dt} = V(c_{m+1} + c_{m-1}) + Wc_\theta, \tag{6.19a}$$

$$i\frac{dc_\theta}{dt} = W\sum_m c_m - \chi|c_\theta|^2 c_\theta, \tag{6.19b}$$

and is the one of interest to us in the present discussion published by Kenkre and Kuś (1992). Let us examine first the method of investigation, obtain with its help an analytic solution for arbitrary initial conditions and then study two issues in particular: the stationary states of the system, and the exact time-dependent solutions for the particular case of initial occupation of the antenna.

6.4.1 Arbitrary Initial Conditions, Analytic Solution

One can visualize our system as consisting of $N+1$ sites with N of them constituting a ring that surrounds a central trap site external to the ring. See Fig. 6.7. Intersite interactions are nearest neighbor within the antenna ring. The central trap is coupled to all the antenna sites equally. In order to solve the governing equations (6.19), let

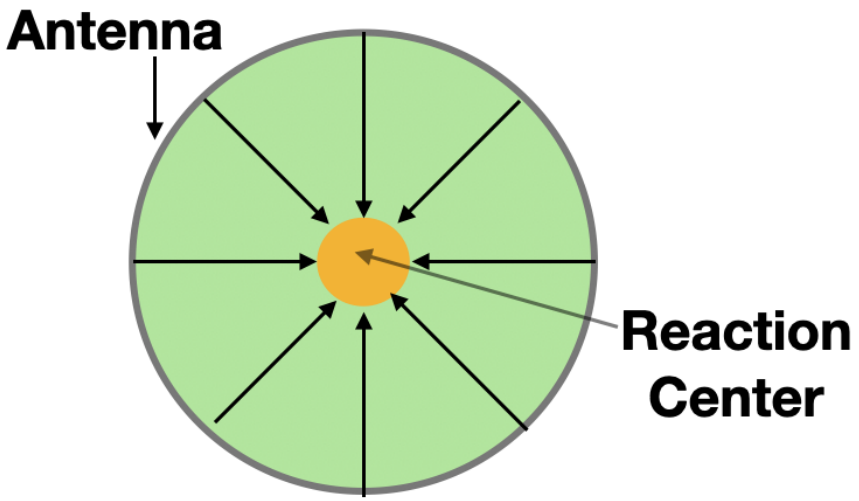

Fig. 6.7 Schematic depiction of the capture model showing the antenna which is the ring of sites surrounding the centrally placed reaction center whose energy is lowered by an amount proportional to χ when it is occupied by the excitation. Excitation moves in the antenna sites through nearest neighbor matrix elements V and communicates with the reaction center via matrix elements W. See text.

us introduce the Bloch state amplitudes

$$c^k = \frac{1}{\sqrt{N}} \sum_{m=1,2,\ldots}^{N} c_m e^{ikm} \tag{6.20}$$

via a simple discrete Fourier transform of the antenna site amplitudes and remember that they can always be inverted into the site amplitudes via

$$c_m = \frac{1}{\sqrt{N}} \sum_{m=0,2\pi/N,\ldots}^{2\pi(N-1)/N} c^k e^{-ikm}. \tag{6.21}$$

In order to find the time dependence of the Bloch amplitudes in the antenna it is straightforward to use Eq. (6.19a). We find the Bloch amplitudes obeying

$$\frac{dc^k}{dt} = -2iV \cos k c^k + \sqrt{N} W \delta k, 0 c_\theta. \tag{6.22}$$

The antenna state with $k = 0$ and the capturing state θ form a closed system of two nonlinear equations

$$\frac{dc^0}{dt} = -2iVc^0 - i\sqrt{N}Wc_\theta, \tag{6.23a}$$

$$\frac{dc_\theta}{dt} = -i\sqrt{N}Wc^0 + i\chi|c_\theta|^2 c_\theta. \tag{6.23b}$$

The remaining Fourier components $c^k(t)$ can be found straightforwardly from the linear homogeneous equation (6.22).

While closely related to the nonlinear nondegenerate dimer that we have analyzed in Chapter 5 and have linked to the N-mer in the preceding sections of the present chapter, what we have here for the capture system is slightly different. Only one of the two sites, θ, has nonlinearity χ associated with it: it alone undergoes energy lowering when occupied by the excitation, the antenna obviously does not. The matrix element that connects the two sites is $\sqrt{N}W$, which we will call from now on w for simplicity, and the nondegeneracy is marked by $2V$.

Let us now rewrite the Fourier mode of the antenna that communicates with the reaction center associating it with the letter s so that $c_s = c^0$, define generally the density matrix elements $\rho_{\mu\nu} = c_\mu c_\nu^*$ with the subscripts μ and ν taking on values s and θ, and introduce the *four* Bloch-like quantities

$$P = \rho_{\theta\theta}, \tag{6.24a}$$

$$Q = i\left(\rho_{\theta s} - \rho_{s\theta}\right), \tag{6.24b}$$

$$R = \left(\rho_{\theta s} + \rho_{s\theta}\right), \tag{6.24c}$$

$$S = \rho_{ss}. \tag{6.24d}$$

Three of these, P, Q, R, have the nature of the components of the Bloch vector that we have encountered in various calculations, S represents the antenna. They obey the evolution equations

$$\frac{dP}{dt} = -\frac{dS}{dt} = wQ, \tag{6.25a}$$

$$\frac{dQ}{dt} = -2w(P - S) - 2VR - \chi PR, \tag{6.25b}$$

$$\frac{dR}{dt} = 2VQ + \chi PQ. \tag{6.25c}$$

It is easy to see that this system of equations has three integrals of motion,

$$I_1 = P + S, \tag{6.26a}$$

$$I_2 = R - \frac{\chi}{2w}P^2 - \frac{2V}{w}P, \tag{6.26b}$$

$$I_3 = 4P(P - I_1) + Q^2 + R^2. \tag{6.26c}$$

The first and the third of these have a simple interpretation for the case of equal population of all antenna sites, i.e., for $c_n(0) = c_1(0)$ for all n. In this case, we can write explicitly,

$$I_1 = |c_\theta|^2 + \left| \frac{1}{\sqrt{N}} \sum_{m=1,2,\ldots}^{N} c_m \right|^2 = 1, \tag{6.27a}$$

$$I_3 = 4P(P-1) + Q^2 + R^2 = 0. \tag{6.27b}$$

from conservation of the total probability.

It is now possible to obtain a single closed equation for the probability P,

$$\frac{d^2P}{d\tau^2} = (1/2)(I_1 - \eta I_2) - (\xi I_2 + \eta^2 + 1)P - 3\xi\eta P^2 - 2\xi^2 P^3, \tag{6.28}$$

in terms of the scaled time as well as scaled nonlinearity and transfer parameters

$$\tau = 2wt, \qquad \xi = \chi/4w, \qquad \eta = V/w. \tag{6.29}$$

It is clear that τ measures the time relative to the transfer time for the excitation to go from antenna to the reaction center and that the parameters ξ and η similarly measure the nonlinearity and the transfer within the antenna, respectively.

We have already shown in section 5.2 of Chapter 5 how to obtain explicit solutions of an equation such as (6.28) by appealing to the method that employs Weierstrass functions. The pathway consists of multiplying Eq. (6.28) by the first τ-derivative of P and arriving at what is essentially Eq. (5.9). Following the notation of (Kenkre and Kuś, 1992), we write it here as

$$P(\tau) = P_0 - \frac{6U'(P_0)}{24\wp(\tau; g_2, g_3) + U''(P_0)}. \tag{6.30}$$

where $\wp$ is the Weierstrass function, $P_0 = P(0)$, and the g's are here given by

$$g_2 = (1/9)h_2^2 + (1/2)h_1 - \xi^2 U(P_0), \tag{6.31a}$$

$$g_3 = (1/216)h_2^3 - (1/16)\xi^2 h_2^2 + (1/24)\xi\eta h_1 h_2 - (1/4)\xi^2(h_1 + \eta^2)U(P_0), \tag{6.31b}$$

in terms of the quantities $h_1 = \eta I_2 - I_1$ and $h_2 = \xi I_2 + \eta^2 + 1$.

Once $P(\tau)$ is known explicitly through Eq. (6.30), related quantities follow through

$$Q(\tau) = 2\frac{dP(\tau)}{d\tau}, \tag{6.32a}$$

$$R(\tau) = I_2 + 2\xi P^2(\tau) + 2\eta P(\tau), \tag{6.32b}$$

$$S(\tau) = I_1 + P(\tau). \tag{6.32c}$$

The phase between the amplitudes c_θ and c_s is also determined explicitly as

$$\cos\psi(\tau) = \frac{R(\tau)}{\sqrt{P(\tau)S(\tau)}}, \quad \sin\psi(\tau) = \frac{Q(\tau)}{\sqrt{P(\tau)S(\tau)}}. \tag{6.33}$$

With $c^k(\tau) = c^k(0)e^{-i\eta\tau\cos k}$ for $k \neq 0$, we have thus the full solution for arbitrary initial conditions.

By using the reexpression of the Weierstrass functions in terms of Jacobian elliptic functions that we have shown in Chapter 5 of this book, see, for instance, Eq. (5.12), it is now possible to cast the reaction center probability and related quantities in terms of squares of sn functions. Because it is a straightforward exercise, I will leave it to the reader. Let us now explore the stationary states of the system followed by an analysis of the particular case of zero initial occupation of the reaction center.

6.4.2 Stationary States of the Reaction Center

Interesting information can be gleaned by examining the stationary states obtained by putting the time derivatives in Eqs. (6.25) equal to zero. We get, with ss as the subscript to denote stationary states,

$$Q_{ss} = 0, \tag{6.34a}$$

$$2w(S_{ss} - P_{ss}) = 2VR_{ss} + \chi P_{ss}R_{ss}. \tag{6.34b}$$

If we restrict attention to the case of homogeneous antenna occupation, $c_n = c_1$ for all n, it is easy to eliminate S_{ss} and R_{ss} by using that, in this case, $I_1 = 1$ and $I_3 = 0$, and obtain a closed nonlinear equation for the stationary state value of the reaction center probability P_{ss}:

$$P_{ss}(P_{ss} - 1)\left(\frac{2V}{w} + \frac{\chi}{w}P_{ss}\right)^2 + (1 - 2P_{ss})^2 = 0. \tag{6.35}$$

This result is highly useful for the purposes of analyzing the effect of the system parameters on the efficiency of the reaction center in the process of collecting the excitation originally placed in the antenna. To get a brief illustrative glimpse, let us plot in Fig. 6.8 the solution of the nonlinear Eq. (6.35), examine its dependence on the nonlinearity ratio $\xi = \chi/4w$ for just two values of the ratio $\chi/4V$ which we will call α.

6.4.3 Dynamics for Initial Zero Occupation of the Reaction Center

Let us now consider the time-dependent evolution for the initial assignment $c_\theta = 0$ which means the reaction center is unoccupied and $c_n(0) = 1/\sqrt{N}$ which represents a uniform distribution of the initial probability among the antenna sites. Now we have,

$$P(0) = Q(0) = R(0) = [dP/d\tau]_{\tau=0} = 0, \quad S(0) = 1. \tag{6.36}$$

The quantities we have introduced earlier take on simple values

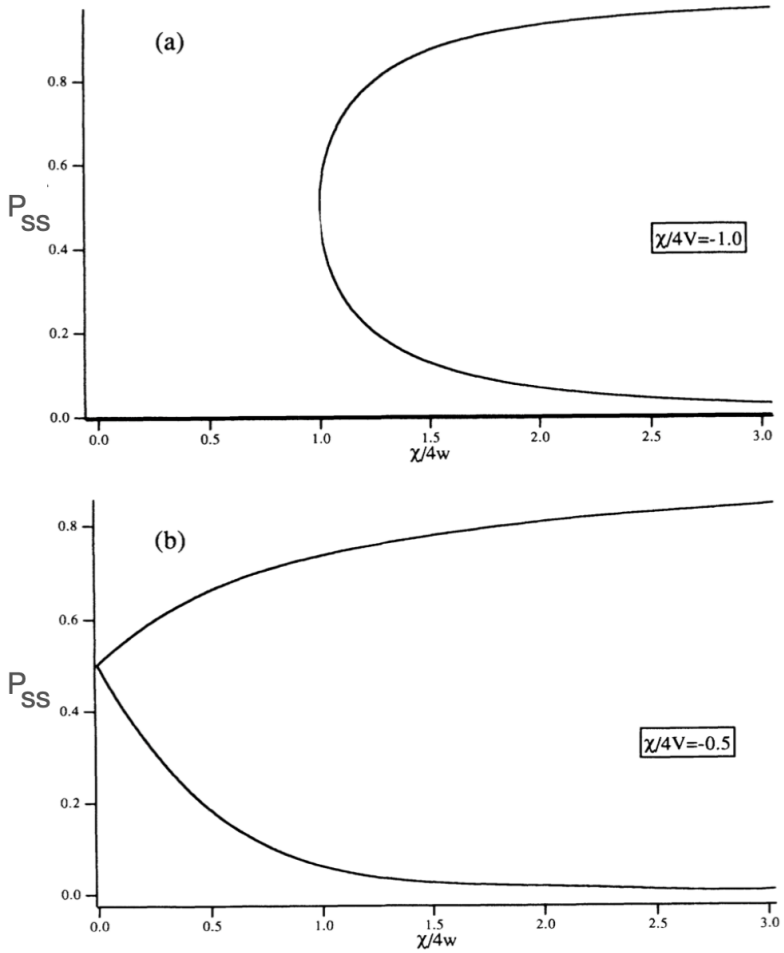

Fig. 6.8 Reaction center probability in the stationary state plotted as a function of the parameter $\xi = \chi/4w$ for two values of $\chi/4V$: (a) -1 and (b) -0.5. Bifurcation behavior is clearly exhibited. Modified with permission from fig. 3 of Ref. (Kenkre and Kuś, 1992); copyright (1993) by American Physical Society.

$$I_1 = 1, \quad I_2 = 0, \quad h_1 = -1, \quad h_2 = 1 + \eta^2. \tag{6.37}$$

And the potential $U(P)$ that is natural to obtain in the standard procedure to solve the nonlinear differential equation of second order for $P(\tau)$ that features in

$$[dP(\tau)/d\tau]^2 = U(P) - U(P_0) + [dP/d\tau]^2_{\tau=0} \tag{6.38}$$

reduces to the simple form $U(P) = PU_1(P)$ with the cubic expression

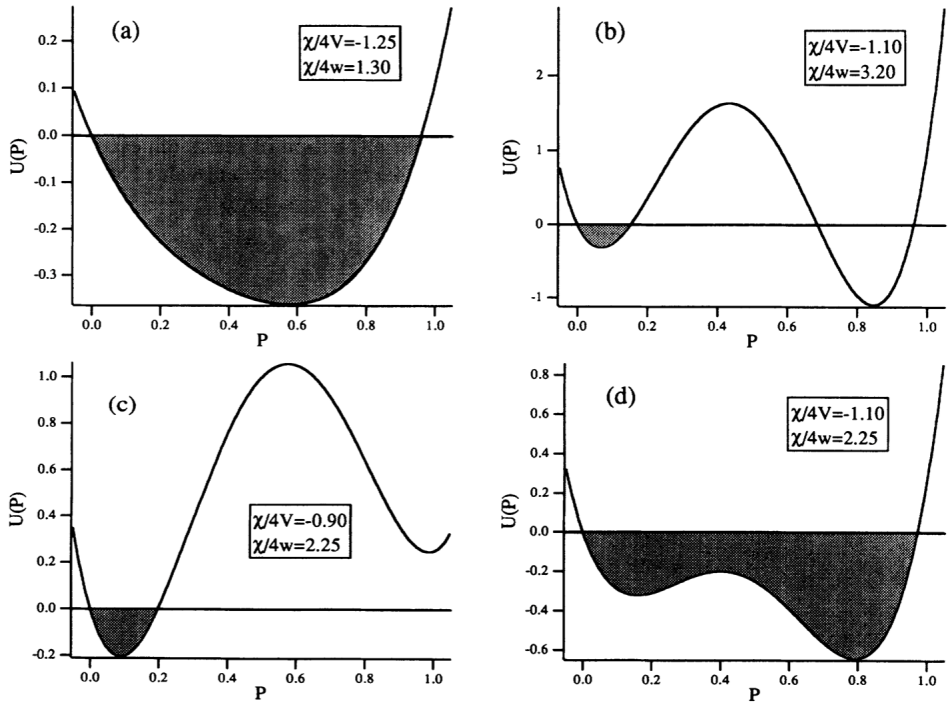

Fig. 6.9 Transfer from antenna to initially unoccupied reaction center illustrated with the help of the quartic potential $U(P)$ for several values of the pair $\alpha = \chi/4V$ and $\xi = \chi/4w$. See text for the physical meaning of these quantities. Shaded regions represent intervals in which excitation motion occurs. Parameter values determine sharply whether the system is confined to the neighborhood of $P = 0$ as in (b) and (c) signifying inefficient transfer to the reaction center or reach values close to $P = 1$ as in (a) and (d) signifying a situation that would be desirable for collecting excitation at the reaction center. Modified with permission from fig. 1 of Ref. (Kenkre and Kuś, 1992); copyright (1993) by American Physical Society.

$$U_1(P) = \xi^2 P^3 + 2\eta\xi P^2 + (1+\eta^2)P - 1. \tag{6.39}$$

The evolution of the system can be said to start from $P = 0$ where $U(P) = 0$. Given that the P-derivative of U at $P = 0$ equals -1, and is thus smaller than 0, means that the motion of the representative point proceeds in the direction of positive P. The system never reaches $P = 1$ corresponding to full occupation of the reaction center with the exception of the case $\eta = -\xi$. This exceptional case occurs if the antenna intersite interaction and the scaled antenna-trap interaction are equal in magnitude but opposite in sign. Note here that $U(1) = (\xi + \eta)^2 \geq 0 = U(0)$. Note also that

$$U_1(P) = \xi^2 P^3 + 2\eta\xi P^2 + (1+\eta^2)P - 1. \tag{6.40}$$

This statement leads us to conclude that there exists at least one positive root P_1 of $U_1(P)$ lying between the values 0 and 1 of P. One can state with confidence that the motion of the representative point is confined to the interval between the values 0 and P_1, the smallest of the values that fulfills the condition $U_1(P_1) = 0, 0 \leq P_1 < 1$.

Through the application of insights obtained from standard treatments such as (Uspensky, 1948), Marek Kuś was successful, in the collaborated work we did, in progressing considerably further in the analysis of the present problem. Following the presentation to be found in detail in (Kenkre and Kuś, 1992), let us point out that the necessary and sufficient condition for $U_1(P)$ to have three real roots is that the discriminant Δ of the third-order equation $U_1(P) = 0$ is smaller than 0. With the notation $\alpha = \chi/4V$, the condition is that the discriminant Δ is less than 0. This inequality is fulfilled if and only if $9+8/\alpha > 0$, and $\beta_- \geq \xi^2 \geq \beta_+$ where one defines

$$\beta_\pm = \left[-\frac{1}{\alpha^2} - \frac{9}{2\alpha} - \frac{27}{8} \mp \frac{(9\alpha+8)^{3/2}}{8\alpha^{3/2}} \right]^{-1}. \tag{6.41}$$

To ensure that all three roots of $U_1(P)$ lie between 0 and 1, one might impose another condition,

$$0 \leq p_{max} \leq p_{min} \leq 1. \tag{6.42}$$

Here,

$$p_{max} = -\frac{1}{3}\left[\frac{2}{\alpha} + \sqrt{\frac{1}{\alpha^2} - \frac{3}{\xi^2}} \right], \tag{6.43a}$$

$$p_{min} = -\frac{1}{3}\left[\frac{2}{\alpha} - \sqrt{\frac{1}{\alpha^2} - \frac{3}{\xi^2}} \right], \tag{6.43b}$$

are the respective values of P at the local maximum and minimum of $U_1(P)$. Because $U_1(\pm\infty) = \pm\infty$, if $U_1(P)$ has three real roots, we must have $U_1(p_{max}) > 0, U_1(p_{min}) < 0$, and $p_{max} \leq p_{min}$. This leads to the conclusion that all roots of $U_1(P)$ lie between 0 and 1 if and only if the condition (6.42) is satisfied. And it implies

$$\alpha < 0, \quad \frac{1}{\xi^2} > 1 - \left(\frac{1}{\alpha} - 2 \right)^2. \tag{6.44}$$

We are now in a position to understand the dynamics of our system graphically on the basis of the analytics we have shown by considering different shapes of the potential corresponding to different regions in the (α, ξ) plane. These two quantities that form the plane represent, as we have seen, the nonlinearity at the reaction center relative to the internal antenna intersite transfer and to the antenna-center transfer, respectively.

We see from Fig. 6.9 that the confining interval within the P-extent depends sensitively on the parameter values and is critical to the efficiency of excitation transfer from antenna to reaction center. In order to understand the source of this behavior, let us examine Fig. 6.10 which shows the potential $U(P)$ for $\alpha = \chi/4V =$

-1 for three different values of $\xi = \chi/4w$. The reader is reminded that the latter is a measure of the nonlinearity of the reaction center relative to the antenna-center transfer.

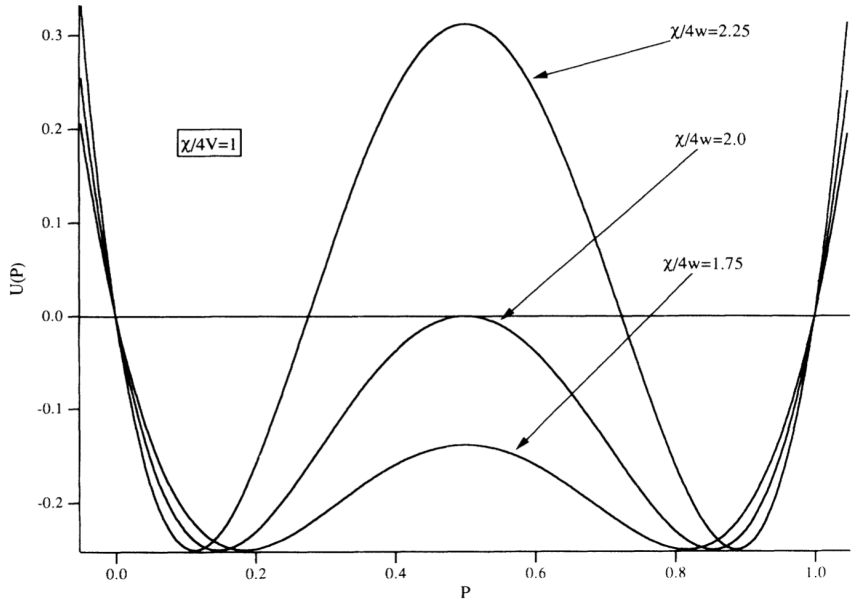

Fig. 6.10 Graphical understanding of how differences in the ratio $\xi = \chi/4w$ of the reaction center nonlinearity to the antenna-center transfer control the efficiency. Plotted is the potential $U(P)$ for a fixed value 1 of $\alpha = \chi/4V$ for three different values, 2.25. 2, and 1.75 of the $\xi = \alpha = \chi/4V$. The values of P are confined to the left well of the potential for the first two cases but spread throughout the region for the third as is clear from the fact that the central peak of the potential is below the 0 line for the third case, above it for the first case and marginally touching the line in the second case. Modified with permission from fig. 2 of Ref. (Kenkre and Kuś, 1992); copyright (1993) by American Physical Society.

Consider in Fig. 6.10 the case $\xi = 2.25$. The potential confines the evolution of the reaction center probability $P(\tau)$ to the interval from 0 to 0.3. Now examine the effect of lowering ξ to the value 2.0. The evolution still has P going from 0 to now 0.5. The excitation is confined primarily to the antenna. If, however, one reduces the nonlinearity by a small amount now to 1.75, P is seen to oscillate fully in the 0 to 1 region. This means that we now have a delocalized state and much more efficient transfer from the antenna to the reaction center. The transition occurs whenever the line $\xi = \pm\beta$ is crossed in parameter space.

6.5 Further Directions of Research and Remarks

The sharp reader has not only appreciated the equivalence between the nonlinear nondegenerate dimer and the globally interacting N-mers that we have stated and explored in the first part of the present Chapter but has surely noticed the similarity of the treatments and identity of some equations to be found in the analysis of the second part of this Chapter as well. Weierstrass functions appear in all three because of the formally similar closed second-order differential equations that need to be solved. Within the contexts of the systems we are discussing in this book, Tsironis invoked them first in his Ph. D. thesis but they were also employed, independently, by Andersen for N-mers and by Kuś for the nonlinear trapping model, respectively. The slight differences in the treatments are consequences of the slightly different points of emphasis the three used.

There are a number of new directions one could explore in the nonlinear trapping model if experimental observations were to show the relevance of such theoretical exercises. I mention two. The first would involve a complete investigation of the transfer of excitation from antenna to the reaction center for arbitrary types of initial conditions in the antenna related to spatially different absorption of light or of initial deposition of the excitation within the antenna. It could also involve scattering processes among the Bloch states in the antenna. Depending on relevance and need for detail, the equations of motion within the Bloch band of antenna states could be of the Boltzmann type leading to relaxation in the band or could involve full density matrix detail. The second interesting project might be to stay within the nondegenerate nonlinear dimer system that the study explained in this second part of this Chapter has covered but to investigate a design feature which might control the nondegeneracy. The extent of nonresonance of the $k = 0$ Bloch state of the antenna with the center state could be dialed to get the most efficient extent of transfer. This is a simple and interesting problem that I hope the reader will undertake as an immediate exercise to tackle. If the communicating Bloch state from the antenna is energetically nonresonant with the reaction center state as it would normally be, the process of transfer which changes the effective energy of the reaction center state could bring it into resonance during the transfer process.

6.6 Chapter 6 in Summary

Equal global interactions between any pair of sites in a system of an arbitrary number of them served as the focus in this Chapter. In its first part, initial conditions with high symmetry were selected for study so that whatever the site number, it was divided into two subgroups, evolution in each of which was identical from site to site but different from the other subgroup. Transitions were noted, analytic solutions were obtained and their averages and frequencies of oscillation were studied. Weierstrass functions entered the study as naturally as they did in the study of the nonlinear nondegenerate dimer in the previous Chapter. This was shown to be more than an accident in that

any N-mer system could be formally recast as a nonlinear nondegenerate dimer with an effective energy mismatch that could be calculated precisely from the symmetry imposed in the N-mer and the extent of nonlinearity. This bridge allowed results from N-mers to be easily (but not trivially) ported over to the nonlinear nondegenerate dimer and vice-versa. In the second half of the Chapter a reaction-diffusion model of a phenomenon like sensitized luminescence was studied which might serve in principle as a crude representation of a photosynthetic unit. Analytic solutions were again obtained in terms of Weierstrass functions and their equivalent Jacobian elliptic functions. Arguments were presented concerning stationary states of the system and their influence on the capture of the excitation and analysis in terms of nonlinear potentials were given. Interesting unsolved questions were explained and suggested for analysis.

Chapter 7
Slow Relaxation: the Nonadiabatic Nonlinear Dimer

In Chapters 4-6 we have explored the effects of slapping various complexities on to the simple DNLSE that we introduced in Chapter 1 and investigated in its simple form in Chapters 2,3. These complexities have covered, in turn, non-cubic nonlinearities, static energy mismatch, and globally interacting spatial extensions. In all of those considerations, the lowering of the energy of the occupied site has been taken to happen infinitely fast: The nonlinear term in the DNLSE has made its presence instantaneously on occupation of the site by the quantum particle. Let us now drop that assumption even as we return to the cubic, symmetrical dimer and ask what the effects of slow relaxation can be. (Kenkre and Wu, 1989a,b)

We could undertake the study by incorporating into the nonlinearity χ a time dependence that makes it rise at a finite rate from 0 to its full value, or use related descriptions. Instead, let us return to the coupled equations (4.5) and simply refrain from making the time disparity assumption whereby the time derivative is omitted. Let us also take the opportunity to consider in the interests of proper representation of damping effects, an additive term proportional to the first-order time derivative. Equation (4.5b) is then replaced by

$$\frac{d^2x_m}{dt^2} + \alpha\frac{dx_m}{dt} + \omega^2 x_m + S|c_m|^2 = 0. \tag{7.1}$$

We will focus most of the analysis on the extreme limits of high damping (Sections 1-3) in which α (and ω as well) is taken to tend to infinity in such a way that the relaxation may be treated with the help of a single rate parameter $\Gamma = \omega^2/\alpha$. We will also briefly tackle the opposite effect of vanishing damping (Section 4) so that there is no α in the system but only a time proportional to $1/\Gamma$. A study with external fields will be mentioned in Section 5.

7.1 Preliminary Considerations

If we take the so-called Aristotelian[1] limit of the vibrational parameters, $\alpha \to \infty, \omega \to \infty$, so that $\omega^2/\alpha \to \Gamma$, where Γ is constant and may be termed the relaxation rate, the replacement of (4.5b) is by

$$\frac{dx_m}{dt} + \Gamma x_m + (S/\alpha)|c_m|^2 = 0, \tag{7.2}$$

provided it is also assumed that $S \to \infty$ (and is proportional to α) so we may keep the last term in the equation.

For a dimer ($m = 1, 2$), the interacting equations take the form

$$i\frac{dc_1}{dt} = Vc_2 + Ex_1c_1, \tag{7.3a}$$

$$i\frac{dc_2}{dt} = Vc_1 + Ex_2c_2, \tag{7.3b}$$

$$\frac{dx_1}{dt} + \Gamma x_1 = -\frac{\Gamma\chi}{E}|c_1|^2, \tag{7.3c}$$

$$\frac{dx_2}{dt} + \Gamma x_2 = -\frac{\Gamma\chi}{E}|c_2|^2. \tag{7.3d}$$

It is therefore clear that the nonlinearity parameter χ of the adiabatic (infinitely fast relaxation) description is given in terms of the internal parameters and the nonlinearity χ is related to the internal parameters by

$$\chi = \frac{SE}{\alpha\Gamma} = \frac{SE}{\omega^2}. \tag{7.4}$$

In the spirit of preview of exciting things to come, let me first display in Fig. 7.1 consequences of Eqs. (7.3), numerically obtained: the time evolution of the probability difference $p(t) = |c_1(t)|^2 - |c_2(t)|^2$ and the relative vibrational coordinate $y(t) = x_1(t) - x_2(t)$ for the initial condition that the particle is localized on site 1 initially, and the vibrational coordinate is random. The caption provides the description of what is displayed.

What we see in the top left panel is the case of a free system (nonlinearity subcritical so there is no self-trapping transition) displaying particle probability oscillations (solid blue line) forever. The oscillator displacement difference (dash-dotted red line) starts from its initial value and falls in step with the probability difference as time evolves. As we move clockwise to the top right panel, the nonlinearity value is the precise critical value, the stationary state is still symmetric, i.e., with equal probability on either site, and that is how the particle settles eventually after attempting to oscillate around that value. The left bottom panel should be inspected next. Agin

[1] The terminology refers to the contrasting beliefs held by the ancient Greek scientist and the more modern Englishman, Newton, about what state a body left to itself, i.e., in the absence of a force acting on it, persists in.

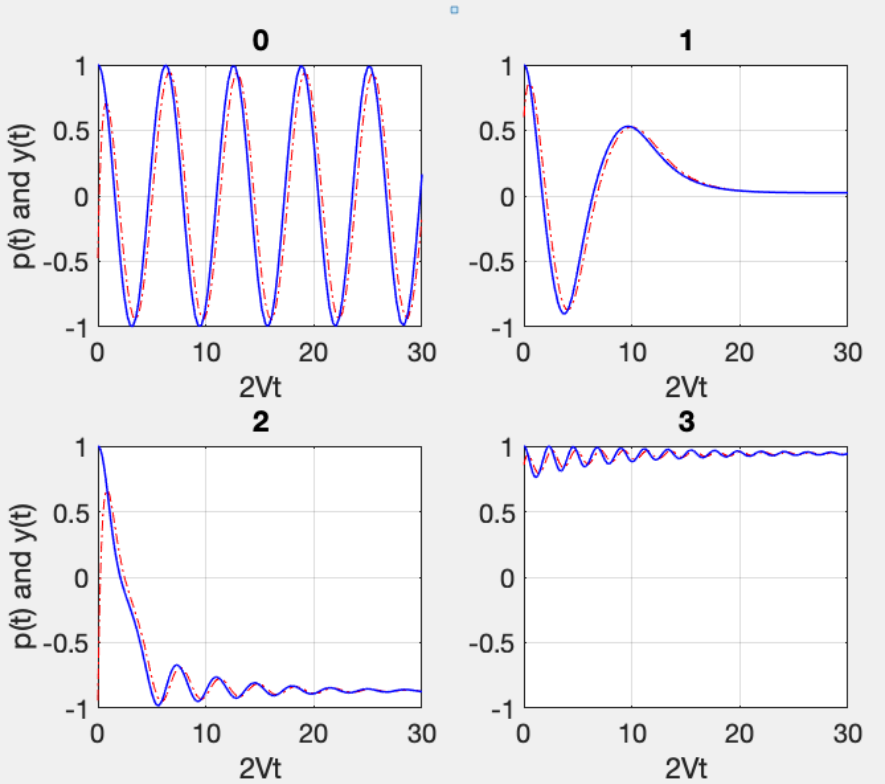

Fig. 7.1 Evolution of the probability difference $p(t)$ (solid blue) and the scaled oscillator displacement $y(t)$ (dash-dot red) in the nonadiabatic nonlinear resonant dimer for four values of the nonlinearity ratio $\chi/2V$ as shown on top of respective panel: 0, 1, 2, 3, respectively. The initial condition for the dimer is localized on site 1 in all cases ($p(0) = 1$) but the initial displacement of the oscillator is random. The relaxation rate Γ scaled to $2V$ is 2.9. Slaving of the oscillator displacement proceeds in time in all cases which means that, whatever its starting value, $y(t)$ attempts to attain the value of $p(t)$. Furthermore, we see p driven to its stationary value p_{ss} which is different in the four cases. For the top two panels, χ is sub-critical (the second case is at the margin) and so there is no self-trapped state: the probability difference is eventually equalized. For the bottom two panels the value of χ exceeds the critical value $2V$. Consequently, the quantum particle settles into the self-trapped state. The eventual probability difference in the self-trapped state has magnitude $\sqrt{1-(2V/\chi)^2}$ and here equals -0.8660 and 0.9428, respectively.

we observe the slaving of the scaled oscillator displacement difference $y(t)$ (started with a random value for each of the four panels) be slaved by the slower $p(t)$, which then evolves into a stationary state which is self-trapped with probability appropriate to the nonlinearity $\chi = 4V$. While this self-trapped state has more of a contribution of the right site in it, the last of the panels shows the same process. It has $\chi = 6V$

and it happens to settle into a *more* self-trapped state and one that happens to have more contribution of the left site in it.

We will see examples of these various behaviors in the following with theoretical explanations of what is happening.

7.2 Relaxation at Finite Rates

The consequence of Eq. (7.3) is that the Bloch vector components develop an interaction with the vibrational coordinate evolution so that

$$\frac{dp}{dt} = 2Vq, \tag{7.5a}$$

$$\frac{dq}{dt} = -2Vp - \chi yr, \tag{7.5b}$$

$$\frac{dr}{dt} = \chi yq, \tag{7.5c}$$

$$\frac{dy}{dt} + \Gamma(y - p) = 0. \tag{7.5d}$$

The consequences of finite relaxation are clear in the evolution equations. Terms that have the nonlinearity parameter χ in them, specifically in Eqs. (7.5b) and (7.5c), are now multiplied by the vibrational coordinate y rather than by the probability difference p; and an additional evolution equation, (7.5d), appears. We see the system drive, as its consequence, y to p at rate Γ. Surely, if the driving is infinitely fast, Eqs. (7.5) reduce to the *adiabatic* Bloch vector equations discussed earlier in the book.

The exact solution of the newly introduced Eq. (7.5d) is

$$y(t) = y(0)e^{-\Gamma t} + \int_0^t ds\, \Gamma e^{-\Gamma(t-s)} p(s). \tag{7.6}$$

The first term on the right hand side carries information about the initial value of the vibrational coordinate. That information is wiped out quickly if Γ is large and can be neglected in that case. In the second term, $\Gamma e^{-\Gamma t}$ plays the role similar to that of a Dirac delta-function if Γ is large enough, thereby slaving $y(t)$ to $p(t)$ at times much larger than $1/\Gamma$.[2] In order to probe into relaxation that is not infinitely fast, we could neglect the first term for $t >> 1/\Gamma$ and rewrite the second term through an integration by parts as $[p(t) - (1/\Gamma)dp(t)/dt]$.

There is another way to solve Eq. (7.5d) that I presented in Kenkre and Wu (1989a). In the Laplace domain the solution is

[2] Let me remind the reader that $\Gamma \exp(-\Gamma t)$, except for an unimportant multiplicative factor of (1/2) which is sometimes used by convention, is an often used representation for the Dirac δ-function.

$$\widetilde{y}(\epsilon) = \frac{y(0)}{\epsilon + \Gamma} + \frac{\Gamma \widetilde{p}(\epsilon)}{\epsilon + \Gamma}. \tag{7.7}$$

We denote the Laplace variable by ϵ and use tildes to indicate Laplace transforms. If we ignore the first term on the right hand side for times t much larger than $1/\Gamma$ as we did earlier, divide both the numerator and denominator of the second term by Γ, and assume that for times much larger than $1/\Gamma$ we can express $[1/(1+\epsilon/\Gamma)]$ by $[1-\epsilon/\Gamma]$, we could approximate

$$y(t) \approx p\left(t - \frac{1}{\Gamma}\right) \approx p(t) - \frac{1}{\Gamma}\frac{dp(t)}{dt}. \tag{7.8}$$

Two approximations have been made here that the reader should attempt to understand from simple Laplace manipulations.

We thus see that the interaction of the vibrational and particle motion in the Aristotelian (very fast but not infinitely fast) approximation forces the former to follow the latter *with a lag* as Eq. (7.8) shows in its first part. That equation also shows from its second part that, as equilibrium is approached, the time derivative of $p(t)$ dies out and y coincides with p leading to the adiabatic evolution into stationary states. It is thus possible to write under the approximation that we are looking at times much larger than $1/\Gamma$, the *closed* set of Bloch vector equations, independently of the vibrational evolution:

$$\frac{dp}{dt} = 2Vq, \tag{7.9a}$$

$$\frac{dq}{dt} = -2Vp - \chi r\left(p - \frac{1}{\Gamma}\frac{dp}{dt}\right), \tag{7.9b}$$

$$\frac{dr}{dt} = \chi q\left(p - \frac{1}{\Gamma}\frac{dp}{dt}\right). \tag{7.9c}$$

It is also interesting to ask, as was done by Kenkre and Wu (1989a,b) ,what we can learn by attempting to derive second order differential equations for the probability difference $p(t)$ alone (eliminating q and r) but maintaining the interaction beween $y(y)$ and $p(t)$. Obviously, we use for this purpose the original Eqs. (7.5) and get

$$\frac{d^2p}{dt^2} = Ap - Bp^3 + C(t), \tag{7.10a}$$

$$\frac{dy}{dt} + \Gamma(y - p) = 0. \tag{7.10b}$$

The second-order equation (7.10a) should be compared to the adiabatic (or infinitely fast relaxation) counterpart: Eq. (1.9) for an initial localized condition and Eq. (2.20) for a general initial condition, respectively. In the finite relaxation case, there appears now a correction term $C(t)$. For the localized initial condition $p(0) = 1$, if calculated from Eqs. (7.5) before the approximation used for getting a closure in p, q, r is applied, we get

$$C(t) = -\chi^2 y(t) \left[\int_0^t ds\, y(s) \frac{dp(s)}{ds} + \frac{p(t) - p^3(t)}{2} \right], \tag{7.11}$$

The quantities A, B in Eq. (7.10a) are given, as in earlier adiabatic descriptions in the book, by $A = \chi^2/2 - 4V^2$ and $B = \chi^2/2$.

The correction term vanishes both at the initial time, because the two terms separately vanish (the first because the upper and lower limits of the integral are equal to each other, the second because the initial localized condition is localized) for an initially localized condition; and and when the system has settled into the stationary states (by $y(t)$ becoming equal to $p(t)$ and the consequent cancellation of the two terms). This means that not only is the system driven by the damping agency into the system stationary states, as would be expected, but that initially, the adiabatic evolution will be visible. This is borne out as we will see in the examples below.

7.3 Numerical Explorations

Because clean analytic solutions are not available in the presence of relaxation at non-infinite rates, let us study the evolution seminumerically and try to understand what emerges via analytic arguments. We do this in two steps, first for localized initial conditions and then for general ones.

7.3.1 Localized Initial Conditions

We begin by presenting a graph that includes, along with the evolution of the probability difference $p(t)$ of the quantum particle from its site-localized state to its stationary state, the new element introduced in this Chapter, i.e., the vibrational coordinate $y(t)$ evolving from its initial value (assumed to be 0), being slaved to the probability difference, and eventually going into the stationary state. The adiabatic approximation would be represented by $y(t)$ jumping instantaneously into coincidence with $p(t)$ at the initial time.

In Fig. 7.2 we see the probability of the particle evolve (solid line) from its initially fully localized value $P_1(0) = 1$ to one of the two stationary state values. The stationary state is seftrapped because the value of the nonlinearity ratio $\chi/V = 4.5$ has been taken to exceed the critical value 4 for the dynamical transition. The relaxation rate Γ has been taken to be 1 in units of V which also scales the time abscissa. We also see how the oscillator displacement rises from its assumed initially value 0 to be slaved by the slower particle probability and eventually coincide with it as the system descends into the stationary state. The internal dynamics on the fast scale is thus described by Fig. 7.2.

Let us now see how the system parameters affect the evolution.

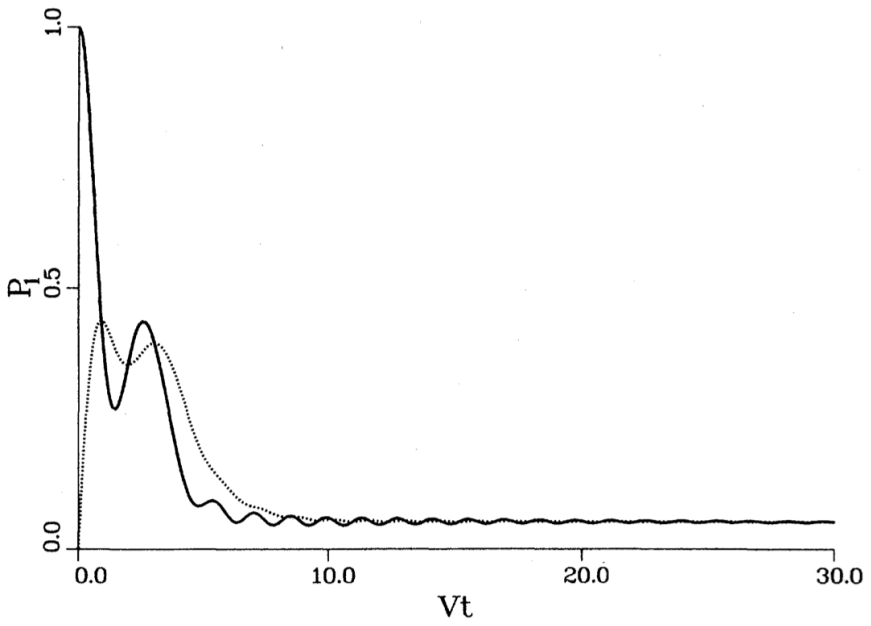

Fig. 7.2 Time evolution of the oscillator displacement $x_1(t)$ (dotted line) along with that of the probability difference $P_1(t)$ (solid line), the occupation probability of the initially localized quantum particle, showing the slaving of the former by the latter as a result of the time scale disparity. The displacement is shown scaled to the probability. The process of settling into the system stationary state is also clear. For infinitely fast relaxation (adiabatic approximation) explored in earlier chapters, $y(t)$ would jump instantaneously at the initial time into coincidence with the probability and stay that way for all time. Reprinted with permission from fig. 6 of Ref. (Kenkre and Wu, 1989b); copyright (1989) by American Physical Society.

In the uppermost curve (dotted line) of Fig. 7.3, the initially localized probability $P_1(t)$ is seen to oscillate symmetrically at first and then tend to the value 0.5. The nonlinearity is subcritical here ($\chi/V = 1$) and so the eventual stationary state the system goes into is free (not self-trapped).

The two lower lines correspond to self-trapped stationary states because the nonlinearity is supercritical: $\chi/V = 2.5$ (dashed line) and $\chi/V = 4.5$ (solid line), respectively. Note, in particular, that the middle line (dashed) refers to the formation of the self-trapped stationary state because $\chi > 2V$ although the nonlinearity parameter is less than $4V$. The latter value is relevant to the *dynamical* transition of the adiabatic (infinitely fast relaxation) system, i.e., to the situation when for an initial condition of localization on a single site the particle undergoes self-trapping. For all three curves, $\Gamma/V = 1$. The stationary state values to which the lower lines tend are both given by $\left(1 - \sqrt{1 - (2V/\chi)^2}\right)/2$.

In the right panel, we consider much faster relaxation than in the left panel, by a factor of orders of magnitude: V/Γ is now 2×10^{-3} rather than 1. The main result to

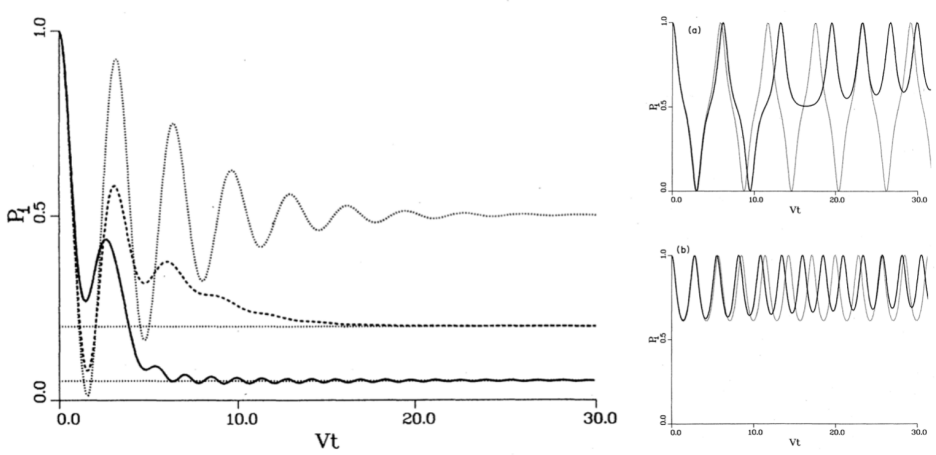

Fig. 7.3 The probability of the initially (fully) occupied site is plotted as a function of the dimensionless time Vt for finite relaxation for various parameter values. In the left panel, the value of the relaxation rate Γ is 1 in units of V and respective values of χ/V are 1 (dotted line), 2.5 (dashed line) and 4.5 (solid line). Evolution to a stationary state is clear in each case. The state is free (symmetric) in the first case and self-trapped in the second as well as the third case. In the right panel $V/\Gamma = 2 \times 10^{-3}$ and adiabatic evolution is seen to be approximately followed at *short* times in both cases even though at long times the probability approaches the value in the stationary state. The nonlinearity parameter χ/V is 3.9 for the upper curves, i.e. below the self-trapping transition but 4.1 , i.e., above the transition value for the lower curves. The solid (dotted) curves represent the actual (adiabatic) evolution. The cn-like shape we are familiar with from the adiabatic evolution is very clear in the dotted curve in the upper panel. Adapted with permission from figs. 1 and 2 of Ref. (Kenkre and Wu, 1989b); copyright (1989) by American Physical Society.

appreciate is that adiabatic evolution is approximately followed at short times even as the system tends to its stationary state at long times. The nonlinearity ratio χ/V has been chosen to be 3.9 (less than the critical value for the *dynamical* transition) in the upper pair of curves but 4.1 (more than that critical value). Solid lines in each case are for the actual, i.e., non adiabatic, dimer and show a tendency to go into the stationary state values given by $\left(1 + \sqrt{1 - (2V/\chi)^2}\right)/2$. The dotted lines in each case represent the adiabatic dimer (infinitely fast relaxation) and are a plot of $\mathrm{cn}(2Vt, \chi/4V)$ in the upper subpanel (a) and of $\mathrm{dn}(2Vt, \chi/4V)$ in the lower subpanel (b).

Now let us appreciate some visually surprising results through $3-d$ representations of the time evolution of $P_1(t)$ in Fig. 7.4. The probability of the initially occupied site is plotted versus the dimensionless time Vt as the nonlinearity is varied in one case (plot versus χ/V in the left panel) and the relaxation rate in the other (plot versus Γ/V in the right panel).

In the left panel we see the probability oscillate initially and then settle into its stationary state value. Towards the left side or the front of the $3-d$ plot, where χ/V is less than the critical value 2, the oscillations decay to the free state value 0.5. But

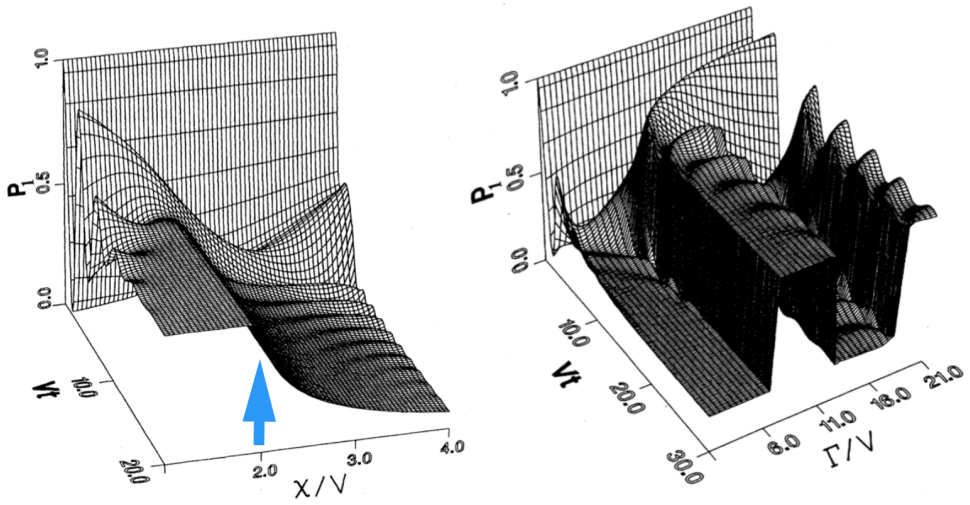

Fig. 7.4 Intriguing effects emerging from evolution at finite relaxation concerning static self-trapping at $\chi = 2V$ reflected in the asymptotic limit of the probability (left panel) and a switching of the stationary state reached as the relaxation rate is varied (right panel). Plotted along the vertical in both panels is the occupation probability $P_1(t)$ of the initially (fully) occupied site, the horizontal axes being the time in units of $1/V$ in both panels and the nonlinearity χ in the left and the relaxation rate $1/\Gamma$ in the right panel. In the left panel, the asymptotic (large-time) limit of the probability is 0.5 for $\chi < 2V$ but clearly undergoes a transition $\chi = 2V$ and begins to decrease for larger nonlinearity. The transition is marked by an arrow. The value of Γ/V is taken to be 2. In the right panel, the limiting values of the stationary probability reached asymptotic is seen to switch as the relaxation rate Γ in units of V increases. The plot shows three switches. The value of χ/V is taken to be 2.5. Adapted with permission from figs. 3 and 5 of Ref. (Kenkre and Wu, 1989b); copyright (1989) by American Physical Society.

at the critical value, the self-trapping transition that occurs in that the asymptotic value to which the probability decays, is visually quite clear. The transition is marked by a blue arrow. Throughout the left panel, $\Gamma/V = 2$.

In the right panel, we observe a curious switching phenomenon as the relaxation rate is varied. The stationary state picked for eventual settling down switches from that localized more towards one side to that towards the other as Γ/V is varied. Throughout the right panel, $\chi/V = 2.5$. For a spatially extended system such as a photosynthetic unit, this could mean that excitation absorbed at one location could be deposited at another unpredictably according to complex conditions such as the value of the relaxation rate.

Let us finally report in this sequence of examples analyzed for localized initial condition a case of a 'misleading' evolution of the probability, Fig. 7.5. The caption explains what is noteworthy.

What have we learned from these explorations? The main physics to emerge has been the recovery of the adiabatic (infinite relaxation rate) evolution at short times and the approach to stationary states of the adiabatic system at long times. The former

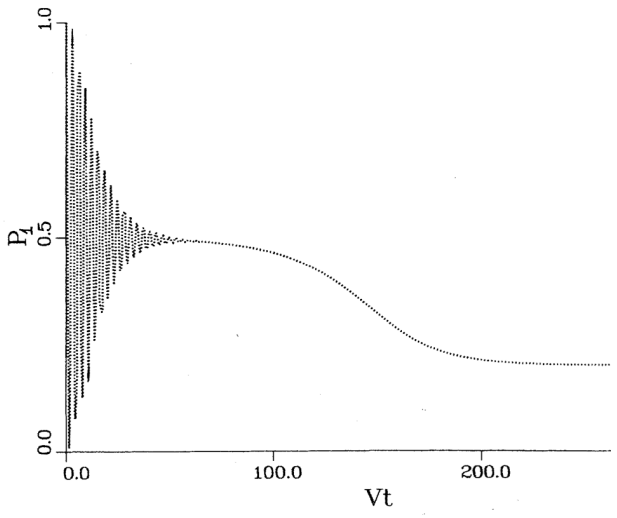

Fig. 7.5 The "misleading" evolution of the probability of the initially occupied site as it first oscillates around the free symmetric state at short times and then swings away to settle into the system self-trapped state with probability 0.2. Measurements with probe times of 100/V or smaller would tend to lead the observer to believe that the system is equilibrating to the free state. Observations with longer probe times would show self-trapping. Here Γ/V has been taken to be 0.15. Reprinted with permission from figs. 3 and 5 of Ref. (Kenkre and Wu, 1989b); copyright (1989) by American Physical Society.

occurs only if relaxation is fast on the scale of the other rate constants of the system, such as V, while the latter occurs for all cases provided only that there is relaxation, i.e., damping effects.

It is important to realize that no damping agents exist in the DNLSE as originally stated and so there is no evolution towards stationary states. Adding damping externally might ensure the removal of energy of the particle but leading it to the stationary states of the DNLSE occurs only if we use the manner we have introduced damping: into the oscillator system.[3]

It is interesting to use the approximate relation (7.8) that shows that y follows p with a delay of time $1/\Gamma$ as it gets slaved to p by substituting it in Eq. (7.11). The result, for times much larger than $1/\Gamma$, is

$$C(t) = \left(\frac{\chi^2}{\Gamma}\right)\left(p(t)\int_0^t ds\,\left[\frac{dp(s)}{ds}\right]^2 - \left(\frac{1}{2}\right)\left[1-p^2(t)\right]\left[\frac{dp(t)}{dt}\right]\right) \qquad (7.12)$$

and yields the following closed equation for the probability difference:

[3] Straightforward additions such as ones we had used earlier, e.g., in (Tsironis et al., 1988), do not achieve the purpose.

$$\frac{d^2p(t)}{dt^2} + \left(\frac{\chi^2}{2\Gamma}\right)\left[1 - p^2(t)\right]\left[\frac{dp(t)}{dt}\right] = A'p(t) - Bp^3(t), \tag{7.13a}$$

$$A' = \left(\frac{\chi^2}{2}\right) - \left(4V^2 - \left(\frac{\chi^2}{\Gamma}\right)\int_0^t ds\,\left[\frac{dp(t)}{dt}\right]^2\right). \tag{7.13b}$$

The term $B = \chi^2/2$ is identical to its form as encountered elsewhere in the book, see, e.g., Eq. (1.9), but A' is augmented relative to A by the integral term in Eq. (7.13b).

This difference between A' and A at long times but their identity at short times has strong significance. Equation (7.13a) shows clearly that the time-dependent damping term in the evolution of $p(t)$ (that would have vanished identically for infinitely fast relaxation, i.e., in the adiabatic limit, because of the Γ in the denominator) drives the system to stationary states. Because $A' \approx A$ at short times, i.e., before the integral term in Eq. (7.13b) has accumulated to a sizable value, the system exhibits oscillations at short times around the values it would in the adiabatic limit. As time proceeds A' acquires values consonant with the stationary states and so the system is driven into those states. On that long time scale it no longer oscillates around the adiabatic values.

This is somewhat clear in Fig. 7.1 but particularly transparent in Fig. 7.3.

If we look upon Eq. (7.13) as describing a fictitious oscillator with displacement p, the new term in A' can be said to represent a dissociative anti-restoring force acting on the oscillator given that the integral term is always positive. As $t \to \infty$, the value of $p(t)$ must either vanish, or oscillate, or tend to a nonzero constant, or grow without limit. The last three possibilities would cause dp/dt to have a positive nonvanishing value. The anti restoring force would then grow without bound and dissociate the fictitious oscillator. It is guaranteed that this cannot happen because the probability difference p is constrained to lie between ± 1. We conclude that dp/dt vanishes as $t \to \infty$.

The long-time evolution of p is, therefore, to stationary values. Ignoring the trivial solution $p(\infty) = 0$, we obtain for the stationary probability difference,

$$\lim_{t\to\infty} p(t) = \sqrt{1 - \left[\frac{8V^2}{\chi^2} - \frac{2}{\Gamma}\int_0^\infty dt\,\left[\frac{dp(t)}{dt}\right]^2\right]}. \tag{7.14}$$

While the approximate equality of A and A' corresponds to the short-time oscillation of the system around the adiabatic values, the neglect of their difference at long times would lead us to the erroneous conclusion that $\lim_{t\to\infty} p(t) = \sqrt{1 - (8V^2/\chi^2)}$. This value corresponds not to the stationary values but to the average values around which the initially localized adiabatic dimer oscillates. The correct result for stationary states is

$$\lim_{t\to\infty} p(t) = \sqrt{1 - \left(\frac{4V^2}{\chi^2}\right)}. \tag{7.15}$$

We see this limit both in our Eq. (7.13) and in the plots we have produced from our numerical solutions of the evolution equations.

7.3.2 Delocalized Initial Conditions

Let us now explore the evolution in the presence of finite relaxation for initial conditions of the quantum particle occupation that are not localized. In Fig. 7.6, we study the interplay of nonlinearity and initial phase relationships between site amplitudes. The magnitude of the probability is the same in both cases shown but the left panel corresponds the in-phase case (the phase difference of the particle at the two sites is 0) and the right to the out-of-phase counterpart (the phase difference is initially π). In both cases we see oscillations followed by coincidence of the oscillator displacement and the particle probability. The oscillations are wilder for the in-phase case of hteleft panel a.

It is easy to see that we can express the version of Eqs. (7.13) slightly differently to cover this more general case of arbitrary phases by keeping Eq. (7.13b) the same but rewriting Eq. (7.13a) as

$$\frac{d^2p(t)}{dt^2} + D(t)\frac{dp(t)}{dt} = A'p(t) - Bp^3(t). \tag{7.16}$$

Here we have a time-dependent damping coefficient given by

$$D(t) = \frac{\chi^2}{2\Gamma}\left[\left(p(0)^2 - p^2(t)\right) - \frac{4V}{\chi}r(0)\right]. \tag{7.17}$$

The damping depends explicitly both on the initial values of p and r and on the

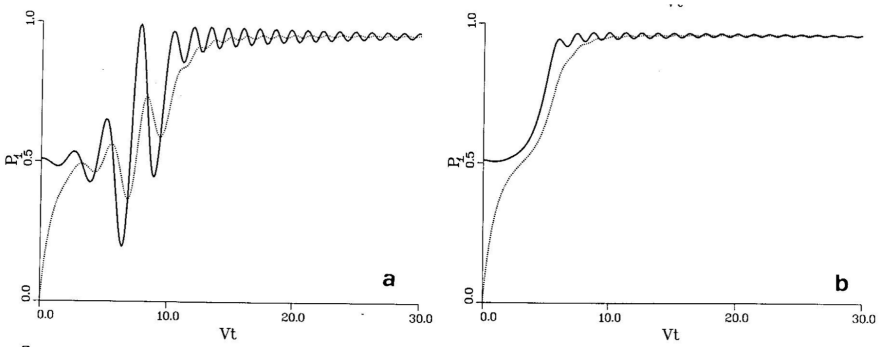

Fig. 7.6 Time evolution of the probability $P_1(t)$ (solid line) of the occupation of one of the two sites, labeled 1, by the quantum particle for a largely delocalized initial condition. The left panel a is for an in-phase condition meaning that the initial amplitude $c_2(0)$ is $\sqrt{0.49}$ while the right panel b is for an out-of-phase condition meaning that the initial amplitude $c_2(0)$ is $-\sqrt{0.49}$. In both cases $c_1(0) = \sqrt{0.51}$. The particle probability (solid line) and the scaled oscillator displacement (dotted line) both reach the same scaled steady state value but with wilder oscillations in the in-phase case. In both cases $\chi = 5V$ and $\Gamma = V$. Reprinted with permission from fig.1 of Ref. (Kenkre and Wu, 1989a); copyright (1989) by Elsevier Publishing.

instantaneous value of p at all times. The sign of $r(0)$ as well as later evolution can make $D(t)$ temporarily positive or negative and lead to oscillations of a different nature in the two panels. Eventually of course, the system settles into the stationary states and all time dependence ceases.

Needless to say, A' in Eq. (7.16) is the sum of A and the time-dependent integral $(\chi^2/\Gamma)\int_0^t ds\,[dp(s)/ds]^2$ which is zero at short times but nonvanishing as time progresses. And A, for this general case with arbitrary initial quantum phases, is itself given by $A = (\chi^2/2) - 4V^2 - 2V\chi r(0)$.

Results of a more detailed study of the effects of the interplay of initial phases with finite rate relaxation are displayed in Fig. 7.7. We start with site 1 occupied with probability 0.8 but study the evolution of the system for all initial phase differences ranging from 0 to π and thus examine the whole gamut from in-phase to out-of-phase extremes. The $3-d$ representation in the left panel shows the switching effect we have encountered earlier as the relaxation rate is varied whereby the eventual stationary state reached is switched.

The right panel shows three cross-sections and illustrates the 'rich-get-richer effect' we discussed in Chapter 3 but now in the presence of finite relaxation. Notice how the probability rises to values higher than the initial 0.8 for the middle curve (dashed) when the initial phase difference at the two sites is $\pi/2$. In the other two cases, for the phase difference equaling 0 and π (solid and dotted curves, respectively) initial movement is to decrease the probability but during evolution one also sees the opposite tendency.

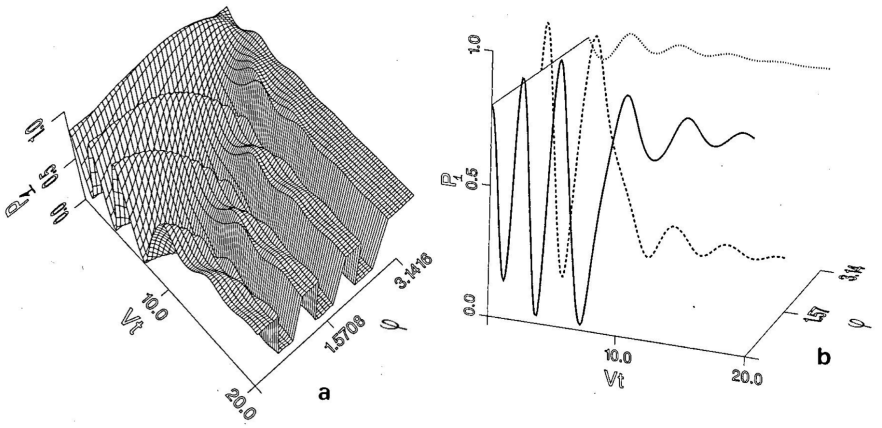

Fig. 7.7 Influence of the initial phases on the evolution of a non-adiabatic (finite relaxation) dimer shown through the evolution of the probability of one of the sites (initial occupation probability 0.8) plotted along the vertical axis. The dimensionless time Vt is along one horizontal axis and the initial phase difference from 0 to pi along the other. The full dependence on the phase is in the 3-d plot of the left panel (a) and the three cross-sections at phase values 0, $\pi/2$ and π in the right panel (b). Parameter values are $\chi/V = 2.5, \Gamma/V = 10$, $P_1(0) = 0.8$. Modified with permission from fig. 2 of Ref. (Kenkre and Wu, 1989a); copyright (1989) by Elsevier Publishing.

7.4 Some Exact Calculations in the Non-adiabatic Regime but in the Absence of Damping

What if the time scale disparity between the vibrational times and the times characteristic of the motion of the particle is not extreme so a non-adiabatic treatment is certainly necessary but what if there is no dissipation or damping? This is the question that we take up in this Section through the examination of a class of unexpected exact solutions obtained by Marek Kuś as part of a long and fruitful collaboration.

The damping coefficient α in the first equation displayed in the present Chapter, Eq. (7.1), is no zero, there is no meaning to the Aristotelian assumption, and the interacting set of equations for the system is, instead of (7.5),

$$\frac{dp}{d\tau} = q, \tag{7.18a}$$

$$\frac{dq}{d\tau} = -p - \chi y r, \tag{7.18b}$$

$$\frac{dr}{d\tau} = \chi y q, \tag{7.18c}$$

$$\frac{d^2y}{d\tau^2} + \omega^2(y - p) = 0. \tag{7.18d}$$

To correspond easily to the original publication in which we analyzed this situation, (Kuś and Kenkre, 1994), I have expressed the time here in the form of the dimensionless $\tau = 2Vt$, and taken the symbols χ, ω, also dimensionless to mean the respective ratios of the nonlinearity and the vibrational frequency to $2V$.

It is wise to begin our considerations knowing that a project to find exact solutions of Eqs. (7.18) for arbitrary initial conditions is doomed to failure. Indeed, it has been shown (Milonni et al., 1983; Belobrov et al., 1976) that an equivalent system ecountered in quantum optics exhibits chaos for some values of parameters and initial conditions. What we will see, however, is that some useful and exact techniques used by Jeleńska-Kuklińska and Kuś (1990) (see also (Kujawski, 1988)) in a related context in quantum optics can be ported over here for our system and used to extract analytic solutions in terms of elliptic functions for our problem in a limited range of parameter values.

7.4.1 The Essence of the Technique and Solutions

We observe that the system represented by Eqs. (7.18) has two integrals of motion,

$$p^2 + q^2 + r^2,$$

which equals 1 from the conservation of the particle probability, and also,

$$\frac{r}{\chi} - py + \frac{y^2}{2} + \frac{1}{2\omega}\left(\frac{dy}{dt}\right)^2,$$

which refers to the conservation of energy in the entire system including both the particle and the vibrations.

In seeking a way of finding the form of the vibrational coordinate y, we note that the adiabatic treatment takes it to be identical to p while the procedures appropriate to inclusion of the large but not infinite damping rate Γ effectively takes it equal p with a time lag: $y(t) \approx p(t - 1/\Gamma)$. Traditional analyses in nonequilibrium statistical mechanics, particularly addressing the interlocked BBGKY hierarchy, have sometimes used the concept of expressing the slower quantities as functions of the faster ones. If, following that idea in the form perfected in (Jeleńska-Kuklińska and Kuś, 1990), we assume that p is a sum of powers of y, and particularly keep only the linear and the cubic term in the expansion, we could try

$$p = \alpha_0 y + \alpha_1 y^3. \tag{7.19}$$

Using this ansatz form in the first of the extended Bloch-like equations (7.18), and employing (7.18d) to express the second derivative of y in terms of y and p, it is possible to obtain

$$\frac{dq}{d\tau} = y\left[6\alpha_1\left(\frac{dy}{d\tau}\right)^2 + \omega^2(\alpha_0 - 1)\alpha_0 + \omega^2(4\alpha_0\alpha_1 - 3\alpha_1)y^2 + 3\omega^2\alpha_1^2 y^4\right], \tag{7.20}$$

whose substitution in Eqs. (7.18), followed by an integration, allows us to express r in the form

$$r = \gamma + \frac{1}{2}\chi\alpha_1 y^2 + \frac{3}{4}\chi\alpha_2 y^4, \tag{7.21}$$

γ being an integration constant. The right hand sides of Eqs. (7.18b) and (7.20) both equal the derivative of q. Consequently, when compared to each other, they produce a closed differential equation for y which can immediately be used to obtain solutions in terms of Jacobian elliptic functions. The differential equation is of the familiar form

$$\left(\frac{dq}{d\tau}\right)^2 = F_0 + F_2 y^2 + F_4 y^4, \tag{7.22}$$

with constant coefficients

$$F_0 = \frac{1}{6\alpha_1}\left[\omega^2(1 - \alpha_0)\alpha_0 - \chi\gamma\right], \tag{7.23a}$$

$$F_2 = \omega^2\left(\frac{1}{2} - \frac{2\alpha_0}{3}\right) - \frac{1}{6} - \frac{\alpha_0}{12\alpha_1}\chi^2, \tag{7.23b}$$

$$F_4 = -\frac{1}{2}\omega^2\alpha_1 - \frac{1}{8}\chi^2. \tag{7.23c}$$

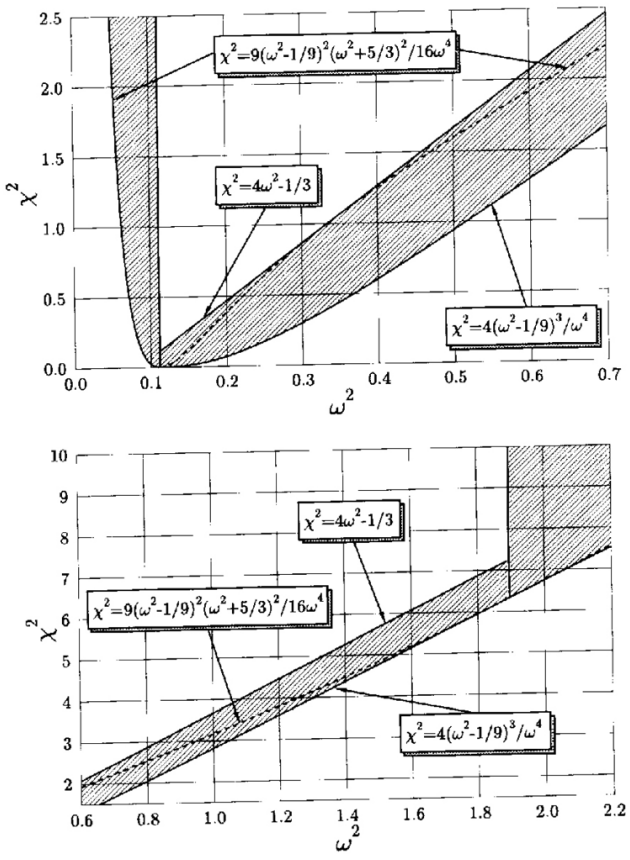

Fig. 7.8 Delineation of regions of parameter space spanned by the vibrational frequency ω and the system nonlinearity χ shown by their squares. Shading shows where exact analytical solutions of the nonadiabatic dimer can be found as indicated in th text. The dashed lines divide regions of free motion from self-trapped motion. Modified with permission from figs. 1 and 2 of Ref. (Kuś and Kenkre, 1994); copyright (1994) by Elsevier Publishing.

The explicit analytic solution satisfying the ansatz for the Bloch vector components as well as for the vibrational coordinate that underlies them, is, thus,

$$p = a\mathrm{cn}(\Omega\tau, k) + b\mathrm{cn}^3(\Omega\tau, k), \tag{7.24a}$$

$$q = -\Omega\mathrm{sn}(\Omega\tau, k)\mathrm{dn}(\Omega\tau, k)\left[a + 3b\mathrm{cn}^3(\Omega\tau, k)\right], \tag{7.24b}$$

$$r = c_0 + c_1\mathrm{cn}^2(\Omega\tau, k) + c_2\mathrm{cn}^4(\Omega\tau, k), \tag{7.24c}$$

$$y = \frac{4\Omega k}{\chi}\mathrm{cn}(\Omega\tau, k) = \frac{4\Omega k}{\chi}\mathrm{dn}(\Omega k\tau, 1/k). \tag{7.24d}$$

The elliptic modulus is related to the frequency through

$$\Omega^2 = \frac{\omega^2 - (1/3)}{2(2k^2 - 1)} \tag{7.25}$$

and is determined from the system parameters through the following complicated relation. With the understanding that

$$B_\pm = \left[\frac{1}{\omega^2 - (1/3)}\right]^2 \left[\pm(4/3)\sqrt{\chi^2\omega^4 - 4(\omega^2 - (1/9))^3} - \Big(\omega^2 - (1/9)\Big)\Big(\omega^2 - (17/9)\Big)\right],$$

it is obtained from

$$2k^2 = 1 - \frac{1}{\sqrt{1 + B_+}}, \quad \text{for } \omega^2 \le (1/9), \quad \chi^2 \ge \frac{9(\omega^2 - (1/9))^2(\omega^2 + (5/3))^2}{16\omega^4}, \tag{7.26a}$$

$$2k^2 = 1 - \frac{1}{\sqrt{1 + B_-}}, \quad \text{for } (1/9) < \omega^2 < (1/3), \quad \frac{4(\omega^2 - (1/9))^3}{\omega^4} \le \chi^2 < 4\omega^2 - 1/3, \tag{7.26b}$$

$$2k^2 = 1 + \frac{1}{\sqrt{1 + B_-}}, \quad \text{for } (1/3) \le \omega^2 \le (17/9), \quad \frac{4(\omega^2 - (1/9))^3}{\omega^4} \le \chi^2 < 4\omega^2 - 1/3, \tag{7.26c}$$

$$2k^2 = 1 + \frac{1}{\sqrt{1 + B_+}}, \quad \text{for } (17/9) < \omega^2, \quad \frac{4(\omega^2 - (1/9))^3}{\omega^4} \le \chi^2. \tag{7.26d}$$

Beware of the misinterpretation that can occur between the elliptic modulus k that we use throughout the book and its square that is called in some circles as $m = k^2$. This cautionary note is particularly aimed at the rare reader who might consult the original publication in which we had used the elliptic parameter m but used the letter k for it, bringing the confusion kettle inadvertently to a super boil![4]

The quantum particle tends to move on both sites in three of the panels of Fig. 7.9 but in the right bottom panel, for which the nonlinearity is supercritical, as indicated, selects one of them.[5] This shows the onset of self-trapping.

Interesting new time dependence showing double peaks is visible in each of the panels of Fig. 7.10 as the system parameters are changed (as indicated in the plot). The frequency has a high value ($\omega^2 = 10$) in both cases. The nonlinearity is subcritical in the upper panel and leads to free motion but it is supercritical in the lower panel where the quantum particle is self-trapped.

---

[4] We seem to have used there the correct symbol convention with the vertical bar | as a separator rather than a comma , but what many would frowningly (and, I must confess, appropriately) call it an incorrect terminology.

[5] All values of the parameters shown in these plots are relative to $2V$ and thus should be considered dimensionless.

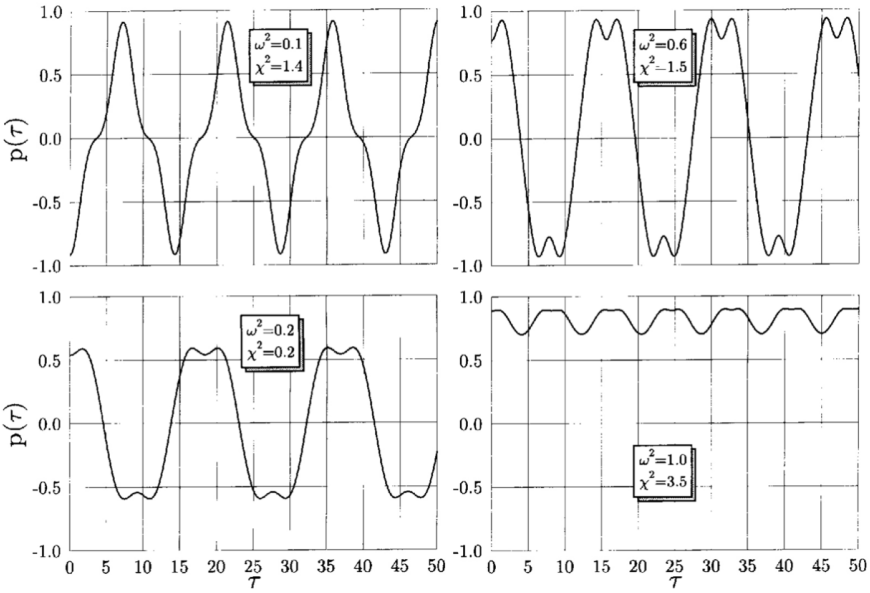

Fig. 7.9 Analytic solutions exhibited for small and moderate values of the vibrational frequency as shown. The nonlinearity is subcritical in three of the four panels and, accordingly, the quantum particle moves on both sites equally. In the bottom right panel, χ^2 equals 3.5, a supercritical value, and so self-trapping occurs. Modified with permission from figs. 3 and 4 of Ref. (Kuś and Kenkre, 1994); copyright (1994) by Elsevier Publishing.

Regions of parameter space in which the exact solutions can be found are shown below in Fig. 7.8. Some of the solutions themselves are exhibited in subsequent plots provided below. The coefficients a, b and the c's are calculated with the understanding that the sign in Eq. (7.26c) corresponds precisely to the sign in Eq. (7.27c).

$$a = 6\frac{\Omega k(\omega^2 - (1/9))}{\chi\omega^2}, \tag{7.27a}$$

$$b = -8\frac{\Omega^3 k^3}{\chi\omega^2}, \tag{7.27b}$$

$$c_0 = \frac{1}{\chi\omega^2}\left[\pm\sqrt{-(3/2)(\omega^2 - (1/9))^2}\right], \tag{7.27c}$$

$$c_1 = 12\frac{(\omega^2 - (1/9))\Omega^2 k^2}{\chi\omega^2}, \tag{7.27d}$$

$$c_2 = -24\frac{\Omega^4 k^4}{\chi\omega^2}. \tag{7.27e}$$

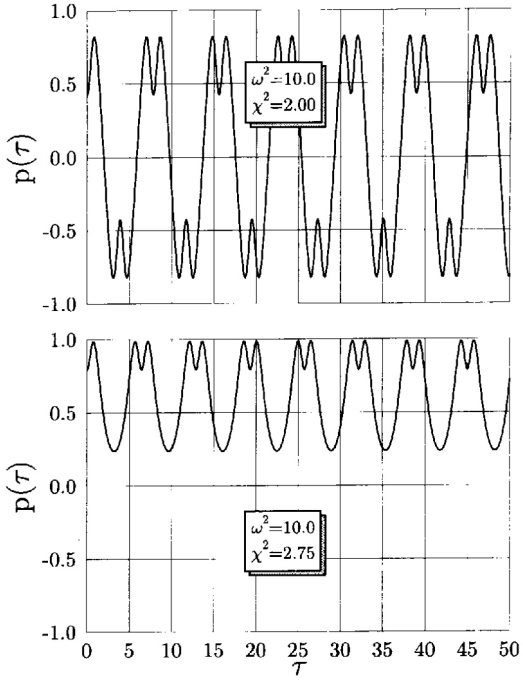

Fig. 7.10 Analytic solutions obtained for even higher values of vibrational frequency as shown. Self-trapping is occurring in the lower panel but the motion is free in the upper panel. The parameter values are visible in the Figure. Modified with permission from fig. 5 of Ref. (Kuś and Kenkre, 1994); copyright (1994) by Elsevier Publishing.

From the multitude of time-dependent solutions exhibited by Kuś and Kenkre (1994) on the base of their analytic work, we show a selection. The lowermost values of the vibrational frequencies are represented in Fig. 7.9 and higher ones in Fig. 7.10. The self-trapping transition from free to bound behavior is clear in Fig. 7.11. It should be kept in mind that the solutions shown are all analytic and without any adiabatic approximation made.

Particularly transparent is the graphical depiction of the transition in Fig. 7.11. In all three cases shown the vibrational frequency is given by $\omega^2 = 1$. Each case corresponds, however, to a different value of the nonlinearity parameter. The intermediate value, $\chi^2 = 256/81$, depicts the transition from free to self-trapped motion. We see that for a very slightly smaller value, $\chi^2 = 3.160$, the motion shows oscillations on both sides which means that the particle is free. For a very slightly larger value, $\chi^2 = 3.161$, the motion is only on one side and the particle is self-trapped. As stated above, the analysis is fully exact with vibrations completely treated.

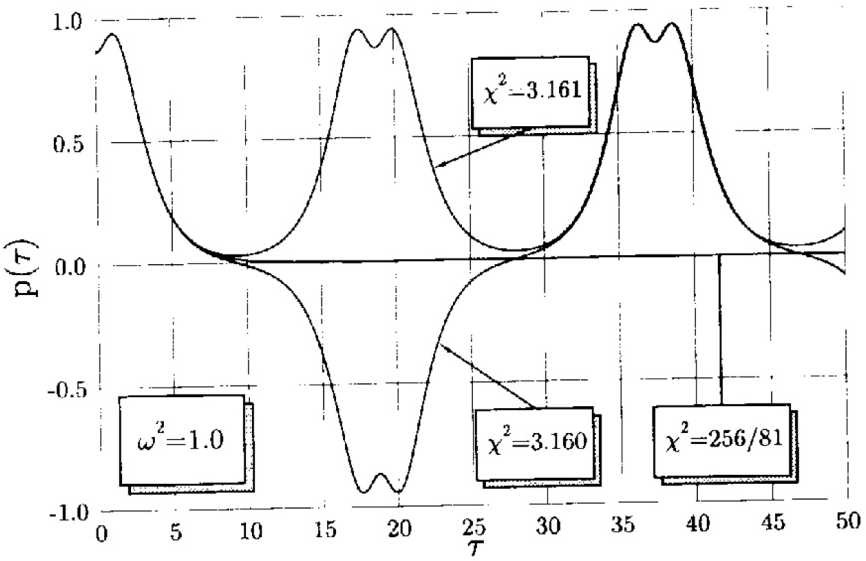

Fig. 7.11 Three different exact solutions exhibiting the self-trapping transition with vibrations fully treated. Vibrational frequency is given in all three cases by $\omega^2 = 1$. The values of the nonlinearity χ are different in the three cases and shown in the Figure. The transition case as well as free and self-trapped state are clearly seen. Reprinted with permission from fig. 6 of Ref. (Kuś and Kenkre, 1994); copyright (1994) by Elsevier Publishing.

7.4.2 Tiptoeing Around Regions with Chaos

The dissipationless quantum dimer treated in Kuś and Kenkre (1994) and described in the preceding sections has a (to me, irritating) propensity towards chaos as any trained eye would suspect on even casual inspection. How has the discussion presented been possible then and what is its value? The question has been answered in the Preface to the present book where allusion has been made to "...The latter analysis tiptoes teasingly around chaotic regions, but can be made to yield precise solutions in terms of elliptic functions for certain values of the system parameters." Marek Kuś performed this delicate tiptoeing during our collaboration decades ago and was able to delineate carefully regions of parameter space where analytic solutions were possible from regions where chaos spoiled the fun. The reader may glean some of the information from Fig. 7.8 above. As explained in (Kuś and Kenkre, 1994), numerical investigations show clearly that the ever present possibility of chaotic behavior means that in a universal manner, "...typical trajectories cannot be classified as representing free and self-trapped motion. Nevertheless it is relatively easy to find initial conditions for which the system exhibits the tendency to stay in a well-localized state characterized by a non-vanishing value of p for a relatively long time." One of the primary points is that the analysis is clear, and free of the influence of chaos, if one sticks to parameter domains indicated. The reader of this book is

referred to the original publication for a lengthier discussion. However, a plot from that publication reproduced here as Fig. 7.12 might be of some help.

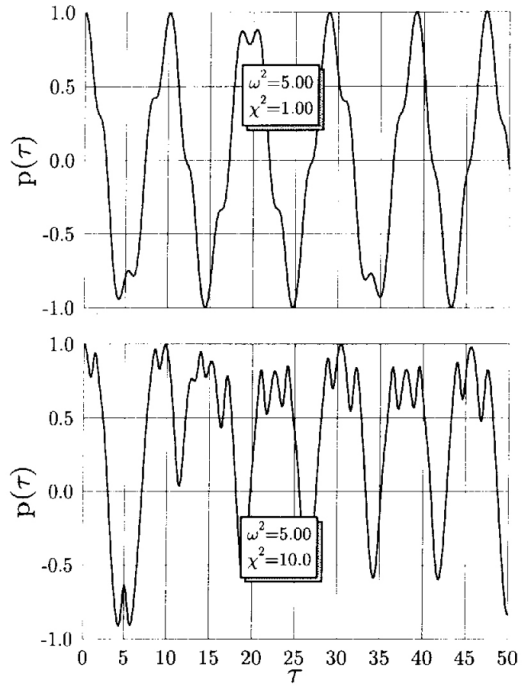

Fig. 7.12 A case in which the parameter values are in the chaotic region and so do not permit analytic solutions in terms of Jacobian elliptic functions. However, by inspection of the mean value of p in the two panels, one can state that the particle is free in the upper but self-trapped in the lower panel. Parameter values are as indicated. See text. Reprinted with permission from fig. 6 of Ref. (Kuś and Kenkre, 1994); copyright (1994) by Elsevier Publishing.

The trajectories in the plot do not fall in the regions for which there are exact solutions in terms of elliptic functions to be found. The oscillations, although not as regular as in the deterministic regions, lead to clearly different mean values of p. For $\omega^2 = 5, \chi^2 = 1$, we can state that the motion is free because p oscillates around zero mean. This is the upper panel. Contrast this with the lower panel in which $\omega^2 = 5$ but $\chi^2 = 10$. There is little question that for the latter case the evolution prefers positive values of p and we can say that the particle has undergone self-trapping.

7.5 Averaging Approximation

There is one more method that we have had the opportunity to apply to the understanding of the evolution of the nonadiabatic dimer. One of the techniques in the tool kit of the investigator of periodic motions of nonlinear systems, it goes under the name of the 'averaging approximation'. It is a powerful procedure to know about. Its application to our system carried out by Wu and Grigolini in collaboration with me allowed us to make progress. However, because I have no deep new insights to share that have emerged from that study (Wu et al., 1990), I will describe it in the briefest of manners and refer the reader to the original publication.

The essence of the method consists of selecting a constant of the motion for the adiabatic case so that in the presence of nonadiabaticity its time evolution is slow, and of employing approximation methods for the description of the full system. We start with the system of equations (7.9) which is closed in the Bloch components p, q, r but which takes into account the nonadiabaticity. Looking around for constants of motion of the *adiabatic* counterpart, we come across the obvious candidate $p^2+q^2+r^2$ which equals 1 as the result of the conservation of probability. However, it is not of use because it is a constant of motion for all values of the relaxation rate Γ, not just the infinite case. We therefore discard it. Another candidate happens to be, as a moment's reflection will show, $r-(\chi/2)p^2$, which we will rewrite, by adding to it a term which we know to be constant, as

$$E(t) = r(t) - (\chi/2)p^2(t) + \chi/2 + 1/2\chi. \tag{7.28}$$

The choice of the additive term makes E vanish in the non-trivial stationary state ($p \neq 0$) in which $R = -1/\chi$ and $p = \pm\sqrt{1-1/\chi^2}$.

In the presence of finite-rate relaxation ($1/\Gamma \neq 0$), i.e., when the adiabatic limit does not apply, the quantity we have selected, $E(t)$, evolves in time, its time derivative being equal to $-(1/\Gamma)\chi q^2(t)$. If χ/Γ can be considered small, the rate of change of E is small, and E can be considered a slow variable relative to p, q and r. One takes advantage of the fact that the latter quantities are oscillating in time. Replacement of $q^2(t)$ by its time average allows us then to approximate the evolution of the slow variable $E(t)$ through

$$\frac{dE(t)}{dt} = -\frac{\chi}{\Gamma}\langle q^2\rangle. \tag{7.29}$$

Expressing q^2 in terms of E itself and one of the Bloch vector components, p, one obtains the possibility of evaluating $E(t)$ to various degrees of approximation. The interested reader will find details of development in Wu et al. (1990).

7.6 Chapter 7 in Summary

To refrain from making the adiabatic approximation, i.e., the assumption of infinitely fast relaxation of the nonlinear system, was the purpose of this Chapter. This was

done by introducing into the system a degree of freedom exemplified by the vibrational coordinate and by investigating situations in which it did not relax with infinite rapidity to the adiabatic limit. The first plot exhibited in the Chapter showed what was to come, the next half a dozen figures considered that there was fast damping of the vibrational coordinate and the remaining plots described the absence of any damping. The basic equation of motion obeyed by the vibrations was considered to be the second order (7.1). Under the Aristotelian limit of high damping, wherein inertial effects were neglected, it was reduced to one that forced the vibration to follow the probability difference exponentially at the relaxation rate Γ. Analytic approximation methods were developed that uncovered an integral relation (7.6) between the vibration and the probability difference which also showed how the former tended to the latter with a lag. Plots such as in Fig. 7.2 showed this behavior visually. Consequences of the finite relaxation investigation were that we could see that adiabatic evolution was recovered at short times and the system was forced into the *stationary states* of the adiabatic system at long times. A number of surprising effects were further noticed in plots such as Fig. 7.4 and Fig. 7.5, and the interplay with initial quantum phases was apparent in Figs. 7.6 and 7.7. In the absence of damping there was chaos to be avoided in the equations if we were seeking deterministic analytic solutions. We were able to obtain such solutions in certain parameter regions. The regions were made clear in Fig. 7.8. The solutions for the vibrational coordinate were obtained as functionals of the probability difference, a ruse borrowed from non-equilibrium statistic mechanics theories and applied in earlier quantum optics contexts (Jeleńska-Kuklińska and Kuś, 1990). These solutions turned out to be Jacobian elliptic functions as in Eqs. (7.24). Their plots in Figs. 7.9, 7.10,7.11, showed interesting features and uncovered self-trapping transitions. A quick description of the application (Wu et al., 1990) of another independent technique of analyzing finite relaxation, the averaging technique, was briefly given.

Chapter 8
Thermal Effects: Phase-Space and Langevin Formulations

Introducing damping into the vibrational part of our system as we did in Chapter 7 meant that we opened the system under study to the universe. The natural follow-up, which is to investigate thermal effects on our system, will occupy us in the present Chapter. My own interest in the subject has been primarily procedural and, accordingly, the Chapter is divided into a part on equilibrium phase-space considerations and a part on a non-equilibrium description of time-dependent equations.

8.1 Introduction: Background on the Davydov Soliton Stability against Thermal Fluctuations

This introduction describes the active but (unfortunately) not conclusive work that had been going on in the 1980's and 90's in the subject of the thermal stability of Davydov solitons.

A surge of interest had appeared in the research community in the subject of Davydov solitons because they had been suggested as being responsible in an essential way for transport, along proteins, of the free energy released by the hydrolysis of adenosine triphosphate. There were two questions that battles were fought over. One of them was whether the traveling state that Davydov had suggested as the carrier of the energy was truly a consequence of the quantum dynamics of the system or simply a hopeful invention of creative minds. Another, and one that is tangentially[1] relevant to the present Chapter, was whether the quantum mechanical state, even if

[1] The word 'tangential' is used here to represent the fact that, as when the debates were going on decades back, my own interest was/is procedural rather than in whether the Davydov idea was tenable in realistic biological systems. I worked on methodologies to describe the thermal effects and was only mildly interested in whether the nonlinear structures were actually stable at the temperatures at which they were invoked. As will become clear in the sequel, the physics intricacies are already delightfully complex in the description part. For that, there is no need to add the debate issues regarding the comparison to observations that make the matter fiercely undecided in the opinion of some.

it were to exist, was stable against thermal interactions with the natural reservoirs that could be said to be in contact with the biological objects at room temperatures. Diametrically opposite opinions were voiced. We learned from some, e.g. (Lomdahl and Kerr, 1985; Kerr and Lomdahl, 1987) that

"...the original soliton proposal does not work at biological temperature. The 'crisis in bioenergetics' is still with us!".

The sentiment was opposed in no uncertain terms by (Kadantsev et al., 1987, 1988) who concluded that

"...thermal vibrations not only do not prevent the soliton transport of energy but...become its necessary condition."

What could lead to such contrast in the opposite views that were held by the researchers? One might attribute it to two quite separate sources. The uncertainty in the values of the physical parameters involved was surely one of them. The other was the great variety of theoretical approaches used to investigate the problem. Typically, when the theoretical situation is full of such conflicts, efforts are naturally made to construct bridges that would lead to an understanding of the interrelations among the diverse methods of attack. Surprisingly, there was the almost complete absence of such bridge work, each subgroup of investigators remaining wedded to its own way of regarding the phenomena. As I understand it, the theoretical approaches were basically five:

(i) direct calculations from the Hamiltonian of the interacting system via perturbation methods such as those carried out by Cottingham and Schweitzer (1989) and Schweitzer (1992), and via variational principles and other procedures (Bolterauer, 1990),
(ii) quantum Monte Carlo calculations taking the full Hamiltonian as the point of departure and avoiding semiclassical approximations such as by Wang et al. (1990),
(iii) semiclassical Monte Carlo methods in which the interacting boson field is represented classically and the moving quasiparticle quantum mechanically as in the work of Cruzeiro et al. (1988); Cruzeiro-Hansson and Takeno (1997),
(iv) numerical simulations of the semiclassical model with stochastic interactions with a thermal reservoir appended explicitly as by (Lomdahl and Kerr, 1985; Kerr and Lomdahl, 1987), as well as by (Lawrence et al., 1986; Forner, 1991), and
(v) analytic calculations via a Fokker-Planck treatment of the semiclassical model in thermal interaction with a reservoir as in the work of Grigolini et al. (1989); Kenkre and Grigolini (1993); Kenkre (1993); Kenkre and Kuś (1994); Kenkre (1994c).

There is, perhaps, a natural reason for the diversity in the literature along these lines. A thermal reservoir has two *different* kinds of consequences on the evolution of a system. For want of a better term, we might distinguish them as phase-space effects and fluctuation effects. The former are associated with the statistical weights

for states of varying energies as taught to us by Boltzmann or Gibbs; they arise from a consideration of equilibrium statistical mechanics. Nonzero temperature is treated here by the introduction of a canonical density matrix involving Boltzmann thermal weights. The analysis is typified by (i)-(iii) above. Such a treatment does address the first of the two effects but not the second. Brownian methodology, often associated with the terms Langevin or Fokker-Planck (generally stochastic), characterized by (iv) and (v) above, tends to take aim at the second effect, and, as a by-product, at the first.

These latter, stochastic, methods are also able, in contrast to the former, to address the *approach to equilibrium* and not merely the nature of the equilibrium state. They suffer from the fact that they are always considerably more difficult to implement, except though numerical techniques. Such techniques can take away from the transparency of what is going on as one moves from assumption to result. Needless to say, whenever properly interpreted, both approaches should yield the same answers about the final (equilibrium) state and therefore about the stability of the soliton. However, inevitable approximations and assumptions along the way disturb this ideal situation. They naturally lead to divergences in the final consequences, making it impossible often to resolve the issue.

As you step into the present Chapter, dear reader, my suggestion is to be aware of the fact that the important question about the stability of Davydov solitons in biological environments is by no means universally settled, that opinions differ sharply about the issues, and that what I am presenting below, while according to me not only useful but fascinating as well to any student of physics, is only procedural. My view is that the responsibility to come to a conclusion about the applicability of the methods set out *for the Davydov problem* is not mine in the setting of the present book but the reader's, if she is so interested.

8.2 Phase-space Considerations and Partition Function Analysis

Let us begin with equilibrium statistical mechanics and carry out first a partition function analysis of the nonlinear structures that we encounter in our system. This will occupy us in Section 2 of the present Chapter.

If we take the Hamiltonian laid out in Eq. (4.1) as applying to a system of two sites only, 1 and 2, we have

$$\hat{H} = V\hat{r} + g\omega\hat{p}\left(\frac{b^\dagger + b}{\sqrt{2}}\right) + \omega\left(b^\dagger b + \frac{1}{2}\right), \tag{8.1}$$

where the particle operators $\hat{p}$ and $\hat{r}$ along with their companion $\hat{q}$ not appearing in the above equation are given by

$$\hat{p} = a_1^\dagger a_1 - a_2^\dagger a_2; \quad \hat{r} = a_1^\dagger a_1 + a_2^\dagger a_2; \quad \hat{q} = -i\left(a_1^\dagger a_2 - a_2^\dagger a_1\right) \tag{8.2}$$

and those describing the intersite vibration are given by[2]

$$\hat{y} = \left(b^\dagger + b\right)/\sqrt{2}; \quad \hat{\pi}_y = \left(b - b^\dagger\right)/i\sqrt{2}. \tag{8.3}$$

The semiclassical approximation inherent in our analysis throughout the book so far replaces the vibration operator $\hat{y}$ and its conjugate momentum $\hat{\pi}_y$ by c-numbers, which we denote by removing the circumflex symbols, leaving the particle operators intact. This results in our being able to express the Hamiltonian as a 2×2 matrix

$$\hat{H} = \begin{pmatrix} g\omega y + (\omega/2)(y^2 + \pi_y^2) & V \\ V & -g\omega y + (\omega/2)(y^2 + \pi_y^2) \end{pmatrix} \tag{8.4}$$

with elements that are functions of the c-numbers y and π_y.

Let us start with the observation that, omitting an unimportant factor of 2, the partition function Q of our semiclassical system, which we know is obtained by evaluating the trace $Tr\, e^{-\beta\hat{H}}$ of the exponential of the Hamiltonian operator, is given by

$$Q = \int_{-\infty}^{+\infty} dz\, e^{-\beta z^2} \cosh\left(\beta\sqrt{v^2 + z^2}\right). \tag{8.5}$$

Note that the meaning of the trace operator includes integrations over the classical vibrational space. Here $gz = y$, the nonlinearity parameter that we have discussed throughout the book is $\chi = 2g^2\omega$, and the parameters in Eq. (8.5) are given by

$$v = 2V/\chi; \qquad \beta = \chi/2k_B T, \tag{8.6}$$

T and k_B being, respectively, the temperature and the Boltzmann constant.

Our first task is to understand how the semiclassical expression (8.5) at vanishing temperature can describe the self-trapped stationary states of the dimer that we have been discussing throughout the book. For low temperatures T, which means large β, the integrand in peaked at a value of z that we will denote by z_m. It is clear that Q can be evaluated to an excellent approximation through

$$Q = \int_{-\infty}^{+\infty} dz\, e^{f(z)} \approx \int_{-\infty}^{+\infty} dz\, e^{\frac{(z-z_m)^2}{2} f''(z_m)} \tag{8.7}$$

provided we define $f(z) = -\beta(z^2/2) + \ln\cosh\left(\beta\sqrt{v^2 + z^2}\right)$, and evaluate its derivative as

$$f'(z) = \frac{df(z)}{dz} = \frac{\beta z}{\sqrt{v^2 + z^2}}\left[\tanh\left(\beta\sqrt{v^2 + z^2}\right) - \sqrt{v^2 + z^2}\right]. \tag{8.8}$$

There are two possible values the peak value $z = z_m$ can take. Either $z_m = 0$ or

$$\sqrt{v^2 + z_m^2} = \tanh\left(\beta\sqrt{v^2 + z_m^2}\right). \tag{8.9}$$

[2] Surely, $\hbar$ has been put equal to 1 as everywhere else in the book.

Additionally, the value of the second derivative of f at the nonzero root[3] is given by

$$f''(z_m) = \left[\frac{d^2 f(z)}{dz^2}\right]_{z_m} = \frac{\beta^2 z_m^2}{v^2 + z_m^2}\left[1 - \frac{1}{\beta} - (v^2 + z_m^2)\right]. \tag{8.10}$$

Eq. (8.9) yields

$$\frac{1}{k_B T} = \frac{1}{2\sqrt{v^2 + z_m^2}} \ln\left[\frac{1 + \sqrt{v^2 + z_m^2}}{1 - \sqrt{v^2 + z_m^2}}\right]. \tag{8.11}$$

At the zero of temperature, each side of this equation is infinite so that

$$z_m^2 = 1 - v^2. \tag{8.12}$$

This result shows that the location of the vibrational coordinate of the system at vanishing temperature has the largest possible value when the intersite interaction is zero, that it decreases as the intersite interaction increases relative to the nonlinearity χ, and that it vanishes at $v = 1$, equivalently at $V = \chi/2 = g^2\omega$. This marks the transition from self-trapped to free behavior. Further increase in V disallows the non-zero solution.

These developments in the evaluation of the partition function suggested to me an obvious magnetic analogy given our nonlinear system and the mean field ferromagnet. To study self-trapping it appeared natural, therefore, to seek out in our system a quantity which would correspond to the magnetization in a magnet and use it as an operator $\hat{O}$ whose average via the standard Gibbs statistical mechanics prescription would serve as a measure of the self-trapping at any temperature of interest via

$$\langle\langle \hat{O} \rangle\rangle = \frac{\int\int dy d\pi_y \, Tr \, \hat{O} e^{-\beta \hat{H}}}{\int\int dy d\pi_y \, Tr \, e^{-\beta \hat{H}}}. \tag{8.13}$$

It is clear that the trace operation would reduce to one over the exponential of the 2×2 matrix of Eq. (8.4) (shown explicitly within the integrand in Eq. (8.13)), followed by an integration over y with Gaussian weights $\exp\left(-\beta\omega y^2/2\right)$: the effects of the π_y integration would cancel in the numerator and the denominator. The program was explained in essence at two conferences (Kenkre, 1994b, 1995), begun for a dimer in (Kenkre and Cruzeiro-Hansson, 1994), continued for spatially extended counterparts of the dimer in (Kenkre et al., 1994), and will be explained in the rest of this section.

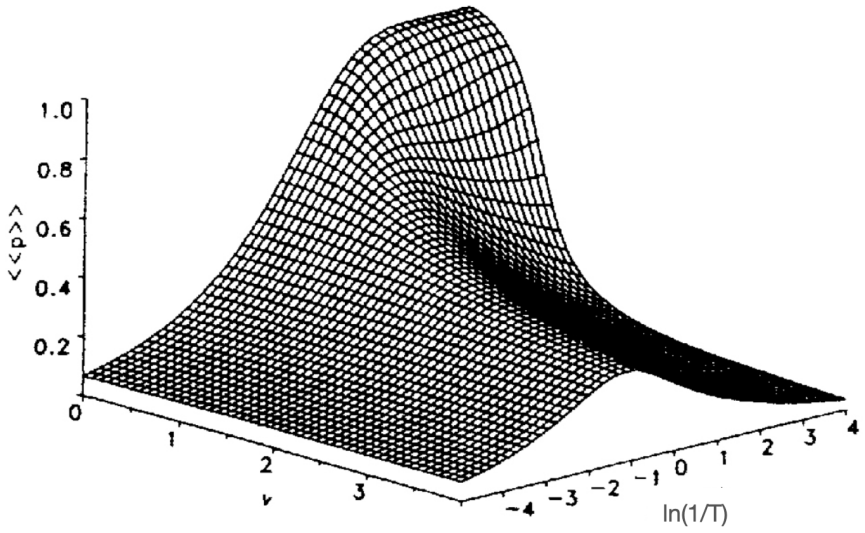

Fig. 8.1 The localization parameter $\langle\langle p\rangle\rangle$ plotted in a $3d$ representation versus the dimensionless intersite transfer $v = V/g^2\omega$ along one horizontal axis and the logarithm of the dimensionless reciprocal temperature $1/T$ in units of $k_B/g^2\omega$ along the other. For large enough v it shows a dual behavior of a rise with temperature increasing and a fall for further increases. For small enough v it shows merely a decrease as temperature increases. Modified with permission from fig. 4 of Ref. (Kenkre and Cruzeiro-Hansson, 1994); copyright (1994) by Springer Publishing.

8.2.1 Choice of Observable, Basic Expression, and Primary Behavior

The magnetic analogy suggests that we select the probability difference $p = P_1 - P_2$ in the case of a dimer as the observable to focus on. The eigenvalues of the Hamiltonian matrix (8.4) are easily seen to be

$$E^{\pm} = \frac{\omega}{2}\left(y^2 + \pi_y^2\right) \pm \sqrt{(g\omega y)^2 + V^2}. \tag{8.14}$$

On calculating the eigenvectors of the matrix, we see that, in each system state, the probability difference depends on the vibrational coordinate y in the form

$$p = \frac{y}{\sqrt{y^2 + (gv)^2}}. \tag{8.15}$$

The selection of the observable to study is guided by the necessity to focus on the correlation between the particle and the vibrational field as the essential signature of the nonlinear structure. We choose $\hat{p}$ as the $\hat{O}$ in Eq. (8.13) and focus on the

[3] This non-zero root in Eq. (8.9) is strikingly similar to what one obtains as a well-known result in the mean field theory of ferromagnetism often associated with the name of Weiss or Néel.

ensemble average of Eq. (8.15),

$$\langle\langle p\rangle\rangle = \frac{\int_0^{+\infty} dz\, e^{-\beta z^2/2} \left(\frac{z}{\sqrt{z^2+v^2}}\right) \sinh\left(\beta\sqrt{z^2+v^2}\right)}{\int_0^{+\infty} dz\, e^{-\beta z^2/2} \cosh\left(\beta\sqrt{z^2+v^2}\right)}, \tag{8.16}$$

which we call the 'localization parameter', to provide a tool for the investigation of thermal stability. Generally, an increase (decrease) in the magnitude of this quantity would mean that temperature aids (hampers) the nonlinear structure. The 'p-dipole' points in a direction which in one of the two states of the dimer is parallel and in the other anti-parallel to the 'magnetic field' represented by the vibrational amplitude y, the energies of the two states being different as seen in Eq. (8.14). To be kept in mind is that in taking the ensemble average we must ensure that a trivial cancellation does not occur simply because of the inherent symmetry of the available phase space. A standard feature of magnetic field treatments in symmetric systems, this means that we average over half the available phase space: the z-integral extends from 0 to ∞ rather than from $-\infty$ to ∞.

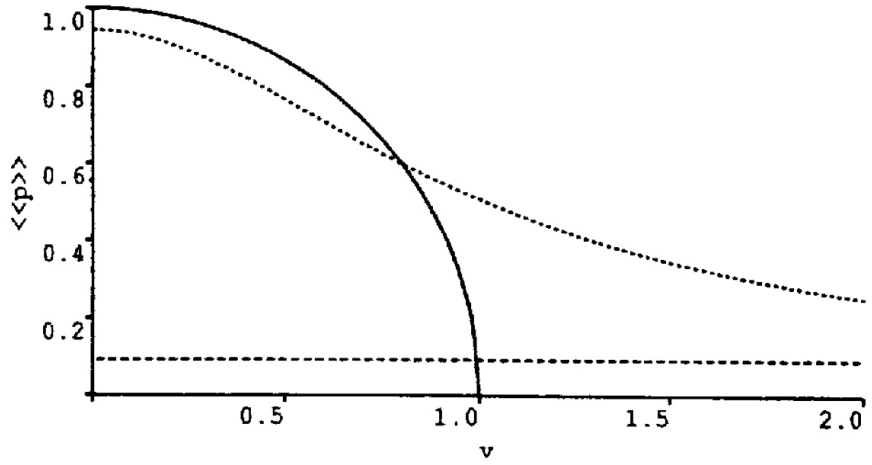

Fig. 8.2 The localization parameter $\langle\langle p\rangle\rangle$ plotted as a function of the dimensionless intersite transfer $v = V/g^2\omega$ for three values of the temperature T expressed relative to $g^2\omega/k_B$, 0 (solid line), 0.27 (dotted line) and a much larger value 72 (dashed line), as shown. Note that similarity in the v-dependence of $\langle\langle p\rangle\rangle$ with the T-dependence of the magnetization in a similar magnetic system. Reprinted with permission from fig. 2 of Ref. (Kenkre and Cruzeiro-Hansson, 1994); copyright (1994) by Springer Publishing.

We are able to evaluate the integral in the numerator of the $\langle\langle p\rangle\rangle$ expression analytically in terms of error functions but that in the denominator requires approximate

analytical or numerical evaluation.[4] Figure 8.1 shows that the localization parameter can show a tendency to initially rise with a rise in temperature and then fall with increases in temperature if the intersite interaction is large enough. This dual behavior represents (dynamic) disorder-induced self-trapping followed by a destruction of the nonlinear structure at high temperatures because of the usual Boltzmann equalization of weights no matter what the energy. If the intersite interaction is smaller than that required for self-trapping at zero temperature, only a decrease is seen in $\langle\langle p\rangle\rangle$ as temperature increases from 0.

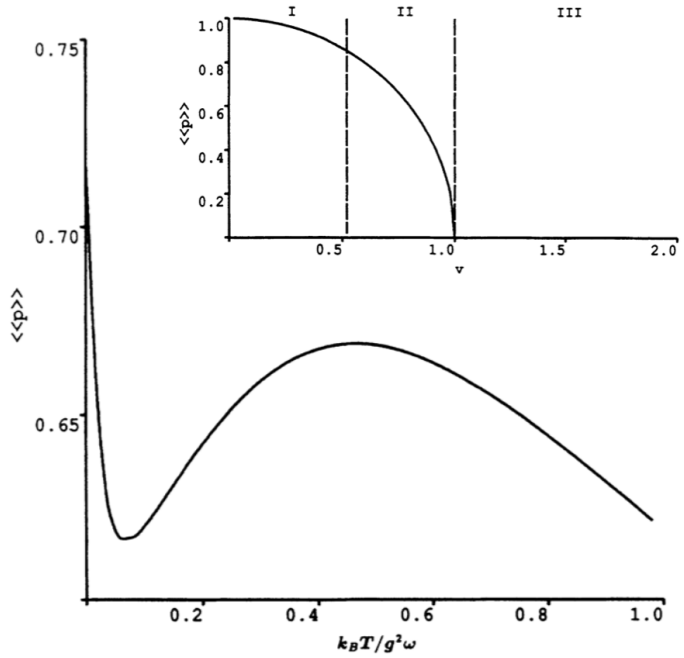

Fig. 8.3 Interesting low-T behavior showing a hindering of the structure at low T, an aiding at intermediate T, and a hampering at high T corresponding to the system being in region II in the inset. The main figure is a plot of the localization parameter versus T (temperature) expressed as a ratio to the characteristic value $g^2\omega/k_B$. The inset is a plot of $\langle\langle p\rangle\rangle$ showing its dependence on v. The other two regions in the inset are less interesting. Modified with permission from figs. 4 and 5 of Ref. (Kenkre et al., 1994); copyright (1994) by American Physical Society.

The primary behavior of the localization parameter is that it can have both tendencies: being aided by an increase in the temperature in one range and hampered

[4] Kenkre et al. (1994) have provided detailed analytical expressions, both exact and approximate but we display here plots based on numerical calculation of the denominator for the sake of maximum accuracy.

by it in the other. To understand this better, we show Fig. 8.2, which is a plot of our localization parameter $\langle\langle p\rangle\rangle$ versus the dimensionless interaction matrix element relative to the energy lowering for three different temperatures T. The solid arc is at the zero of temperature. We see in this case that $\langle\langle p\rangle\rangle$ disappears abruptly beyond $v = 1$ in a manner reminiscent of the magnetization plotted versus the *temperature*: in the latter case, the magnetization disappears abruptly beyond a critical temperature. It is clear that the general tendency of the system is as follows. An increase in T causes $\langle\langle p\rangle\rangle$ to decrease if v is rather small but it increases, and then decreases if v is larger than the critical value 1. If it lies in the intermediate range (lying between 0 and 1), varied behavior occurs at low temperatures.

8.2.2 Low Temperature Behavior

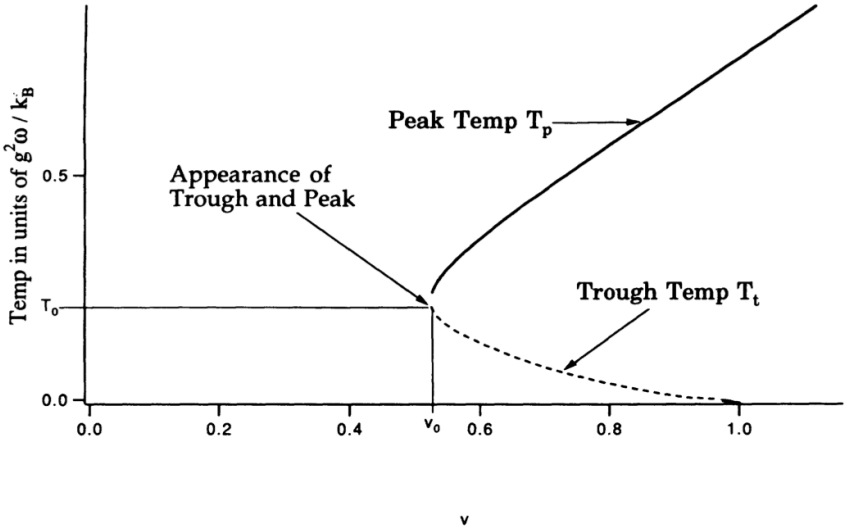

Fig. 8.4 Plot of the v-dependence of the two characteristic temperatures T_t and T_p. See text. Reprinted with permission from fig. 6 of Ref. (Kenkre et al., 1994); copyright (1994) by Springer Publishing.

Fig. 8.3 shows what can happen when v has a value intermediate between 0 and 1. The localization parameter can decrease as T increases from 0 and reach a minimum that we call a 'trough' and whose temperature we denote by T_t. On increasing T further, $\langle\langle p\rangle\rangle$ rises from the trough to a maximum that we associate with the word 'peak'. The temperature at this point is called T_p. Further increase in temperature causes the eventual expected decrease of $\langle\langle p\rangle\rangle$ as the nonlinear structure is destroyed.

All this is shown in Fig. 8.4 in a graph versus v. The reader should consult the original publication for more detailed analysis.

8.2.3 Extension Beyond the Dimer

What we have explained so far has addressed a two-site system for the quantum particle, i.e., we considered a dimer as in most of this book, interacting with what can be regarded as a single (classical) vibrational coordinate representing the difference in displacements of the two sites. Whether there are new insights to gain in generalizations of this system was the question raised by Kenkre et al. (1994). They considered for the most part a crystal ($1d$ for simplicity) interacting with two vibrational modes of equal frequency and coupling constant so analytic considerations could be used and also, separately, a particle dimer interacting with an *arbitrary* number of vibrational modes with different coupling constants and frequencies. I have refrained from showing the calculations for both extensions in the book because they uncover no surprises but lead to expected behavior reinforcing the picture we have constructed of the behavior of the localization parameter. The interested reader should consult the original publication. We start with the spatial extension to N sites and write the semiclassical Hamiltonian as (Kenkre et al., 1994)

$$\begin{aligned}\hat{H} =&\epsilon \sum_m a_m^\dagger a_m + \sum_{m,n} V_{m-n} a_m^\dagger a_n + \frac{1}{2}\sum_q \omega_q \left(y_q y_{-q} + \pi_q \pi_{-q}\right) + \\ &+ \frac{2}{N}\sum_m g_k \omega_k \left(e^{ikm} y_k + e^{-ikm} y_{-k}\right) a_m^\dagger a_m \end{aligned} \tag{8.17}$$

with the translational invariance explicit in the interaction matrix elements V being functions of differences in location and in the equal site energies ϵ at all sites and k and $-k$ being the two specific modes with which the particle interacts.

Consider N to be even for simplicity, take the interacting mode to be $k = \pi$ for simplicity so we can take $y_k = y_{-k} = y$ and, although the results can be generalized to any number of dimensions, assume the crystal to be a $1d$ chain.

Diagonalizing as done earlier for the dimer system but assisted also by a Bloch transformation as a result of the chain translational invariance, we obtain the extension of Eq. (8.14) to be

$$E_q^{\pm} = (\omega/2)\sum_r \left(y_r^2 + \pi_r^2\right) + \sqrt{(g\omega y)^2 + V_q^2}. \tag{8.18}$$

Here $\omega = \omega_k = \omega_{-k}$ is the frequency of the interacting mode $k = \pi$, the band energy V_q equals $2V\cos(q/2)$ if we consider only nearest neighbor interaction matrix elements for the particle on the chain, which we assume from now on for simplicity. Also, we have dropped the constant site energy ϵ without loss of generality.

The partition function is evaluated as in the dimer analysis. The choice of the localization parameter in this extended case falls again on the variable conjugate to y in the Hamiltonian:

$$p = (2/N) \sum_m P_m \cos km, \tag{8.19}$$

where P_m is the probability of the particle occupation of site m and k is the wave vector of the vibrational mode(s) that interacts with the particle. For the N-site chain interacting with the π mode, this gives

$$p = -(2/N)(P_1 - P_2 + P_3 - P_4 + ... - P_N). \tag{8.20}$$

Among explicit calculations of the localization parameter performed with this preparation are those for

- Arbitrary size of crystal, interaction with a single vibrational mode,
- Details for a tetramer ($N = 4$) with explicit evaluations of eigenvectors and eigenvalues and peculiarities of interaction with the $\pi/2$ mode,
- Details for a hypermer (also called an N-mer) that is a system with an arbitrary number of sites with equal intersite interaction as in the systems analyzed in the first part of Chapter 6,
- Dimer interacting with an arbitrary number of modes.

The exercises are interesting to perform but all reinforce the picture we have explained.

8.3 Langevin/Fokker-Planck Analysis of Brownian Motion

In this second part of the present Chapter, we undertake Brownian motion studies in order to understand the effect that thermal interactions with a reservoir can have on the simple nonlinear system we have been investigating in this book. As in the analysis published by Lomdahl and Kerr (1985), our interest is in studying how robust nonlinear entities such as solitons and polarons remain against bath fluctuations induced by heightened temperatures. The difference is that our treatment is analytical, our system is much simpler (a dimer rather than a Davydov soliton), and we focus on the procedure rather than values of parameters obtained from experimental data in the Davydov debate.

The question we pose, expressed in a form appropriate to dimer investigations, is as follows. We know already that the nonlinear nonadiabatic dimer analyzed in the last Chapter settles into localized states (the stationary states of the adiabatic dimer) at $T = 0$. Is there a characteristic temperature T_c such that, while the dimer settles into those localized states for $T < T_c$, it escapes from them at higher temperatures and attains equal population in the two sites for $T > T_c$? In other words, how do we describe quantitatively the destruction of the localization phenomenon that presumably occurs at high temperatures?

Our studies will be found to have a dual outcome. Not only will we have conclusions to draw about how to describe the stability of the nonlinear structure against thermal fluctuations at any given temperature but we will also derive time-dependent equations that govern the evolution of the system in the presence of bath interactions. Setting up a Langevin equation to describe the effect of thermal interactions in a simple manner is our first task. Converting that stochastic equation into a partial differential equation for the probability distribution function in the standard manner is the second task. Our resultant Fokker-Planck viewpoint allows us to calculate a Kramer's escape rate addressing, directly, the question of thermal stability of the nonlinear structure we study. It additionally presents us with a time-dependent density matrix equation with intriguing predictions such as the phenomenon of Hopf bifurcations. We dedicate a section to effects that are observable in principle in a fluorescence depolarization scenario.

This Langevin approach to the description of thermal effects begins (Grigolini et al., 1989) with the incorporation of a stochastic or random force $F(t)$ into the evolution, specifically of the vibrational coordinate y, so that Eqs.(7.5) become now

$$\frac{dp}{dt} = 2Vq, \tag{8.21a}$$

$$\frac{dq}{dt} = -2Vp - \chi yr, \tag{8.21b}$$

$$\frac{dr}{dt} = \chi yq, \tag{8.21c}$$

$$\frac{dy}{dt} + \Gamma(y - p) + F(t) = 0. \tag{8.21d}$$

We have taken $F(t)$, arising from thermal kicks received by the dimer from the heat bath, to be proportional to the difference of terms appropriate to the two sites $F_1(t) - F_2(t)$, and to represent white Gaussian noise with vanishing mean value:

$$\langle F(0)F(t)\rangle = 2\Gamma\langle y^2\rangle_{eq}\delta(t). \tag{8.22}$$

Of importance are the physical assumptions that the noise is not colored, by which we mean that the correlation of the forces is proportional to a δ-function in time, and that it is proportional to the relaxation rate Γ as well as to the equilibrium value of the square of the displacement $\langle y^2\rangle_{eq}$. In the absence of the interaction term in Eq. (8.21d), that equilibrium value would be proportional to the temperature and inversely proportional to the nonlinearity,

$$\langle y^2\rangle_{eq} = \frac{2k_BT}{\chi}. \tag{8.23}$$

We have assumed that the stochastic forces acting on the individual sites are uncorrelated with each other.

8.3.1 Kramer's Escape Time as Representative of Thermal Stability

Our application of the techniques developed over the years by various investigators, but particularly by Grigolini and his collaborators through the use of the projection formalism (Grigolini, 1989; Fonseca et al., 1985; Faetti et al., 1988), leads us to focus on a Langevin set of equations rewritten to involve the quantity

$$z(t) = y(t) - p(t).$$

Details may be found in the original publication (Grigolini et al., 1989) where it is shown how three useful results can be obtained. The first is a Fokker-Planck equation for the evolution of the probability distribution of the vibrational coordinate as well as of the Bloch components of the quasiparticle. The second is a *reduced* Fokker-Planck equation for the nonlinear dimer alone after elimination of the vibrational coordinate. It governs the time dependence of the density matrix elements of the quasiparticle with no reference to the vibrational coordinate. The third is an even further reduced evolution equation for a slow variable that is an appropriate energy in the system. That variable is proportional to

$$r(t) - (\chi/2)p^2(t) + \chi/2 + 1/2\chi.$$

The slow variable has been defined and discussed in the context of Eq. (7.28) earlier and leads to the calculation of the Kramers escape rate. The first of the two Fokker-Planck equations serves as an intermediate step in the derivation of the second. This second equation describes the effect on the nonlinear structure that is the dimer, produced by vibrations and the reservoir both of which are eliminated in the evolution equation.

An excellent exposition of the standard apparatus of the first-time-passage formalism may be found in the work of Weiss (1967). Its application to our system as carried out by Grigolini et al. (1989) has two outcomes. One is an approximate, analytic expression for the Kramer's escape time that is also especially convenient for applications. The other is a more precise version of the same result with the shortcoming that it can only be analyzed numerically. We plot both in the accompanying Fig. 8.5, the solid (dotted) line being the numerical (analytic) prediction. Both show Arrhenius behavior marked by essentially the same characteristic temperature (about $0.5(V/k_B)$ in the plot displayed). What this means physically is that, if our nonlinear dimer is placed initially in one of the localized stationary states, it tends to remain localized for temperatures below this characteristic temperature T_c. The approximate but analytic expression for T_c is

$$T_c = \text{constant}\left(\frac{(\chi/4) + (V^2/\chi) - V}{k_B}\right) \approx \text{constant}\left(\frac{\chi}{4k_B}\right). \tag{8.24}$$

The system escapes if the temperature exceeds that value. The approximation on the extreme right in Eq. (8.24) applies if the nonlinearity χ is much larger than V.

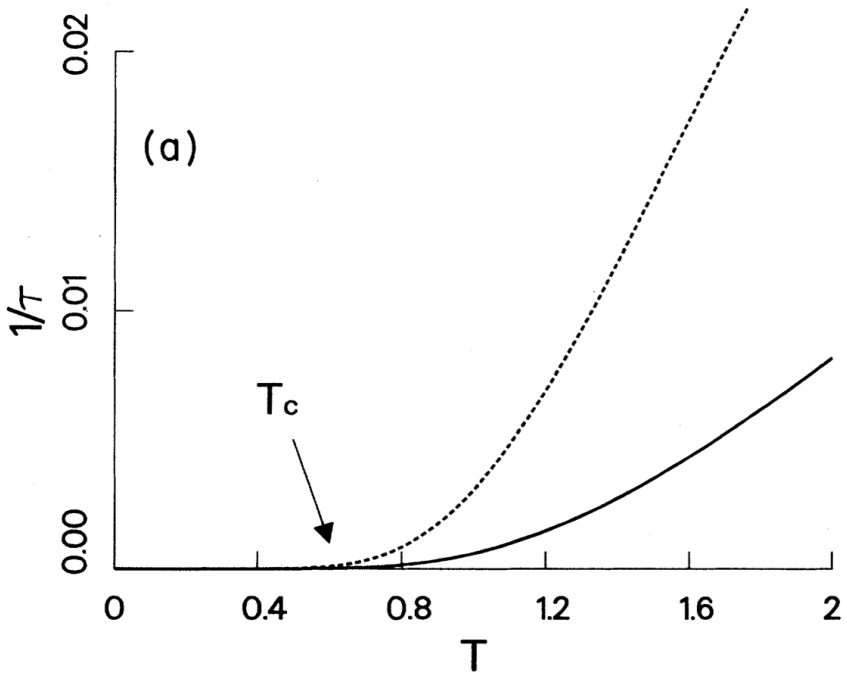

Fig. 8.5 Arrhenius temperature dependence of the escape rate for the system from its nonlinear state plotted on a linear scale as a function of temperature T, the units of rate and temperature being, respectively, V and V/k_B. The solid line, which represents the numerical and more precise result, corresponds to essentially the same characteristic temperature as the approximate but analytic Kramers-like result as given by Eq. (8.24). Parameter values chosen for illustrative purposes are $\Gamma = 50$, $\chi = 10$, in units of V. Reprinted by permission from fig. 1 of Ref. (Grigolini et al., 1989). Copyright 1989 by American Physical Society.

Here is a physical description of what happens. Consider the quasiparticle localized on one of the two sites initially at $T = 0$ and assume that we have $2V < \chi < 4V$. The quasiparticle will perform oscillations between the two sites. The representative point will 'lose energy' as a result of the non-infinite relaxation rate Γ. When this 'energy' decreases below the barrier-top value, the quasiparticle falls into one of the two 'wells' and is practically localized around one of the two sites. The initial conditions and the relaxation rate determine *delicately* which of the two sites is selected for localization. The delicate nature of the selection is associated with the interesting aspect of the right panel of Fig. 7.4. On further reduction of the 'energy' as the reservoir performs its function, the quasiparticle settles into the localized state. These goings-on, described in Chapter 7 at the zero of temperature, are now modified for finite T. The quasiparticle will diffuse as a result of thermal fluctuations and will attain energies characteristic of thermalization with the reservoir. While the fluctuations will be extremely slow below T_c, the barrier will be surmounted easily when

the temperature exceeds T_c. To be kept especially in mind is that the temperature dependence is Arrhenius (or activated) so that, quiet for temperatures below T_c, the system 'awakens' at that characteristic temperature. Equilibration (equal population at the two sites) occurs. The nonlinear entity is then destroyed.

8.3.2 The Ecumenical Equation and its Unification Capabilities

The analysis of the escape rate provided above is appropriate particularly at small temperatures. Let us now describe what happens at arbitrary temperatures with particular validity for high temperatures, following (Kenkre and Grigolini, 1993; Kenkre, 1993). We have mentioned above that two Fokker-Planck equations were derived following the calculation scheme set up by Grigolini for numerous similar systems. The reduced version obtained after elimination of both the reservoir and the vibrational coordinate governs the probability density $\sigma(p, q, r; t)$ that the three Bloch components of the quasiparticle density matrix have values p, q, r at time t is

$$\frac{\partial \sigma(p.q.r;t)}{\partial t} = L\sigma(p, q, r; t), \tag{8.25}$$

where the operator L is given by

$$\begin{aligned} L =& 2V\left(p\frac{\partial}{\partial q} - q\frac{\partial}{\partial p}\right) + \chi p\left(r\frac{\partial}{\partial q} - q\frac{\partial}{\partial r}\right) + \left(\frac{2V\chi}{\Gamma}\right) q\left(q\frac{\partial}{\partial r} - r\frac{\partial}{\partial q}\right) \\ &+ \left(\frac{2\chi k_B T}{\Gamma}\right)\left(r^2\frac{\partial^2}{\partial q^2} - \frac{\partial}{\partial q}r\frac{\partial}{\partial r}q - \frac{\partial}{\partial r}q\frac{\partial}{\partial r}r + q^2\frac{\partial^2}{\partial q^2}\right). \end{aligned} \tag{8.26}$$

In equilibrium, either side of (8.25) vanishes and the equilibrium distribution is obtained to be, with N_1 a normalizing constant,

$$\sigma_{eq}(p, q, r) = N_1 \exp\left[-(V/k_B T)[r - (\chi/4V)p^2]\right]. \tag{8.27}$$

Using the notation

$$\langle f\rangle = \int\int\int dpdqdr\, f(p, q, r)\sigma(p, q, r; t)$$

for any function $f(p, q, r)$ of the Bloch vector components, we obtain from the above Fokker-Planck equation,[5]

[5] The full equilibrium distribution, including for the vibrational coordinate, is proportional to the product of the $\sigma_{eq}(p, q, r)$ given in Eq. (8.25) and the Gaussian factor $\exp[-(\chi z^2/2k_B T)]$.

$$\frac{d\langle p\rangle}{dt} = 2V\langle q\rangle, \tag{8.28a}$$

$$\frac{d\langle q\rangle}{dt} = -2V\langle p\rangle - \chi\langle pr\rangle + \frac{2V\chi}{\Gamma}\langle qr\rangle - \alpha\langle q\rangle, \tag{8.28b}$$

$$\frac{d\langle r\rangle}{dt} = \chi\langle pq\rangle - \frac{2V\chi}{\Gamma}\langle q^2\rangle - \alpha\langle r\rangle. \tag{8.28c}$$

A temperature-dependent expression for the dephasing rate α emerges approximately but naturally from the formalism:

$$\alpha = (2\chi/\Gamma)k_B T. \tag{8.29}$$

While, as we shall see below, Eqs. (8.28) are remarkable in what they predict under standard approximation procedures, they suffer from the same disease that plagues contracted equations in the famous BBGKY kinetic hierarchy (Reichl, 2009; Balescu, 1975). Unless we decouple the products that appear, we have no way of solving these equations as obtained because they are not closed. Factorization assumptions such as $\langle qr\rangle \approx \langle q\rangle\langle r\rangle$ are crude at best. In order to make progress, let us stay within the factorization procedure but employ (Kenkre and Grigolini, 1993) a version that has a slightly more sophisticated aspect (a, b, c being integer exponents):

$$\langle p^a q^b r^c\rangle \approx \langle p\rangle^a\langle q\rangle^b\langle r\rangle^c + \left(\langle p^a q^b r^c\rangle - \langle p\rangle^a\langle q\rangle^b\langle r\rangle^c\right)_{eq}. \tag{8.30}$$

This factorization assumes that, at any time, the thermal average of products of powers of the Bloch components may be approximated by the products of the thermal average of the respective powers plus a correction factor. The correction factor equals the difference of the two quantities at thermal equilibrium. This subterfuge ensures that the assumption is correct at thermal equilibrium even if the simple product assumption is not generally valid.

Substituting (8.30) in (8.28) and dropping the angular brackets, we obtain

$$\frac{dp}{dt} = 2Vq, \tag{8.31a}$$

$$\frac{dq}{dt} = -2Vp - \chi pr + (2V\chi/\Gamma)qr - \alpha q, \tag{8.31b}$$

$$\frac{dr}{dt} = \chi pq - (2V\chi/\Gamma)q^2 - \alpha(r - r_{eq}). \tag{8.31c}$$

The single difference between Eqs. (8.31) and what we would get if we had simply applied a product assumption to Eqs. (8.28) is the replacement of r by its *difference from the thermal equilibrium value* r_{eq} in the last (dephasing) term in (8.31c). One might have expected p_{eq} and q_{eq} also to appear. However, they are absent from the evolution because they vanish identically, the first because of symmetry, i.e., degeneracy of the dimer, and the second from Eq. (8.31a) coupled to the fact that time derivatives vanish in equilibrium.

What evolution equation would we get if we generalize Eqs. (8.31) through no more than an inductive leap to apply to an infinite chain of sites m, n etc., making sure only that they reduce naturally to simpler evolution equations that we believe in as providing an appropriate description? The answer to this question may be found in a suggestion made in (Kenkre, 1993),

$$i\frac{d\rho_{mn}}{dt} = [V,\rho]_{mn} - \chi(\rho_{mm} - \rho_{nn})\rho_{mn} - i\frac{\chi}{\Gamma}\rho_{mn}\left([V,\rho]_{mm} - [V,\rho]_{nn}\right) - i\alpha\left(1-\delta_{mn}\right)\left(\rho_{mn} - \rho_{mn}^{eq}\right), \quad (8.32)$$

and given the appellation 'the ecumenical equation'.[6] This was in an article I wrote in celebration of Al Scott's research.

The reader is invited to reexamine Eq. (1.6) that was presented in Chapter 1 and to realize that the ecumenical equation (8.32) is the augmented form that that density matrix equation adopts when opened to heat reservoirs and prepared for stochastic activities through the introduction of dissipation and fluctuation. In the augmented form, it incorporates non-infinite relaxation and thermal interactions with the reservoir and is capable of resolving the competition and conflicts of nonlinearity and damping, or of fluctuation and dissipation. Indeed, it unifies the description of all those effects in one fell swoop.

It should be remembered that the subject under investigation is the dynamics of a low or intermediate mobility quasiparticle under strong interactions with vibrations. Examples could be a light interstitial such as a muon or proton in a metal; or a vibrational or electronic excitation in a polymer; or even an electron in a narrow-band material. The ρ in the equation would be the density matrix of the quasiparticle, the matrix elements taken in a set of Wannier localized states or a similar representation. The four terms on its right hand side can be said to arise, respectively, from intersite transfer, nonlinearity stemming from interactions with vibrations, finiteness of vibrational relaxation (nonadiabaticity), and thermal fluctuations. The ecumenical equation can be said to be the nonadiabatic version of the nonlinear stochastic Liouville equation (SLE) employed by Tsironis et al. (1988) The latter is obtained by adding ad hoc dephasing terms to the density matrix equation corresponding to the DNLSE. It may be called the adiabatic version of a nonlinear version of the original SLE introduced into exciton transport by Haken, Strobl, and particularly by Reineker (see, e.g., (Haken and Strobl, 1973; Haken and Reineker, 1972; Kenkre and Reineker, 1982)). See also a book of mine, Kenkre (2021) ,for a recent discussion of the conceptual issues surrounding the SLE. A careful comparison of the two nonlinear versions has been given in (Kenkre and Grigolini, 1993).

---

[6] Calculations to be presented below do justify regarding Eq. (8.32) as 'all-embracing' and 'all-inclusive', terms you will find ascribed to the word 'ecumenical' if you refer to the dictionary. I must confess the suggestion for the term came from someone else, a friend whose name, alas, I have, unforgivably, forgotten. I can assure you that I associate the terminology with a moment of weakness when we were deeply embroiled in discussions regarding comparative religions. Luckily perhaps, the name has not stuck.

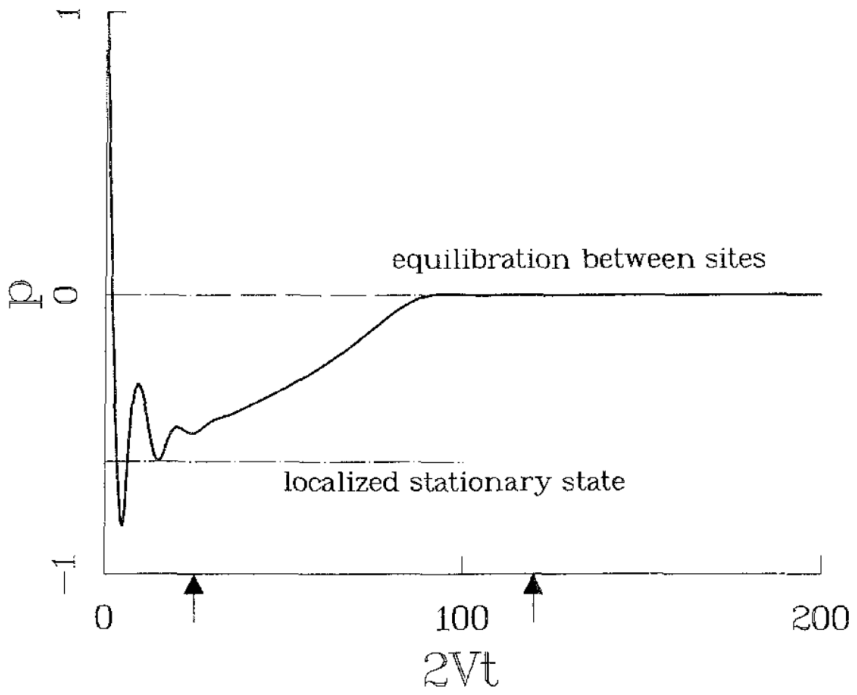

Fig. 8.6 Time evolution of the probability difference $p(t)$ in the dimer as governed by Eq. (8.31) for initial occupation of a single site. Two separate processes, the formation of the self-trapped state and its later destruction as a consequence of thermal fluctuations are seen clearly. Arrows on the time axis indicate the different time regimes. Parameter values in units of $2V$, which are also used to mark time on the x-axis, are: nonlinearity $\chi = 1.25$, relaxation rate $\Gamma = 3$ and temperature dephasing rate $\alpha = 4 \times 10^{-3}$. The localized state value of p seen in the plot is $-\sqrt{1-(2V/\chi)^2}$ precisely according to theory. Reprinted by permission from fig. 1 of Ref. (Kenkre and Grigolini, 1993). Copyright 1993 by Springer Publishing.

For a dimer, the ecumenical equation is the set (8.31). For $\chi = 0 = \alpha$, it describes the trivial linear dimer; if χ vanishes but α does not, it describes the damped linear dimer; for finite χ but infinite Γ, the nonlinear nonadiabatic dimer if α vanishes; a relatively crude but interesting extension (Tsironis et al., 1988) of the nonlinear dimer to dissipative situation if χ is finite, Γ is infinite and α vanishes; and to the nonlinear nonadiabatic dimer if χ, Γ are both finite but α vanishes. We will now begin by examining the unifying abilities of the equation. Let us first consider temperatures so large that $r_{eq} = \tanh(V/k_BT)$ vanishes.

Let us assume that the temperature is large enough ($T >> V/k_B$) to justify such a neglect of r_{eq} and plot the probability difference $p(t)$ in a dimer if the governing equation is (8.31) so that nonlinearity and finite relaxation are envisaged along with initial occupation of site 1. We plot in Fig. 8.6 the time evolution for the parameter values $\chi = 1.25, \Gamma = 3, \alpha = 4 \times 10^{-3}$ all in units of $2V$. We obtain a unified de-

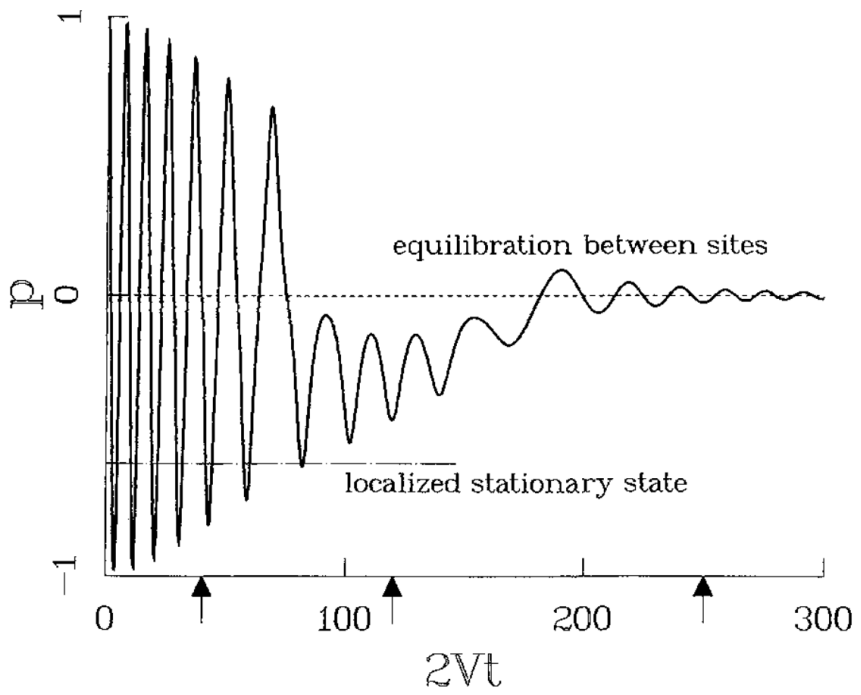

Fig. 8.7 Time evolution of the probability difference $p(t)$ as in Fig. 8.6 with the same value of the nonlinearity $\chi = 1.25$, but for different values of other parameters (in units of $2V$): much larger relaxation rate $\Gamma = 30$ and smaller temperature dephasing rate $\alpha = 1.6 \times 10^{-3}$. All three phases of the evolution are clear: pre-trapping oscillations, formation of the localized structure, and destruction of the state resulting in the equilibration between the two sites. Reprinted by permission from fig. 3 of Ref. (Kenkre and Grigolini, 1993). Copyright 1993 by Springer Publishing.

scription of not only the passage (with oscillations) into the localized stationary state (that corresponds to the value $p_{ss} = -\sqrt{1 - (2V/\chi)^2}$ of the probability difference exactly as theory would predict) but also of escape from that state caused by thermal fluctuations so that the probability equilibrates between the two states.

The same two processes of self-trapping and escape from the self-trapped state are visible in Fig. 8.7 for the same nonlinearity parameter as in Fig. 8.6 but for a much faster relaxation rate $\Gamma = 3$. The relaxation rate is here larger by an order of magnitude but the dephasing rate remains almost the same, $\alpha = 1.6 \times 10^{-3}$. Additionally, the pretrapping oscillations are also seen clearly. Arrows are displayed on the time-axis marking the regions characterizing the various processes in both plots.[7]

[7] The interested reader should consult analysis and plots in (Kenkre and Grigolini, 1993) that compare the old (adiabatic) SLE with the new (nonadiabatic) counterpart introduced here.

8.3.3 Onset of Bifurcations and Limit Cycles

A striking consequence of the ecumenical equation that one can discover through straightforward numerical exploration is that, if the temperature is not so large that the new *driving* term r_{eq} vanishes, its effects can produce unexpected and delightful consequences such as limit cycles and bifurcations (Kenkre, 1993).[8] Kuś was successful in determining that they were Hopf bifurcations and in providing a satisfactory mathematical analysis. What we published as a result (Kenkre and Kuś, 1994) is explained in brief below.

We know from standard texts (see, for example, (Reichl, 2009; Balescu, 1975)) that

$$r_{eq} = \tanh\left(\frac{V}{k_B T}\right) \approx \tanh\left(\frac{\chi}{\Gamma\alpha}\right), \tag{8.33}$$

where the first equality is a consequence of elementary equilibrium considerations[9] of a quantum dimer and the second is based on an approximate description for α,

$$\alpha \approx \frac{\chi k_B T}{\Gamma V}. \tag{8.34}$$

For a large enough nonlinearity χ, an increase in the dephasing rate α results in surprising bursts of the probability difference at short times. The bursts recur with a certain time period. Thus, observe that the initially localized dimer in Fig 8.8a (with parameter values $\chi = 2V = \Gamma$ and time t plotted in units of $1/2V$) first shows oscillations in its probability difference $p(t)$ that damp out within 30 time units signifying descent into its localized self-trapping state. This is followed by destruction of that localized structure after about 200 units of time. Both these processes are ones we have been seeing in the examples studied so far. If however, the dephasing rate α which had been taken to be 0.002 in units of $2V$ in (a), is increased to 0.005, the surprise depicted in (b) of Fig 8.8 happens: a sudden burst of p occurs around $t = 260$ and soon dies out. Although not visible in the plot that

[8] These results remained as curiosities in my notebook serving as no more than material for intriguing remarks during talks until Marek Kuś was able to recognize the nature of the bifurcations.

[9] A rather interesting observation made in Kenkre and Grigolini (1993) deserves mention here. The equilibrium distribution in Eq. (8.27) leads exactly to

$$r_{eq} = \coth(V/k_B T) - (k_B T/V),$$

not to the tanh function. This is surely expected from the fact that the quantum mechanical dimer has been represented in our Fokker-Planck treatment as a dipole rotating in three dimensions in the space spanned by the Bloch vector components. Although this *Langevin function* has the same qualitative shape as the tanh function, they certainly differ quantitatively. Where did this discrepancy come from? The answer is that we have not used the second postulate of quantum statistical mechanics, viz. the assumption of random phases, in our derivation of Eq. (8.27). That derivation treats a classical bath in interaction with a quantum mechanical dimer. When the second postulate is invoked through the construction of an ensemble, removing thereby the contribution of the (random) phases, the Langevin function expression does collapse onto the quantum mechanical tanh result.

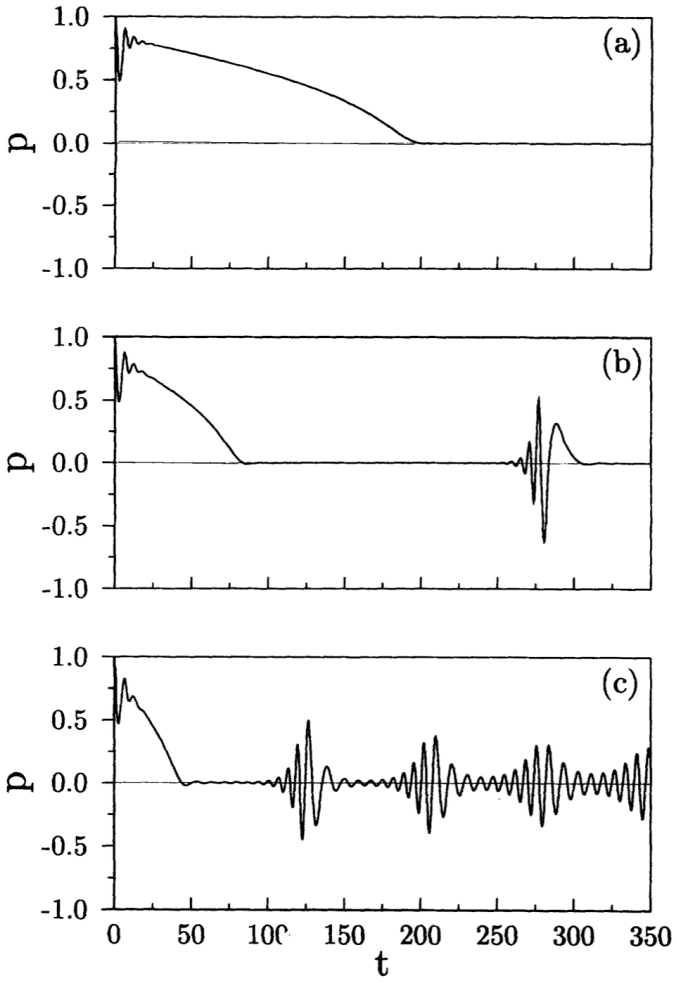

Fig. 8.8 The probability difference $p(t)$ of the quasiparticle localized initially on one site plotted as a function of the dimensionless time $2Vt$ showing a number of different processes. The earliest is initial oscillations, followed by self-trapping and escape from the self-trapped state due to thermal fluctuations. When the dephasing rate α is changed, bursts of $p(t)$ occur as explained in the text. $\chi = 2V = \Gamma$ in all cases but α is varied. In units of $2V$ it is 0.002 in (a), 0.005 in (b) and 0.01 in (c). The increase in α makes the bursts more frequent and therefore visible. Reprinted by permission from fig. 1 of Ref. (Kenkre and Kuś, 1994). Copyright 1994 by American Physical Society.

relates to (b), the bursts recur at larger times. On making α ten times larger as in (c), the multiple bursts recurring periodically become clear because they emerge closer to one another.

This prediction of the ecumenical equation is certainly worthy of note. Where do the bursts come from? Do they occur in the evolution of all three Bloch components?

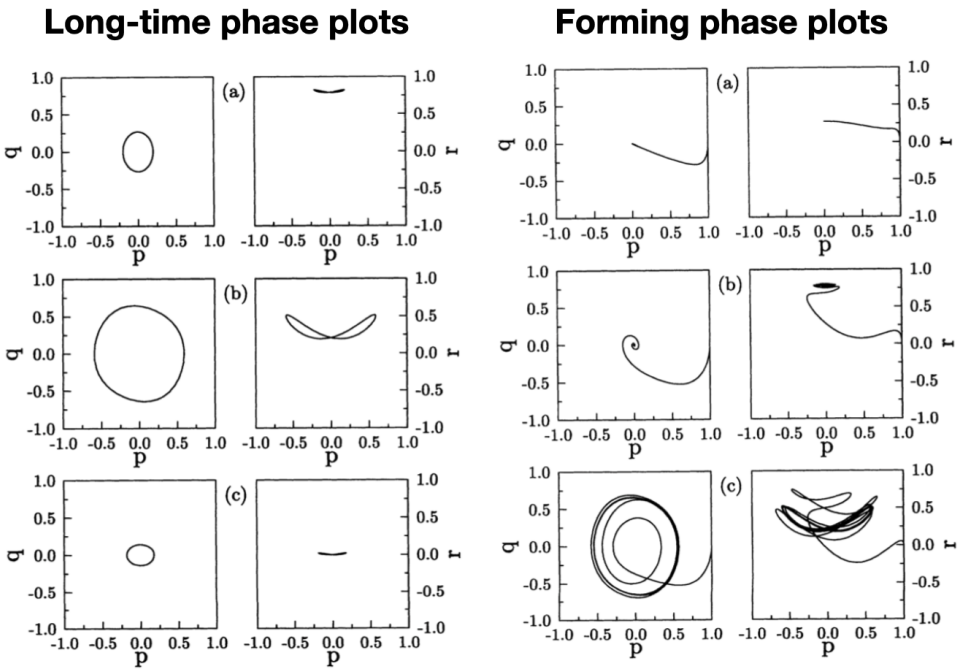

Fig. 8.9 Phase plots of p versus q, and p versus r, showing the formation of limit cycles. The left panel shows them at long times when they have been formed and the right panel at short times during their formation. $\chi = 2V = \Gamma$ in all of them but the dephasing rate α has in units of $2V$ specific values (a) 0.8, (b) 0.33, and (c) 0.01 in the left panel, and (a) 0.33, (b) 0.9, and (c) 3.5 in the right panel. Modified by permission from figs. 5 and 6 of Ref. (Kenkre and Kuś, 1994). Copyright 1994 by American Physical Society.

In order to answer these and similar questions, it is helpful to prepare *phase plots* of the Bloch components p, q, r. We see what happens in such phase plots in Fig. 8.9 where they are displayed two by two.

The left panel in Fig. 8.9 shows the limit cycles at long times, thus, their formed shapes. The right panel shows them at short times, i.e., as they are forming. We see closed circular shapes in the p, q case and butterfly shapes in the p, r case. Parameter values are $\chi = 2V = \Gamma$ in all of them but α varies: (a) 0.8, (b) 0.33, and (c) 0.01 in the left panel but (a) 0.33, (b) 0.9, and (c) 3.5 in the right panel. We have varied the values to show different situations.

What precisely do these phase plots signify? It should be clear that the quasiparticle is in a dynamic steady state, tending to stay in that state forever as a result of thermal energy exchange with the reservoir and of dissipation. If we return to time evolution graphs and examine all three Bloch components, see Fig. 8.10, we note more clearly the tendency for limit cycles to form.

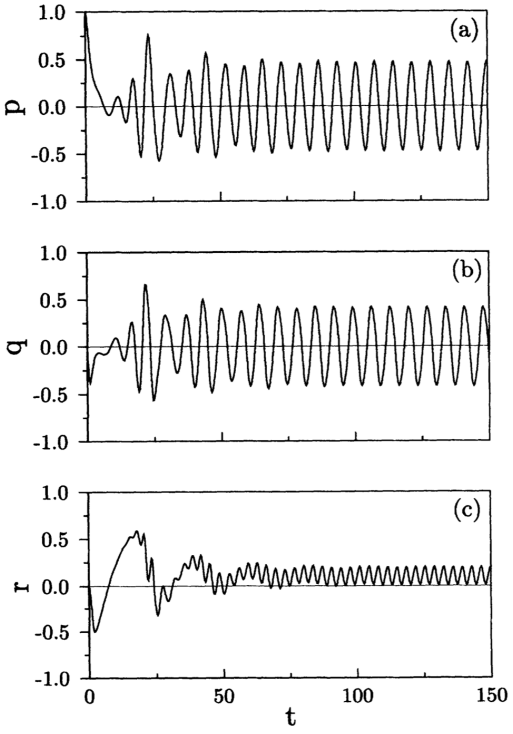

Fig. 8.10 Limit cycles forming in the time evolution of all three Bloch components. Parameter values are $\chi = 2V = \Gamma$ and $\alpha/2V = 0.33$. Reprinted by permission from fig. 2 of Ref. (Kenkre and Kuś, 1994). Copyright 1994 by American Physical Society.

8.3.4 Linear Stability Analysis

Standard stability theory applied around the solutions $p = p_{eq} = 0, q = q_{eq} = 0, r = r_{eq}$ of Eqs. (8.31) leads, as shown in Kenkre and Kuś (1994), to the eigenvalues $\lambda_{\pm}$ and λ_3 of the linearization matrix. They are

$$\lambda_{\pm} = \frac{1}{2}\left[\frac{\chi}{\Gamma} r_{eq} - \alpha \pm \sqrt{\left(\frac{\chi}{\Gamma} r_{eq} - \alpha\right)^2 - 4(1 + \chi r_{eq})}\right], \tag{8.35a}$$

$$\lambda_3 = -\alpha. \tag{8.35b}$$

It is clear from an examination of these expressions that the dephasing rate α has a damping effect that opposes the thermal driving of r_{eq} and that when the dissipation is large enough, the former overtakes the latter. The explicit condition for this to happen is

$$\alpha > \frac{\chi}{\Gamma} r_{eq} \tag{8.36}$$

The critical demarcation value of α that separates the stable and unstable regions is thus $(\chi/\Gamma)r_{eq}$. If α is large enough for the imaginary parts of the eigenvalues $\lambda_{\pm}$ to vanish, the approach of p and q to their equilibrium values is monotonic. This occurs for

$$\alpha > \frac{\chi}{\Gamma} r_{eq} + 2\sqrt{1 + \chi r_{eq}}. \tag{8.37}$$

If α lies between the two demarcation values, i.e.,

$$\frac{\chi}{\Gamma} r_{eq} + 2\sqrt{1 + \chi r_{eq}} > \alpha > \frac{\chi}{\Gamma} r_{eq}, \tag{8.38}$$

the real parts of $\lambda_{\pm}$ continue to be negative but their imaginary parts do not vanish any longer. Spiraling trajectories towards equilibrium in the phase plots are a consequence as is visible in Fig. 8.9. The third eigenvalue, $\lambda_3 = -\alpha$, governs the equilibration of r. It is always real (and negative). Accordingly, for large enough time, the approach along that direction is always monotonic.

The value

$$\alpha_H = \frac{\chi}{\Gamma} r_{eq} \tag{8.39}$$

is clearly significant. We use the subscript H to emphasize that these are Hopf bifurcations. The real parts of the eigenvalues $\lambda_{\pm}$ become zero at $\alpha = \alpha_H$ and positive for even smaller values of α. The interplay of dissipation characterized by α and thermal excitation measured by r_{eq} becomes subtle. The excitation sustains oscillations in the system with non-diminishing amplitude and the equilibrium solution bifurcates to a periodic kind. This is what justifies the identification with what is called a Hopf bifurcation.

The reader might want to consult the book by Marsden and McCracken (1976) for a general theory of Hopf bifurcation and our original paper for details of application to the present system. It can be shown that the oscillation amplitude grows as $\sqrt{\alpha - \alpha_H}$ as the rephrasing rate departs from the Hopf bifurcation. The frequency of revolution along the closed orbit is approximately given by the imaginary part of $\lambda_{\pm}$ at the bifurcation point α_H. How the limiting closed orbit depends on α can be gleaned by inspecting the left panel of Fig. 8.9. I recommend to the reader an examination in detail of the simple but powerful analysis made available in (Kenkre and Kuś, 1994).

8.4 Bursts and Limit Cycles of Time-dependent Fluorescence Depolarization

Let us now examine how the noteworthy predictions of bifurcation and limit cycle phenomena that we have noted could be observed at least in principle in the laboratory in the context of fluorescence depolarization.[10]

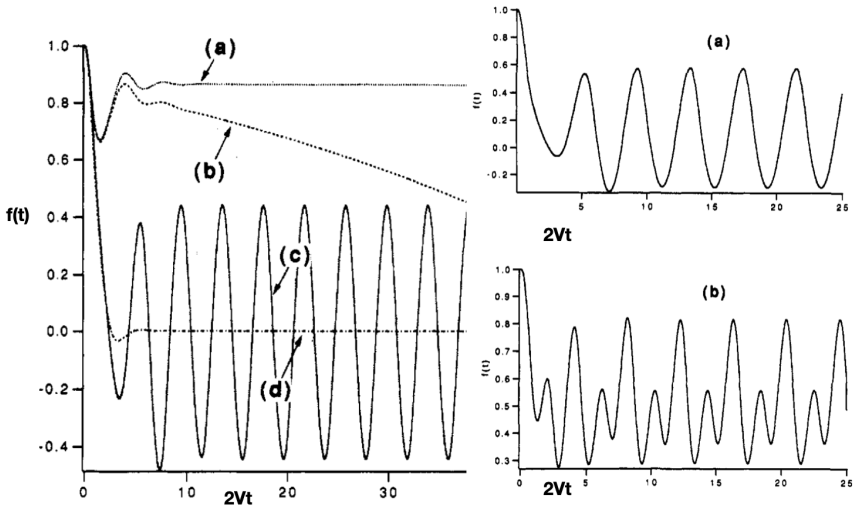

Fig. 8.11 Limit cycles in the fluorescence depolarization arising from thermal fluctuations interacting with nonlinearity. The left panel shows plots of $f\ (t)$ for four values of the dephasing rate α in units of $2V$: (a) 0, (b) 0.01, (c) 1, (d) 4. Respectively, we see straightforward evolution towards the stationary state, removal of the excitation from that state by thermal fluctuations, limit cycles that do not ever decay on account of the combination of nonlinearity and dissipation, and the destruction of the limit cycles from the dephasing rate crossing a threshold. Other parameters: $\phi = 0$ deg, $\chi/2V = 2$, and $\Gamma/2V = 1$. The right panel shows the limit cycles differing when you change the initial polarization angle ϕ. In (a) it is 6 deg and in (b) it is 36 deg. In units of $2V$, α, Γ, χ are 1, 2, 1 respectively.Reprinted by permission from figs. 1, 2, 3, 4 of Ref. (Kenkre, 1994c). Copyright 1994 by the American Chemical Society.

The reader is already familiar with the experiment from the detailed discussion given in Section 3.3 in this book. I found it a simple matter to incorporate the analysis of (Kenkre and Kuś, 1994) into a fluorescence depolarization context because the experimental observable $f(t)$ defined in Eq. (3.8) is given by a simple linear superposition of two of the nonlinear dimer Bloch components via Eq. (3.10). The

[10] This was a topic I had learnt long ago from Robert Knox during a collaboration with him and his then-student Talat Rahman (Rahman et al., 1979). Bob has written about the experiments and various theoretical aspects of the phenomenon in publications with his other students as well including in (Knox and Gülen, 1993).

coefficients in the superposition are trigonometric functions of the initial angle of inclination ϕ made by the polarization of the incident light with the induced dipole moment. The straightforward analysis I presented in a festschrift article written in honor of Raoul Kopelman showed interesting possibilities concerning thermally induced limit cycles (Kenkre, 1994c). For this book, I have combined all four figures of that publication into a single one with two panels, Fig. 8.11 here, to focus on the findings.

For the purposes of the calculation that produces the plots displayed, we take the nonlinearity χ and the relaxation rate Γ to be $4V$ and $2V$, respectively. Let us start by noticing that in (a) of the left panel, for which the angle of initial inclination of the polarization is $\phi = 0$ deg, we see the consequence on $f(t)$ of the fact that the system oscillates and falls into its stationary state. The dephasing rate α for this case is 0. If we change the value of $\alpha/2V$ to 0.01, we see the consequence of the destruction of the nonlinear state by thermal fluctuations. On making α equal to $2V$, we see limit cycles in $f(t)$. This is case (c). The degree of fluorescence depolarization falls into a periodic oscillation that persists forever. This is perhaps the most striking observation. Dissipation and thermal fluctuations join hands to produce this dynamic state that lives for all time. On increasing $\alpha/2V$ still further, making it 4 in the case (d) shown, the limit cycle is destroyed.

The left panel thus shows the varied effect of increasing the dephasing rate α from 0 to higher values leading to escape from the localized state, limit cycles and their destruction.

In the right panel, we see the simple consequence of changing the angle of initial inclination of the plane of polarization of the incident light. In both cases there are limit cycles but in (a) of the right panel we see a single oscillation while in (b) we see a structure with two oscillations both repeating themselves forever. The inclination ϕ is 6 deg in (a) but 36 deg in (b).

8.5 Remarks about the Non-equilibrium Considerations of Thermal Effects

If I were a reader (rather than the author) casting my eyes for the first time on the contents of this Chapter, I would come away with two questions plaguing me. Are the Davydov solitons that made such a splash in the literature a few decades ago (for very understandable reasons given they were invented to bridge serious gaps in our understanding of biological systems) really stable against thermal fluctuations at biological (for instance room) temperatures? And, given the remarkable predictions in the second part of the Chapter about bifurcations and limit cycles, how frequently should we expect to see them actualized in experimental observations in systems we encounter?

I have already washed my hands of the first question during the introductory discussion. I find the Davydov system too complex for me to be able to say authoritatively one way or the other. I know of respectable scientists even now holding on

fast to their opinion that Davydov solitons have no chance to survive at temperatures that matter in biology. I know of other respectable scientists who, as vehemently, believe the opposite.[11]

The second is an important question because on one hand the predictions of the ecumenical equation are striking. On the other hand, the assumptions we have had to make, typified by the cutting of the hierarchy via factorization procedures, should make us suspicious of the connection of the final form of the equation to the original point of departure. Of course, such a state of affairs is met with in the context of much more venerable equations in physics such as the Master equation and the Boltzmann equation although this is not always openly recognized. So should we consider the equations as actually derived or as appearing on a monolith outside our window, or encountered near a burning bush, or heard through what the Hindus call Akashvani (pronouncement from the heavens)? Honestly I do not know. My goal regarding both questions is modest. As to the first, I describe procedures and leave the reader to make her own applications and draw her own conclusions. As to the second, I remain even more silent. Inwardly, I feel the predictions are so intriguing that they are well worth the ingenuity of experimental probers even if the approximations used by theorists in arriving at them are crude.

8.6 Chapter 8 in Summary

Description of thermal effects in the dynamics of nonlinear structures occupied us in this Chapter. Questions of the thermal stability of the Davydov soliton served as a backdrop for the investigations although they were not the focus of the analysis. The conflicting situation in the literature about the fate of that soliton, originally suggested as the carrier of the energy released by the hydrolysis of adenosine triphosphate, was described as an introduction and the rest of the Chapter was dedicated not to any resolution of that issue but to provide two different modes of description, the first based on equilibrium considerations and partition function analysis and the second based on a Langevin formulation and a Fokker-Planck analysis. In the first, a magnetic analogy was utilized to set up a localization parameter which would measure the nonlinearity in the structure that develops in the system. It was shown to

[11] David Brown, Katja Lindenberg, Bruce West belonged in the old days to the former group while Leonor Cruzeiro, Chris Eilbeck and Peter Christiansen belonged to the latter group. Paolo Grigolini wondered whether Davydov solitons existed at all even at zero temperature while Bob Knox worried about how they could be launched, i.e., put into the system realistically. Yet other colleagues smiled enigmatically when I asked for clarification. Several of these scientists had been my collaborators and I could swear by their thoroughness, careful scrutiny and inventiveness. The methods used by some of them in coming to their conclusions were to me rather involved. I had been myself quite unable to come to an opinion and it is not for want of trying. I do not know about the opinions held at the present moment by the investigators I have identified in this footnote but, for the interested, I mention a relatively recent review authored by Cruzeiro (2009), a scientist highly versed in Monte Carlo methods. She collaborated with me on some of these questions in the past but has opinions that have often diverged from mine on these matters.

have a tendency to both increase and eventually decrease as the system temperature increased. Eventual Boltzmannization[12] ensured a destruction of the nonlinear structure at high enough temperatures but the behavior at lower temperatures could be complex. The description was first developed for a two-site system interacting with a single vibration but then extended to a translationally invariant system of an arbitrary number of sites interacting with a single representative vibrational mode and then to a two-site system interacting with any number of vibrational modes. Results were shown to emerge as expected. In the second part of the Chapter, standard methods were applied to start with a Langevin picture and develop a Fokker-Planck equation. The ensuing density matrix equation was shown to be capable of describing in a unified manner, nonlinear behavior known for an adiabatic system, the onset of dissipation from non-adiabacity (finite relaxation), and even of predicting novel phenomena such as bifurcations and limit cycles. These were analyzed and it was shown how they could arise in observations of fluorescence depolarization. The first part of this Chapter, which dealt with equilibrium considerations, showed expected behavior. The second, which addressed non-equilibrium phenomena and invoked some approximations that could be considered a bit bold, presented us with effects that were surprising and certainly interesting.

[12] I realize this term will fill the minds of many respectable users of the English language with ire and wrath but it does explain the process succinctly.

Chapter 9
Microscopic Origin Issues about the DNLSE for Polarons

The microscopic foundation of the DNLSE for polarons is the subject matter for this Chapter 9. Let us follow here a format opposite to the one adopted for Chapter 8 in that we will focus first on the microscopic origin issues for the simplified system central to the book: quasiparticle moving on a dimer in strong interaction with vibrations. Only at the very end of the Chapter will we come to the Davydov soliton backdrop and mention, in highly compressed form, the questions that were causing profound splits among investigators in the 1980's and 1990's about whether the Davydov soliton was really a consequence of the quantum mechanics of the biological system in which it was thought to exist.

The DNLSE for spatially extended systems, as well as for small systems that is the subject matter of the present book, has been for long supposed to be the consequence of strong electron-phonon (generally carrier-phonon) interactions in crystals. The word 'carrier' here covers, additionally, quasiparticles such as an exciton or a vibron. The topic of carrier transport under such conditions has been investigated in multiple ways over the years–long before Davydov suggested solitons for his purpose in biological systems. The theory has been developed simultaneously *and* at different times, without intercommunication in different groups within condensed matter physics. For instance, some know it as constructed by Lee, Low, Pines; others by Firsov, Kudinov. Some have learnt it from publications of Holstein and Fröhlich; others from textbooks by Haken and Mahan.[1] My own first education in the theory of such systems happened in the context of excitons in molecular crystals and photosynthetic systems. I learned the many polaronic tricks of the trade often from the published work of Robert Silbey with his collaborators such as Munn, Grover, Rackovsky and Yarkony (Silbey, 1976; Silbey and Munn, 1980; Grover and Silbey, 1971; Rackovsky and Silbey, 1973; Yarkony and Silbey, 1977).

Prior to addressing the validity issues of the microscopic derivation of semiclassical equations of motion including the DNLSE in the polaron context, let us briefly reacquaint ourselves with the dressing transformation (Grover and Silbey, 1971;

[1] It is practically impossible to remove the parochial element of where we acquired such instruction and I apologize in advance to those who know it well but tend to associate it with other sources.

Kenkre, 1975) and the memory function procedure (Kenkre and Rahman, 1974; Kenkre, 1975) applied specially to the dimer in strong interaction with vibrations. In addition to the original papers cited, two books, a recent one (Kenkre, 2021) and an older one (Kenkre and Reineker, 1982), might be of assistance to the reader for details.[2]

9.1 Preliminary Concepts

Let us begin with the prototypical Hamiltonian in Eq.(4.1) and write it for a two-site resonant system as in section 2 of Chapter 8 as

$$H = V\hat{r} + g\omega\hat{p}\hat{y} + \frac{1}{2}\omega\left(\hat{y}^2 + \hat{\pi}_y^2\right). \tag{9.1}$$

The first term describes the quasiparticle, the third the vibration, and the second stands for the interaction between them. While the interaction can be treated perturbatively if the coupling constant g is small, it presents a problem if it is large.

9.1.1 Dressing Transformations and the Memory Function

The crucial technique for such a situation is to apply a transformation that goes under the name of the *displaced-oscillator transformation* to the bare operators, say $\hat{a}$, to convert them into transformed or 'dressed' operators $\hat{A}$, through the prescription

$$\hat{A} = e^{\left(-ig\hat{\pi}_y\hat{p}\right)}\hat{a}e^{\left(+ig\hat{\pi}_y\hat{p}\right)}. \tag{9.2}$$

Our notation here is to capitalize the respective bare operator to represent the dressed (transformed) operator. The connection between the bare operators appearing in the Hamiltonian (9.1) and their dressed versions is then

[2] Having spent years in the subject of carrier transport under strong interactions with vibrations before I had heard of the Davydov idea, I had a bit of a surrealistic experience when I attended conferences and seminars focused on that idea. People would rehash old concepts and fight ancient battles in the subject matter as if they had been invented anew, often seemingly unaware of what was known, believed, or practiced in the wider community. This is not uncommon. We typically like to think and calculate (rather than read) when we take a fresh look at difficult problems. Surely, it is unreasonable to expect familiarity with science discussed in all branches of our field. Nevertheless, the large disconnect in the Davydov soliton community with general polaronic practice was a bit disorienting and practically inconvenient. The leaders in the field, Al Scott in particular, who organized opportunities for scientists with multiple backgrounds to meet and tackle the Davydov issue in a complementary fashion, were genuinely interested in resolving questions in the field. Despite this, I must confess that shades of the tower of Babel I witnessed in the conferences despite the great ingenuity and creativity of participating researchers (and especially their willingness to learn and cooperate) left an impression. It has motivated me to include a few essential items from polaron knowhow in the beginnings of the present Chapter.

$$\hat{p} = \hat{P}, \tag{9.3a}$$

$$\hat{q} = \hat{Q}\cos(2g\widehat{\Pi}_y) - \hat{R}\sin(2g\widehat{\Pi}_y), \tag{9.3b}$$

$$\hat{r} = \hat{R}\cos(2g\widehat{\Pi}_y) + \hat{Q}\sin(2g\widehat{\Pi}_y), \tag{9.3c}$$

$$\hat{y} = \hat{Y} - g\hat{P}, \tag{9.3d}$$

$$\widehat{\pi}_y = \widehat{\Pi}_y. \tag{9.3e}$$

In terms of the dressed operators, the Hamiltonian can be expressed as[3]

$$\widehat{H} = V\left[\hat{R}\cos(2g\widehat{\Pi}_Y) + \hat{Q}\sin(2g\widehat{\Pi}_Y)\right] + \frac{1}{2}\omega\left(\hat{Y}^2 + \widehat{\Pi}_Y^2\right) - \frac{1}{2}g^2\omega\widehat{1}. \tag{9.4}$$

The transformation derives its name from Eq. (9.3d): it shows that the dressed oscillator has its equilibrium position displaced by the coupling constant g times the probability difference of the quasiparticle. We also see from a comparison of Eq. (9.1) and Eq. (9.4) that the frequency of the dressed oscillator is the same, ω, as that of the bare counterpart. The trigonometric functions signify clouds of oscillator excitations (bosons) surrounding the particle. The last term of Eq.(9.4) shows a lowering of the energy proportional to the product of the square of the coupling constant g and the frequency ω, i.e., to $g^2\omega$. Except for a multiplying constant 2, this is the nonlinearity parameter χ that we have encountered throughout the book. The first term of Eq.(9.4) shows that, in contrast to the first term on the right side of Eq. (9.1), the transfer in the dressed case is accompanied by exchanges of phonons in the 'virtual cloud'. The reader acquainted with more standard expositions of the dressing transformations may find our discussion specialized for a dimer a bit unfamiliar. This form has been used in our group in Kenkre et al. (1996a), Kenkre (1998a) and Kenkre and Giuggioli (2004) and has also appeared in the work of others, for instance, (Steib et al., 1998).

The role of the transformation is to account for a large part of the effect of the coupling term (second in Eq.(9.1)) in the displacement of the equilibrium of the dressed oscillator. The transfer is then treated through a perturbation analysis of the first term on the right side of Eq.(9.4). One can calculate Fermi Golden Rule rates of transfer using $V\left[\hat{R}\cos(2g\widehat{\Pi}_y)\right]$ as the interaction but our method consists of calculating memory functions, instead.

For the purpose, we use the projection operators of Zwanzig (1964) in a form specialized to trace over the vibrations as well as diagonalize in the site-representation for the dimer and produce, without any approximation,

$$\frac{dp(t)}{dt} + 2\int_0^t ds\, \mathcal{W}(t-s)p(s) = \mathcal{I}(t). \tag{9.5}$$

[3] This reduction is exact for a dimer because $\hat{P}^2$ equals the identity operator $\hat{1}$. In extended systems it is customary and necessary to neglect the term proportional to $\hat{P}^2$, the justification requiring either diluteness or the nature of the carrier if it is a fermion.

Flexibility in the choice of projection operators (see, e.g., (Kenkre, 2021)) allows us to make $\mathcal{I}(t) = 0$ identically, if the initial state is diagonal in the dimer site-representation for the quasiparticle and a product of the quasiparticle and vibrational states.

Equation (9.5) is an integrodifferential equation for the c-number $p(t)$ that is the probability difference of the two sites. Features of the memory function $\mathcal{W}(t)$ determine its evolution. Given that the dressing transformation takes into account a large part of the effect of the strong coupling, the memory is calculated perturbatively in orders of the *left-over* interaction between the dressed states. Details may be found in numerous places, especially in Kenkre (1975), but also explained in a tutorial fashion in Kenkre (2021). The result (Kenkre and Rahman, 1974; Kenkre, 1975) is

$$\mathcal{W}(t) = 2V^2 \mathrm{Re}[e^{h(t)-h(0)}]. \tag{9.6}$$

If the number of vibrational modes is arbitrary rather than 1 as in our simplified system here, the $h(t)$ in Eq.(9.6) is given by (Kenkre and Rahman, 1974)

$$h(t) = 2\sum_q g_q^2 [\exp(-i\omega_q t + 2n_q \cos(\omega_q t)], \tag{9.7}$$

but reduces in our single-mode zero-temperature case to

$$h(t) = 2g^2 [\exp(-i\omega t]. \tag{9.8}$$

The q in Eq. (9.7) is a mode label (has nothing obviously to do with the second Bloch vector component) that is summed over, and $n_q = [\exp(\beta\omega_q) - 1]^{-1}$ is the Bose factor with $\beta = 1/k_B T$ and T the temperature.

This means that for our single-mode system at $T = 0$, the probability difference $p(t)$ is explicitly given, for the initial condition stated, by the solution of

$$\frac{dp(t)}{dt} + 4V^2 \int_0^t ds\, e^{-2g^2[1-\cos\omega(t-s)]} \cos[2g^2 \sin\omega(t-s)] p(s) = 0. \tag{9.9}$$

9.1.2 Success of the Memory Approach

How good is the memory method for accuracy of calculation? The memory procedure had been considered a successful approximation technique when it had been used to address a long-debated puzzle involving experiments on naphthalene. Specifically, the data concerned the temperature dependence of the mobility of photo-injected holes in naphthalene. A thorough investigation carried out by Andersen and collaborators of about a dozen theoretical attempts to explain the data showed (see, e.g., Andersen et al. (1983, 1984)) that they were all reasonable but flawed. The one exception (Kenkre et al., 1989) used the memory procedure. The reader is referred to a detailed discussion of this use of the memory method (as well as of the naphthalene

story) in the book by Pope and Swenberg (1982, 1999) where, on pages 968-971 (of the 2nd edition) in particular, the matter has been discussed.

The Hamiltonian used for the naphthalene system was as given in Eq. (4.1) and described a spatially extended crystal, the carrier being in strong interaction with many modes of vibration. The relevant modes were librational. The memory function was calculated explicitly and the velocity autocorrelation function of the carrier was deduced from it. This autocorrelation function was integrated to get the mobility. The reader is referred for an explanation to the original papers or to Chapter 6 of my recent book (Kenkre, 2021) where a pedagogically oriented exposition is provided.

As a visual reminder of how successful the theory based on the memory method was in providing an explanation of the temperature dependence of the mobility in naphthalene, Fig. 9.1 displays the theoretical fits.

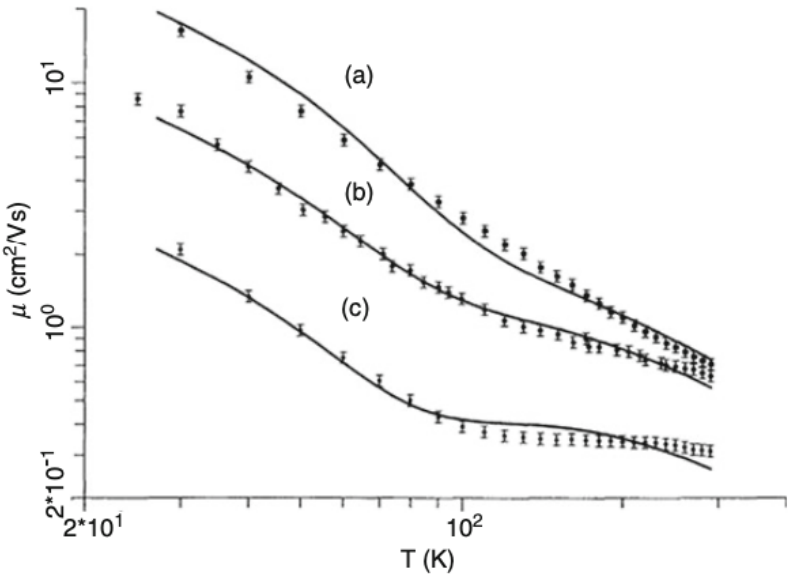

Fig. 9.1 Comparison of the observed mobility data of photo-injected holes in naphthalene in the three directions 1, b, 3, represented by (a), (b), (c), respectively, with the theory based on the memory function procedure, indicating a successful explanation. Reprinted with permission from fig. 2 of Ref. (Kenkre et al., 1989). Copyright 1989 by American Physical Society.

However, the question remains: how good is the memory method for accuracy for the simple system of a dimer in interaction with a single vibrational mode at zero temperature? In order to answer this question, it is straightforward to solve the integro-differential Eq. (9.9) for any given values of the coupling constant g, oscillator frequency ω and intersite transfer interaction V.

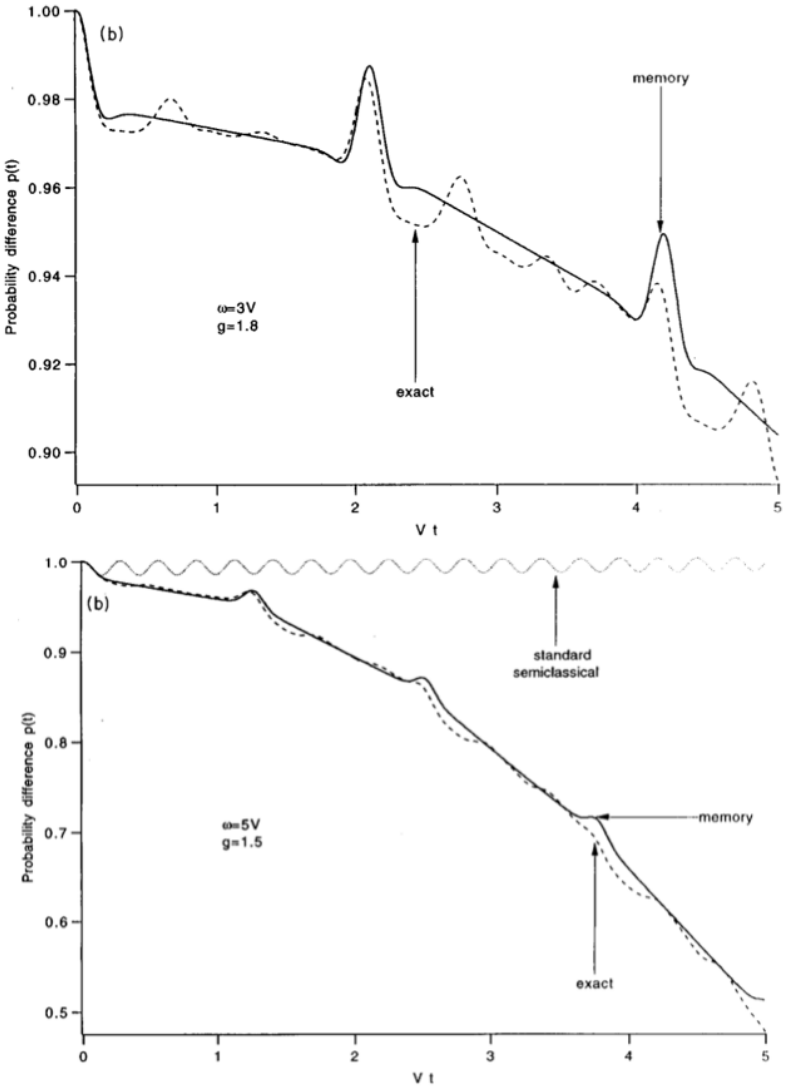

Fig. 9.2 Comparison of the exact (i.e., obtained numerically from the quantum dynamics) and approximate (i.e., obtained via the memory procedure) evolutions of the probability difference $p(t)$. They are denoted, respectively by a dashed and a solid line. The upper panel uses one set of parameter values while the lower panel uses a different set. Both are as indicated. The agreement of the exact and approximate predictions is not perfect but is impressive. Modified by permission from figs. 2 and 3 of Ref. (Kenkre et al., 1996a). Copyright 1996 by American Physical Society.

Fig 9.2 displays[4] a comparison of the solution obtained from such a memory approximation (solid line) to the exact evolution (dashed line) obtained numerically

[4] The additional trace in the lower panel labeled 'standard semiclassical' is not relevant to the present discussion and will be discussed later.

from the given Hamiltonian. The plot shows the results for two sets of parameters, one in the upper panel and one in the lower panel (as indicated) and for an initial condition localized on one site for the quasiparticle.

The details of the vibrational initial condition as well as of the numerical procedure used will be explained in the sequel. We see that the agreement is impressive both in the upper panel where p varies from 1 to 0.9 and in the lower panel where it has a much wider span from 1 to 0.5. Not only does the approximation stay close to the exact evolution in an overall sense but tends, quite remarkably, to change curvature and produce humps at or near the ones in the exact curve.

9.1.3 Nature of the Memory Function and Hierarchy of Time Scales

We have seen that Eq. (9.5) shows how the probability difference $p(t)$ emerges from the memory function. The memory function itself, given generally by Eq. (9.6), becomes, for a single mode at zero temperature,

$$\mathcal{W}(t) = 2V^2 e^{-2g^2(1-\cos\omega t)} \cos(2g^2 \sin\omega t). \tag{9.10}$$

What can we learn from an inspection of the right hand side of (9.10)?

We notice a hierarchy of time scales. We can identify three characteristic times as reciprocals of ω, $g\omega$ and $g^2\omega$. Their presence in the memory is particularly apparent in the limit of small ω. In this limit, the memory becomes a product of a cosine of a period proportional to the $2g^2\omega$, the quantity that we have called the nonlinearity parameter χ, and a Gaussian in time of width proportional to the reciprocal of $g\omega$:

$$\mathcal{W}(t) \approx 2V^2 e^{-g^2\omega^2 t^2} \cos(2g^2\omega t). \tag{9.11}$$

This means that the memory decays in a time equal to the reciprocal of $g\omega$. And that, within the decaying envelope, there are rapid oscillations whose period is characterized by the reciprocal of $g^2\omega$.

The behavior of the memory function is clear from Fig. 9.3 where the ratio of the memory function to its value $2V^2$ at the origin of time is plotted as a function of time in units of $1/V$ for two parameter value sets as shown. For constructing the plots, we use the exact expression (9.10) rather than the low-ω approximation (9.11). The oscillation within the envelope and the decay are visible for either set but we also see an interval in time in which the memory function remains constant at the value of zero before recurring. This last feature is responsible for similar constant periods in the evolution of the probability difference $p(t)$. We call those the *silent runs*.[5]

[5] I seem to remember it was some submarine movie that suggested to me that terminology. My collaborators attempted to object but I was unrelenting and they were kind to me.

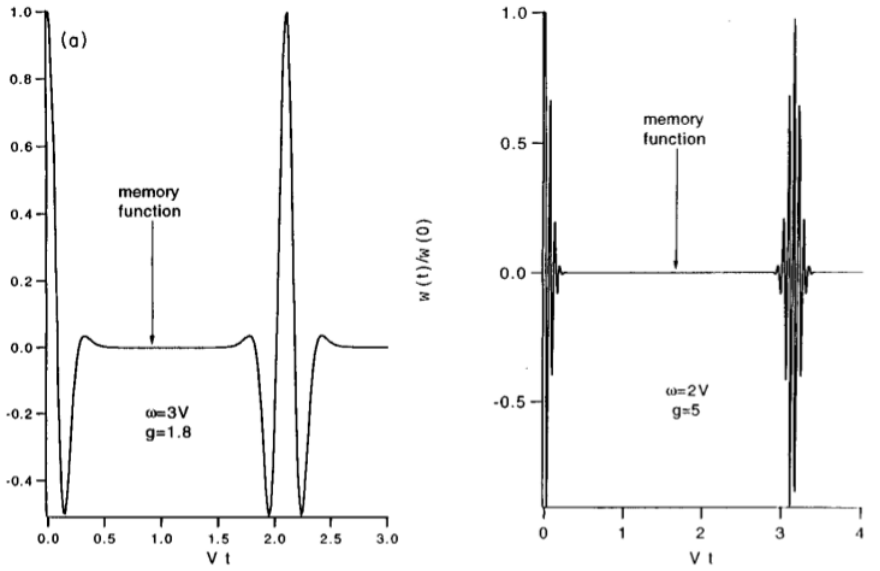

Fig. 9.3 The time-dependence of the memory function itself showing a hierarchy of time scales. Plotted is the ratio $\mathcal{W}(t)/\mathcal{W}(0)$ of the memory function to its value at $t = 0$, as a function of the dimensionless time Vt for two sets of parameter values, as indicated in the left and right panels. Note the decay, the oscillation within the envelope, the period of constant value at 0, and the recurrence. See text. Modified by permission from fig. 2 of Ref. (Kenkre et al., 1996a). Copyright 1996 by American Physical Society.

9.2 Criticism of the Semiclassical Treatment/DNLSE, Numerical Confirmation, and Timescale Hierarchy

Through several papers written in collaboration with his students and colleagues (Vitali and Grigolini, 1990; Vitali et al., 1992; Bonci et al., 1993; Vitali et al., 1994), Grigolini presented an incisive criticism of the semiclassical procedures then current along with the use of the DNLSE.[6] They studied our dimer quasiparticle in strong interaction with a vibrational mode by analyzing the equivalent spin system microscopically, pointed out the connection to work in other fields and generally called into question assumptions and procedures that were being followed in the literature.

Rather than grappling with the analytic approximations (such as Hartree) and procedures (such as Wigner function formulations) discussed by Grigolini and collaborators, I thought a direct comparison with controllable numerical solutions of the simple quantum system would help in getting to the heart of the matter quicker. Following such a procedure resulted (Salkola et al., 1995; Kenkre et al., 1996a) in

[6] He had been earlier an active collaborator of mine on thermal aspects of the DNLSE work that has been described in Chapter 8 of this book.

the firm validation of some of the issues raised by Grigolini and collaborators. We begin the discussion in this Section.

An important point made by Grigolini and his collaborators was about the effect that ω/V, the ratio of the vibrational energy to the intersite transfer interaction would have on the validity of the semiclassical approximation representing the actual quantum evolution of the quasiparticle-vibration system. They pointed out that the approximation gets worse as the ratio becomes large and that, consequently, the slaving idea as usually put forward would not work. This invalidates the often used argument that the vibrations are so fast that they adapt, close to instantaneously, to a slower quasiparticle. Surely, one can have a situation starting from the semiclassical equations wherein the quasiparticle moves slowly and thereby slaves the faster vibrations that adapt. However, Grigolini et al argued that the replacement of the quantum evolution by its semiclassical counterpart itself requires small ω/V. The two suppositions needed to arrive at the DNLSE, they argued, are thus in contradiction. They suggested that the DNLSE is therefore not to be trusted.

My plan to use a direct quantum mechanical calculation to test this conclusion was based on calculations that I had done in the early 1970s to study the comparative validity of two approximation schemes, one carried out by Silbey and collaborators and the other by my collaborators and me on the basis of the memory method. The detail of those calculational schemes is not relevant to the present discussion although the reader will find a thorough exposition in appropriate references (Kenkre, 1975; Kenkre and Reineker, 1982; Kenkre, 2021). What is relevant is that, when our system is stripped to its essentials, its evolution can be calculated by solving the Schrödinger equation easily by numerical methods. The method consisted in writing out the amplitude equations corresponding to the Hamiltonian (9.1), taking a finite number of vibrational levels to approximate the actual semi-infinite situation and diagonalizing the (finite) Hamiltonian matrix, by brute force if necessary, to obtain the evolution.

Thus, if $c_{R,m}$ is the amplitude that our system under investigation has the quasiparticle on the site R (1 or 2), and the oscillator whose displacement is the difference in the displacements of the two sites is in the oscillator number state m (m=0, 1, ...∞) with energy $(m+1/2)\hbar\omega$, the following equations describe the evolution of the system among the vibrational states m, n, etc. with the quasiparticle on site 1 or 2:

$$i\frac{dc_{1,m}}{dt} = \left(m+\frac{1}{2}\right)\omega c_{1,m} + Vc_{2,m} + g\omega\left(\sqrt{m+1}c_{1,m+1} + \sqrt{m}c_{1,m-1}\right), \quad (9.12a)$$

$$i\frac{dc_{2,m}}{dt} = \left(m+\frac{1}{2}\right)\omega c_{2,m} + Vc_{1,m} - g\omega\left(\sqrt{m+1}c_{2,m+1} + \sqrt{m}c_{2,m-1}\right) \quad (9.12b)$$

for $m > 0$, and

$$i\frac{dc_{1,0}}{dt} = \left(\frac{1}{2}\right)\omega c_{1,0} + Vc_{2,0} + g\omega c_{1,1}, \quad (9.13a)$$

$$i\frac{dc_{2,0}}{dt} = \left(\frac{1}{2}\right)\omega c_{2,0} + Vc_{1,0} - g\omega c_{2,1}. \quad (9.13b)$$

for $m = 0$. The square root factors arise from the matrix elements of the displacement among harmonic oscillator states and the difference in sign in the terms multiplying $g\omega$ stems from the fact that the interaction must scatter 'Bloch' states of the dimer.

The numerical approximation consists in taking the upper limit of integers m to a finite number $N - 1$ instead of to what is actually correct, which is infinity. The practical way to implement this is to do the calculation for a finite N and then increase N until there is no discernible change in the results. The probability difference is given by

$$p(t) = \sum_{m=0}^{N} \left(|c_{1,m}|^2 - |c_{2,m}|^2 \right) . \tag{9.14}$$

In our practical computations we found convergence much before N came close to 100 so that we never had to diagonalize matrices larger than 200×200.

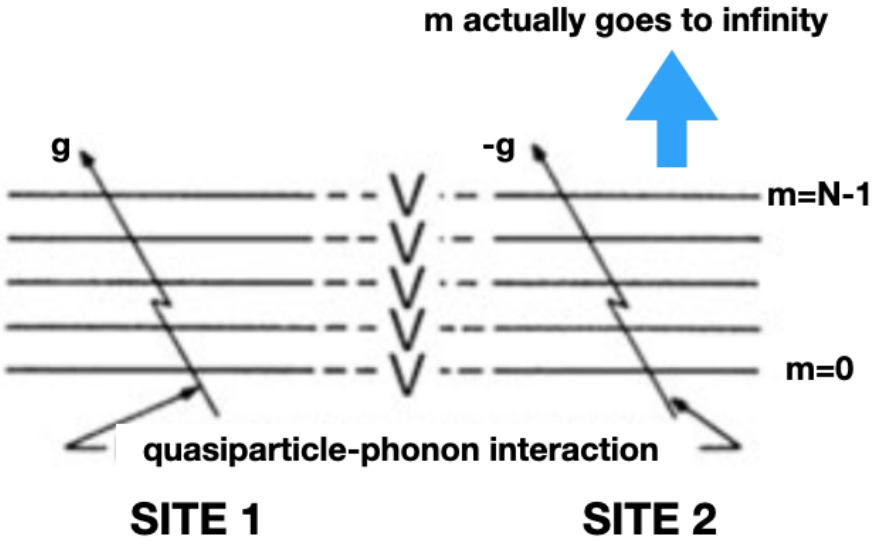

Fig. 9.4 Schematics of the numerical program to obtain the evolution of the probability difference $p(t)$ labeled as 'exact'. See text.

This was the program (see the schematic depiction in Fig. 9.4) that I had followed for the comparative study of the two competing perturbation methods used after the dressing transformation.[7] It had been carried out by hand for $N = 5$ then and has been mentioned in various perturbation discussions, e.g., in Kenkre and Reineker (1982) and in section 4.1 of Kenkre (2021). It was also the precise program that I

[7] It is mentioned explicitly at the end of the paper Kenkre (1975) as a Note Added in Proof.

had suggested to Raghavan[8] to implement numerically when we were surprised to learn from Salkola and Bishop from Los Alamos that they had just achieved not only this calculation but had gone a good deal further in the understanding of the system. We were able to pool results and publish almost half a dozen papers together on the subject matter, clarifying the issues quite thoroughly.[9]

Salkola et al. (1995) showed unequivocally that not only were Grigolini and collaborators correct in asserting that the semiclassical approximation was better (worse) for smaller (larger) values of ω/V but that there was a well-defined non-trivial limit in which semiclassical dynamics coincided with quantum dynamics. In addition, they identified a clear hierarchy of time scales over which the quantum dynamics can be rationalized, time scales that can be related to counterparts in the memory function $\mathcal{W}(t)$ quite simply.

That all was not well with the semiclassical approximation for high frequencies of the vibrations ($\omega/V >> 1$) was known already earlier than the Grigolini papers, for instance to Brown et al. (1987), and independently later, e.g., to Steib et al. (1998). The 'massive oscillator limit' that Salkola et al. (1995) identified as being one in which the semiclassical equations were perfectly valid was $\omega \to 0, g \to \infty$ with $2g^2\omega = \chi$, a constant. The hierarchy of time scales they mentioned was associated with the fact that, for appropriate parameters, the probability evolution exhibits rapid oscillations on a time scale we may call τ_χ, a decay on a time scale τ_γ, a revival on the time scale τ_Δ, and an overall oscillation on the scale τ_T. These are all visible in the exact evolution (dashed line) in both panels of Fig. 9.2. In the limit of small ω and large g, three of these four time scales can be seen very clearly as being $\tau_\chi \approx 1/g^2\omega$, the time characteristic of the oscillations within the recurring envelope, $\tau_\gamma \approx 1/g\omega$, the time extent of the envelope (burst), and $\tau_\Delta \approx 1/\omega$, over which the revivals occur after each silent run. These three are particularly obvious in Fig. 9.5 which we show for a situation with low oscillator frequency ω and high coupling constant g: $\omega = 0.1V$, $\chi = 2g^2\omega = 6V$.

The fourth time scale, not seen in the plot, marks the tunneling of the quasiparticle from one site to the other and is of the order of e^{g^2}/V. In the massive oscillator limit $\omega \to 0, g \to \infty$ with $2g^2\omega = \chi$, the vibrational distortion is essentially frozen from the viewpoint of the quasiparticle and so we have a static energy mismatch proportional to χ. In this limit, the memory function is $2V^2 \cos \chi t$. The probability difference can be said to be, (for initial placement on one of the sites),

$$p(t) = \left(\frac{\chi^2}{\chi^2 + 4V^2}\right) + \left(\frac{4V^2}{\chi^2 + 4V^2}\right) \cos\left(t\sqrt{\chi^2 + 4V^2}\right). \tag{9.15}$$

[8] Srikanth Raghavan was a gifted student with quick wit and a highly developed sensitivity to play upon words. I could not decide which I enjoyed during our time together more, his sense of humor or his enthusiasm and work ethic as well as his sharpness in physics matters. We spent oodles of time discussing P. G. Wodehouse during his thesis work with me. The reader will meet him again in Chapter 10 in connection with his brilliant work with Smerzi, Shenoy and others on tunneling in Bose-Einstein condensates.

[9] The brief four-way collaboration with Markku Salkola, Alan Bishop, and Srikanth Raghavan around 1995 was one of the most enjoyable and productive ones that I remember. Srikanth and I learned much from our Los Alamos collaborators.

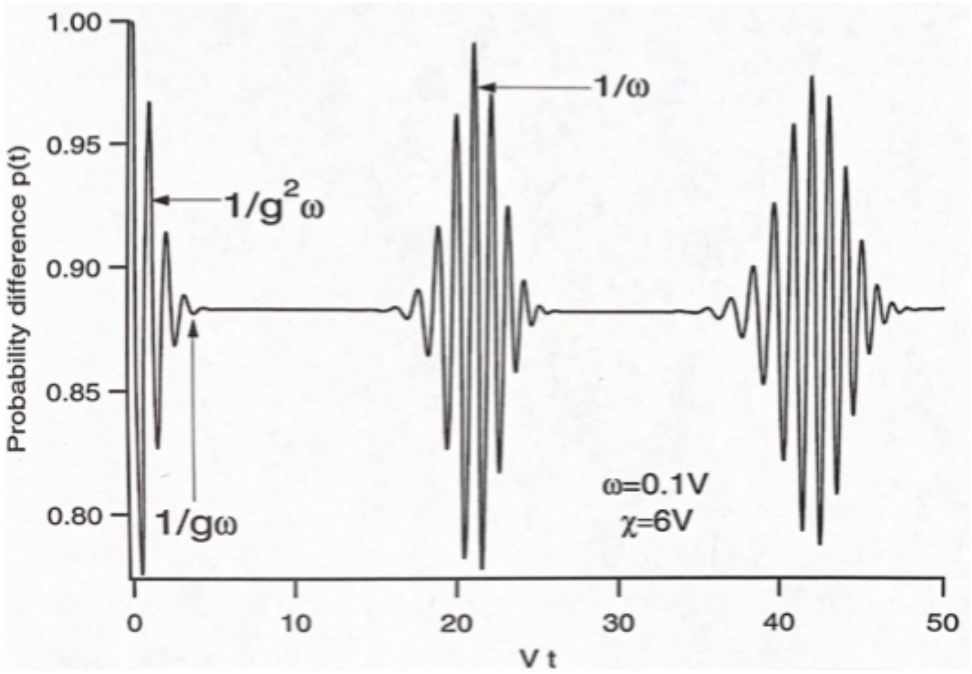

Fig. 9.5 Three of the four time scales in the time evolution of $p(t)$, the probability difference: τ_χ, τ_γ, and τ_Δ. The tunneling timescale is not visible. The time scales indicated are clear in this low-frequency high coupling constant situation as $1/g^2\omega, 1/g\omega, 1/\omega$, respectively. Parameter values, as shown on the plot, are $\omega = 0.1$ and $\chi = 2g^2\omega = 6$ in units of V. Compare Fig. 9.3 that displays memory functions (rather than $p(t)$ that is shown here) and uses another set of parameter values. See text.

What does this equation tell us about the evolution? The quasiparticle is self-trapped: oscillations of frequency proportional to $\sqrt{\chi^2 + 4V^2}$, which is approximately equal to χ for the case $\chi >> V$, occur about a mean value $\chi^2/(\chi^2 + 4V^2)$.

The tunneling time scale e^{g^2}/V can be understood easily also. It is the reciprocal of the tunneling matrix element Ve^{-g^2} after the transformation. The matrix element is reduced from its bare value V because of the reduction in overlap.

Why we use the phrase 'massive oscillator limit' should be clear from the fact that the oscillator mass μ appears as $g\omega \propto \mu^{-1/4}$ and $\omega \propto \mu^{-1/2}$. The limit $\omega \to 0, g \to \infty$ with $2g^2\omega = \chi$ may be looked upon as the limit $\mu \to \infty$.

The correctness of the warning (Brown et al., 1987; Vitali and Grigolini, 1990; Vitali et al., 1992; Bonci et al., 1993; Vitali et al., 1994; Steib et al., 1998), that the semiclassical approximation could be quite inadequate unless ω/V was small, already verified in (Salkola et al., 1995), was supported impressively in (Kenkre et al., 1996a). Thus, let me now point out that the lonely trace oscillating high up in Fig. 9.2 (lower panel) signifying self-trapping is the result of the semiclassical

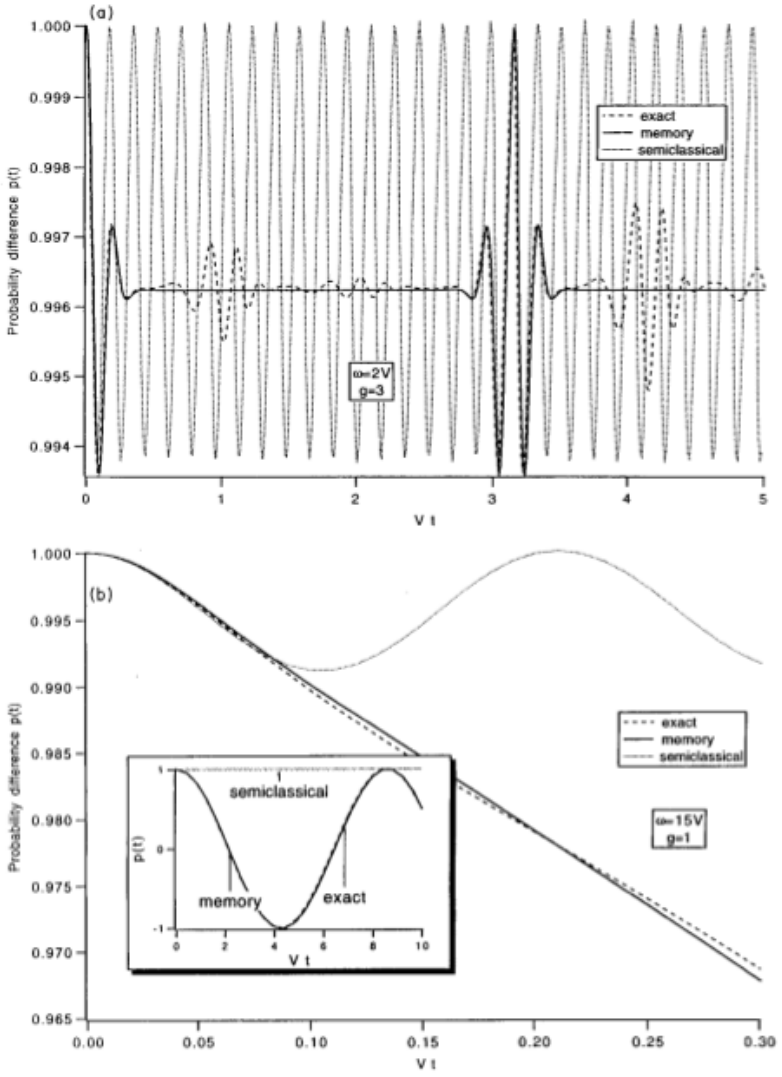

Fig. 9.6 Agreement of the approximations with the exact evolution for low frequency (upper panel (a)) and failure of the semiclassical approximation but success of the memory procedure for high frequency (lower panel (b)). See text. Reprinted by permission from fig. 1 of Ref. (Kenkre et al., 1996a). Copyright 1996 by American Physical Society.

description. The actual evolution as given both by the exact numerical (dashed) and the memory approximation (solid) is shown to be very different: tunneling from

one site to the other.[10] From the repeated instances of the comparative analysis of numerically exact and the two approximate predictions (semiclassical and memory) that we carried out systematically in Kenkre et al. (1996a), we show one more in Fig. 9.6.

The upper (lower) panel is for low (high) frequency. We notice impressive reproduction of the silent runs and oscillation detail by the memory approximation in (a), the low-ω case. Here, $\omega/V = 2$ (and $g = 3$). We also see agreement with the semiclassical approximation in that the latter correctly reproduces the bounds of the oscillation (but is unable to describe the silent runs).

The striking failure of the semiclassical approximation as well as the striking success of the memory method are obvious in (b) where the frequency is high: $\omega/V = 15$ (and $g = 1$). The semiclassical description shows self-trapping whereas the memory approximation and the exact evolution stay together and represent tunneling. The inset in the lower panel describes the long-time evolution and again emphasizes both the inadequacy of the semiclassical representation and the success of the memory approximation.

9.3 Additional Investigations into the Validity Question

A systematic study of the analysis of the approximations reported by Salkola, Raghavan, Bishop and Kenkre will reveal to the reader numerous interesting findings in addition to following the time dependence of $p(t)$. They include monitoring the correlation that measures the effect of quantum fluctuations on the system and that is the missing term from the semiclassical description (Salkola et al., 1995). They involve studies of the spin-boson system and its features such as entropy maximization far from equilibrium with the help of Husumi distributions (Salkola et al., 1996). They also include studies for this purpose of the energy transfer rate in sensitized luminescence (Kenkre et al., 1996a), studies of the fluorescence depolarization (Raghavan et al., 1996), of anharmonicity in the vibrations particularly with the validity of semiclassical equations in mind (Raghavan et al., 1999a), and investigations also of varying the initial condition (Kenkre et al., 1996a). Some of these will be addressed in the sequel.

The main features of the exact evolution can be understood in terms of a representative two-state system in interaction with vibrations in such a way that there is a *time dependence* both to the energy mismatch, $\chi(t)$, and to the transfer interaction, $V(t)$. The DNLSE or the semiclassical approximation describes the self-trapping transition by treating properly the effect of $\chi(t)$ but not of $V(t)$. If the coupling constant g is large enough, the overlap between the wave functions on the two sites becomes repeatedly near-zero during the vibrational oscillations.[11] The enormous

[10] It should be kept in mind that this disagreement means that the semiclassical approximation gives here *even qualitatively* incorrect predictions.

[11] This corresponds to the overlap reduction or band narrowing that is described by the exponential reduction in V going to $V e^{-g^2}$.

reduction of intersite interaction suppresses the motion of the quasiparticle. This goes on for some time until the vibrational oscillation unmakes the mismatch. The overlap returns to the original value and revival occurs. This happens repeatedly and causes the *silent runs*. The period is inversely proportional to ω. One can assert that, while the semiclassical description covers the energy mismatch $\chi(t)$ but not the time-dependent transfer $V(t)$, it stays inferior as an approximation relative to the memory procedure that does both.

9.3.1 A Linear Four-State Model

Worth mentioning here is a clever *linear* 4-state model that Raghavan invented on the basis of sum rule arguments such as those put forward in Kenkre (1975). He has described it in his Ph. D. thesis (1996). In Chapter 4 of the present book, we have learned pictorially the Stokes sliding of the parabolic potential in which the oscillator moves. See Fig. 4.1. In the dimer, it can be considered to slide leftwards and downwards (from the dotted to the solid curve as shown) if the quasiparticle occupies the left site, and rightwards and downwards, similarly, if it occupies the right site. Raghavan took the bottom points of the displaced parabolas as states 1 and 2 and the points energetically higher up on the opposite parabolas reached by a Franck-Condon vertical transition as 3 and 4, respectively. He envisaged the bottom states 1 and 2 to be connected by the tunneling matrix element $V_d \equiv Ve^{-g^2}$. Through sum rule arguments (Kenkre, 1975), he introduced a representative matrix element $\mathcal{V} = \sqrt{V^2 - V_d^2}$ between states 1 and 3. Requiring that the matrix element V_u between 3 and 4, together with $V - d$, absorb the interactions responsible for the 'zero-phonon line' in the original problem,[12] and keeping in mind that χ is the energy difference between the upper and the lower states, Raghavan described the evolution in terms of the amplitudes $C_{1.2.3.4}$ that the system is in the four states:

$$i\frac{dC_1(t)}{dt} = V_d C_2(t) + \mathcal{V} C_3(t), \tag{9.16a}$$

$$i\frac{dC_2(t)}{dt} = V_d C_1(t) + \mathcal{V} C_4(t), \tag{9.16b}$$

$$i\frac{dC_3(t)}{dt} = \chi C_3(t) + V_u C_4(t) + \mathcal{V} C_1(t), \tag{9.16c}$$

$$i\frac{dC_4(t)}{dt} = \chi C_4(t) + V_u C_3(t) + \mathcal{V} C_2(t). \tag{9.16d}$$

Exact solutions of the linear model are trivial to obtain not only in the dimer system but even in the infinite chain. What is remarkable is that Raghavan showed that the results captured a great deal of the exact evolution (although not delicate ingredients

[12] The curious reader might be helped by a perusal of (Kenkre, 1975).

such as the silent runs) that we have had to obtain through tortuous practice of numerical methodology.

9.3.2 Extreme Limits of the Transformation: Bare and Fully Dressed

A moment's reflection shows that there is not a single semiclassical approximation that one should be considering but as many as allowable values of the coupling constant used in the transformation. The bare limit would be appropriate to small coupling constants and the full limit to large ones. Let us first study these two limits. It is quite clear hat the semiclassical approximation anchored in the bare picture should correspond to removing the circumflexes on the operators in

$$\frac{d\hat{p}}{dt} = -2V\hat{q}, \tag{9.17a}$$

$$\frac{d\hat{q}}{dt} = 2V\hat{p} - 2g\omega\hat{y}\hat{r}, \tag{9.17b}$$

$$\frac{d\hat{r}}{dt} = 2g\omega\hat{y}\hat{q}, \tag{9.17c}$$

$$\frac{d\hat{y}}{dt} = \omega\widehat{\pi}_y, \tag{9.17d}$$

$$\frac{d\widehat{\pi}_y}{dt} = -\omega\hat{y} - g\omega\widehat{\pi}_y. \tag{9.17e}$$

Kenkre and Giuggioli (2004) found, however, that there was a problem in assigning the opposite limit in the fully dressed picture. After full dressing , we have

$$\frac{d\hat{P}}{dt} = -2V\left[\hat{Q}\cos(2g\widehat{\Pi}_Y) + \hat{R}\sin(2g\widehat{\Pi}_Y)\right], \tag{9.18a}$$

$$\frac{d\hat{Q}}{dt} = 2V\hat{P}\cos(2g\widehat{\Pi}_Y), \tag{9.18b}$$

$$\frac{d\hat{R}}{dt} = 2V\hat{P}\sin(2g\widehat{\Pi}_Y), \tag{9.18c}$$

$$\frac{d\hat{Y}}{dt} = -2gV\left[\hat{Q}\cos(2g\widehat{\Pi}_y) + \hat{R}\sin(2g\widehat{\Pi}_Y)\right] + \omega\widehat{\Pi}_Y, \tag{9.18d}$$

$$\frac{d\widehat{\Pi}_Y}{dt} = -\omega\hat{Y}. \tag{9.18e}$$

Removing the circumflexes on the operators on these dressed equations shows that they have a tendency to get better at representing the actual quantum evolution in the limit of large ω/V, i.e., opposite to the case with the bare semiclassical approximation. However, they consistently predict a *shift in the probability difference* $p(t)$. This is seen clearly in Fig. 9.7. In contrast to the bare case, the semiclassical procedure of replacing the vibrational operators by c-numbers has a double approximation effect.

Assuming

$$\cos(2g\widehat{\Pi}_Y) \approx \cos(2g\langle\widehat{\Pi}_Y\rangle)$$

involves, in addition to the replacement of the operator $\widehat{\Pi}_Y$ by its expectation value, the replacement of *all powers* of $\widehat{\Pi}_Y$, resident in the cosine in the form of its infinite series by powers of the expectation values.

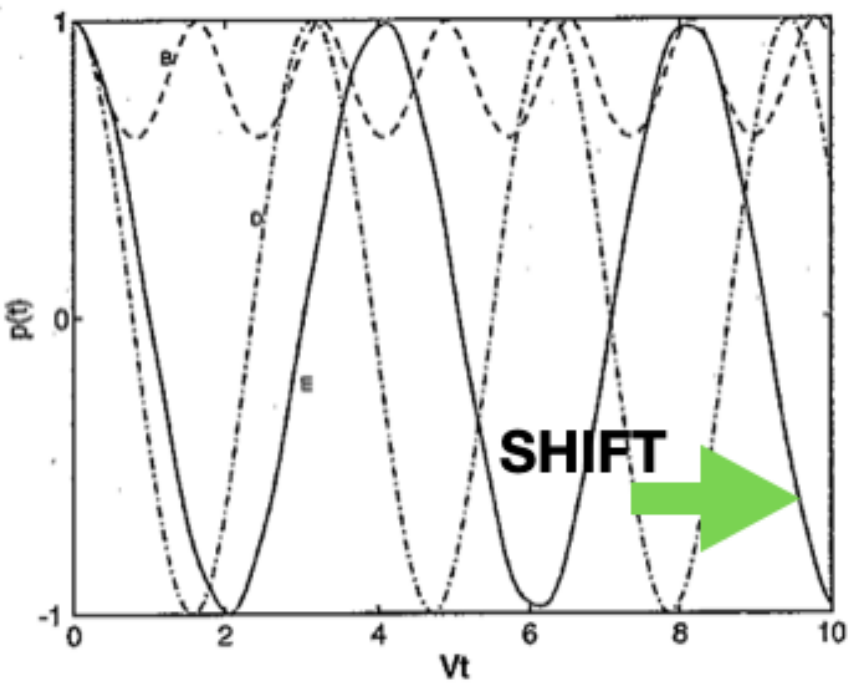

Fig. 9.7 Comparison of the exact evolution of the exact probability difference $p(t)$ (solid line E) with two extreme semiclassical approximations: one made after full dressing (dash-dotted line D) that is otherwise a good approximation to the exact evolution in that it describes the qualitatives correctly but produces a consistent shift; and one in which no dressing transformation is performed (dashed line B). This latter is hopelessly inadequate as it shows self-trapping, oscillating asymmetrically as it does with a mean that is much larger than 0. Parameters are $g = 0.5$ and $\omega/V = 10$ and the quasiparticle initially occupies one site. Modified with permission from fig. 2 of Ref. Kenkre and Giuggioli (2004). Copyright 2004 by Elsevier Publishing.

This shift problem can be resolved satisfactorily in a pragmatic manner, as discussed in Kenkre and Giuggioli (2004), by following the prescription suggested by Reineker and collaborators (Steib et al., 1998) on the basis of the application of the time-dependent variational principle (Kramer and Saraceno, 1980). When the circumflexes are removed from the operators in Eqs. (9.19), one multiplies V by the Huang-Rhys factor e^{-g^2}. It is well-known that the factor appears

from the overlap of the displaced oscillator and is related to the known identity $\langle \exp(\theta b + \phi b^\dagger)\rangle = \exp[\theta\phi(\langle b^\dagger b\rangle + 1/2)]$ where $\langle ...\rangle$ denotes a thermal average over the boson Hamiltonian.

As a consequence, the equations of motion in the fully dressed semiclassical approximation take the form

$$\frac{dP}{dt} = -2Ve^{-g^2}\left[Q\cos(2g\Pi_Y) + R\sin(2g\Pi_Y)\right], \tag{9.19a}$$

$$\frac{dQ}{dt} = 2Ve^{-g^2}P\cos(2g\Pi_Y), \tag{9.19b}$$

$$\frac{dR}{dt} = 2Ve^{-g^2}P\sin(2g\Pi_Y), \tag{9.19c}$$

$$\frac{dY}{dt} = -2gVe^{-g^2}\left[Q\cos(2g\Pi_y) + R\sin(2g\Pi_Y)\right] + \omega\Pi_Y, \tag{9.19d}$$

$$\frac{d\Pi_Y}{dt} = -\omega Y. \tag{9.19e}$$

We find that this set removes the shift problem displayed in Fig. 9.7 by the application of the e^{-g^2} factor and does an acceptable job of approximating the exact evolution for high values of ω/V. The reader is reminded that this is the limit opposite to that in which the bare semiclassical approximation (obtained by removing the circumflexes over the operators in Eqs. (9.17)) works well, as pointed out in (Salkola et al., 1995) and earlier.

We have seen that the exact quantum mechanical analysis of the dimer shows remarkable features in its evolution such as not only self-trapping but silent runs as well.[13] The suggestion, probably made by many authors independently, see, e.g., Kenkre et al. (1996a), that these phenomena arise from an effective time-dependent energy mismatch and an effective time-dependent intersite transfer matrix element can be given a firm footing from Eqs. (9.19) and (9.17), respectively. Define for this purpose the time-dependent *complex* interaction

$$V_R(t) + iV_I(t) = Ve^{-g^2}e^{i2g\Pi_Y(t)} = Ve^{-g^2}[\cos 2g\Pi_Y(t) + i\sin 2g\Pi_Y(t)]. \tag{9.20}$$

One deduces from the set. (9.19) that its first three equations can be written as the following torque equation for the precession of a rigid rotator:

$$\frac{d}{dt}\begin{pmatrix} P \\ Q \\ R \end{pmatrix} + \begin{pmatrix} 0 & 2V_R(t) & 2V_I(t) \\ -2V_R(t) & 0 & 0 \\ -2V_I(t) & 0 & 0 \end{pmatrix}\begin{pmatrix} P \\ Q \\ R \end{pmatrix} = 0. \tag{9.21}$$

The real quantities $V_R(t)$ and $V_I(t)$ evolve trigonometrically with the dressed momentum $\Pi_Y(t)$ that is changing in time as their argument. As a consequence, the time-dependent interaction can periodically collapse and produce the silent runs in

[13] Such features have been well known in related fields such as quantum optics. See, e.g., (Allen and Eberly, 1987).

$P(t) = p(t)$. The dressed picture for the full semiclassical system makes this quite clear.

Cast in a similar torque form, the bare semiclassical equations (9.17) yield

$$\frac{d}{dt}\begin{pmatrix} p \\ q \\ r \end{pmatrix} + \begin{pmatrix} 0 & 2V & 0 \\ -2V & 0 & 2E(t) \\ 0 & -2E(t) & 0 \end{pmatrix}\begin{pmatrix} p \\ q \\ r \end{pmatrix} = 0. \tag{9.22}$$

They show that the (bare) quasiparticle shuttles with constant intersite transfer V between two *energetically mismatched* states. The effective mismatch $E(t)$ is time-dependent and proportional to the displacement of the bare oscillator:

$$E(t) = g\omega y(t). \tag{9.23}$$

We know, of course, that energy mismatch in the dimer leads to probability oscillations that are not complete, signifying self-trapping.

We see thus that the disruption of transfer, equivalently localization, occurs in two separate ways. What emerges from the discussion is that the bare limit is representative of energy mismatch, which is one of them, whereas the fully dressed limit is representative of reduced intersite transfer, which is the other way. By 'reduced' I refer here not merely to what the Huang-Rhys (sometimes called the Debye-Waller) factor e^{-g^2} does, but also, and particularly, to the time variation that can *periodically collapse the effective transfer.*

A rather detailed comparative investigation of the bare and the fully dressed semiclassical approximations has been carried out in Kenkre and Giuggioli (2004).[14] One of the quantities studied was an objectively calculated least-squares error between the exact evolution and each of the semiclassical approximations. Particularly two regions in g, ω space were explored. In the first, the oscillator frequency was varied relative to the transfer over three orders of magnitude between values 10^{-1} and 10^{+2} of ω/V, the coupling constant g being varied from 0 to 14. In the second, the variation of ω/V was over five orders of magnitude between 10^{-2} and 10^{+3} and that of the coupling constant g from 0.1 to 3. A normalized (least-squares) discrepancy factor

$$\eta \propto \sqrt{\sum_k \left[\frac{p_{exact}(t_k) - p_{semiclass}(t_k)}{|p_{exact}(t_k)| + |p_{semiclass}(t_k)|}\right]^2}, \tag{9.24}$$

where the suffix 'semiclass' stands for the respective semiclassical approximation and k marks the points selected for the least squares estimate. The reader is referred to the original publication for plots and discussion. The overall conclusion to be drawn from those studies was that the bare semiclassical approximation is excellent and its dressed counterpart is totally inapplicable if the oscillator frequency is

[14] This was a review article I was invited to write by Abraham Nitzan for a special issue of Chemical Physics that covered various approaches to the spin-boson problem. The issue, masterfully edited by Grabert and Nitzan, is full of nuggets of research into the topic and I recommend all its articles heartily to the reader.

small whereas in the opposite, high frequency, case ($\omega/V > 5$ for instance), the dressed approximation can practically coincide with the exact evolution while the bare approximation is way off.

Half of the findings thus support the observations of Grigolini and collaborators and agree with (Salkola et al., 1995)'s 'massive oscillator limit' argument. The other half of them are new and should provide food for fresh thought.

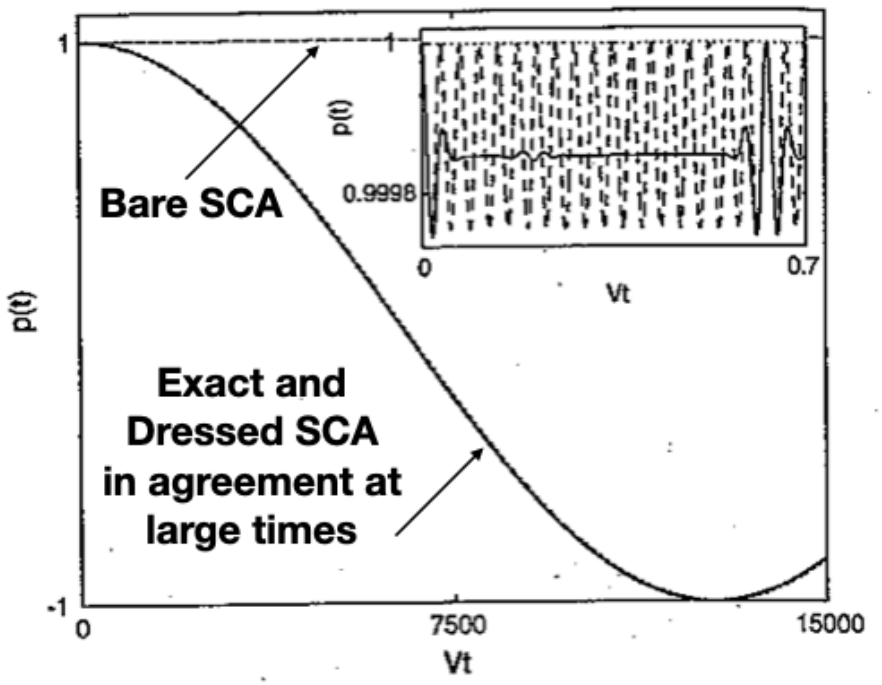

Fig. 9.8 Evolution of the agreement of which semiclassical procedure approximates the exact evolution better as time progresses. The coupling constant and frequency ratio are here given by $g = 3$ and $\omega/V = 10$. The probability difference $p(t)$ is plotted in the long time domain in the main plot and in the short time domain in the inset. Excellent agreement is noticed with the dressed semiclassical (dotted line) as it approximates the tunneling of the quasiparticle (overall oscillation between 1 and -1). The bare semiclassical (dashed line) is hopeless in its depiction of the constant at 1 signifying self-trapping. In the inset however, where the time in units of $1/V$ goes not to 15000 but only to 0.7, we see the opposite situation! The dressed semiclassical (dotted line) is remaining constant on this time scale at the very top whereas the bare semiclassical (dashed line) reproduces the bounded oscillations of the exact evolution (solid line) faithfully although it is unable to produce the silent runs. Modified with permission from fig. 5 of Ref. Kenkre and Giuggioli (2004). Copyright 2004 by Elsevier Publishing.

There is another conclusion, one that could be unexpected for some investigators in the field, that can be drawn from the work of Kenkre and Giuggioli (2004). It is about the *evolution of the validity as time progresses* for a fixed coupling

constant and frequency-interaction ratio. As emerges quite clearly from that work, the reliability of the approximation method passes from the bare to the dressed version of the semiclassical procedure as time evolves. Tests were carried out in that publication over really large time spans: focusing attention on $0 < Vt < 1$ as well as on $0 < Vt < 15000$ for the same set of parameters and a single initial condition, and keeping track of the comparison of the approximation to the exact result. Fig. 9.8, reproduced here from Kenkre and Giuggioli (2004), should convince the reader. This *time evolution of validity from bare to dressed* might have been missed by investigators in the field.

Yet another observation that we made in Kenkre and Giuggioli (2004) deserves notice. The bare result in the inset of Fig. 9.8, which clearly approximates rather well the exact evolution on the short time scale (except for the silent run), is *practically indistinguishable* from the prediction of the fully adiabatic[15] nonlinear dimer (Kenkre and Campbell, 1986; Kenkre, 1989, 1994a) that started for me this entire nonlinear adventure. Its prediction has the simple analytic form

$$p(t) = \mathrm{dn}\left(\frac{\chi t}{2}, \frac{4V}{\chi}\right) \tag{9.25}$$

expressed in terms of the dn Jacobian elliptic function with argument $\chi t/2 = g^2\omega t$ and elliptic parameter (whose square is the elliptic modulus) $4V/\chi = 2V/g^2\omega$.

What does this mean? It shows that the DNLSE depicts the short time evolution excellently so long as demand is not made on it to describe tunneling–a long time phenomenon outside its reach. All those who have felt on the basis of objections raised in the literature that the DNLSE ought to pack its bags, should take note.

It goes without saying, surely, that the two limiting forms of the semiclassical approximation are not identical to each other. Accordingly, one should stop the current practice of referring to '*the* semiclassical' approximation. This cautionary suggestion goes beyond the fact that the Huang-Rhys factor appears firmly in one limit but not the other. While p and P happen to be identical to each other (and so too π_y and Π_Y), this is not true of q, r, and y and their respective dressed counterparts. More to the point, the equations of evolution are not all identical in the two versions.

This sets the scene for our discussion of the next Section, which is primarily conjectural in nature.

9.3.3 An Infinite Number of Semiclassical Approximations

The dressing transformation that we have mentioned throughout the development uses the full coupling constant g in its implementation. While this may be reasonable for a situation in which the coupling is very strong, it may be inaccurate to use it for every case. The idea of using an intermediate amount of dressing with a coupling

[15] The word 'adiabatic' here follows the clear usage employed in this book that signifies infinitely fast relaxation rate Γ, which means the DNLSE is being used; it does not refer to any ω/V ratio.

constant G intermediate between 0 and the actual g was introduced into the field in conjunction with a variational treatment. These concepts were originally discussed by Merrifield and later by Toyozawa at a conference in 1975 (Shionoya et al., 1976) and were continued by various investigators including (Yarkony and Silbey, 1977; Silbey and Harris, 1984; Harris and Silbey, 1985; Parris and Silbey, 1985). They were also used for applications by (Parris and Kenkre, 2004; Cheng and Silbey, 2008). In these treatments it was argued that G, that surely lies in between 0 and the g in the Hamiltonian, should be calculated through a variational principle applied to an appropriate free energy function.

Thus, now the transformed operator corresponding to the bare $\hat{a}$ is $\hat{A}'$ through

$$\hat{A}' = e^{(-iG\hat{\pi}_y\hat{\rho})}\hat{a}e^{(+iG\hat{\pi}_y\hat{\rho})}, \tag{9.26}$$

and leads to modified versions of the Hamiltonian as expressed on the other operators and of the semiclassical equation set for the c-numbers (primed to denote partial dressing). This has been written down explicitly in Kenkre and Giuggioli (2004). The important point to note is that the counterpart of the torque-like equations for the partially dressed case now is

$$\frac{d}{dt}\begin{pmatrix} P' \\ Q' \\ R' \end{pmatrix} + \begin{pmatrix} 0 & 2V_R(t) & 2V_I(t) \\ -2V_R(t) & 0 & 2E(t) \\ -2V_I(t) & -2E(t) & 0 \end{pmatrix}\begin{pmatrix} P' \\ Q' \\ R' \end{pmatrix} = 0, \tag{9.27}$$

with *both* $E(t)$ and the complex $V(t)$ present and given by

$$E(t) = (g - G)\omega Y'(t), \tag{9.28a}$$

$$V(t) = V_R(t) + iV_I(t), \tag{9.28b}$$

$$V_R(t) = V' \cos(2G\Pi'_Y), \tag{9.28c}$$

$$V_I(t) = V' \sin(2G\Pi'_Y). \tag{9.28d}$$

The V' is an intermediate quantity between the bare limit V and the fully dressed limit Ve^{-g^2}, conjectured to be approximated by Ve^{-G^2}. Obviously, the partial dressing program is mentioned above only in the form of a conjecture, if at all, is highly unfinished and in need of a great deal of work.[16]

9.4 Relations to Other Approximation Programs

Comments have been already made about the connections between our memory method and some other investigations such as the analysis of Reineker and collaborators (Steib et al., 1998). Let us remark on links to three other studies, the so-called noninteracting blip approximation by Leggett et al. (1987), an action angle variables

[16] You, the reader, are invited to give it proper despatch if it strikes your fancy. You might find useful some comments on it made in Kenkre and Giuggioli (2004).

formalism by Lu and Dunlap (2003) and the Grigolini papers that started some of the validity studies.

9.4.1 Leggett et al's Noninteracting Blip Approximation and its Equivalence to the Memory Method

We have seen repeatedly in this Chapter that the memory method has met with considerable success in its description of the dynamics of our system of a quasiparticle interacting with vibrations.[17] The memory method was developed a good deal further, in concept as well practice for exciton dynamics in Kenkre (1975), and was explained in that context thoroughly in the book (Kenkre and Reineker, 1982).

Indeed, a particularly useful application of that method was made a few years later to resolve a puzzle in naphthalene experiments that had remained as an unsolved problem for several years (Duke and Schein, 1980). (See Fig. 9.1 and the related discussion at the beginning of this Chapter.) That resolution (Kenkre et al., 1989), was done primarily in collaboration with my then-student John Andersen as well as with Charlie Duke of Xerox. The theory explained the so-called (incorrectly suspected) band-hopping transition data in the temperature dependence of the mobility of charge carriers on the basis of polaron ideas. It was reviewed and commented upon in books on this latter subject such as by Pope and Swenberg (1982, 1999), and articles such as by Wu and Conwell (1997). It has also received coverage in my own books, (Kenkre and Reineker, 1982; Kenkre, 2021).

Remarkably, Grigolini and collaborators have shown, apparently without realizing these earlier references I have mentioned, and the uses we have put our memory method to over the years, that the method is equivalent to the much discussed 'noninteracting blip approximation' authored by Leggett et al. (1987). I do not know how important to the current reader it might be to see the following demonstration explicitly but the reader might want to start with Eq. (3.6) of Vitali and Grigolini (1990). These authors have stated that that equation *coincides exactly with the result of the non-interacting blip approximation* of Leggett et al. (1987).

If you merely substitute the symbols $2V^2$ and g_i, that we have used in this book, to (respectively) replace ω_0^2 and $g\Gamma_i/\omega_i$ in Eq. (3.6) of (Vitali and Grigolini, 1990), you convert that equation into

$$\frac{d\langle\sigma_x(t)\rangle}{dt} + 2\int_0^t ds\, \mathcal{W}(t-s)\langle\sigma_x(s)\rangle = 0, \tag{9.29}$$

with $\mathcal{W}(t)$ given precisely by our expression in Eq. (9.6) with its $h(t)$ spelled out in Eq. (9.7) in terms of the temperature factors, the coupling constants and the frequencies.

---

[17] It started as a calculation I worked out in collaboration with Talat Rahman (Kenkre and Rahman, 1974), basically on a lark while on a break in our regular pursuits, during friendly conflicts I had with Robert Silbey on the best way of analyzing exciton transport in molecular aggregates.

What this means is that the identification of $\langle \sigma_x(t) \rangle$ with the probability difference $p(t)$, which is what it is, immediately yields a noteworthy consequence. What Vitali and Grigolini (1990) have called their 'central equation', as well as the expression representing the non-interacting blip approximation of Leggett et al. (1987), is nothing other than our memory result![18] Like the results of Leggett et al. or of Vitali and Grigolini, our memory expressions were always expressed in their fully general form at any temperature with any number of modes and for any values of parameters.

Bishop, Salkola, Raghavan and I mentioned in Kenkre et al. (1996a) that the memory approach, specifically the evolution equation (2.14) in that paper, "...appears to be closely related, for all practical purposes identical, to the more recent noninteracting blip approximation given on the basis of a quite different and (at least in the general context) considerably more complex formalism..."

We thought at that time remarkable that the connection had remained undiscovered for so long. We made further such remarks in Kenkre (1998a) and in Kenkre and Giuggioli (2004). However, that lack of communication between communities of researchers has continued for another 20 years.[19]

9.4.2 Dunlap's Action Angle Formalism and Connection to Dynamic Localization

In a clear and crisp paper written in collaboration with his student, David Dunlap applied (Lu and Dunlap, 2003) an action angle variables formalism to the dimer in interaction with vibrations for the case when the vibrational frequency is large with respect to the intersite transfer. The result obtained was that, for an initial coherent (or high phonon number) state in the phonons, the bandwidth reduction went not via the exponential Huang-Rhys factor but through the Bessel function of zero order with the coupling constant as its argument.

In order to understand the connection of such a result to our memory function in a simple way, let us cast Eq. (9.10) in a form wherein its last factor is expressed through an expansion in terms of Bessel functions,

$$\cos(2g^2 \sin \omega t) = J_0(2g^2) + 2 \sum_{m=1}^{\infty} J_{2m}(2g^2) \cos 2m\omega t, \tag{9.30}$$

---

[18] Obtained almost half a century ago now in Kenkre and Rahman (1974) and used, as stated above, subsequently for excitons by Kenkre (1975), for photo-injected charge carriers in Kenkre et al. (1989) and for the validity of semiclassical approximations in one-mode model calculations in Kenkre et al. (1996a).

[19] Vitali and Grigolini (1990) mentioned that Aslangul et al. (1986) applied Zwanzig projections after the Hamiltonian transformation to derive the non-interacting blip approximation result. This was *exactly* the technique, first transforming and then applying Zwanzig projections, that was used by Kenkre and Rahman (1974). No wonder our result, with a different purpose and direction, is the same as the one derived eleven years later by Aslangul et al. (1986). Surely, the value of the latter reference is great and lies in their demonstration of how easy it is to get *the non-interacting blip result* without using complex formalisms.

and the middle factor similarly in terms of modified Bessel functions,

$$\exp(2g^2\cos\omega t) = I_0(2g^2) + 2\sum_{m=1}^{\infty} I_m(2g^2)\cos m\omega t. \tag{9.31}$$

Substitution produces, see, e.g., Kenkre and Giuggioli (2004),

$$\mathcal{W}(t) = 2V^2 e^{-2g^2}\left[I_0(2g^2) + 2\sum_{m=1}^{\infty} I_m(2g^2)\cos m\omega t\right] \times\left[J_0(2g^2) + 2\sum_{m=1}^{\infty} J_{2m}(2g^2)\cos 2m\omega t\right]. \tag{9.32}$$

It is clear that, in the high frequency limit, the neglect of rapid oscillations yields the proportionality of the memory function,

$$\mathcal{W}(t) \approx 2V^2 e^{-2g^2} I_0(2g^2)[J_0(2g^2) + J_2(2g^2)], \tag{9.33}$$

to a sum of Bessel functions $J_0(2g^2)$ and $J_2(2g^2)$. This brings some understanding to the Lu- Dunlap result that the motion is sensitive to the Bessel function of argument proportional to the square of the coupling constant[20].

The Bessel zeros connection opens the analysis to delightfully complex areas of research involving what is known in various circles under the names of *dynamic localization* (Dunlap and Kenkre, 1986b, 1988b,c; Raghavan et al., 2000; Kenkre and Raghavan, 2000), *coherent destruction of tunneling* (Großmann and Hänggi, 1992; Grifoni and Hänggi, 1998), and *quantum control* (Kenkre, 2000). Although the topics fall outside the purview of this book, they are closely related and offer exciting physics. I recommend to the reader a recent review by Bukov et al. (2015).

9.4.3 Grigolini's Analysis, its Importance and Risks of its Mistinterpretation

Through their work published in the 1990's, Grigolini and his collaborators made valuable contributions by pointing out the possibilities of missed terms and the adiabatic-nonadiabatic confusion in the analysis of spin-boson problems. We emphasized the importance of their contributions in several papers and conferences exemplified by the statement in (Salkola et al., 1995) that we "...support their earlier finding that the antiadiabatic limit, leading to the DNLSE according to the usual semiclassical arguments, does *not* produce the correct low-energy physics...", the assertion in (Kenkre, 1998a) that the work "has addressed issues lying at the heart of the problem and their analysis has led to the conclusion that much could be

[20] I am indebted to David Dunlap for a conversation regarding this old argument during the writing of this book.

amiss in the semiclassical approximation" and in (Kenkre et al., 1996a) that our own work "supports the conclusions drawn by them that semiclassical equations of motion...could be questionable in many physically relevant cases." Nevertheless, there are risks in possible misinterpretations of their work that I briefly mention here.

We have learnt from their work, and confirmed independently by our own (Salkola et al., 1995; Kenkre et al., 1996a) that the semiclassical approximation in our system of the dimer interacting with vibrations gets worse for large ω/V and, conversely, is more accurate for small ω/V. It is important to remember that we have shown that the semiclassical approximation happens to be exact in Salkola's massive oscillator limit (Salkola et al., 1995). The limit is characterized by $g \to \infty, \omega \to 0, g^2\omega \to$ const., and can be ascertained not only from the expression for $p(t)$ as we have done in Eq. (9.15), but also in the comparison between panels in Fig. 9.6, and also directly by inspecting our expression for the memory function $\mathcal{W}(t)$ in Eq. (9.10).

The danger of misinterpretation of the analysis of Grigolini et al. and possible misuse of their result lies in assuming that this limit of small ω/V, that validates the semiclassical treatment, is in contradiction to the limit used by us, for instance in Kenkre and Wu (1989b,a), to set up the DNLSE. Such a supposition would be patently incorrect. The fast time assumption we use to get the DNLSE form the semiclassical dynamics is NOT that associated with the vibrational frequency ω at all *but with the relaxation rate* Γ. A careful examination of Chapter 7 of this book, as well as of our original publications (Kenkre and Wu, 1989b,a), will make this quite clear to the reader.

We can certainly have a situation with small ω/V for the isolated dimer. This would make the semiclassical treatment an accurate approximation. If we now consider the dimer in interaction with a bath as explained in Chapter 7 or originally in (Kenkre and Wu, 1989b,a), we have a perfectly valid passage to the DNLSE if the relaxation is fast. The confusion between the uses of adiabatic versus nonadiabatic as phrases for the process has sometimes occurred in the literature but in our own arguments it has not.[21] Our treatment has never used a high ω/V argument to pass to the DNLSE; instead, it has always used for that purpose damping produced, for instance, by the environment in which the dimer is embedded. If the Grigolini analysis makes the reader lean towards thinking that there is a contradiction involved, it is important that this misconclusion be corrected.

9.5 A Brief Return to Davydov Solitons

Let us now return at the end of the Chapter to what served sometimes as a backdrop for the investigations we carried out: the Davydov soliton. It is my belief that the

[21] As explained already elsewhere in the book, I have used 'adiabatic' to represent instantaneous appearance of the (cubic) nonlinear term in the DNLSE and not to mean a vibrational frequency that is high with respect to intersite transfer. This latter terminology has been unfortunately used by some others in the literature. A sentiment similar to ours has been expressed on page 341 of their book by Dauxois and Peyrard (2006).

original idea in the field was to posit a soliton so it could oppose within itself the destructive effects of dissipation and dispersion and convey signals without loss over what was unimaginably long distances through nerves in living beings. The idea did not survive in that context but received much support generally in the context of the conveyance along proteins, of the free energy released by the hydrolysis of adenosine triphosphate. When Alwyn Scott heard of the idea from Davydov, he decided to give it support and did a great job through his leadership of an international group that produced many publications and conferences. The rest of this brief section will describe, compactly, some of the ideas and goings-on.

The original conception of Davydov was based on an ansatz for the assumed combined state of the moving quasiparticle and vibrations interacting strongly with it. The ansatz was modified with the passage of time and survived longest under the name of *the D_2 ansatz*.

Essentially, the state considered was a more or less (spatially) localized excitation of the moving quasiparticle with the vibrations in a coherent state (coherent in the sense of Sudarshan and Glauber). Although the system was fully quantum mechanical, it was postulated (or assumed by some to have been derived) that the vibrational subsystem could be described by classical equations of motion. Thus,

$$i\frac{da_n}{dt} = -J(a_{n+1} + a_{n-1} - 2a_n) + \chi(\beta_{n+1} - \beta_n)a_n, \tag{9.34a}$$

$$m\frac{d^2\beta_n}{dt^2} = K(\beta_{n+1} + \beta_{n-1} - 2\beta_n) + \chi(|a_n|^2 - |a_{n-1}|^2). \tag{9.34b}$$

I have suppressed the $\hbar$ that multiplies the left hand side of (9.34a) for compatibility with usage in this book but have otherwise kept to the symbols in the Davydov literature.

The quantum mechanical amplitude of the quasiparticle to be at site n in the representative single chain is a_n. The quasiparticle tends to move with nearest-neighbor transfer interaction J (but was, perhaps surprisingly, arranged to have diffusive-like terms) and a strong interaction through the coupling parameter χ with what can be thought of as the (discrete) spatial derivative of the chain oscillator displacement: the site energy of the quasiparticle is taken to be proportional, thus, to the spatial derivative. The displacement of the oscillator in the chain from its equilibrium is β_n. It evolution equation follows the standard (classical) Newton's oscillator dynamics. The mass of the oscillators at each site is m, the spring constant is K.

It is easy to see that the assumption that time derivatives of the oscillator displacements β_n may be neglected (for whatever reason), if made at this point, leads to a modified version of the DNLSE for the quasiparticle amplitudes,

$$i\frac{da_n}{dt} = -J(a_{n+1} + a_{n-1} - 2a_n) - \frac{\chi^2}{K}|a_n|^2 a_n, \tag{9.35}$$

whose continuum limit is, even more easily than from Eq. (1.2) of Chapter 1, the standard continuum form of the nonlinear Schrödinger equation. Soliton behavior is

expected including dispersion and nonlinearity combining into smooth transport if you neglect discreteness effects.[22]

Soliton aficionados were delighted while condensed matter types were worried. The delight was caused by the opportunity to utilize numerous concepts and techniques existing already in soliton physics and mathematics. The worries were about whether the interactions in the Hamiltonian were indeed of the kind postulated, whether the Davydov ansatz made sense at the time of preparation and what kind of state preparation this entailed precisely, whether, even if the ansatz were initially correct, the state maintained that form as time evolved, and, even if these nonlinear desirable states could exist, how cold did the environment have to be for them not to be exterminated by thermal fluctuations in short order.

As I have said a few times now in these pages, this is not a book about the Davydov soliton. It is just closely connected in its problems and the tricks used in the solution of these problems to the simple dimer system (the true system of interest to the book) that came my way accidentally in my research. For further details, let me, therefore, refer you in the briefest manner possible to two books I have mentioned in the Preface, (Christiansen and Scott, 1990) and (Dauxois and Peyrard, 2006). The first of these makes quite an effort to have opponents and proponents of the Davydov concept have their say,[23] and is a fine compendium of activities on the Davydov soliton until 1989. The second book is a favorite of mine for the way it is written, and happens to be a much later compilation. Unfortunately, it is on the general subject of solitons and has just a chapter among many on the Davydov kind. For a recent review that is favorable to the Davydov-Scott model, the reader might take a look at Cruzeiro's article (Cruzeiro, 2009) that I have already mentioned in Chapter 8.

There has been an unfortunate, and remarkable, dearth of incisive data fueling, challenging and stimulating the theoretical discussions of the Davydov soliton community. The work by Careri and their collaborators on acetanilide crystals (Careri et al., 1984) seemed to many to be associated with polaron features and spatial localization rather than dispersionless transport of energy by solitons. I will now describe, briefly, a crude estimate that was published in Kenkre et al. (1996a) as part of the application of the *dimer* theory to three different systems. One of the three represented (a dimer version of) the Davydov problem.

The three caricature versions of experimental systems we considered with the help of our memory method and the semiclassical approximation have as their respective observables, charge mobility in aromatic hydrocarbons such as naphthalene, thermal diffusivity in high-T thermoelectrics such as boron carbide, and vibrational energy transfer in biological systems such as protein. Although surely the dimer calculations we attempted could not really represent extended crystals, we assumed as a working

---

[22] Not to forget that a, $-J$, χ^2/K in the Davydov soliton equations bear kinship, respectively, to the amplitude c, the intersite transfer V, the nonlinearity χ in the DNLSE notation used in this book.

[23] I myself resisted contributing to the book initially. Eventually, I included a one-page article on my work that I considered relevant to the subject matter (after repeated kind and warm requests by Al Scott to do so); at all the conferences of that sub-community I had been a curious, interested, and vocal member of the audience.

hypothesis that the essential physics might be captured *in a skeleton sense*. Here are two of the examples.

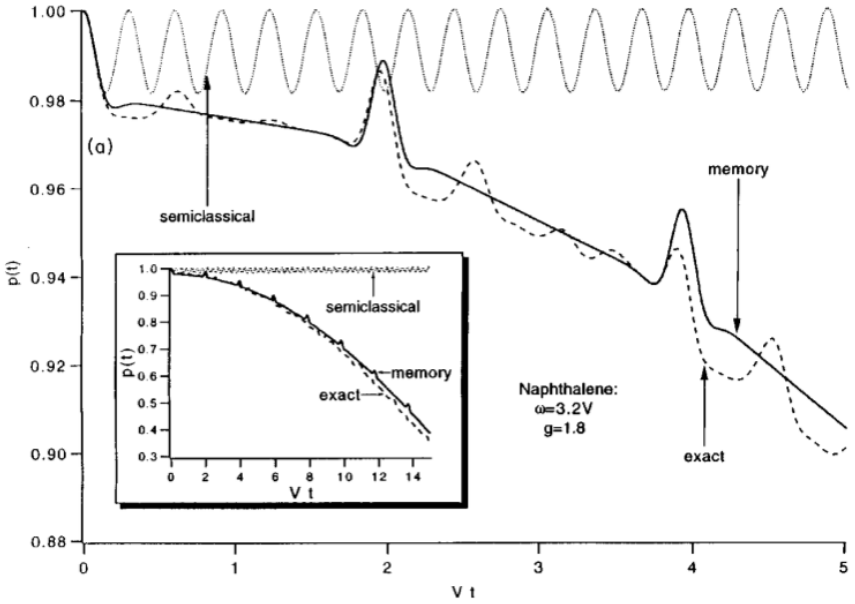

Fig. 9.9 A crude representation of the photo-injected carrier in an aromatic hydrocarbon crystal. Parameter values are estimated from experiment. See text. The semiclassical approximation appears to do very poorly for this system while the memory method follows the exact evolution well. Modified with permission from fig. 6 of Ref. Kenkre et al. (1996a). Copyright 1996 by American Physical Society.

The first of these, see Fig. 9.9, involves data on the mobility of photo-injected charge carriers in naphthalene, the moving quasiparticle being a hole or electron interacting strongly with librational phonons. Parameters were obtained from independent experiments and gave the coupling constant $g = 1.8$, the carrier bandwidth 10.5 meV, and vibrational phonon energy as 16 meV. In the notation we have used in the book this means $g = 1.8, V = 60K, \omega/V = 3.2$.

Compared in Fig. 9.9 are the exact quantum calculation, semiclassical approximation, and memory function analysis. Clearly, the semiclassical approximation, maintaining as it does, its distance from the other two curves (it is the lone curve at the top both in the inset and the main figure), fails badly; the memory function analysis recovers all the salient features of the exact evolution for the assumed parameters. In particular, the short-time evolution at a frequency of $g^2\omega$, decay of the initial oscillations on the order of a time of $1/g\omega$, oscillations revival at a frequency of ω and the tunneling to the other site at time of the order of e^{g^2} are all shown by the memory calculation.

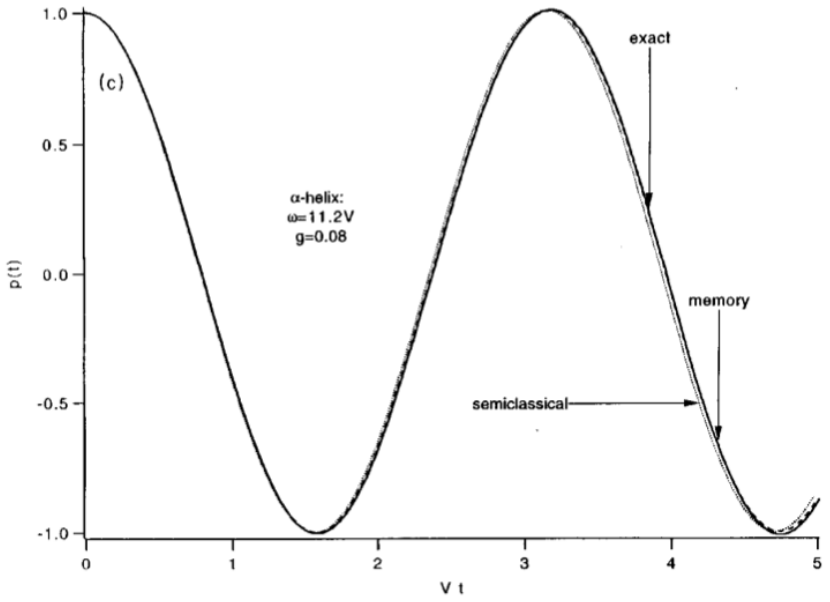

Fig. 9.10 A crude representation of the Davydov system but with parameter values estimated from experiment and theory. See text. The semiclassical approximation appears to do as well as the memory method in following the exact evolution. Modified with permission from fig. 6 of Ref. Kenkre et al. (1996a). Copyright 1996 by American Physical Society.

The second of these, see Fig. 9.10, is a crude representation of the Davydov soliton. The coupling parameter χ (not to be confused with the nonlinearity parameter represented by that symbol throughout this book) has been estimated to be 35 pN in Scott (1992) and 67 pN in Careri et al. (1984). The longitudinal spring constant is three times that for a single hydrogen bond which in turn, is estimated to be 13 N/m from experiments in Itoh and Shimanouchi (1972) and from *ab initio* calculations (Scott, 1992) to be 19.5 N/m. The reader is referred to Kenkre et al. (1996a) for detailed explanations for the rest of the parameter values. The coupling constant that we call g turns out to vary between 0.035 and 0.084 and the ratio of the phonon energy to the intersite transfer, $\hbar\omega/V$, to lie between 11.2 and 13.8.

The result of the calculations is seen in Fig. 9.10 as revealing that the memory approach is slightly better in representing the exact evolution but the difference is *not significant* for the particular parameter set used: the semiclassical approximation is also quite acceptable. This is completely different as a conclusion reached relative to the first system treated.

My purpose in displaying the (two of the three) examples treated in Kenkre et al. (1996a) is solely to show that the semiclassical approximation can do well in some systems and poorly in others. No conclusive results are to be attributed to this graphical demonstration about the actual Davydov soliton.

In closing out this brief description of the work on the Davydov soliton that I had occasion to watch so many decades ago from my vantage point as an interested active *outsider* to the subject, I would like to recommend to the curious reader to pay particular attention to the writings that originated with three groups: Al Scott (and his immediate collaborators) who was the prime mover and shaker while the activity lasted; Kerr and Lomdahl who (with clear derivations) in simple terms zeroed in on whether the Davydov soliton has a quantum mechanical past and a statistical mechanical (i.e., thermal) future; and Brown, Lindenberg and West who, coming from a condensed matter and statistical mechanics background, left no stone unturned in investigating theoretically the foundations of the concept.[24]

9.6 Chapter 9 in Summary

The DNLSE is typically thought to arise in polaronic systems in which a quasiparticle interacts strongly with vibrations or other motions involving bosons through time scale disparity of the quasiparticle and the vibrations. Many have interpreted this argument as requiring fast vibrations that are slaved by the slower quasiparticles. To facilitate the reader's understanding of the problem as well as suggested remedies to come later on in the Chapter, the discussion began with the elucidation of standard polaron concepts such as the displaced oscillator transformation and the calculation of memory functions. The memory method was recalled to have been accurate, consequently highly successful, in the description of the temperature dependence of carriers in complex organic crystals. It was applied to zero T, one-mode model under investigation and was also found to be remarkably accurate. By contrast, the standard (bare) semiclassical approximation was found to fail for several frequency-transfer ratios. Studies confirmed the concerns raised in the literature that where the (bare) semiclassical approximation seemed to fail in the worst way was the *high* vibrational frequency limit. This appeared to be opposite to the limit in which the DNLSE could be then obtained from the semiclassical equations. Numerical solutions of the one-mode zero-T system showed that the semiclassical equation worked in the massive oscillator limit in which the vibrational frequency is very low compared to the intersite transfer. A hierarchy of time scales was noted in the evolution of the probability difference. A corresponding time scale hierarchy was noticed in the memory function making possible an understanding of the evolution in terms of the system parameters: coupling constant g and its square, the oscillator frequency ω and their simple combinations. It was shown that the system in which

[24] David Brown, who had been my Ph. D. student as I have mentioned in the Preface, knew all about how to apply powerful projections to polarons; Katja Lindenberg was a colleague well versed in every aspect of condensed matter physics necessary for this subject, and Bruce West was a well known authority in modern statistical physics. A fascinating treat awaits the reader who decides to analyze their many publications on this subject. If you do, please pay attention to the exquisite puns that David Brown sprinkled throughout the writings of this San Diego group just as he did in papers he published with me during his thesis work.

our considerations worked best in the adiabatic extreme were at the low frequency end making possible the massive oscillator limit. Furthermore the DNLSE could then arise from such a system if it is coupled to a damping agency that produced fast removal of the vibrational energy as detailed in Chapter 7. Validity studies were carried out for dressed vibrations and it was shown that bare and dressed semiclassical approximations (a) work best in opposite limits of the frequency-transfer ratio, respectively low and high, and (b) improve remarkably from short-time for bare to long-time for the dressed cases. With the help of other published results in the literature we showed that the so-called noninteracting blip approximation of Leggett et al. was precisely the same as our memory method. We also touched upon some other approaches including by Reineker et al. based on the time-dependent variational principle and Dunlap's action angle variables approach. A brief explanation was also given of how some related questions in the Davydov soliton backdrop play out.

Chapter 10
Bose-Einstein Condensate Tunneling: the Gross-Pitaevskii Equation

First some verbiage.

10.1 A Lookalike of the DNLSE in BEC Condensate Dynamics

10.2 Transitions and Tunneling in Condensates via the DNLSE Techniques

10.3 Validity of the DNLSE in the light of Quantum Dynamics

10.4 Recent Results in Quantum Oscillations in BEC Condensates

10.5 Chapter 10 in Summary

John D. Andersen, Srikanth Raghavan, V. M. Kenkre, http://arxiv.org/abs/2108.08711

Chapter 11
Miscellaneous Topics and Summary of the Book

C. B. Duke, known to his friends and foes as Charlie, was an active collaborator of mine in the 1980s when I was on the faculty at the University of Rochester and he at the Xerox Research Laboratory in Webster. Brilliant in his science, he had a sharp tongue and a keen sense of humor. Framed in his office was this statement:

All those of you who think you know it all, are very annoying to us, who do.

He let me take a copy of the statement. It has been hanging in my office ever since. Every time I have written a book, as I arrive at the last Chapter where I summarize, I have a sinking feeling in the pit of my stomach that illustrious experts among my readers might be thinking that thought, addressing it aggressively at my book and me. I am experiencing the feeling in my stomach this moment but have decided to continue any way.

This final Chapter of the book is in two parts. In the first, some miscellaneous topics are touched upon to complete the story that has been woven so far. In the second part, a brief summary is given of the contents of the book.

11.1 Assorted Subjects and Directions

There are a few directions in nonlinear science that my collaborators and I pursued that do not quite fit as parts of the development in the first 10 Chapters of the book. Mentioning them might help the reader complete the picture. Nine topics suggest themselves to me in this regard. I will explain six of them in the next section, each in its own subsection. The first three deal with (i) the application of Zwanzig projections to the nonlinear von Neumann equation corresponding to the DNLSE, (ii) a treatment of external fields applied to the nonlinear dimer, and (iii) an investigation of how anharmonicities in the vibration affect the validity of the semiclassical approximation through the study of the Pöschl-Teller potential. In the next three we step out into spatial extended systems to (iv) investigate soliton

propagation in mixtures of bosons and fermions, (v) consider self-trapping transitions when a localized nonlinear impurity is embedded in an extended linear system, and (vi) to consider the only classical system treated in this book, inspired nevertheless by quantum considerations, related to excimers in molecular aggregates. Although the purpose of the studies reported in the book has been to focus on small systems, those three are exceptions. They are included as lying naturally on the borders of our theme.

The three topics I will not explain but only give references to are: an investigation of the thermal conductivity of boron carbides that my student Ximing Fan undertook with me using some related nonlinear methods and the dressing idea: (Kenkre and Fan, 1987, 1988; Fan and Kenkre, 1989); work that Kalosakas published with Alan Bishop and me on the multiple-timescale quantum dynamics of interacting bosons and on the Hubbard model (Kalosakas et al., 2003a,b); and the analysis of the bound rotator that Raghavan undertook with me as support study for further investigations of the rotational polaron (Raghavan and Kenkre, 1994).[1]

11.1.1 Application of Projection Techniques to the Nonlinear Dimer: Generalized Master Equations

A problem that had received a great deal of attention from clever minds in the field of statistical mechanics in the 1950s was the derivation of the Master equation for the probabilities of state occupation starting from the (von Neumann) density matrix equation of quantum mechanics. The activity had to do with a central problem of physics as it was associated with the understanding of the onset of macroscopic irreversibility in systems obeying reversible equations of motion at the microscopic level. In order to cut through the confusion that existed in that earlier work (seminal though it was), because of the complex methodology used, Zwanzig (and Nakajima, independently) introduced diagonalizing projection operators. (Nakajima, 1958; Zwanzig, 1961, 1964) That projection technique showed how to get, rather directly, equations for the quantum mechanical probabilities in a chosen representation that were essentially closed in those probabilities.

An obvious question that one might ask is what happens if we apply such diagonalizing projection operators to the nonlinear density matrix equation (1.6) that is a consequence of the DNLSE. Superficial considerations might lead one to think that it is not legitimate to apply a *linear* technique such as that of projections to a nonlinear equation such as (1.6). Wu showed that this line of reasoning was flawed. He was successful in carrying the program through as is evident in Wu and Kenkre (1989). See also (Kenkre, 2021, 2000). A description of the method and results follows.

[1] The decision to omit a fuller commentary on these is almost arbitrary. The interested reader should look up the references.

Let us begin by recasting the nonlinear von Neumann equation in terms of two 'Liouville operators'[2], the first of which is the standard commutation operator $L_V O = [V, O]$. For nearest-neighbor interactions, we are assuming in Eq.(1.6) that, for any ordinary operator O, its matrix elements are given by $(L_V O)_{mn} = V(O_{m+1,n} + O_{m-1,n} - O_{m,n+1} - O_{m,n-1})$. The m, n label eigenstates of a part H_0 of the full Hamiltonian and what is being sought is the evolution of the probabilities (diagonal elements of the density matrix) of occupation of these states m, n. The second Liouville operator is defined as

$$(L_\chi O)_{mn} = \chi(\rho_{mm}(t) - \rho_{nn}(t))O_{mn}, \tag{11.1}$$

and the nonlinear density matrix equation (1.6) is reexpressed as

$$\frac{d\rho}{dt} = -i\left(L_V \rho + L_\chi(t)\right)\rho = -iL(t)\rho. \tag{11.2}$$

Note that I have explicitly indicated the time dependence of L_χ because it necessitates a slightly more complicated treatment of the solution of an otherwise linear differential equation. As is well-known, the complication is that it involves time ordering of operators; I expect it to be standard fare to the reader.

The next step in the Zwanzig development is to define a projection (super)operator that in the selected representation extracts the diagonal part of the operator on which it acts. Let us give it the symbol $\mathcal{D}$ rather than the usual $\mathcal{P}$ to follow Zwanzig's original terminology (Zwanzig, 1961, 1964) particularly because there are no traces over phonons or baths involved. Specifically,

$$(\mathcal{D}O)_{mn} = O_{mm}\delta_{m,n}$$

for any operator O. The application of $(1 - \mathcal{D})$ to Eq. (11.2), where 1 is the identity matrix, produces

$$\frac{d\rho''(t)}{dt} = -i(1 - \mathcal{D})(L_V + L_\chi(t))\rho''(t) - i(1 - \mathcal{D})(L_V + L_\chi(t))\rho'(t) \tag{11.3}$$

as the equation of evolution for the off-diagonal part of the density matrix, $\rho'' \equiv (1-\mathcal{D})\rho$. Because we were clever enough to interpret the action of L_χ as being linear although time-dependent, in other words because we did *not* commit the strategic error of defining it via $(L_\chi O)_{mn} = \chi\left(O_{mm}(t) - O_{nn}(t)\right) O_{mn}$, rather used (11.1) for the definition, we avoided the nonlinearity. Given the retention of the linearity in relation to O in the definition for L_χ, we can find the Green function and solve the evolution of $\rho''(t)$ in terms of the driving term (the last term in Eq.(11.3) that involves the diagonal part $\rho'(t)$.

---

[2] Such operators, surely more exotic than garden-variety operators like the Hamiltonian that act *merely* on state vectors, are sometimes called *super*operators because they act on operators. In working with them, one must not forget their kryptonite-like weakness that they work only on what is on their right, and, indeed, on all of what is on the right.

The application of $\mathcal{D}$ instead of $(1-\mathcal{D})$ to (11.2) yields, for the diagonal part $\rho'(t)$,

$$\frac{d\rho'(t)}{dt} = -i\mathcal{D}(L_V + L_\chi(t))\rho'(t) - i\mathcal{D}(L_V + L_\chi)\rho''(t). \tag{11.4}$$

If we substitute the solution of the off-diagonal equation we obtained via the Green function formalism in this diagonal evolution equation, we get

$$\frac{d\rho'(t)}{dt} + \mathcal{D}L(t)\int_0^t ds\left[e^{-i\int_s^t dt'(1-\mathcal{D})L(t')}\right](1-\mathcal{D})L(s)\rho'(s) = \\ -i\mathcal{D}L(t)e^{-i\int_s^t dt'(1-\mathcal{D})L(t')}\rho''(0). \tag{11.5}$$

We have recombined the two Liouville operators into a single sum for the sake of space. We continue to keep in mind that the time-dependence in $L_\chi(t)$ requires that we use time ordering in the integrals.

Typically, this Zwanzig equation (11.5) displays the derivative of the projected $\rho(t)$ as being the sum of three terms. But as Zwanzig himself has shown in his first few papers on the subject, the combination of the diagonalizing nature of $\mathcal{D}$ and the commutation nature of $L(t)$ makes one of the terms disappear identically. We are left with the two terms shown, the memory term and the initial value term. The latter is identically zero if the density matrix is initially diagonal, i.e., if $\rho''(0) = 0$).[3]

The generalized master equation (GME) obeyed by the probabilities P_m for such an initial condition can now be written down explicitly from

$$\frac{dP_m(t)}{dt} = \int_0^t ds\sum_n\left[\mathcal{W}_{mn}(t,s)P_n(s) - \mathcal{W}_{nm}(t,s)P_m(s)\right], \tag{11.6}$$

if the density matrix is initially off-diagonal in the m, n representation. If this condition is not met, a driving term $\mathcal{I}_m(t)$ is appended on its right side that arises from the non-vanishing off-diagonal elements of the initial density matrix, $\rho(0)$. The result (11.6) differs in two respects from the usual GMEs that one normally encounters. One is that the memories $\mathcal{W}(t,s)$ are *not* functions of the difference combination $t-s$ but depend on the two times independently; the other that they depend on the probabilities themselves. The approximate evaluation of the memory functions $\mathcal{W}_{mn}$ for a spatially extended system may be found elsewhere (Wu and Kenkre, 1989; Kenkre, 2021) along with a number of related results that, while not of direct relevance here, are quite interesting in their own right. What we are interested in here are the GME for the two probabilities $\rho_{11}(t)$ and $\rho_{22}(t)$. With the understanding that the driving terms $\mathcal{I}_1(t)$ and $\mathcal{I}_2(t)$ vanish identically for the initial condition that the density matrix is diagonal, the probability equations are, for arbitrary initial conditions,

[3] I have refrained from crossing all the t's and dotting all the i's here because the projection equation application to the DNLSE has been described in another recently published book Kenkre (2021). The results and the flow of the logic are, however, important to display here.

$$\frac{d\rho_{11}(t)}{dt} = 2V^2 \int_0^t ds\ [\rho_{22}(s) - \rho_{11}(s)] \cos\left(\int_s^t dz\chi\ [\rho_{22}(z) - \rho_{11}(z)]\right) + \mathcal{I}_1(t), \tag{11.7a}$$

$$\frac{d\rho_{22}(t)}{dt} = 2V^2 \int_0^t ds\ [\rho_{11}(s) - \rho_{22}(s)] \cos\left(\int_s^t dz\chi\ [\rho_{11}(z) - \rho_{22}(z)]\right) + \mathcal{I}_2(t). \tag{11.7b}$$

Expressions for $\mathcal{I}_{1,2}(t)$ can be evaluated from the last term of Eq. (11.5)). In terms of the initial values of the density matrix element combinations

$$r_0 = [\rho_{12}(0) + \rho_{21}(0)], \quad q_0 = i[\rho_{12}(0) - \rho_{21}(0)],$$

the explicit expressions for $\mathcal{I}_1(t)$ and $\mathcal{I}_2(t)$ to be respectively added to the GME equations for $P_1(t)$ and $P_2(t)$ are[4]

$$\mathcal{I}_1(t) = \left(-V\sqrt{1-p_0^2}\right) \cos\left(\Delta_0 - \chi \int_0^t dz\, p(z)\right), \tag{11.8a}$$

$$\mathcal{I}_2(t) = \left(V\sqrt{1-p_0^2}\right) \cos\left(\Delta_0 - \chi \int_0^t dz\, p(z)\right), \tag{11.8b}$$

satisfying, as they must, the sum rule $\mathcal{I}_1 + \mathcal{I}_2 = 0$ at all times t. The symbol Δ_0 stands for $\tan^{-1}(r_0/q_0)$.

Note that Eq. (11.7) is a simple two-site GME except for the fact that its memories are functions of the (time integrals of) probability differences, thus making the GME itself certainly nonlinear. What evolution does Eq. (11.7) predict for the probability difference $p = \rho_{11} - \rho_{22}$? The answer is obtained by subtracting its two lines to get

$$\frac{dp(t)}{dt} + 4V^2 \int_0^t ds\, p(s) \cos\left(\chi \int_s^t dz\, p(z)\right) = 0. \tag{11.9}$$

But there is more. If one introduces a new variable $\xi(t)$ as an integral of the probability difference,

$$\xi(t) = \int_0^t ds\, p(s), \tag{11.10}$$

a remarkable result, certainly unexpected if you are not familiar with it, emerges. We get a second order differential equation for the integral $\xi(t)$,

$$\frac{d^2\xi}{dt^2} + \left(\frac{4V^2}{\chi}\right) \sin(\chi\xi) = 0. \tag{11.11}$$

This equation is identical to the evolution equation of the physical pendulum in which one has *not* made the small angle approximation that would simplify it to the

[4] For the benefit of those who might compare the expressions to the ones in the original publication, a typo has been corrected from Eqs. (A7), (A8) of (Wu and Kenkre, 1989) and expressions rewritten to make them more compact.

simple harmonic motion of an oscillator.[5] Indeed, the explicit solution of (11.11) in terms of the inverse trigonometric and direct elliptic sine functions may already be known to you:

$$\xi(t) = (2/\chi)\sin^{-1}\left[\mathrm{sn}\left(\chi t/2|4V/\chi\right)\right].$$

Differentiation of this result gives

$$p(t) = \frac{d\xi}{dt} = \mathrm{cn}\left(2Vt|\chi/4V\right). \tag{11.12}$$

This result for the probability difference in a nonlinear dimer is part of the literature (see, e.g., Kenkre and Campbell (1986)), is known to satisfy a simple cubic nonlinear differential equation with coefficients determined by initial conditions in the dimer (Kenkre and Tsironis, 1987). You, the reader, have learned that already in Chapter 2.

In summary, the application of diagonalizing projections to the discrete nonlinear Schrödinger equation (1.6) shown here brings out the following points: it is possible to to apply this linear technique despite the nonlinearity of the starting equation; the resulting memory functions turn out to be nonlinear in that they depend on the integrals of the probabilities (actually their differences) and are not of the simple difference form. Surprisingly, for the two-site system, the passage from the probability difference p to its time integral ξ happens to be a well-known transformation that changes the cubic nonlinearity in an equation such as (1.2) to a sinusoidal nonlinearity characteristic of the equation for a physical pendulum, Eq. (11.11).

11.1.2 External Fields Considered via Time-dependent System Parameters

The effect of external fields on a system, for instance consequences of applying an electric field or thermal gradient to a metal containing carriers of charge or energy, is typically investigated nowadays with the help of the linear response theory due to Kubo. In this formalism, the external fields are typically represented by *additive* terms in the Hamiltonian of the system, the well-known expression for that additive part used in the response theory being $-\lambda f(t)\hat{A}$ where λ and $f(t)$ are c-numbers signifying a strength parameter and the time-dependence of the applied external field, respectively, $\hat{A}$ being an operator typical for the particular application. In the following I will make very brief remarks about the treatment of our nonlinear system under the application of external stimuli through a set-up that does not involve this traditional addition of external terms in the Hamiltonian. Rather our interest will lie in making the system parameters time- and strength-dependent.

A glance at Eqs. (5.1) shows that we might be focus, thus, on $V(t)$, $\Delta(t)$ and $\chi(t)$... TO BE COMPLETED

[5] When Wu and I were publishing our result, we discovered that the equation had also just appeared in the work of Cruzeiro-Hansson et al. (1988) although not through this memory route. Needless to say, the publication is duly credited in Wu and Kenkre (1989).

11.1.3 The Semiclassical Approximation for *Anharmonic* Vibrations

We have observed numerous features such as silent runs, revivals, recurrences during our study of the dimer in interaction with harmonic vibrations, particularly from the point of view of the validity of the semiclassical approximation. An obvious question of interest to pose here is whether the introduction of *anharmonicity* in the vibrations modifies in any way the answers obtained. Clearly, the focus in such a study should be *not on slight* anharmonicities that can be always treated via perturbation developments. We must seek an oscillator that can be dialed continuously from a harmonic nature to behavior that is substantially different from harmonic behavior. Such an oscillator is the Pöschl-Teller potential (see Fig.11.1). Basically proportional to the square of a trigonometric tangent, the potential $U(x)$ can be changed continuously from harmonic into a box potential. One may write it as being proportional to $\tan^2(ax)$ in which case it is clear that it will correspond in a limiting sense to a (1-dimensional) box of extent π/a. It is convenient to write the constant of proportionality in a form that allows

$$U(x) = \lambda(\lambda - 1)\left(\hbar^2 a^2/2m\right)\tan^2(ax), \tag{11.13}$$

where m is the mass of the quantum particle subjected to it. Then it is easy to show (Nieto and Simmons, 1979) that the energy eigenvalues of the Schrödinger equation may be labeled by integers $n = 0, 1, 2, ...$ as

$$E_n = \frac{\hbar^2 a^2}{2m}(n^2 + 2n\lambda + \lambda). \tag{11.14}$$

We see that, for $\lambda = 1$, the energy spectrum is precisely that of a particle of mass m in a box of length π/a. We also see that if $\lambda \to \infty, a \to 0$ such that λa^2 remains a constant of finite value, the spectrum becomes that of a harmonic oscillator. It is also straightforward (Nieto and Simmons, 1979) to obtain the eigenfunctions corresponding to the eigenvalues given above as generally products of trigonometric cosines and associated Legendre functions $P_\alpha^\beta(t)$ whose arguments are trigonometric sines,

$$\phi_n(x) = N_n\sqrt{\cos ax}\, P^{1/2-\lambda}_{n+\lambda-1/2}(\sin ax). \tag{11.15}$$

The normalization constant is given by $N_n = \sqrt{a(n+\lambda)\Gamma(n+2\lambda)/\Gamma n + 1}$.

Thus, we have a system that, through a manipulation of λ from 1 to ∞, can be dialed continuously to introduce anharmonicity to the extent desired. We can use it to study the effects of anharmonicity in vibration on the dynamics of a particle moving between the two sites of a dimer and simultaneously interacting strongly on the vibration. What about the particle-vibration interaction? In the standard (harmonic) case, it is linear in the vibrational amplitude and, *consequently*, connects eigenstates that are nearest-neighbor in energy space. In setting up our system we have a choice of taking either an interaction that is linear in the vibrational amplitude *or* one that connects nearest-neighbor states. Let us examine the results of exploring the

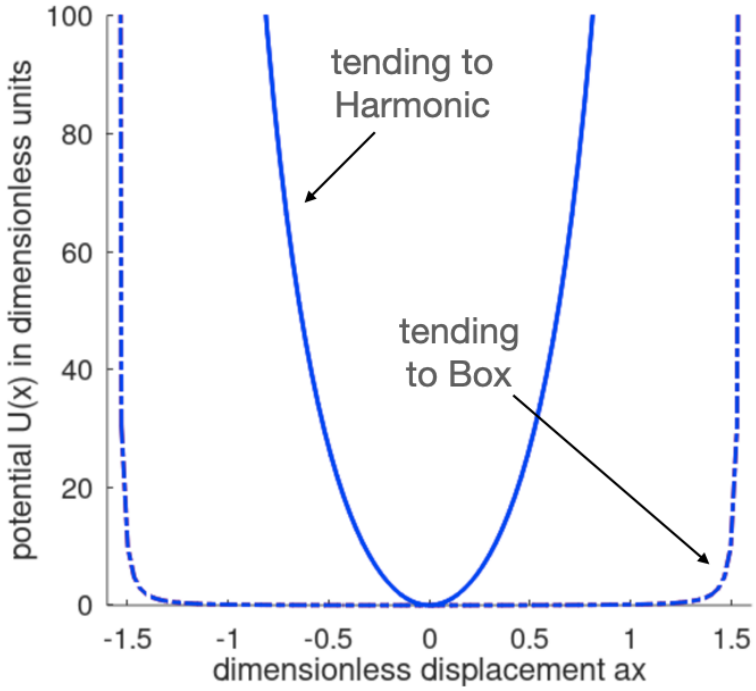

Fig. 11.1 The anharmonic potential for the vibrations in strong interaction with the quantum particle. It goes under the name of Pöschl-Teller and can be dialed continuously from the harmonic to the box limit by changing a parameter λ: see text. The potential is plotted (in arbitrary but dimensionless units) versus the displacement from equilibrium x in units of $1/a$ and extremes shown are one near the harmonic limit (solid), and one close to the box limit (dash dot). The factor $(\hbar^2 a^2/2m)$ has been suppressed from the potential expression in the text for the sake of the graph. The respective values of λ are 10 (solid) and 1.05 (dash dot). Curves for intermediate cases would lie between these. When $ax = \pi/2$, the potential blows up to infinity. For $\lambda = 1$, it is zero everywhere in the 'box' and becomes infinite at the box wall.

second choice. Nieto and Simmons (1979) as well as Crawford and Vrscay (1998) have shown that such a nearest-neighbor connection is provided by a sinusoidal interaction. The two elements of the Hamiltonian H we must choose are thus clear: we adopt the Pöschl-Teller potential for the vibrational dynamics and the sinusoid for the interaction.

From Eq. (11.14), it is clear that the difference between the energies of the first excited state and the ground state of the particle subjected to the Pöschl-Teller potential is

$$\omega_0 = \left(\frac{a^2}{m}\right)\left(\lambda + \frac{1}{2}\right). \tag{11.16}$$

In terms of this quantity and of the dimensionless oscillator coordinate $z = ax$ let us write the Hamiltonian of the system we wish to study to ascertain the role of anharmonicity in the vibrations as

$$H = \left(\frac{\omega_0}{1+2\lambda}\right)\left[\hat{\pi}_z^2 + \lambda(\lambda-1)\tan^2\hat{z}\right] + g\omega_0\sqrt{\left(\lambda+\frac{1}{2}\right)}\hat{p}\sin\hat{z} + V\hat{r}, \qquad (11.17)$$

and carry out the program explained in Chapter 9 performed in Salkola et al. (1995) and in Kenkre et al. (1996a) for the simpler case of harmonic vibrations and linear interactions. The results of such a task (Raghavan et al., 1999a) are displayed below even though they did not produce any surprises. It is important to know whether anharmonicities do or do not introduce substantial modifications.

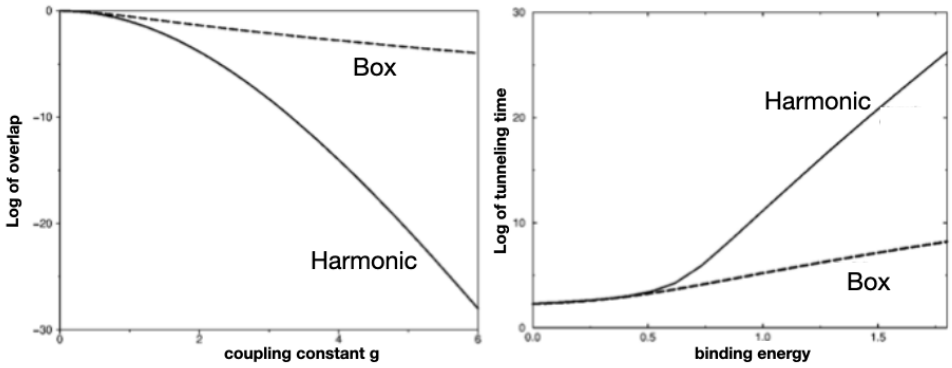

Fig. 11.2 Semilogarithmic plots of the coupling constant dependence of two key quantities in the system of Eq. (11.17). In the left panel, the logarithm of the overlap factor between undisplayed and displaced oscillator ground state functions is plotted as a function of the coupling constant g for the Pöschl-Teller potential obtained from our system by freezing transfer ($V = 0$). In the right panel, the logarithm of the tunneling time for the system with transfer is plotted as a function of the polaron binding energy. The box (harmonic) limit in each case is represented by a dashed (solid) line. See text for discussion. Modified with permission from figs. 3 and 5 of Ref. (Raghavan et al., 1999a); copyright (1999) by American Physical Society.

Plots of the variation of the overlap of the displaced ground-state wave-functions with their undisplayed counterparts with the coupling constant are displayed in the left panel of Fig. 11.2 to show a comparison in the two extreme limits of the Pöschl-Teller potential: box ($\lambda \to 1$) and harmonic ($\lambda \to \infty$). In the same Figure, plots of the variation of the polaron tunneling time scale with the binding energy are displayed in the right panel. These preliminary displays show that λ, thus the extent of the anharmonicity, certainly controls the dependence as the values of the coupling constant and binding energy increase from 0, substantial differences appearing quickly. There are, however, no abrupt changes.

Furthermore, it is easy to see from the expressions for the Hamiltonian itself that the polaron binding energy is proportional to $g^2\omega$ in the harmonic oscillator limit but in the opposite limit of the infinite square well, because the width of the well remains finite, the lowering of the energy is proportional to g. This cross-over behavior of the exponent of g from 2 to 1 is quite interesting, its elucidation was made possible only because of our choice of the Pöschl-Teller potential wherein dialing the anharmonicity is so straightforward, and has been made crystal-clear graphically in the original publication (Raghavan et al., 1999a).[6]

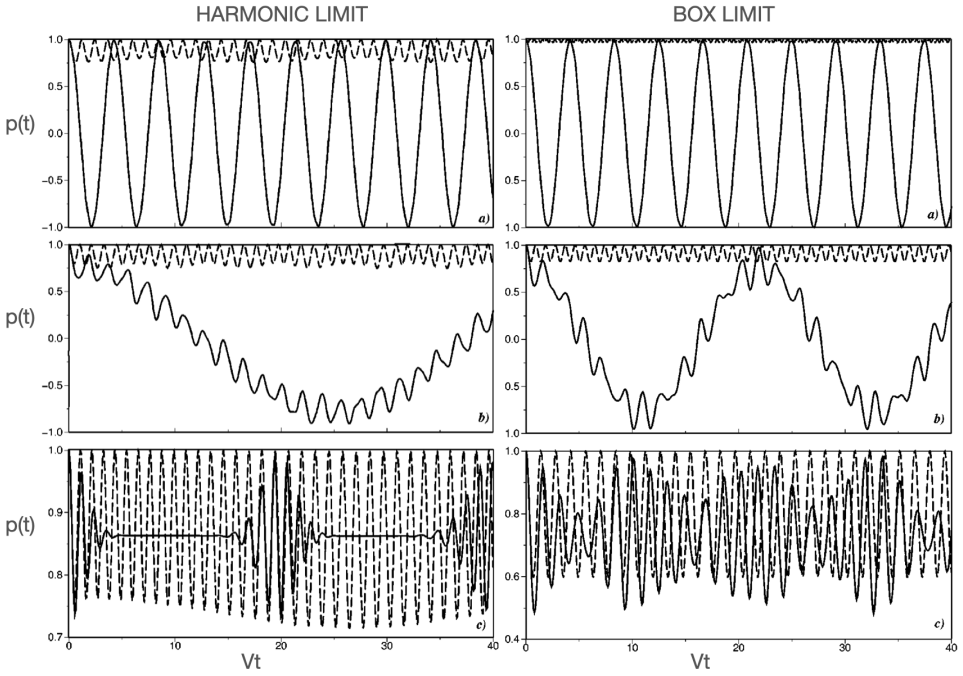

Fig. 11.3 Time dependence of the probability difference $p(t)$ between the two sites, plotted as a function of the dimensionless time Vt, for a usual initial condition that is discussed in the text, for a particle in strong interaction with vibrations obeying a Pöschl-Teller potential characterized by an anharmonicity measured by λ. The harmonic limit ($\lambda \to \infty$) is represented in the left panel and the box limit ($\lambda \to 1$) in the right panel. The actual values taken for λ are 200 and 1, respectively. Rows a,b,c represent decreasing values of ω_0/V from the top down: 10, 1, and 0.1, respectively. The semiclassical approximation gets better as expected as one goes down the figure towards lower ω_0/V. Primary characteristics are unaffected by the anharmonicity. See text. Adapted with permission from figs. 2 and 6 of Ref. (Raghavan et al., 1999a); copyright (1999) by the American Physical Society.

[6] The interested reader should consult the original publication for that graphical demonstration.

The plot in the right panel of Fig. 11.2, in which the logarithm of the tunneling time is displayed against the binding energy, shows that, for small values of the binding energy, the tunneling time for both cases is weakly dependent on the energy. On the other hand, for larger coupling (binding energy), both show a clear linear dependence *but with different slopes* in the two cases. We see that, even for the box limit of the potential, the polaron tunneling time is exponentially dependent on the binding energy. The result, well known for harmonic polarons, is a new finding of our analysis for their anharmonic counterparts.

We explored the system for numerous values of the anharmonicity parameter λ and found that the behavior is continuous from one limit to the other. The initial condition used for the quantum system, as in the harmonic system studies carried out in (Salkola et al., 1995; Kenkre et al., 1996a), is the ground state of the particle-oscillator projected onto the one-site localized part of the Hilbert space, such that $\langle \hat{p} \rangle (0) = 1$. For the semiclassical calculation it is $p(0) = 1, (z)_0 = 0, (\pi_z)_0 = 0$. In all cases in the plot, the quantum (semiclassical) evolution is indicated by a solid (dashed) line. The polaron binding energy has been kept constant at 1.5 in units of V. The value corresponds to $g^2\omega_0/2$ in the harmonic limit. We have displayed the explicit time dependence of the probability difference $p(t)$ in the primary plots of this investigation in Fig. 11.3. The three rows coming down from the top of the figure correspond to the three respective values 10, 1 and 0.1 of the ratio ω_0/V.

The left panel, marked as the harmonic limit, for which we have taken $\lambda = 200$, shows behavior that we are familiar with from Chapter 9: we have the same situation with initial conditions, the onset of the recurrences, selftrapping, silent runs and revivals in the appropriate parameter ranges. For the right panel, marked as the box limit, $\lambda = 1$. The behavior is qualitatively similar to that in the left panel: the semiclassical approximation incorrectly shows self-trapping while the correct quantum behavior is complete oscillations between the two sites for high ω_0/V (upper two rows). However, the representation is good for the lowest row, for which $\omega_0/V = 0.1$, strengthening the massive oscillator result of Salkola et al. (1995) or the warnings of (Vitali and Grigolini, 1990; Vitali et al., 1992) and others. In that row, the behavior is qualitatively similar for the harmonic and the extreme anharmonic (box) cases except that the silent runs are of very short or zero duration. Our careful examination of intermediate anharmonicities (λ) (not shown here but accessible in Raghavan et al. (1999a)), establishes unequivocally there are silent runs also for the anharmonic case: they just become shorter and shorter as one approaches the extreme box limit, collapses and revivals *intruding* into each other. Furthermore, the agreement between semiclassical and quantum evolutions becomes quantitatively worse as the anharmonicity grows.

The overall conclusion is that self-trapping is robust as a phenomenon and that it maintains its principal characteristics in the presence of anharmonicity in the vibrations even if the latter is very strong, although worse agreement between the exact quantum evolution and its semiclassical approximation is obtained for greater anharmonicity. Nevertheless, the dynamical tendencies are by and large preserved.

11.1.4 Boson-Fermion Mixtures and Soliton Propagation

This is the first of three consecutive studies of extended systems. They constitute a departure from the focus on spatially restricted systems that has pervaded all the rest of the studies in this book. The first deals with soliton propagation in boson-fermion mixtures. Our work on this topic was led by Vladimir Konotop in Lisbon, and carried out primarily by him, Jayanthi Santhanam from my research group and by Budov, a colleague of Konotop.[7] (Santhanam et al., 2006; Bludov et al., 2006)

People have worried about boson-fermion mixtures 4,5 and the variety of properties that they can exhibit. To complement studies in the literature 8,9 that address a mixture of a relatively small number of fermions embedded in a much larger bosonic component, we studied the opposite situation: a relatively small number of bosons embedded in a much larger fermionic component.

The starting coupled mean-field equations for a mixture of bosons and spin-polarized fermions with such a dominant fermions component were derived in 6 for the boson order parameter Psi(rat) and the fermion density n=n0+deltan. Here n0=

From this by rescaling, psi and rho we get eps 5 and 6

3d

Transverse dimension of the Fermi RF is much larger than transverse of Bose RB

Ref 10 multiple scale expansions provide a onecomponetn 1d GrossP ref 11 . Question we ask is a BoseFermi mixture gives such a reduction?

Section IV shows how a mutolitple scale analysis is possible and results in eq 20 for A and 17,18 also???

FIG1

concluL boson fermion mixture in a strongly anisotropic trap with fermions much more than bosons

Solitons involve most of the bosons etc Single nonlinear S eon ==========

11.1.5 Nonlinear Impurity in an Extended Chain

Let us consider next, a problem that can be regarded as having simultaneously to do with both a localized system in space and an extended one. Our interest is in the dynamics of a nonlinear impurity of small spatial extent embedded in an infinite lattice. As an example, the system could be an infinite linear chain wherein a quantum mechanical particle moves via nearest-neighbor transfer matrix elements, there being a single site, considered to be the origin without loss of generality, where the DNLSE effect is operative. My interest in this system originally came from the doping of host molecular crystals such as anthracene with guest molecules such as tetracene in the pursuit of sensitized luminescence and of the related phenomenon

[7] My own role in this investigation was restricted largely to watching Konotop teach us how this is done as much as anything.

of photosynthesis.[8] The primary motivation to present the analysis here is to show how a combination of numerical and analytic methods may be fashioned to solve a problem not accessible to purely analytic attack.

As is well known, the dynamics of a quasiparticle moving in a linear chain of infinite extent via nearest-neighbor interactions can be written down analytically in explicit form involving ordinary Bessel functions. Our interest is in studying a particle whose amplitude to be at a site m on the linear chain at time t is $C_m(t)$ via the equation of motion[9]

$$i\frac{dC_m}{dt} = V(C_{m+1} + C_{m-1}) - \delta_{m,0}\chi|C_0|^2C_0, \tag{11.18}$$

in notation that should be completely familiar to the reader. We will consider only the initial condition that the particle occupies the impurity site (origin) at $t = 0$. It finds itself with an instantaneously lowered site energy by an amount χ relative to all the other sites in the chain. Those sites have energy 0. The particle is not in resonance with its neighbors initially but as it attempts to move out of the initial site, the lack of resonance decreases. The dynamics can then be just as interesting as in the case of the dimer we have studied thoroughly in earlier Chapters of the book. However, here the motion outside the impurity site is in a system with infinite extension. This makes the problem difficult (actually impossible) to solve by the same methods as earlier.

If there were no nonlinearity in the system, the impurity at the origin being merely static, but lower in energy than the rest of the sites in the chain by an amount Δ, the equation of motion would be

$$i\frac{dC_m}{dt} = V(C_{m+1} + C_{m-1}) - \delta_{m,0}\Delta C_0, \tag{11.19}$$

instead of Eq. (11.18). The difference, that the site energy is here the given constant Δ rather than determined *dynamically* by the particle probability of occupation itself, $\chi|C_0|^2(t)$, is substantial and makes the analytic solution a non-trivial problem.

How would we solve the static impurity problem? A technique, tailored for such problems, is the so-called defect technique consisting of two steps. The first step is to write a Green function solution of Eq. (11.19) using the Bessel-function propagators of the linear chain without the impurity. The second step is to take advantage of the fact that the impurity is of finite extent to write down an explicit solution. The technique was used widely by Montroll and collaborators in elucidating the effect of defects in lattices and has been explained in great detail in a different book I published recently (Kenkre, 2021). The solution of Eq. (11.19) for the initial condition stated is, in terms of J_0, the Bessel function of order zero,

---

[8] The work to be described was done primarily by my then-student David Dunlap also in collaboration with my long-time friend and colleague Peter Reineker of Ulm who, on a sabbatical, was visiting my research group at that time.

[9] As usual, we suppress $\hbar$ and have used capital C's in keeping with the terminology of the original paper (Dunlap et al., 1993).

$$C_0(t) = J_0(2Vt) + i\Delta \int_0^t ds\, e^{i\Delta s} J_0\left(2V\sqrt{t^2 - s^2}\right). \tag{11.20}$$

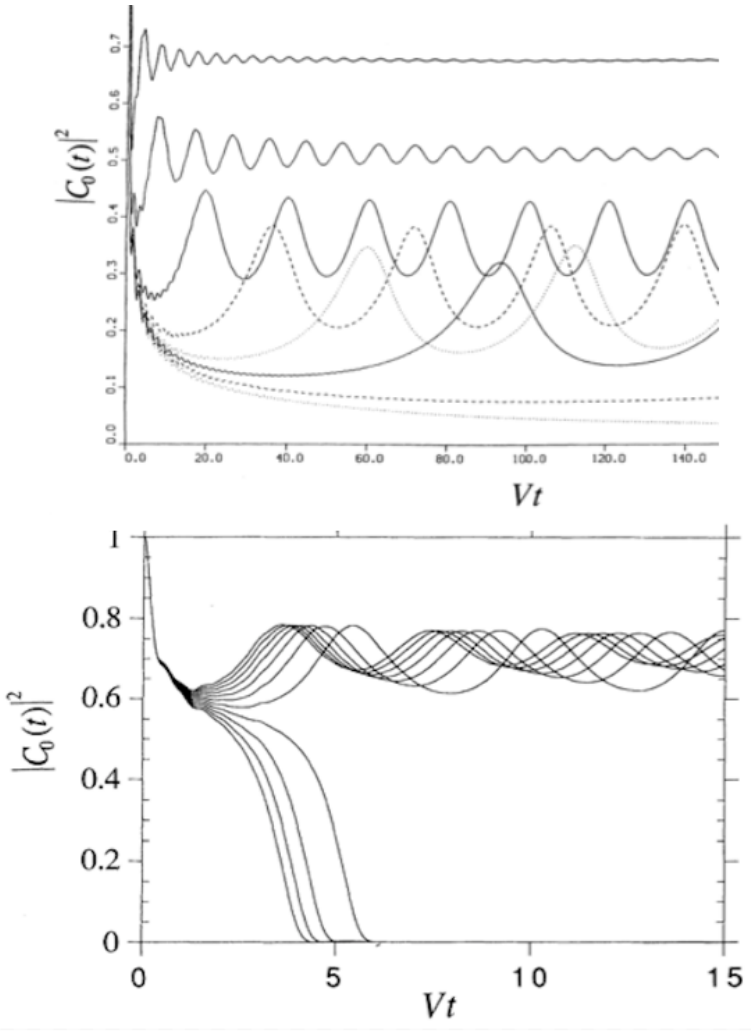

Fig. 11.4 Self-trapping transition at the initially occupied impurity site in a 1-dimensional chain of infinite extent in the upper panel and in a simple cubic 3-dimensional crystal, also of infinite extent, in the lower panel. The probability of the initially occupied impurity site is plotted versus the dimensionless time Vt for various values of the nonlinearity ratio χ/V. See text. Modified with permission from figs. 1 and 4 of Ref. (Dunlap et al., 1993); copyright (1993) by American Physical Society.

The presence of nonlinearity in our actual problem allows us to perform the first step of the procedure outlined but not the second. We can state with confidence that the solution of Eq. (11.18) must satisfy

$$C_0(t) = J_0(2Vt) + i\chi \int_0^t ds\, |C_0(s)|^2 C_0(s) J_0\left(2V(t-s)\right). \tag{11.21}$$

However, an explicit solution does not appear possible because of the appearance of $C_0(t)$ within the integral in a nonlinear form on the right hand side of the equation.

What happens if we carry out a numerical solution along the lines explained in relation to Fig. 1.1 and the DNLSE without impurity? The answer is displayed in Fig. 11.4. In the upper panel the results for the problem as stated in a 1-dimensional chain are shown; the lower panel is a straightforward extension to a 3-dimensional (simple cubic) crystal.[10] Both are plots of the probability to remain at the the initially occupied impurity site versus the dimensionless time Vt for various values of χ/V.

An abrupt self-trapping transition as we vary the nonlinearity ratio χ/V is indicated in both panels. The top curve of the upper panel (1-dimensional chain) shows self-trapping at $|C_0(t)|^2 \approx 0.67$ calculated at $\chi/V = 4.00$. As the value of χ is reduced, so is the probability remaining at long times. The next two lower curves are for χ/V values 3.5 and 3.3. Then come 3.25 (dashed), 3.23 (dotted), 3.22 (solid), 3.21 (dashed) and the lowest 3.20 (dashed). There should be no doubt that self-trapping occurs for χ/V greater than 3.22.

The reader might want to take special notice now of how one might move between a blend of numerical and analytic techniques. We see probability oscillations in Fig. 11.4. In order the investigate the transition, let us focus on the recurrence period of the probability oscillations as we get close to what we suspect as the transition value of χ/V. On approaching it from the self-trapped side ($\chi/V > 3.205$), the period is found to become *very* long as χ/V tended to 3.205. Dunlap et al. (1993) have given a careful and thorough report of the procedures followed. I recommend the reader to consult them in detail.

To quantify their observations, they recorded the time τ for the first recurrence in probability as a function of χ/V. A plot of τ for χ/V in the neighborhood of 3.2 is shown in Fig. 11.5. It is not easy to determine whether the transition is real. A true transition would correspond to the recurrence period becoming infinite. For the nonlinearity ratio χ/V equal to 3.21, it appears there is complete decay of probability if you look at short times but a longer interaction shows this not to be the case. As Dunlap et al. (1993) have stated, one can be only sure that, for times t less than approximately $800/V$ one can suggest that there might be a transition that occurs at a value of the nonlinearity ratio between 3.20 and 3.21.

One argument presented is based on an examination of the dependence of τ on the nonlinearity ratio observed in the neighborhood of 3.2, assuming it can be fitted by

[10] It is easy to show that for simple isotropic higher-dimensional extensions (for instance to a simple square and simple cubic cases in 2 and 3 dimensions respectively), Eq. (11.21) is maintained in form except for the replacement, both inside the integral and outside, of J_0 by $[J_0]^n$ where n is the dimensionality of the infinite crystal.

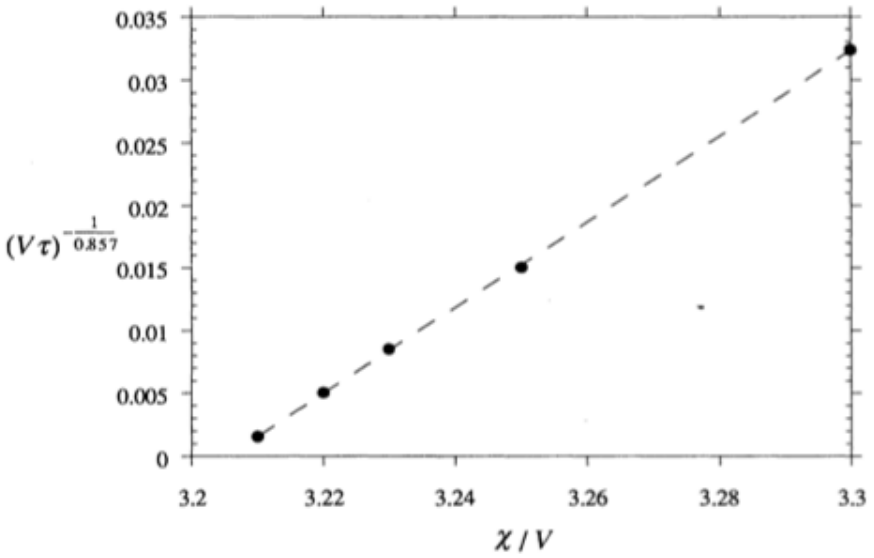

Fig. 11.5 Determination of whether recurrences of probability oscillations from Fig. 11.4 are really indicative of an abrupt transition. The oscillation period τ extracted from those numerical observations is built into the dimensionless quantity $(1/V\tau)^{1/0.857}$ and plotted against the nonlinearity ratio χ/V, the black dots showing the values extracted. Relation (11.22) conjectured in the text suggests a transition that is indeed abrupt to infinite recurrence time when χ/V attains approximately the value 3.20, when the fitted straight line hits the x-axis. Modified with permission from figs. 1 and 4 of Ref. (Dunlap et al., 1993); copyright (1993) by American Physical Society.

a power law, and finding a best fit. It appears that the power law fit can be described by

$$V\tau = \left[\frac{2.924}{(\chi/V) - (\chi/V)_{cr}}\right]^{0.857}, \tag{11.22}$$

the critical value $(\chi/V)_{cr}$ of the nonlinearity, thus found empirically, being 3.205.

Equation (11.22) is chock full of information extracted from the numerical work reflected in Fig. 11.4: From that work comes the *form* of the relation between $V\tau$ and the nonlinearity ratio χ/V. From those numerical results come the numbers 2.924 and 0.857. Finally, that work has given us the critical value $(\chi/V)_{cr} = 3.205$. Equation (11.22) implies that the recurrence period becomes infinite at the critical value of the nonlinearity and thus signifies an abrupt transition from free to self-trapped behavior. Fig. 11.5 displays the relation as a straight line making the inspection process understandable.[11]

[11] There are additional arguments in support of our methodology that we presented in the original publication that the reader might find interesting. Briefly stated, recognizing that an analytical (explicit) solution of Eq. (11.21) is not available, we considered an approximate representation

For obvious reasons, stemming from intellectual interest as well as applications, this impurity problem that we analyzed in 1992 in the context of sensitized luminescence and photosynthesis has attracted the attention of a number of investigators. There is new work that is being done as recently as during the current year with a fractional operator replacing the standard discrete Laplacian.[12] Compare also in this general connection the discussion I have given in Section 6.4 of global interactions between an antenna and the reaction center performed by Kenkre and Kuś (1992) and a study by Molina et al. (1997) of the difference between DNLSE consequences and more general predictions.

11.1.6 Excimer Formation as a Nonlinear problem: a Classical Treatment

Unlike all other problems studied in this book, this last of the topics investigated is approached *classically*. The governing equation is not Schödinger's for the quantum amplitude or von Neumann's for the density matrix but Newton's for a nonlinear oscillator. The equation and the quantities calculated are intimately connected, however, to observables analyzed via quantum mechanics such as the light emission spectrum. Although the system has similarities to the nonlinear impurity in a crystal that we analyzed in the preceding Section, the two items that set apart the present study are the crucial role that nonlinearity in the potential plays here and the fact that no quantum dynamics is involved. Three of our four original publications on the subject were part of Dunlap's Ph.D. dissertation (Dunlap and Kenkre, 1984, 1986a, 1988a), the fourth had Grigolini as a coauthor. (Kenkre et al., 1990)

In contrast to the other investigations described in the book, our excimer work was strongly motivated by experimental observations. My own contributions to this subject came from a concerted collaborated analysis over a summer with two very well-known and accomplished molecular crystal experimentalists from the University of Stuttgart, H. C. Wolf and his one-time student, and an internationally respected scientist in his own right, Helmut Port.[13] The intense discussions that the three of us had together led to the unique theoretical model that we developed with the able implementation skills of David Dunlap who was just starting his research activities in physics. The model will be found to be well entrenched in experimental observations and suggestions such as those of Collins and Craig but to be quite

---

of $\chi|C_0(s)|^2$ inside the integrand in terms of a simple time-dependent function of increasing complexity and determined it by a non-standard iterative procedure.

[12] See, e.g., Mario Molina, The fractional nonlinear impurity: a Green function approach, http://arxiv.org/abs/2108.08711.

[13] Unfortunately, neither of them is living now. Although both had a serious approach to their profession, Helmut Port's quick wit would surface on many an occasion. Here is what he said to me once when I had been invited at his house for dinner. I was attempting to make small talk and asked him if he appreciated science fiction. Without blinking an eye, he retorted 'Oh yes, I like all the papers you have written.'

different in flavor from a number of more comprehensive but different investigations carried out by others Da et al. (1994); Yudson et al. (1994). My reason to describe it here is because of the simple, different, and instructive role that nonlinearity in classical dynamics plays in its development.

Structured optical absorption accompanied by a broad structureless emission with characteristically long lifetimes and dependence of the spectrum on temperarture are the hallmark of excimers. The process of their formation in crystals such as pyrene and also in some cases their migration have often been scrutinized. At the time I began to analyze excimer physics, experimental work had made substantial leaps in time-resolving excimer formation, 1-4, but theory had lagged behind experiment. Collins and Craig had invoked a treatment of classical vibrational relaxation in a finite linear chain with Morse potentials but it was based on a computer simulation and its function was to select between two configurations of the molecules, one of which was thought to be a *precursor* to excimer formation. Borrowing from CC, I decided to consider the classical relaxation of an oscillator that changes character on being electronically excited. However, the procedure followed was not to do a computer simulation for a few molecules but to present a solution to the relaxation problem of a nonlinear impurity in a classical linear chain. The solution, while numerical, was accurate to an arbitrary degree. We show in the following the approach first and an extension to the problem of Y-states (an intriguing peculiarity of excimers in some materials) next.

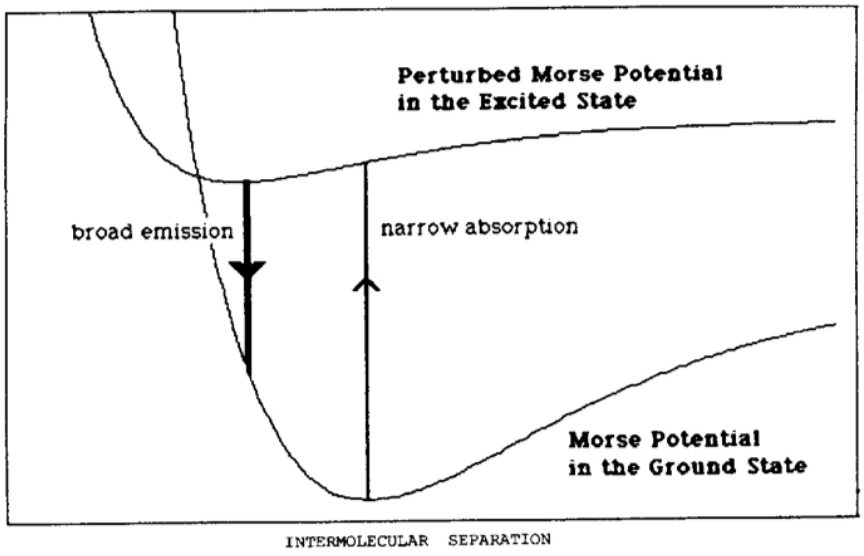

Fig. 11.6 Schematic depiction of nonlinearity in the potential required to address excimer spectra. Reprinted with permission from fig. 1 of Ref. (Dunlap and Kenkre, 1984); copyright (1984) by Elsevier Publishing.

Because the vibrational structure of the monomer is reflected in the absorption spectrum with no contribution from the vibration of the molecular pair that constitutes the excimer vibrations but the emission spectrum is characterized by the excimer vibration, the transition must be to the tail of the excited state pair potential (Dunlap and Kenkre, 1984) (see Fig. 11.6). Surely, the forces initially drawing the molecular pair together must be weak, the pair potential in the crystal must fall off extremely quickly, demanding thus that the contracting force be highly nonlinear. We consider the contraction of the defect pair in an infinite linear chain of molecules wherein the displacement $x_m(t)$ from equilibrium of the mth molecule obeys

$$M\frac{d^2x_m}{dt^2} = -k_0(2x_m - x_{m-1} - x_{m+1}) - (\delta_{m,r} - \delta_{m,r+1})[k_0(x_r - x_{r+1}) - V'(x_{r+1} - x_r)]. \tag{11.23}$$

Here, M is the mass of each molecule, k_0 is the chain spring constant, and $V'(x)$ is the derivative of the nonlinear defect potential $V(x)$ that acts between molecules at r and $r+1$ when one of th the two molecules is excited. It is straightforward to define y_m as the difference $x_{m+1} - x_m$, write a solution for it in the Laplace domain, and invert it into

$$y_r(t) = \eta_r(t) + \int_0^t dt'\,\phi(t-t')h[y_r(t')]. \tag{11.24}$$

Here $y_r(t)$ is the time domain solution for the departure from equilibrium of the difference $x_{r+1} - x_r$ that can be obtained explicitly via a finite difference method with $\eta_r(t)$ as the solution in the absence of the defect spring (that can be written down analytically in terms of Bessel functions), the 'memory' $\phi(t)$ is $(2/\omega_0)J_1(2\omega_0 t)$, with J_1 as the Bessel function of order 1 and $\omega_0 = \sqrt{k_0/M}$. The important nonlinear function$h$ is given from the potential as

$$h[y_r(t)] = \omega_0^2 y_r(t) - (1/M)V'[y_r(t)]. \tag{11.25}$$

We analyzed several different forms of the nonlinear potential, the Morse potential, the Rydberg potential and the Beckel-Findley polynomial potential given respectively in

$$V(x) = D(e^{-2bx} - 2e^{-bx}), \tag{11.26a}$$

$$V(x) = -D(1+bx)e^{-bx}), \tag{11.26b}$$

$$V(x) = D(1+bx)/[x(1+x^6)]. \tag{11.26c}$$

Dunlap's meticulous work allowed us to determine many relevant aspects of relaxation in the time domain and spectra in the frequency domain. Fig. 11.7 shows an example of the results of some of his work (Dunlap and Kenkre, 1984, 1986a) where a Morse potential was assumed with $k_1 = k_0$.

In this manner, in order to model excimer formation in crystals such as dichloroanthracene10 that possess a stack structure we studied linear chains, to study crystals

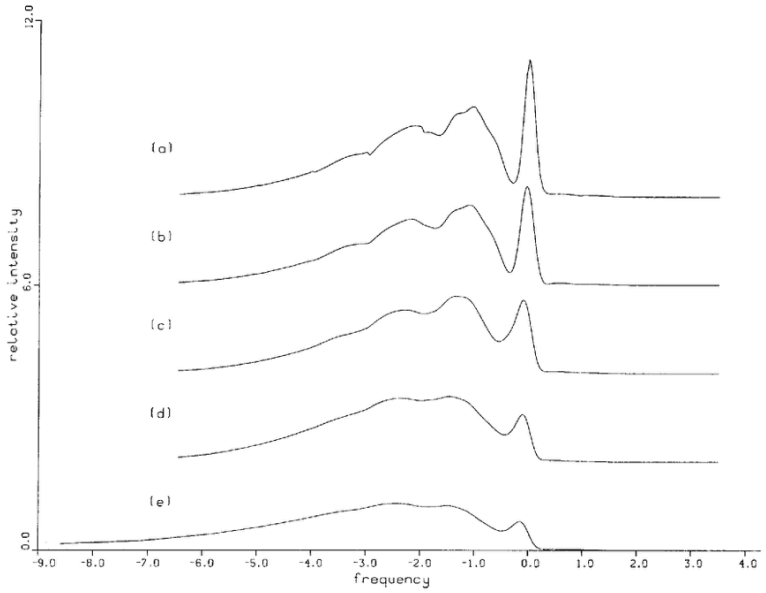

Fig. 11.7 Cumulative time-resolved early time emission spectra calculated under the assumption of a typical shape for the monomer spectrum for several times after excitation: (a) 0, (b) $5/\omega_0 \equiv 5/\sqrt{k_0/M}$, (c) $10/\omega_0$, (d) $15/\omega_0$, and (e) $20/\omega_0$. The last value corresponds to the excimer passing through the its equilibrium position for the first time. The frequency along the x-axis is in units of the assumed monomer characteristic frequency. Modified with permission from figs. 1 and 4 of Ref. (Dunlap and Kenkre, 1986a); copyright (1986) by Elsevier Publications.

such as pyrene25 that consist of preformed dimers we studied chains in which there are two sites per unit cell.

As especially intriguing aspect of excimer formation that we studied was the phenomenon of Y-states observed, for instance, in α-perylene, and supposedly caused by the incomplete relaxation of the excimer pair coordinate due to the hindering of the lattice 13,19,26. In a 1-dimensional system, excimer formation is hindered by the lattice only in the sense that it provides an effective viscosity in which the excimer must contract. In a higher-dimensional system, however, more restrictive forces occur given that horizontal, vertical and diagonal interactions simultaneously occur. We took the spring constants in the horizontal and vertical directions to be k_0 and that in the diagonal direction to be k_1. Equation (11.24) emerges again with, however, the modification that the kernel $\phi(t)$ is complicated by the interplay between he horizontal and vertical interactions and the diagonal interactions. See Fig.11.8. Numerical solution from this higher-dimensional version of Eq. (11.24) shows rich behavior for several values of k_1/k_0. The equilibrium excimer-pair separation increases monotonically with k_1/k_0 because the neighboring molecules are interconnected via an infinite number of indirect diagonal paths. These interactions

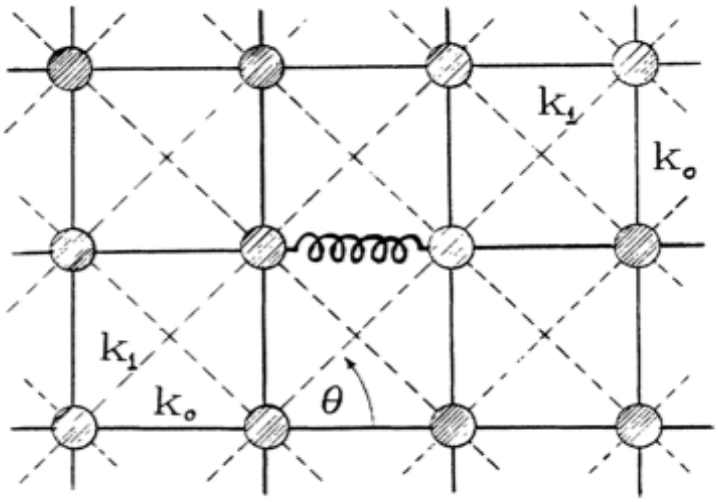

Fig. 11.8 The 2-dimensional square lattice with 'horizontal' and 'vertical' harmonic springs with spring constant k_0, 'diagonal' springs with spring constant k_1 making an angle θ with the horizontal axis, and the nonlinear excimer, represented by the explicitly drawn coiled spring, which is turned on by the process of light absorption. Reproduced with permission from fig. 1 of Ref. Dunlap and Kenkre (1988a); copyright (1988) by American Physical Society.

tend to oppose the lattice distortion that accompanies the contraction for the excimer pair, and their effect increases with the strength of the diagonal spring.

There is a striking result that comes out of these considerations. The equilibrium separation of the molecular pair undergoes a *sudden* transition as k_1/k_0 is varied. We proposed this phenomenon as signifying the formation of the Y-state in (Dunlap and Kenkre, 1988a; Kenkre et al., 1990). In order to understand its essence with the shortest effort expended, let us rewrite Eq. (11.24) with the context expanded to higher dimensions by symbolically replacing $y(t)$ by $\zeta(t)$ and $(1/M)V'(y_r)$ by $u'(\zeta)$, and crossing over into the Laplace domain where ϵ is the Laplace variable and tildes denote Laplace transforms. We now have

$$\tilde{\kappa}(\epsilon)\tilde{\zeta}(\epsilon) = -\int_0^\infty dt\, e^{-\epsilon t} u'[(\zeta(t)], \tag{11.27}$$

with

$$\tilde{\kappa}(\epsilon) = \frac{1}{\tilde{\phi}(\epsilon)} - \omega_0^2. \tag{11.28}$$

An Abelian theorem allow us to write down an *exact* consequence of Eq. (11.27) for the equilibrium value that the excimer coordinate attains. This is the limit of $\zeta(t)$ as $t \to \infty$. What is needed is the simple multiplication of Eq. (11.27) by the Laplace

variable ϵ and the limit $\epsilon \to 0$. The consequence is

$$\tilde{\kappa}(0)\zeta(\infty) = \left[\frac{1}{\tilde{\phi}(0)} - \omega_0^2\right]\zeta(\infty) = -u'[\zeta(\infty)]. \tag{11.29}$$

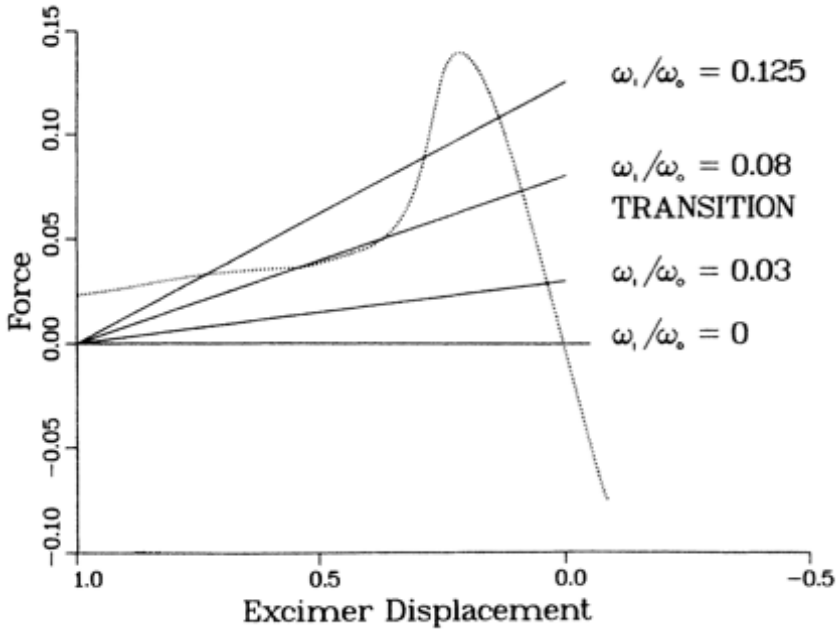

Fig. 11.9 Exact analysis of the emergence of a Y-state based on Eq. (11.29). The dotted curve represents the nonlinear excimer force and the four solid lines the effective restoring force of the lattice for respective values of ω_1/ω_0 as shown. The intersection of the solid lines with the dotted curve gives the equilibrium excimer coordinate ζ at infinite time. Only an Modified with permission from figs. 1 and 4 of Ref. (Dunlap et al., 1993); copyright (1993) by American Physical Society.

Much has been accomplished. We know the time integral $\tilde{\phi}(0)$ of the propagator of the lattice without a defect (simply in terms of Bessel functions) and the nonlinear force $-U'[\zeta(\infty)]$. It is entirely straightforward, therefore, to solve Eq. (11.29) to obtain the equilibrium value of the excimer coordinate. Moreover, the equation gives us immediately insight into the formation of the Y-state as per our model: the Y-state appears only when Eq. (11.29) has more than one solution for $\zeta(\infty)$. The situation is precisely as in mean field theories of ferromagnetism!

The physical situation is as follow. At equilibrium, the excimer pair is acted upon by two forces. The nonlinear excimer pair force is represented by the right hand side of Eq. (11.29) and tends to pull the molecular pair together. An effective restoring force caused by the lattice tends to oppose the contraction of the molecular pair, is

represented by the left hand side of Eq. (11.29) and signifies and effective spring constant $[1/\tilde{\phi}(0)] - \omega_0^2$. If, as in the 1-dimensional chain, hindering interactions stemming from the (diagonal) k_1 springs are absent, $1/\tilde{\phi}(0)$ equals ω_0^2, and the effective spring constant $\tilde{\kappa}(0)$ vanishes. The equilibrium state of the excimer is then at the minimum of the nonlinear potential V, and there is only a *single* excimer state. That is the E-state. In the presence of the hindering interactions, two effects occur, one of which is the simple shift of the E-state equilibrium coordinate caused by the addition of the lefthand side term in Eq. (11.29). The other effect, which occurs when the effective spring constant $\tilde{\kappa}(0)$ exceeds a critical value, is that multiple minima in the total potential $u(\zeta) + \tilde{\kappa}(0)\zeta^2/2$ appear . The additional minimum in the effective potential when occupied is the Y-state.

Although the topic of the study in this subsection lies on the margins of the book's topics, I have included it because of the simple, and yet exciting, physics in terms of which it has been constructed.[14]

11.2 Review of Topics Covered in the Book

The time[15] has come in the second half of this final Chapter to spend a few wise words to summarize what we have covered in the book. As I said in the Preface[16], this was a side adventure I happened to take into something that was outside the mainstream of my research. I have no claims whatsoever to have shared with you, the reader, any profound insights that the title of the book might have (mis)led you into anticipating. What I have presented are simple results that have given delight to me as also to my friends who played along with me in the analysis of these topics.

The general aim of the research described in the book has been to elucidate the effects of the interaction of nonlinearity with quantum mechanics, introduced into the latter as an approximate representation of the partial dynamics. This has been done by specifically focusing on systems of small spatial extent. The smallest size is obviously two sites and it is, therefore, dimers that we concentrated on, although we started the book with a numerical solution of the DNLSE on a chain of a 100 sites or more. Our restriction in size was motivated by the ability thereby to obtain exact solutions in most cases. The central idea was to base our intuition on analytic procedures rather than numerical. The latter constitute a powerful method of study but always run the risk of artifacts being confused with actual consequences of the physical system. The trick of the trade is to make progress by combining insights obtained from exact

[14] It has come out directly from the experimental discussions I had with my two departed colleagues Port and Wolf, and from the unique theoretical skills practiced in all his work by my ex-student Dave Dunlap. The interested reader will find more in the original publications and the hints given about work on thermal fluctuations that I started with Paolo Grigolini and that has been briefly alluded to in Kenkre et al. (1990).

[15] Or space! We physicists have Einstein's assurance that they are not really different.

[16] If you stilll have not read the Preface, hurry and go back to it. It is essential in understanding the message of the rest of my book.

calculations for unrealistically small systems with insights obtained from numerical (therefore in a puristic sense always inexact) calculations for larger, realistic, systems. Even in small systems, however, the need was sometimes felt to use numerical methods.[17] Given that I have young forming theoretical physicists in mind as the readers of this book, may I suggest that the attitude of shunning numerics is nothing short of immature ignorance.[18] Here are some specific examples from this book. MORE ime and again I have found it not only necessary but immensely useful even for ...MORE HERE Mention kenkrewu and other examples of such combined work and also Dunlap's scotch tape inf furnaces.

A few words why retaining the focus of the book on systems of small spatial extent is not at all similar to restricting oneself to toy investigations. One would not dream of faulting a painter for not undertaking sculpture as well, or take to task an artist who does only black and white sketches only, for refusing to break his monochromatic practice. There is plenty of complexity and profundity to drawing without color or painting on a two-dimensional canvass. There are also plenty of deep questions of the kind relevant to spin-boson dynamics that relate to a two-state system behavior. The complexity in such a case comes from the intricacies of the interactions with phonons. We have seen this throughout the book. A number of readers of the book will realize it immediately or at least after reading the book. Those who do not should think about the analogous situation in statistical mechanics wherein an Ising model provides rich problems for the physicist to solve despite only two values that a spin at a site takes in the Ising system. The complexity there comes from the geometry of interactions in an infinite n-dimensional space. The complexity in our dimers comes from the infinite manifold of the bosons that the dimer interacts with. Much fundamental research can be, and is, done in the Ising model without having to employ extensions to Heinseberg, clock, or Potts models. The primary activity of the theoretical physicist seems to me to be slicing a system into parts that are significant yet solvable. Without the divide-and-conquer approach that this entails, the pursuit of theoretical physics would gain little success.

In chapter 1 we met with the DNLSE and learned the graphical tool of potential plots aided by the analytic technique of elliptic functions. We introduced a pedagogically interesting manner of introducing the latter through a stretching transformation applied to ordinary trigonometric functions. We studied an application to the familiar physical pendulum oscillating with arbitrarily large amplitudes as well as the unfamiliar evolution of bacterial population in Petri dishes. In the process we armed ourselves with cn-dn transitions, Landen and Jaboi transformations and similar unusual tools for further use.

---

[17] My own training was pure theoretical and I grew up with an antiquated snobbish attitude towards numerical practices. My wife reminded me the other day that during a walk on the campus at Stony Brook during my graduate student days, some of my theoretical physicist friends had pointed out to her the Computer Sciences department and remarked "That is where the not-so-smart people work." I am glad I freed myself from such a ridiculously arrogant view as I grew wiser in my work.

[18] With the advent of computers on every desk and in a sense in every pocket, this need not be spelled out in this manner perhaps. Nevertheless, for the rare person who might not have understood this lesson, I emphasize that numerical methods are as useful and must-employ tool as analytical although the character of the tools are different.

In chapter 2 we applied the tools to understand completely the occurrence of the self trapping transition in the DNLSE, identifying probability difference oscillations on both sides of the resonant dimer as free motion and those oscillations when restricted to one side only as self-trapped motion. XXXXXX MENTION THE AL SCOTT CONVERSATIO about the use of KC.

In chapter 3 we studied the interplay of initial phases on the evolution in a non-linear dimer...

In chapter 4 we saw the striking effects of nonlinearity that are more complex than cubic we began the study in the particular context of rotational polarons but extended the investigation to many different aspects including his statuses in chapter 5 return to the cubic nonlinearity and studied the non-resident that is non-degenerate nonlinear dimer in chapter 6 we studied a bit of systems of great especially extent but restricted ourselves to global interactions both in the context of tremors in inmates and in trapping of excitation by an antenna in chapter 7 will begin the study of relaxation that is not infinitely first and then chapter 8 we studied thermal effects into different ways in chapter 9 we investigated the microscopic arguments for Poloron whatever in chapter 10 we studied the gross bitterThe gross but I was scared equation for the tunneling a Bose Einstein condensates finally a number of miscellaneous topics were covered in chapter 11 we have in this man that tried to move around many different and difficult topics about the interplay of non-linearity with quantum mechanics

.... TO BE COMPLETED What is on the wish-list? EXAMPLES AND HINTS?

11.3 Parting Words

Robert Frost is one of my favorite poets in the English language. While we have pranced around the topics that I have described in the interplay of quantum mechanics with nonlinearity, wondering about the validity of adding nonlinear terms to the linear structure of quantum mechanics and marveling at the (sometimes weird but always intriguing) consequences, pondering about the efficacy of procedures such as the memory method while questioning the justification for their success, and contemplating, surely with some anxiety, the legitimacy of approximations such as the semiclassical, I have been continually reminded, and quite acutely, of Frost's lines in his poem *The Secret Sits*:

We dance round in a ring and suppose
But the Secret sits in the middle and knows.

References

Ablowitz M, Ladik J (1976) Nonlinear differential–difference equations and fourier analysis. Journal of Mathematical Physics 17(6):1011–1018

Ablowitz MJ, Prinari B, Trubatch AD (2004) Discrete and Continuous Nonlinear Schrödinger Systems. Cambridge University Press

Abramowitz M, Stegun IA (1965) Handbook of mathematical functions with formulas, graphs, and mathematical tables. Dover, New York

Agarwal GS, Harshawardhan W (1994) Realization of trapping in a two-level system with frequency-modulated fields. Physical Review A 50(6):R4465

Allen L, Eberly JH (1987) Optical resonance and two-level atoms, vol 28. Courier Corporation

Amritkar RE, Kenkre VM (1999) Nature of transitions in augmented discrete nonlinear schrödinger equations. Physical Review E 59(6):6306

Andersen JD, Kenkre VM (1993a) Exact solutions for the quantum nonlinear trimer. physica status solidi (b) 177(2):397–404

Andersen JD, Kenkre VM (1993b) Self-trapping and time evolution in some spatially extended quantum nonlinear systems: Exact solutions. Physical Review B 47(17):11134

Andersen JD, Duke C, Kenkre VM (1983) Injected electrons in naphthalene: Band motion at low temperatures. Physical review letters 51(24):2202

Andersen JD, Duke C, Kenkre V (1984) Application of the silbey-munn theory to interpret the temperature dependence of the mobilities of injected electrons in naphthalene. Chemical physics letters 110(5):504–507

Anderson PW (1997) Concepts in solids: lectures on the theory of solids, vol 58. World Scientific

Aslangul C, Pottier N, Saint-James D (1986) Spin-boson systems: equivalence between the dilute-blip and the born approximations. Journal de Physique 47(10):1657–1661

Balescu R (1975) Equilibrium and nonequilibrium statistical mechanics. John Wiley & Sons, New York

Belobrov P, Zaslavskii G, Tartakovskii GK (1976) Stochastic breaking of bound states in a system of atoms interacting with a radiation field. Sov Phys JETP 44(5):945

Bishop AR, Krumhansl JA, Trullinger S (1980) Solitons in condensed matter: a paradigm. Physica D: Nonlinear Phenomena 1(1):1–44

Bludov YV, Santhanam J, Kenkre V, Konotop V (2006) Matter waves of bose-fermi mixtures in one-dimensional optical lattices. Physical Review A 74(4):043620

Bolterauer H (1990) Temperature effects on the davydov soliton. In: Davydov?s Soliton Revisited, Springer, pp 309–323

Bonci L, Grigolini P, Roncaglia R, Vitali D (1993) Nonlinear schrödinger equation and wave-function collapse: An unreliable consequence of the semiclassical approximation. Physical Review A 47(5):3538

Bowman F (1953) Introduction to elliptic functions: with applications. Dover Publications, New York

Brizard AJ (2009) A primer on elliptic functions with applications in classical mechanics. European Journal of Physics 30(6):729

Brown DW, Kenkre VM (1983) Quasielastic neutron scattering in metal hydrides: Effects of the quantum mechanical motion of interstitial hydrogen atoms. In: Electronic structure and properties of hydrogen in metals, Springer, pp 177–182

Brown DW, Kenkre VM (1987) Neutron scattering lineshapes for hydrogen trapped near impurities in metals. Journal of Physics and Chemistry of Solids 48(9):869–876

Brown DW, Lindenberg K, West BJ (1986a) Applicability of hamilton's equations in the quantum soliton problem. Physical Review A 33(6):4104

Brown DW, Lindenberg K, West BJ (1986b) On the dynamics of polaron formation in a deformable medium. The Journal of chemical physics 84(3):1574–1582

Brown DW, West BJ, Lindenberg K (1986c) Davydov solitons: New results at variance with standard derivations. Physical Review A 33(6):4110

Brown DW, Lindenberg K, West BJ (1987) Nonlinear density-matrix equation for the study of finite-temperature soliton dynamics. Physical Review B 35(12):6169

Bukov M, D'Alessio L, Polkovnikov A (2015) Universal high-frequency behavior of periodically driven systems: from dynamical stabilization to floquet engineering. Advances in Physics 64(2):139–226

Byrd P, Friedman M (1971) Handbook of elliptic integrals for scientists and engineers

Cai D, Bishop A, Grønbech-Jensen N (1994) Localized states in discrete nonlinear schrödinger equations. Physical review letters 72(5):591

Campbell DK (1987) Nonlinear science. Los Alamos Science 15:218–262

Careri G, Buontempo U, Galluzzi F, Scott A (1984) E. gratton and e. shyamsunder. Phys Rev B 30:4689

Chandrasekhar S (1992) Liquid Crystals. Cambridge University Press

Cheng YC, Silbey RJ (2008) A unified theory for charge-carrier transport in organic crystals. The Journal of chemical physics 128(11):114713

Chester G, Thellung A (1959) On the electrical conductivity of metals. Proceedings of the Physical Society 73(5):745

Christiansen PL, Scott AC (1990) Davydov's soliton revisited: self-trapping of vibrational energy in protein, vol 243. Plenum Press, New York

Cottingham JP, Schweitzer JW (1989) Calculation of the lifetime of a davydov soliton at finite temperature. Physical review letters 62(15):1792

Crawford M, Vrscay E (1998) Generalized coherent states for the pöschl-teller potential and a classical limit. Physical Review A 57(1):106

Cruzeiro L (2009) The davydov/scott model for energy storage and transport in proteins. Journal of biological physics 35(1):43–55

Cruzeiro L, Halding J, Christiansen PL, Skovgaard O, Scott AC (1988) Temperature effects on the davydov soliton. Physical Review A 37(3):880

Cruzeiro-Hansson L, Takeno S (1997) Davydov model: The quantum, mixed quantum-classical, and full classical systems. Physical Review E 56(1):894

Cruzeiro-Hansson L, Christiansen PL, Elgin J (1988) Comment on "self-trapping on a dimer: Time-dependent solutions of a discrete nonlinear schrödinger equation". Physical Review B 37(13):7896

Da H, Yudson V, Reineker P, et al. (1994) Organic molecular crystals: formation of excimers. Journal of luminescence 60:454–457

Dauxois T, Peyrard M (2006) Physics of Solitons. Cambridge University Press

Duke CB, Schein L (1980) Organic solids: is energy-band theory enough? Physics Today 33(2):42–48

Dunlap D, Kenkre V (1984) Analysis of excimer migration observations in molecular crystals. Journal of Luminescence 31:753–755

Dunlap D, Kenkre V (1986a) Excimer formation as the relaxation of a non-linear oscillator. i. model calculations in a linear chain. Chemical physics 105(1-2):51–58

Dunlap D, Kenkre V (1988a) Excimer formation as the relaxation of a nonlinear oscillator: Theory of y states. Physical Review B 37(9):4390

Dunlap D, Kenkre V, Reineker P (1993) Self-trapping transition for a nonlinear impurity embedded in a lattice. Physical Review B 47(22):14842

Dunlap DH, Kenkre VM (1986b) Dynamic localization of a charged particle moving under the influence of an electric field. Physical Review B 34(6):3625

Dunlap DH, Kenkre VM (1988b) Dynamic localization of a particle in an electric field viewed in momentum space: Connection with bloch oscillations. Physics Letters A 127(8-9):438–440

Dunlap DH, Kenkre VM (1988c) Effect of scattering on the dynamic localization of a particle in a time-dependent electric field. Physical Review B 37(12):6622

Eilbeck JC, Lomdahl P, Scott AC (1985) The discrete self-trapping equation. Physica D: Nonlinear Phenomena 16(3):318–338

Enol'skii V, Salerno M, Kostov N, Scott A (1991) Alternate quantizations of the discrete self-trapping dimer. Physica Scripta 43(3):229

Enol'skii V, Salerno M, Scott AC, Eilbeck J (1992) There's more than one way to skin schrödinger's cat. Physica D: Nonlinear Phenomena 59(1-3):1–24

Faetti S, Fronzoni L, Grigolini P, Mannella R (1988) The projection approach to the fokker-planck equation. i. colored gaussian noise. Journal of statistical physics 52(3):951–978

Fan X, Kenkre V (1989) A model calculation for vibrational propagation in a chain of nonlinear oscillators ii: Effects of optical dispersion and of initial conditions. Zeitschrift für Physik B Condensed Matter 77(3):425–429

Fonseca T, Grigolini P, Pareo D (1985) Classical dynamics of a coupled double-well oscillator in condensed media. iii. the constraint of detailed balance and its effects on chemical reaction process. The Journal of chemical physics 83(3):1039–1048

Forner W (1991) Davydov soliton dynamics: temperature effects. Journal of Physics: Condensed Matter 3(24):4333

Grifoni M, Hänggi P (1998) Driven quantum tunneling. Physics Reports 304(5-6):229–354

Grigolini P (1989) Noise in nonlinear dynamical systems vol 1, ed f moss and pve mcclintock

Grigolini P, Wu HL, Kenkre VM (1989) Brownian motion and finite-temperature effects in the discrete nonlinear schrödinger equation: Analytic results for the nonadiabatic dimer. Physical Review B 40(10):7045

Gross EP (1961) Structure of a quantized vortex in boson systems. Il Nuovo Cimento (1955-1965) 20(3):454–477

Gross EP (1963) Hydrodynamics of a superfluid condensate. Journal of Mathematical Physics 4(2):195–207

Großmann F, Hänggi P (1992) Localization in a driven two-level dynamics. EPL (Europhysics Letters) 18(7):571

Grover M, Silbey R (1971) Exciton migration in molecular crystals. The Journal of Chemical Physics 54(11):4843–4851

Gupta S, Campa A, Ruffo S (2018) Statistical Physics of Synchronization. Springer

Haken H, Reineker P (1972) The coupled coherent and incoherent motion of excitons and its influence on the line shape of optical absorption. Zeitschrift für Physik 249(3):253–268

Haken H, Strobl G (1973) An exactly solvable model for coherent and incoherent exciton motion. Zeitschrift für Physik A Hadrons and nuclei 262(2):135–148

Harris RA, Silbey R (1985) Variational calculation of the tunneling system interacting with a heat bath. ii. dynamics of an asymmetric tunneling system. The Journal of chemical physics 83(3):1069–1074

Hennig D, Tsironis GP (1999) Wave transmission in nonlinear lattices. Physics Reports 307(5-6):333–432

Holstein T (1959a) Studies of polaron motion: Part i. the molecular-crystal model. Annals of Physics 8(3):325–342

Holstein T (1959b) Studies of polaron motion: Part ii. the "small" polaron. Annals of Physics 8(3):343–389

Itoh K, Shimanouchi T (1972) Vibrational spectra of crystalline formamide. Journal of Molecular Spectroscopy 42(1):86–99

Jackson EA (1989) Perspectives of Nonlinear Dynamics,Volume 1, vol 1. Cambridge University Press

Jackson EA (1990) Perspectives of Nonlinear Dynamics, Volume 2. Cambridge University Press

Jeleńska-Kuklińska M, Kuś M (1990) Exact solution in the semiclassical jaynes-cummings model without the rotating-wave approximation. Physical Review A 41(5):2889

Jordan TF (2009) Why quantum dynamics is linear. In: Journal of Physics: Conference Series, IOP Publishing, vol 196, p 012010

Kadantsev V, Lupichov L, Savin A (1987) Intramolecular excitation dynamics in a thermalized chain. i. formation of autolocalized states in a cyclic chain. physica status solidi (b) 143(2):569–579

Kadantsev V, Lupichev L, Savin A (1988) Intramolecular excitation dynamics in a thermalized chain. ii. formation of autolocalized states in a chain with free ends. physica status solidi (b) 147(1):155–161

Kalosakas G, Bishop A, Kenkre V (2003a) Multiple-timescale quantum dynamics of many interacting bosons in a dimer. Journal of Physics B: Atomic, Molecular and Optical Physics 36(15):3233

Kalosakas G, Bishop A, Kenkre V (2003b) Small-tunneling-amplitude boson-hubbard dimer. ii. dynamics. Physical Review A 68(2):023602

Kehr KW, Kitahara K (1987) Spin depolarization of particles in tunnelling states. Journal of the Physical Society of Japan 56(3):889–892

Kehr KW, Kitahara K (1988) Spin depolarization of a quantum particle on a liner chain with alternating larmor frequencies. Journal of the Physical Society of Japan 57(8):2819–2825

Kenkre V (1975) Relations among theories of excitation transfer. ii. influence of spectral features on exciton motion. Physical Review B 12(6):2150

Kenkre V (1998a) Four stages in the study of quasiparticle-phonon interactions. Journal of luminescence 76:511–517

Kenkre V, Fan X (1987) A theoretical approach to the thermal conductivity of boron carbides. MRS Online Proceedings Library (OPL) 97

Kenkre V, Fan X (1988) A model calculation for vibrational propagation in a chain of nonlinear oscillators. Zeitschrift für Physik B Condensed Matter 70(2):223–228

Kenkre V, Raghavan S (2000) Dynamic localization and related resonance phenomena. Journal of Optics B: Quantum and Semiclassical Optics 2(5):686

Kenkre V, Raghavan S, Bishop A, Salkola M (1996a) Memory-function approach to interacting quasiparticle-boson systems. Physical Review B 53(9):5407

Kenkre VM (1989) The quantum nonlinear dimer and extensions. In: atikos SPM, Bountis T, atikos SPM (eds) Singular behaviour and nonlinear dynamics, World Scientific, London

Kenkre VM (1993) An ecumenical nonlinear von neumann equation: fluctuations, dissipation, and bifurcations. Physica D: Nonlinear Phenomena 68(1):153–161

Kenkre VM (1994a) Nonlinear dynamics of polarons. In: Lakhno VD (ed) Polarons and Applications, Wiley & Sons, Leeds, UK, pp 383–403

Kenkre VM (1994b) Recent developments in the quantum nonlinear dimer: Hopf bifurcations, time evolution, and thermal stability. In: Nonlinear Coherent Structures in Physics and Biology, Springer, pp 15–18

Kenkre VM (1994c) Thermally induced limit cycles in the nonlinear theory of fluorescence depolarization. The Journal of Physical Chemistry 98(30):7371–7375

Kenkre VM (1995) Thermal effects in nonlinear structures such as the davydov soliton: the brownian motion approach and the gibbs approach. In: Fluctuation Phenomena: Disorder and Nonlinearity, World Scientific, pp 124–130

Kenkre VM (1998b) What do polarons owe to their harmonic origins? Physica D: Nonlinear Phenomena 113(3):233–241

Kenkre VM (2000) Memory formalism for quantum control of dynamic localization. Journal of Physical Chemistry B 104(16):3960–3966

Kenkre VM (2021) Memory Functions, Projection Operators, and the Defect Technique: Some Tools of the Trade for the Condensed Matter Physicist. Springer Nature

Kenkre VM, Brown DW (1985) Exact solution of the stochastic liouville equation and application to an evaluation of the neutron scattering function. Physical Review B 31(4):2479

Kenkre VM, Campbell DK (1986) Self-trapping on a dimer: time-dependent solutions of a discrete nonlinear schrödinger equation. Physical Review B 34(7):4959

Kenkre VM, Cruzeiro-Hansson L (1994) Thermal stability of nonlinear structures: a gibbs analysis of the semiclassical system. Zeitschrift für Physik B Condensed Matter 95(3):379–383

Kenkre VM, Dresden M (1971) Exact transport parameters for driving forces of arbitrary magnitude. Physical Review Letters 27(1):9

Kenkre VM, Giuggioli L (2004) Study of some approximation schemes in the spin-boson problem. Chemical physics 296(2-3):135–148

Kenkre VM, Giuggioli L (2020) Theory of the Spread of Epidemics and Movement Ecology of Animals: an Interdisciplinary Approach Using Methodologies of Physics and Mathematics. Cambridge University Press, Cambridge, U.K.

Kenkre VM, Grigolini P (1993) A new nonlinear stochastic liouville equation. Zeitschrift für Physik B Condensed Matter 90(2):247–253

Kenkre VM, Kumar N (2008) Nonlinearity in bacterial population dynamics: Proposal for experiments for the observation of abrupt transitions in patches. Proceedings of the National Academy of Sciences USA 105(48):18752–18757

Kenkre VM, Kuperman MN (2003) Applicability of the fisher equation to bacterial population dynamics. Physical Review E 67(5):051921

Kenkre VM, Kuś M (1992) Model calculations for the phenomenon of nonlinear trapping in molecular aggregates. Physical Review B 46(21):13792

Kenkre VM, Kuś M (1994) Bifurcations in the quantum nonlinear dimer. Physical Review B 49(9):5956

Kenkre VM, Rahman TS (1974) Model calculations in the theory of excitation transfer. Physics Letters A 50(3):170–172

Kenkre VM, Reineker P (1982) Exciton dynamics in molecular crystals and aggregates, vol 94, Springer Tracts in Modern Physics. Springer, Berlin, Germany

Kenkre VM, Tsironis GP (1987) Nonlinear effects in quasielastic neutron scattering: exact line-shape calculation for a dimer. Physical Review B 35(4):1473

Kenkre VM, Tsironis GP (1988) Theory of fluorescence depolarization of dimers from the nonlinear schrödinger equation. Chemical physics 128(1):219–226

Kenkre VM, Wu HL (1989a) Interplay of quantum phases and non-linearity in the non-adiabatic dimer. Physics Letters A 135(2):120–124

Kenkre VM, Wu HL (1989b) Time evolution of the nonadiabatic nonlinear quantum dimer. Physical Review B 39(10):6907

Kenkre VM, Tsironis GP, Campbell DK (1987) Energy transfer, self-trapping, and solitons on a nonlinear dimer. In: Nonlinearity in Condensed Matter, Springer, pp 226–231

Kenkre VM, Andersen JD, Dunlap D, Duke C (1989) Unified theory of the mobilities of photoinjected electrons in naphthalene. Physical review letters 62(10):1165

Kenkre VM, Dunlap D, Grigolini P (1990) Excimers in molecular crystals: The relaxation of a nonlinear oscillator. In: Davydov's Soliton Revisited, Springer, pp 457–464

Kenkre VM, Raghavan S, Cruzeiro-Hansson L (1994) Thermal stability of extended nonlinear structures related to the davydov soliton. Physical Review B 49(14):9511

Kenkre VM, Wu HL, Howard I (1995) Effects of interaction-potential nonlinearities and restoring-force anharmonicities in the discrete nonlinear schrödinger equation. Physical Review B 51(22):15841

Kenkre VM, Jørgensen MF, Christiansen PL (1996b) Exponential nonlinearity and saturation in quantum nonlinear dimers. Physica D: Nonlinear Phenomena 90(3):280–292

Kerr WC, Lomdahl P (1987) Quantum-mechanical derivation of the equations of motion for davydov solitons. Physical Review B 35(7):3629

Kevrikidis PG (2009) The Discrete Nonlinear Schrödinger Equation: Mathematical Analysis, Numerical Computations and Physical Perspectives. Springer-Verlag

Knox RS, Gülen D (1993) Theory of polarized fluorescence from molecular pairs: Förster transfer at large electronic coupling. Photochemistry and photobiology 57(1):40–43

Kramer P, Saraceno M (1980) Geometry of the time-dependent variational principle in quantum mechanics. In: Group theoretical methods in physics, Springer, pp 112–121

Kubo R (1957) Statistical-mechanical theory of irreversible processes. i. general theory and simple applications to magnetic and conduction problems. Journal of the Physical Society of Japan 12(6):570–586

Kujawski A (1988) Exact periodic solution in the semiclassical jaynes-cummings model without the rotating-wave approximation. Physical Review A 37(4):1386

Kumar N, Kenkre VM (2011) Effects of gradual spatial variation in resources on population extinction: analytic calculations for abrupt transitions. Physica A: Statistical Mechanics and its Applications 390(2):257–262

Kuś M, Kenkre VM (1994) The non-adiabatic nonlinear quantum dimer in the absence of dissipation: exact solutions. Physica D: Nonlinear Phenomena 79(2-4):409–415

Landau LD (1933) Electron motion in crystal lattices. Physikalische Zeitschrift der Sowjetunion 3:664

Landauer R (1987) Nonlinearity: Historical and technological view. In: Bishop A R KP Campbell D K, E TS (eds) Nonlinearity in Condensed Matter, Springer, pp 2–22

Lawrence AF, McDaniel JC, Chang DB, Pierce BM, Birge RR (1986) Dynamics of the davydov model in alpha-helical proteins: Effects of the coupling parameter and temperature. Physical Review A 33(2):1188

Leggett AJ (2001) Bose-einstein condensation in the alkali gases: Some fundamental concepts. Reviews of Modern Physics 73(2):307

Leggett AJ (2002) Testing the limits of quantum mechanics: motivation, state of play, prospects. Journal of Physics: Condensed Matter 14(15):R415

Leggett AJ, Chakravarty S, Dorsey AT, Fisher MP, Garg A, Zwerger W (1987) Dynamics of the dissipative two-state system. Reviews of Modern Physics 59(1):1

Lin AL, Mann BA, Torres-Oviedo G, Lincoln B, Käs J, Swinney HL (2004) Localization and extinction of bacterial populations under inhomogeneous growth conditions. Biophysical Journal 87(1):75–80

Lomdahl P, Kerr W (1985) Do davydov solitons exist at 300 k? Physical review letters 55(11):1235

Lu T, Dunlap DH (2003) Band narrowing in semiclassical nonadiabatic electron transfer. Physical Review B 67(1):012301

Marsden J, McCracken M (1976) Introduction to stability and bifurcation in dynamical systems and fluid mechanics. In: The Hopf Bifurcation and Its Applications, Springer, pp 1–26

Milonni P, Ackerhalt J, Galbraith H (1983) Chaos in the semiclassical n-atom jaynes-cummings model: Failure of the rotating-wave approximation. Physical Review Letters 50(13):966

Molina M (1999) Self-trapping on a generalized nonlinear tetrahedron. Modern physics letters B 13(08):225–232

Molina M, Tsironis G (1995) Disorder in the discrete nonlinear schrödinger equation. International Journal of Modern Physics B 9(16):1899–1932

Molina M, Rössler J, Tsironis G (1997) Quantum vibrational impurity embedded in a one-dimensional chain. Physics Letters A 234(1):59–63

Nakajima S (1958) On quantum theory of transport phenomena: steady diffusion. Progress of Theoretical Physics 20(6):948–959

Newell AC (1985) Solitons in mathematics and physics. SIAM

Nicolis G (1995) Introduction to nonlinear science. Cambridge university press

Nieto M, Simmons JL (1979) p. 429 in coherent states, ref.[1]; mm nieto and lm simmons, jr. Phys Rev D 20:1321

Parris PE, Kenkre V (2004) Variational considerations in the study of carrier transport in organic crystals. Physical Review B 70(6):064304

Parris PE, Silbey R (1985) Low temperature tunneling dynamics in condensed media. The Journal of chemical physics 83(11):5619–5626

Pekar S (1954) Untersuchung über die Elektronentheorie der Kristalle, Berlin, Akad. Akademie Verlag, Berlin

Perry N (2005) Experimental validation of a critical domain size in reaction–diffusion systems with escherichia coli populations. Journal of the Royal Society Interface 2(4):379–387

Pitaevskii LP (1961) Vortex lines in an imperfect bose gas. Sov Phys JETP 13(2):451–454

Pope M, Swenberg CE (1982, 1999) Electronic processes in organic crystals and polymers. Oxford University Press

Pudlik T, Hennig H, Witthaut D, Campbell DK (2014) Tunneling in the self-trapped regime of a two-well bose-einstein condensate. Physical Review A 90(5):053610

Rackovsky S, Silbey R (1973) Electronic energy transfer in impure solids: I. two molecules embedded in a lattice. Molecular Physics 25(1):61–72

Raghavan S, Kenkre V (1994) Quantum mechanical bound rotator as a generalized harmonic oscillator. Journal of Physics: Condensed Matter 6(47):10297

Raghavan S, Kenkre V, Bishop A, Salkola M (1996) Validity of the discrete nonlinear schrödinger equation in the context of the fluorescence depolarization of a spin-boson system. Physical Review B 53(13):8457

Raghavan S, Kenkre VM, Bishop AR (1997) Phase-nonlinearity interplay in small quantum systems. Physics Letters A 233(1-2):73–78

Raghavan S, Bishop A, Kenkre V (1999a) Quantum versus semiclassical description of self-trapping: Anharmonic effects. Physical Review B 59(15):9929

Raghavan S, Smerzi A, Fantoni S, Shenoy S (1999b) Boson josephson junction with trapped atoms. International Journal of Modern Physics B 13(05n06):633–641

Raghavan S, Smerzi A, Fantoni S, Shenoy S (1999c) Coherent oscillations between two weakly coupled bose-einstein condensates: Josephson effects, π oscillations, and macroscopic quantum self-trapping. Physical Review A 59(1):620

Raghavan S, Smerzi A, Kenkre VM (1999d) Transitions in coherent oscillations between two trapped bose-einstein condensates. Physical Review A 60(3):R1787

Raghavan S, Kenkre V, Bishop A (2000) Dynamic localization in spin systems. Physical Review B 61(9):5864

Rahman TS, Knox RS, Kenkre VM (1979) Theory of depolarization of fluorescence in molecular pairs. Chemical Physics 44(2):197–211

Reichl LE (2009) A modern course in statistical physics, 3rd edn. John Wiley & Sons, Hoboken, NJ, USA

Salkola M, Bishop A, Kenkre V, Raghavan S (1995) Coupled quasiparticle-boson systems: The semiclassical approximation and discrete nonlinear schrödinger equation. Physical Review B 52(6):R3824

Salkola M, Bishop A, Kenkre V, Raghavan S (1996) Coupled spin-boson systems far from equilibrium. Physical Review B 54(18):R12645

Santhanam J, Kenkre V, Konotop V (2006) Solitons of bose-fermi mixtures in a strongly elongated trap. Physical Review A 73(1):013612

Schweitzer JW (1992) Lifetime of the davydov soliton. Physical Review A 45(12):8914

Scott A (1992) Davydov's soliton. Physics Reports 217(1):1–67

Scott AC (1990) A non-resonant discrete self-trapping system. Physica Scripta 42(1):14

Scott AC (2007) The Nonlinear Universe: Chaos, Emergence, Life. Springer Science & Business Media

Scott AC, Christiansen PL (1990) A generalized discrete self-trapping equation. Physica Scripta 42(3):257

Shionoya S, Nagakura S, Sugano S (1976) Proceedings of the 1975 International Conference on Luminescence, Tokyo, Japan, September 1-5, 1975, vol 12. North-Holland

Silbey R (1976) Electronic energy transfer in molecular crystals. Annual Review of Physical Chemistry 27(1):203–223

Silbey R, Harris RA (1984) Variational calculation of the dynamics of a two level system interacting with a bath. The Journal of chemical physics 80(6):2615–2617

Silbey R, Munn R (1980) General theory of electronic transport in molecular crystals. i. local linear electron–phonon coupling. The Journal of Chemical Physics 72(4):2763–2773

Sköld K (1978) Quasielastic neutron scattering studies of metal hydrides. Springer, pp 267–287

Steib R, Schoendorff J, Korsch H, Reineker P (1998) Quantum-mechanical and quasiclassical dynamics of coupled quasiparticle-boson systems. Physical Review E 57(6):6534

Strogatz SH (2018) Nonlinear dynamics and chaos: with applications to physics, biology, chemistry, and engineering. CRC Press, Boca Raton, FL

Stryer L, Haugland R (1967) Probing polyproline structure and dynamics by photoinduced electron transfer provides evidence for deviations from a regular polyproline type ii helix. Proc Natl Acad Sci USA 58:719–726

Tiwari M, Kenkre VM (2014) Approach to equilibrium of a nondegenerate quantum system: decay of oscillations and detailed balance as separate effects of a reservoir. The European Physical Journal B 87(4):86

Tsironis G (1993) Dynamical domains of a nondegenerate nonlinear dimer. Physics Letters A 173(4-5):381–385

Tsironis G (2011) Exact dynamics for fully connected nonlinear networks. Physics Letters A 375(10):1304–1308

Tsironis GP, Kenkre VM (1988) Initial condition effects in the evolution of a nonlinear dimer. Physics Letters A 127(4):209–212

Tsironis GP, Kenkre VM, Finley D (1988) Effects of dissipation on nonlinearity in transport: Evolution and integrability properties in a molecular dimer. Physical Review A 37(11):4474

Uspensky JV (1948) Theory of equations. Tata McGraw-Hill Education

Van Hove L (1954) Time-dependent correlations between spins and neutron scattering in ferromagnetic crystals. Physical Review 95(6):1374

Vitali D, Grigolini P (1990) Nonlinear effects in quantum dissipation. Physical Review A 42(12):7091

Vitali D, Bonci L, Mannella R, Grigolini P (1992) Localization breakdown as a joint effect of nonlinear and quantum dissipation. Physical Review A 45(4):2285

Vitali D, Allegrini P, Grigolini P (1994) Nonlinear quantum mechanical effects: real or artefact of inaccurate approximations? Chemical physics 180(2-3):297–318

Wang X, Brown DW, Lindenberg K (1990) Quantum monte carlo simulations of the davydov model. In: Davydov's Soliton Revisited, Springer, pp 83–98

Wannier GH (1959) Elements of solid state theory. Cambridge University Press Archive

Weinberg S (1989) Testing quantum mechanics. Annals of Physics 194(2):336–386

Weiss GH (1967) First passage time problems in chemical physics. Advances in Chemical Physics 13:1–18

Wu HL, Kenkre VM (1989) Generalized master equations from the nonlinear schrödinger equation and propagation in an infinite chain. Physical Review B 39(4):2664

Wu HL, Kenkre VM (1995) Multiple stationary states and saturation effects for rotational polarons. Physics Letters A 199(1-2):61–64

Wu HL, Grigolini P, Kenkre VM (1990) Analytical evaluation of the time evolution of a nonadiabatic nonlinear quantum dimer under the averaging approximation. Journal of Physics: Condensed Matter 2(19):4417

Wu M, Conwell E (1997) Transport in α-sexithiophene films. Chemical physics letters 266(3-4):363–367

Yarkony DR, Silbey R (1977) Variational approach to exciton transport in molecular crystals. The Journal of Chemical Physics 67(12):5818–5827

Yudson V, Däubler H, Reineker P (1994) Excimer formation in molecular crystals. Journal of luminescence 58(1-6):371–373

Zwanzig R (1961) Statistical mechanics of irreversibility. Lectures in theoretical physics 3:106–141

Zwanzig R (1964) On the identity of three generalized master equations. Physica 30(6):1109–1123